

The interplay between Natural Killer cells and Pancreatic Stellate cells in Pancreatic Ductal Adenocarcinoma

Rachel Elizabeth Ann Fincham

Submitted in partial fulfilment of the requirements of the Degree of
Doctor of Philosophy

October 2023

This work was supported by Barts and the London Charity (UK) and
A*STAR Research Attachment Programme (Singapore)

Queen Mary University of London

Barts Cancer Institute

Centre for Tumour Biology

John Vane Science Centre

Charterhouse Square

London

EC1M 6BQ

Statement of Originality

I, Rachel Elizabeth Ann Fincham, confirm that the research included within this thesis is my own work or that where it has been carried out in collaboration with, or supported by others, that this is duly acknowledged below and my contribution indicated. Previously published material is also acknowledged below.

I attest that I have exercised reasonable care to ensure that the work is original, and does not to the best of my knowledge break any UK law, infringe any third party's copyright or other Intellectual Property Right, or contain any confidential material.

I accept that Queen Mary University of London has the right to use plagiarism detection software to check the electronic version of the thesis.

I confirm that this thesis has not been previously submitted for the award of a degree by this or any other university.

The copyright of this thesis rests with the author and no quotation from it or information derived from it may be published without the prior written consent of the author.

Signature: Rachel Elizabeth Ann Fincham

Date: 9th October 2023

List of Publications

Fincham REA, Bashiri H, Lau MC, et al. Editorial: Multiplex

Immunohistochemistry/Immunofluorescence Technique: The Potential and Promise for Clinical Application. *Frontiers in Molecular Biosciences* 2022;9.

Fincham REA, Delvecchio FR, Goulart MR, et al. Natural killer cells in pancreatic cancer stroma. *World J Gastroenterol* 2021;27:3483-3501.

Delvecchio FR, Goulart MR, **Fincham REA**, et al. B cells in pancreatic cancer stroma. *World J Gastroenterol* 2022;28:1088-1101.

Delvecchio FR, **Fincham REA**, Spear S, et al. Pancreatic Cancer Chemotherapy Is Potentiated by Induction of Tertiary Lymphoid Structures in Mice. *Cell Mol Gastroenterol Hepatol* 2021;12:1543-1565.

Goulart MR, Stasinou K, **Fincham REA**, et al. T cells in pancreatic cancer stroma. *World J Gastroenterol* 2021;27:7956-7968.

Acknowledgments

Firstly, I would like to take this opportunity to thank both Hemant and Joe for giving me this incredible opportunity. Thank you for all of your help, support, advice, guidance and encouragement throughout this journey, it has meant so very much to me. I would also like to thank Barts Charity and A*STAR for funding this project and allowing me to experience research both in the UK and Singapore.

Secondly, thank you to the Kocher Lab, old and new, and JY Lab for making my PhD journey so wonderful! To Abi, Michelle, Gabriel and Christine, thank you for all of your help and encouragement, for showing me the ropes and for helping me through countless rounds of troubleshooting! To Kostas, Mo, Daniel, Francesca, Sath, Christos, Pramod, Akil and Haz, thank you for making my time in the lab so enjoyable and for keeping my spirits up during the thesis writing! To the original cast of G23, thank you for the chats, laughs and wonderful memories. Thanks in particular to Demi, Shayin, Litsa, Nick and Reza for your kindness, laughter and friendship. To my 'buddy', Justina, thank you for your friendship, for laughing at my jokes and for always being there to help! Thanks too to Felicia, Craig, Jeffrey, Xinru, Hema, Parthiban and Zhen Wei for all of your help, advice, and friendship and for educating my western palate! Krish, thanks for being a little bit of England in Singapore!

Finally I would like to thank my incredible friends and family for their continual love and support. Thank you for always believing in me, for always being my biggest supporters, for all of your love, care, understanding and patience – I could not have done this without you!

Table of Contents

Statement of Originality	2
List of Publications.....	3
Acknowledgments	4
Table of Contents	5
List of Figures.....	10
List of Tables	15
List of Appendices.....	17
List of Abbreviations	18
Abstract	23
Chapter 1 - Introduction	24
1.1 Pancreatic cancer	25
1.2 Pancreatic ductal adenocarcinoma risk factors	25
1.2.1 Development and Subtypes of pancreatic cancer.....	28
1.2.2 PDAC development and progression.....	29
1.2.3 PDAC treatment.....	33
1.2.4 PDAC Tumour Microenvironment	35
1.3 Pancreatic Stellate Cells.....	39
1.3.1 PSC signalling pathways.....	40
1.3.2 PSC interaction with stromal cells	44
1.4 Fibroblasts	48
1.4.1 Cancer Associated Fibroblasts.....	49
1.4.2 CAF cells of origin	50
1.4.3 CAF Heterogeneity in PDAC.....	53
1.5 Natural Killer Cells	57
1.5.1 NK cell receptors.....	61
1.5.2 NK Cytotoxicity	65
1.5.3 NK in Cancer	71
1.5.4 NK cells in PDAC.....	72
1.6 NK cells and Pancreatic Stellate cells	76
1.7 Project Aims and Hypotheses.....	77
Chapter 2 - Materials and Methods	79

2.1 Cell Culture	80
2.2 Media co-culture experiments	84
2.3 WST-1 validation of media co-coculture experiments	86
2.4 CD107 Degranulation Assay	86
2.5 CD107 Troubleshooting	87
2.5.1 Alternative staining protocol – CD56 incubation	87
2.5.2 24-hour Degranulation Assay	88
2.5.3 Primary NK cell degranulation assay	88
2.5.4 CD107 Degranulation assay alternative staining protocol	89
2.5.5 Post-Acquisition analysis	91
2.5.6 Full effector to target ratio experiments.....	92
2.6 Cytotoxicity Assays	92
2.6.1 WST-1 Cytotoxicity Assays.....	92
2.6.2 Calcein AM Cytotoxicity Assays	97
2.7 Flow Antibody Titration.....	98
2.7.1 NKG2A Antibody Troubleshooting	102
2.8 Receptor expression and phenotype analysis.....	105
2.9 Flow cytometry Panel design - Cytex Aurora (Cytex biosciences)	107
2.9.1 Development of an 18-colour panel for full spectrum flow cytometry	107
2.9.2 Antibody titration	113
2.9.3 Staining Protocol	115
2.9.4 Sample Acquisition	116
2.9.5 Spectral unmixing	116
2.9.6 Post-Acquisition analysis	117
2.9.7 Marker troubleshooting	117
2.9.8 Full Panel Trial	118
2.10 Characterisation of Cancer Cell lines.....	119
2.11 Characterisation of PS1 Cells.....	120
2.12 PSC-Educated NK cell WST-1 Cytotoxicity Assays	120
2.13 Degranulation Assay against PSC	122
2.14 Educated Degranulation Assay.....	125
2.15 Calcein AM Cytotoxicity Assays against PSC.....	127
2.16 Educated NK cytotoxicity assay	129

2.17 Receptor/Phenotype Expression Assay	131
2.17.1 Direct Contact and Transwell™ Experiments	133
2.17.2 Conditioned Media Experiments	137
2.18 Luminex ELISA	141
2.19 Proteomics	141
2.19.1 Cell culture	143
2.19.2 Dead cell exclusion	143
2.19.3 Peptide Preparation	144
2.19.4 C18 Peptide Clean-up	145
2.19.5 Peptide Estimation	146
2.19.6 Acquisition on the Mass Spectrometer	146
2.19.7 Post-Acquisition analysis	147
2.19.8 RNA- Seq analysis	147
2.20 Immunofluorescent staining of NK cells in Human spleen tissue	148
2.20.1 Antibody Titration	148
2.20.2 Background troubleshooting	149
2.20.3 Antibody Titration using a different immunofluorescent staining protocol	151
2.20.4 Immunohistochemical evaluation of antibody signal	154
2.20.5 IHC antibody optimisations for Multiplex Immunohistochemistry	158
2.20.6 Slide setup	160
2.20.7 Antibody preparation	160
2.20.8 Slide Dehydration and Mounting	164
2.21 Multiplex Immunohistochemistry	165
2.21.1 TMA staining panels	167
2.21.2 Preparation of OPAL dyes	169
2.21.3 Automated mIHC staining	171
2.21.4 Mounting slides	172
2.21.5 Spectral Unmixing	172
2.21.6 HALO analysis	173
2.22 Proximity Analysis	178
2.23 Statistical Analysis	181
Chapter 3 - Results – <i>In vitro</i> Optimisations	182
3.1 Introduction	183

3.2 NK92 and PS1 media co-culture experiments	184
3.3 WST-1 incubation and seeding density optimisation for cytotoxicity assays	187
3.4 Initial CD107 Degranulation assay trial	189
3.4.1 CD107 Degranulation Assay Optimisations and Troubleshooting	191
3.5 CD107 Degranulation Assay using the Cytex Aurora Flow cytometry system	199
3.6 Calcein AM Cytotoxicity Assay optimisation and troubleshooting	206
3.7 Initial flow cytometric antibody titrations.....	208
3.7.1 NKG2A Troubleshooting	211
3.8 Development of Spectral flow cytometry panels for receptor/phenotypic expression assays.....	219
3.9 Receptor/Phenotypic expression assay trial	226
Chapter 4 - Results 2 – <i>In Vitro</i> Experiments.....	230
4.1 Introduction.....	231
4.2 Characterisation of pancreatic stellate cells and pancreatic cancer cell lines	231
4.3 WST-1 Cytotoxicity Assays.....	234
4.4 CD107 Degranulation Assays.....	240
4.5 Calcein AM Cytotoxicity Assays	242
4.6 Receptor/Phenotypic Expression Assays.....	244
4.6.1 Initial NK cell receptor expression experiment	244
4.6.2 Initial PSC Phenotypic Expression.....	247
4.6.3 Spectral Flow cytometry.....	250
4.6.4 Luminex Analysis	259
4.7 Proteomics.....	262
Chapter 5 - Results 3 – <i>Ex Vivo</i> Optimisations.....	267
5.1 Introduction.....	268
5.2 Immunofluorescent staining	268
5.2.1 Antibody titration	269
5.2.2 Background Troubleshooting	271
5.2.3 Antibody titration using a different immunofluorescent protocol	274
5.3 Immunohistochemical Evaluation of Antibody signal	276
5.4 IHC Optimisations for multiplex immunohistochemistry.....	280
5.5 mIHC full panel trials	285
5.5.1 NKG2D Troubleshooting.....	289
Chapter 6 - Results 4 – <i>Ex Vivo</i> Experiments	293

6.1 Introduction	294
6.2 Multiplex Immunohistochemical analysis of PDAC samples	294
6.2.1 Immune cell infiltrate in PDAC	305
6.2.2 The importance of immune cell proximity to CAFs in PDAC	309
6.2.3 CAF subtypes in PDAC.....	315
6.2.4 Correlation between NK cell infiltrate and CAFs in Short/ Long survivors	317
Chapter 7 – Discussion	319
7.1 PSC activation confers protection from NK cell lysis whilst qPSC education impairs NK cytotoxicity	320
7.1.1 3D <i>in vitro</i> models of NK cell function	323
7.2 NK cells modulate PSC phenotype	326
7.3 PSCs reciprocally modulate NK phenotype and functional markers.....	330
7.4 Co-culture secreted factors	332
7.5 qPSC/aPSC and NK cells demonstrate a significant bi-directional relationship at the proteomic level.....	333
7.6 Prognostic implications of NK cell infiltrate and proximity to CAFs in PDAC.....	339
7.6.1 Absolute NK cell infiltrate does not confer prognostic impact	339
7.6.2 NK proximity to CAFs demonstrates prognostic significance and may be used for patient stratification	340
7.7 Limitations	341
7.8 Future directions	342
7.9 Conclusions.....	344
References	346
Appendix.....	380

List of Figures

Figure 1.1: Pathogenesis of PDAC development.	32
Figure 1.2: The PDAC tumour microenvironment.	38
Figure 1.3: Autocrine and paracrine PSC signalling pathways in PDAC.	43
Figure 1.4: PSC interaction with stromal cells.	47
Figure 1.5: CAF cells of origin.	52
Figure 1.6: CAF heterogeneity in PDAC.	54
Figure 1.7: Activation and inhibition of NK cells.	60
Figure 1.8: LFA-1 conformation.	66
Figure 1.9: Cytotoxic granule convergence and MTOC polarisation.	68
Figure 1.10: Complete and incomplete fusion of lytic granules.	70
Figure 1.11: NK cell dysfunction caused by tumoural and stromal cells in PDAC.	75
Figure 2.1: A schematic representation of the plate layout used for each cancer cell line during WST-1 optimisation.	94
Figure 2.2: Experimental workflow of co-culture experiments for flow cytometric analysis of receptor and phenotype expression.	106
Figure 2.3: Spectral emission of the 18-marker flow cytometry panel.	109
Figure 2.4: Spectral emission of NK flow cytometry markers.	111
Figure 2.5: Spectral emission of PSC flow cytometry markers.	112
Figure 2.6: Schematic representation of the WST-1 Cytotoxicity assay time-course.	121
Figure 2.7: Schematic workflow of CD107 degranulation Assay.	124
Figure 2.8: Experiment workflow of Educated NK cell degranulation assay.	126
Figure 2.9: Experimental workflow of Calcein AM cytotoxicity assays against quiescent and activated PSCs.	128
Figure 2.10: Schematic workflow of educated NK cell cytotoxicity assays against cancer cell lines.	130
Figure 2.11: Flow cytometry workflow.	132
Figure 2.12: Schematic representation of the workflow for direct contact receptor/phenotypic expression assays.	135
Figure 2.13: Schematic representation of the workflow for Transwell™ receptor/phenotypic expression assays.	136

Figure 2.14: Schematic diagram of the experimental workflow for PSCs treated with NK conditioned media.	139
Figure 2.15: Schematic diagram of the experimental workflow for NK cells treated with qPSC/aPSC conditioned media.	140
Figure 2.16: Schematic workflow of proteomic sample preparation and acquisition.	142
Figure 2.17: Overview of the mIHC workflow.....	166
Figure 2.18: Schematic workflow of the major steps involved in the creation, and running of scoring algorithms within HALO software.	177
Figure 2.19: HALO Proximity analysis workflow.	180
Figure 3.1: NK92 and PS1 cell viability following culture in one of five conditions of Alpha MEM and DMEM Hams/F12.	185
Figure 3.2: NK92 and PS1 WST-1 proliferation assays.	186
Figure 3.3: WST-1 incubation and seeding density optimisations.	188
Figure 3.4: Initial CD107 degranulation assay against MiaPaca2 cells	190
Figure 3.5: CD107 Degranulation Assay Troubleshooting.	193
Figure 3.6: Results of a 24h degranulation assay.	196
Figure 3.7: Primary NK cell Degranulation Assay.....	198
Figure 3.8: CD107a/b antibody titration.....	200
Figure 3.9: CD107 Degranulation Assay using the Cytex Aurora Flow cytometry system. ...	202
Figure 3.10: Initial comparison CD107 Degranulation assay against PDAC cell lines using the Cytex Aurora flow cytometry system.	203
Figure 3.11: CD107 Incubation length and effector to target ratio optimisation.	205
Figure 3.12: Calcein AM optimisation and troubleshooting.....	207
Figure 3.13: NK flow cytometry antibody titration.....	209
Figure 3.14: PSC flow cytometry antibody titration.	210
Figure 3.15: Western blot analysis of NKG2A expression.	212
Figure 3.16: NKG2A expression on NK92 cells using surface and intracellular staining protocols.	214
Figure 3.17: NKG2A troubleshooting.	216
Figure 3.18: Flow cytometry staining of NK92 cells using an APC conjugated anti-NKG2A antibody.	218
Figure 3.19: NK marker antibody titration results.....	221

Figure 3.20: PSC Marker Titration.....	222
Figure 3.21: Optimisation of re-sourced antibodies for alpha SMA and NKG2D.	223
Figure 3.22: NK Cell Functional Marker Titration.	224
Figure 3.23: PSC full panel trial.	227
Figure 3.24: NK cell full panel trial.	229
Figure 4.1: Characterisation of PS1 cells.....	232
Figure 4.2: Characterisation of pancreatic cancer cell lines.	233
Figure 4.3: WST-1 cytotoxicity assays	235
Figure 4.4: WST-1 cytotoxicity assay troubleshooting.	237
Figure 4.5: Incucyte images of Capan2 cells following 24h incubation with NK92 cells	239
Figure 4.6: NK cell degranulation against PSCs and the impact of PSC education on NK functional efficacy.....	241
Figure 4.7: Calcein AM Cytotoxicity assays.....	243
Figure 4.8: Representative plots of NK92 receptor expression following co-culture with qPSC or aPSC.	245
Figure 4.9: Percent positive and Geometric Mean Fluorescence intensity of NKG2D and NKG2A in mono- and co-culture conditions.	246
Figure 4.10: Representative plots of phenotypic markers in qPSC and aPSC following co-culture with NK92 cells.	248
Figure 4.11: Percent positive and Geometric Mean Fluorescence intensity of alpha SMA and GFAP in mono- and co-culture conditions.	249
Figure 4.12: The presence of NK cells encourages a myofibroblastic phenotype in both quiescent and activated PSCs.	252
Figure 4.13: PSC marker expression following 24h culture with NK cells separated by 0.4µm Transwell inserts.	253
Figure 4.14: PSC marker expression following 24h culture in NK conditioned media.	254
Figure 4.15: Schematic summary of the changes in qPSCs and aPSCs invoked by direct co-culture with NK cells.	255
Figure 4.16: PSCs influence receptor expression on natural killer cells.	257
Figure 4.17: NK marker expression at the population level in response to direct culture. ..	258
Figure 4.18: Chemokines and Cytokines up and down regulated in response to Direct and Transwell™ culture.....	260

Figure 4.19: Schematic summary of the changes in NK cells invoked by qPSC/ aPSCs direct co-culture.	261
Figure 4.20: NK cells and qPSCs/aPSCs exhibit differentially expressed proteins.....	264
Figure 4.21: Biological Processes down- and up- regulated in NK cells cultured with aPSCs vs those cultured with qPSCs	265
Figure 4.22: Biological Processes down- and up- regulated in qPSCs and aPSCs cultured with NK cells.....	266
Figure 5.1: Immunofluorescent antibody titration of anti-CD56, anti-NKG2D and anti-NKG2A antibodies in human spleen tissue.	270
Figure 5.2: Troubleshooting immunofluorescent staining of human spleen tissue.....	272
Figure 5.3: Immunofluorescent staining of human spleen tissue with different blocking agents.....	273
Figure 5.4: Immunofluorescent staining of human spleen tissue using a new protocol.	275
Figure 5.5: Immunohistochemical evaluation of antibody signal strength.	277
Figure 5.6: Titration of CD56 antibody from DAKO in human spleen tissue.	279
Figure 5.7: Periostin antibody optimisation.	281
Figure 5.8: Myosin-11 antibody optimisation.....	282
Figure 5.9: CD105 antibody optimisation	283
Figure 5.10: NKp46 Antibody optimisation.	284
Figure 5.11: mIHC images of Panel 1 trial staining.	286
Figure 5.12: mIHC images of Panel 2 trial staining.	287
Figure 5.13: mIHC images of Panel 3 trial staining.	288
Figure 5.14: NKG2D incubation optimisation.	290
Figure 5.15: mIHC images of Panel 2 trial staining – modified NKG2D incubation.	292
Figure 6.1: Representative image of CAF staining in PDAC.	300
Figure 6.2: Representative images of NK cell staining in PDAC.	301
Figure 6.3: Cancer associated fibroblast marker expression across patients.	303
Figure 6.4: NK cell marker expression across patients.	304
Figure 6.5: Survival analysis of short and long survivors.	306
Figure 6.6: NK immune cell infiltrate in short and long survivors.	308
Figure 6.7: Proximity of NK cells and CAFs in PDAC.....	310

Figure 6.8: Violin plots showing results of proximity analysis between NK and CAF cells in PDAC.....	312
Figure 6.9: Risk of short survival associated with immune cell infiltrate and CAF marker expression.	314
Figure 6.10: Survival analysis based on CAF marker expression.	316
Figure 6.11: Correlation matrices between cancer associated fibroblast (CAF) markers and NK cells in PDAC.	318

List of Tables

Table 2.1: Cell lines utilised within the current project with their required media.	81
Table 2.2: Mutational and differentiation status of pancreatic cancer cell lines used within this project.	83
Table 2.3: Media conditions trialled to determine optimal co-culture conditions for NK92 and PS1 cells.....	85
Table 2.4: Protocol modifications used to troubleshoot confounder identified in WST-1 Cytotoxicity Assays.....	96
Table 2.5: Antibodies used for flow cytometry staining.....	99
Table 2.6: Antibody dilution for initial flow cytometry antibody titration.....	100
Table 2.7: Key protocol steps involved in NKG2A troubleshooting.....	104
Table 2.8: Flow cytometric panel design.	108
Table 2.9: Antibody and titration details for Spectral Flow Cytometric Staining.....	114
Table 2.10: Blocking conditions and secondary antibody dilutions trialled to troubleshoot the high level of background staining observed in human spleen tissue.....	150
Table 2.11: Key difference between Immunofluorescent staining protocols trialled.....	152
Table 2.12: Antibody dilutions tested in spleen and tonsil tissue using a new immunofluorescent protocol.....	153
Table 2.13: Dilutions, antigen retrieval method and tissue type used for immunohistochemical analysis of anti-CD56, anti-NKG2D and anti-NKG2A antibodies.....	156
Table 2.14: Dilutions, antigen retrieval method and tissue type used for immunohistochemical analysis of the anti-CD56 antibody from DAKO.....	157
Table 2.15: Antibodies optimised prior to mIHC staining.....	159
Table 2.16: Positive control tissue, antibody dilutions and antigen retrieval conditions tested for each optimised marker.	162
Table 2.17: Positive control tissue, antibody dilution, antigen retrieval condition and incubation length tested for NKG2D.....	163
Table 2.18: Multiplex immunohistochemistry staining panels with epitope retrieval conditions (ER), antibody dilutions and positive control tissues.....	168
Table 2.19: Dilutions of OPAL dyes	170
Table 2.20: Description of cellular phenotypes assessed in PDAC TMA samples.	175

Table 3.1: Optimised antibody dilutions for NK and PSC flow cytometric staining.	225
Table 6.1: Clinical details of patient samples included within TMA blocks.	296
Table 6.2: Details of tissue types included within TMA slides.	297
Table 6.3: Sources of normal adjacent tissue included within TMA slides.	298
Table 7.1: Clinical Trials involving NK cell therapies (clinicaltrials.gov).	338

List of Appendices

Appendix 1: CD107 degranulation assay protocol provided by the Samson Lab.....	381
Appendix 2: Gating strategy for CD107 degranulation assays.	382
Appendix 3: Gating strategy for flow cytometric analysis of PSC markers in response to co-culture with NK cells.	383
Appendix 4: Gating strategy for flow cytometric analysis of NK cell markers in response to co-culture with quiescent or activated PSCs.	384
Appendix 5: FGF2 expression in response to Direct and Transwell™ culture.	385
Appendix 6: Concentrations of secreted cytokines and chemokines identified in direct and Transwell™ co-culture.	386
Appendix 7: Fold change in analyte concentration (identified by Luminex multiplex ELISA) observed between Transwell™ separated and direct co-culture conditions.	387
Appendix 8: Top upregulated and downregulated proteins in PSCs and NK cells in response to co-culture.....	388
Appendix 9: Initial antibody titrations for periostin using a second antibody clone.	389
Appendix 10: Additional antibody titration for periostin (second clone).	390
Appendix 11: Number of cores analysable for each patient.	391
Appendix 12: Representative images of Panel 1 staining with HALO scoring masks.	392
Appendix 13: Representative images of Panel 2 staining with scoring masks.	393
Appendix 14: Representative images of Panel 3 staining on TMA sections with scoring masks.	394
Appendix 15: Comparison of lineage markers between panels 2 and 3.	395
Appendix 16: Kaplan Meier survival analysis dichotomised by high and low expression of NK cell markers.....	396

List of Abbreviations

ACC	Acinar Cell Carcinoma
ADCC	Antibody Dependent Cellular Cytotoxicity
apCAF	Antigen Presenting Cancer Associated Fibroblast
aPSC	Activated Pancreatic Stellate Cell
ATRA	All Trans Retinoic Acid
Bcl2	B-Cell Lymphoma 2
BRAF	B-Type Raf Proto-Oncogene
BRCA1	Breast Cancer Gene 1
CDKN2A	Cyclin Dependent Kinase Inhibitor 2A
cMET	Mesenchymal-Epithelial Transition Factor
CTGF	Connective Tissue Growth Factor
CTLA-4	Cytotoxic T-Lymphocyte-Associated Protein 4
CXCL	Chemokine (C-X-C motif) Ligand
CXCR	Chemokine (C-X-C motif) Receptor
DNMT1	DNA Methyltransferase 1
EGFR	Epidermal Growth Factor Receptor
EtOH	Ethanol
FAP	Fibroblast Activation Protein
FGF	Fibroblast Growth Factor

GFAP	Glial Fibrillary Acidic Protein
GLI	Zinc Finger Protein GLI1/ Glioma-Associated Oncogene
GRB2	Growth Factor Receptor Bound Protein 2
HLA-E	Human Leukocyte Antigen (Class 1 Histocompatibility Antigen) Alpha Chain E
HSC	Hepatic Stellate Cell
iCAF	Inflammatory Cancer Associated Fibroblast
ICAM1	Intercellular Adhesion Molecule 1
IDO	Indoleamine 2, 3 Dioxygenase
IFN- γ	Interferon- γ
IL	Interleukin
IOPN	Intraductal Oncolytic Papillary Neoplasm
IPMN	Intraductal Papillary Mucinous Neoplasm
ITPN	Intraductal Tubulopapillary Neoplasm
JAK	Janus Kinase
KIR	Killer Immunoglobulin-Like Receptor
KRAS	Kirsten Rat Sarcoma Viral Oncogene Homolog
LAG3	Lymphocyte Activation Gene 3
LFA-1	Leukocyte Function-Associated Antigen 1
MAPK	Mitogen-Activated Protein Kinase
MCN	Mucinous Cystic Neoplasm

MDSC	Myeloid Derived Suppressor cell
MEK	Methyl Ethyl Ketone
MHC-1	Major Histocompatibility Complex Class 1
MICA/B	MHC Class 1 Related Genes A/B
MMP	Matrix Metalloproteinase
MTOC	Microtubule Organising Center
MUC	Mucin
myCAF	Myofibroblastic Cancer Associated Fibroblast
MYH-11	Myosin-11
NCR	Natural Cytotoxicity Receptor
NF- κ B	Nuclear Factor Kappa B
NK cell	Natural Killer Cell
NKG2A	Natural Killer Group 2A
NKG2D	Natural Killer Group 2D
Nrf2	Nuclear Factor Erythroid 2–Related Factor 2
PALB	Partner and Localiser of BRCA
PanIN	Pancreatic Intraepithelial Neoplasm
PD-1	Programmed Cell Death Protein 1
PDAC	Pancreatic Ductal Adenocarcinoma
PD-L	Programmed Cell Death Ligand

PDPN	Podoplanin
PI3K	Phosphoinositide 3-Kinases
POSTN	Periostin
PRF1	Perforin-1
PSC	Pancreatic Stellate Cell
PTCH	Patched
PTEN	Phosphatase and Tensin Homolog Deleted on Chromosome Ten
qPSC	Quiescent Pancreatic Stellate Cell
RAE-1	Retinoic Acid Receptor
SHH	Sonic Hedgehog
SMAD4	Mothers Against Decapentaplegic Homolog 4
SMO	Smoothed
SOCS	Suppressor of Cytokine Signalling
SPN	Solid Pseudopapillary Neoplasm
STAT	Signal Transducers and Activators of Transcription
TAM	Tumour Associated Macrophage
TAN	Tumour Associated Neutrophil
TGFBR1	Transforming Growth Factor Beta Receptor 1
TGFβ	Tumour Growth Factor-β
TIM-3	T-cell Immunoglobulin and Mucin-Domain Containing-3

TME	Tumour Microenvironment
TNF- α	Tumour Necrosis Factor- α
TP53	Tumour Protein p53
Treg	Regulatory T-Cell
ULBP	UL-16 Binding Proteins
WST-1	2-(4-Iodophenyl)-3-(4-Nitrophenyl)-5-(2,4-Disulfophenyl)-2H-Tetrazolium
α -SMA	Alpha Smooth Muscle Actin

Abstract

Pancreatic ductal adenocarcinoma (PDAC) is a disease with dismal prognosis. With five-year survival rates of less than 11%, PDAC is set to become the second leading cause of cancer related deaths by 2040. The role of pancreatic stellate cells in pancreatic ductal adenocarcinoma has been well established. However, to date, little remains known about the interaction between these crucial stromal cells and the innate lymphocytes, natural killer (NK) cells, in PDAC. Herein we demonstrate that naïve NK cells possess the functional efficacy to target and kill both quiescent (qPSC) and activated (aPSC) pancreatic stellate cells. Furthermore, qPSC, but not aPSC education of NK cells resulted in decreased NK cell-mediated cancer cell cytotoxicity. NK-PSC direct co-culture was found to modulate both PSC and NK phenotype, as well as functional changes within NK cells, an effect not observed with Transwell™ separation. Multiplex Luminex ELISA further revealed upregulation of IFN- γ and related chemokines in NK cells co-cultured with PSC (activated/quiescent), suggesting that this pathway may be involved in phenotypic modulation. Through global proteomic analysis we demonstrate NK cell-induced differential protein changes in aPSC versus qPSC. Furthermore, we demonstrate changes in intracellular NK pathways as a result of direct contact with PSCs, indicating a dynamic, bidirectional interaction between these two key players. Using multiplex immunohistochemical analysis, we demonstrate that NK cell proximity to CAFs, and not total NK cell infiltrate is correlated with overall survival in PDAC. Consequently, we suggest that the spatial biology of NK/CAFs may play a prognostic role in PDAC and may potentially be used as a tool for patient stratification. Taken together, our results demonstrate a significant bidirectional relationship between NK cells and PSC/CAFs in the context of PDAC, providing novel insight into this crucial cell-cell interaction.

Chapter 1 - Introduction

1.1 Pancreatic cancer

Pancreatic cancer is a malignancy with a dismal prognosis. With five-year survival rates of ~11%¹, pancreatic cancer is set to become the second leading cause of cancer related deaths by 2040.²⁻⁵ To date, the only potential curative treatment for pancreatic cancer is surgery, however due to the lack of early symptoms and aggressive disease biology, patients typically present with advance stage disease, rendering the majority of patients unresectable.⁶ Furthermore, with approximately 80% of surgery patients relapsing, frequently within two years, pancreatic cancer remains one of medicine's most urgent areas of unmet need.⁷

1.2 Pancreatic ductal adenocarcinoma risk factors

Risk factors associated with pancreatic cancer can be either modifiable or non-modifiable. When reviewing all modifiable risk factors, smoking was found to have the strongest positive correlation with pancreatic cancer development.⁸ Meta-analysis from multiple case-control and cohort studies have revealed that smoking can increase risk in current and former smokers by 74% and 20%, respectively.⁹ Similarly, Molina-Montes *et al.* observed that current smokers had a 72% greater risk of developing pancreatic cancer than did never smokers. Moreover, they also note a dose response relationship between smoking intensity and smoking duration with the risk of developing pancreatic cancer. Smoking cessation was found to lower the risk.¹⁰

Recently, evidence has also suggested a significant relationship between alcohol consumption and risk of developing pancreatic cancer. A large meta-study revealed heavy drinkers were at much greater risk of developing pancreatic cancer (19%) than were light or moderate drinkers. Moreover, this trend was found to be consistent between men and women.¹¹ Naudin *et al.* also determined significant positive associations between baseline and lifetime

alcohol consumption and risk of pancreatic cancer in men, however hazard ratios did not reach significance for women.¹²

Reports on the impact of diet on pancreatic cancer risk have been inconsistent.¹³ Meta-analysis of epidemiological studies has revealed a significant decrease in risk with the increased consumption of fruit and vegetables (RR 0.73 and 0.76, respectively). However, methodological variation between observational studies included within the analysis may have impacted the magnitude of the associations observed and therefore further work is needed to confirm these findings.¹⁴ Conversely, red-meat consumption has been found to positively associate with pancreatic cancer risk in men. Moreover, cooking method was also observed to play a role in risk, with high temperature cooking correlating with worse outcome.¹⁵

Obesity is being increasingly recognised as a strong, but modifiable risk. Both meta-analysis and cohort studies have identified a positive association between obesity and pancreatic cancer.¹⁶ Aune *et al.* report a 10% increase in relative risk for every 5 additional BMI units, a finding consistent between men and women.¹⁷ Similarly, Bethea *et al.* demonstrate increased risk of 25% and 32% in participants with a BMI of 25.0 to 29.9 and 30.0 to 34.9, respectively. Interestingly a stronger association in BMI and pancreatic cancer was observed in never smokers, than amongst smokers.¹⁸ Furthermore, pooled analysis of population based cohort studies in Japan revealed a significant association between men with high BMI (≥ 30 kg/m²) and risk of pancreatic cancer; HR 1.71, when compared to BMI 23 to <25 kg/m². No clear association was observed in women.¹⁹

Non-modifiable risk factors include; age, gender, ethnicity, blood group and family history.⁹ Whilst age of incidence differs between countries, patients are typically diagnosed after the

age of fifty-five, with most patients presenting in their seventies and eighties. Within the US, 89.4% of new cases are diagnosed in patients over 55, with a median age at death of 72.⁸ Incidence of pancreatic cancer below the age of 30 is very rare worldwide and thus, it is often considered a disease of the elderly.⁸

Males display a higher incidence rate than do females, with age-standardised rates suggesting a ratio of 5.5: 4.0.²⁰ A disparity in risk is also evident between ethnicities, for example, within the United States, African-Americans exhibit greater risk than their Caucasians counterparts.²¹ Incidence rates were lowest in Asian-Americans and Pacific Islanders. Whilst this may be linked to exposure to modifiable risk factors, there may be some underlying genetic and gene-environment interactions which may explain this disparity.⁹

When comparing blood groups, several studies have revealed that individuals with non-O blood groups (A, B or AB) were at significantly greater risk of developing PDAC than those with group O.^{22, 23} It is thought that this may be a result of the differing inflammatory states and glycosyltransferase specificity between blood groups.⁹

Familial PDAC (characterised by two or more first degree relatives being diagnosed with the disease) accounts for 5-10% of new cases. Individuals with familial risk have a nine-fold higher chance of developing PDAC than those without.^{8, 24} Genetically, the presence of *BRCA1* and *PALB* mutations within first degree relatives increases the risk exponentially.⁹

Diabetes mellitus (specifically type II) has long been recognised to have a significant association with the development of pancreatic cancer. Recent evidence has shown that patients with type II diabetes have an increased risk of developing pancreatic cancer (OR: 2.50), this was even more striking in patients diagnosed with new onset type II diabetes (OR:

6.39).²⁵ This significance was also noted by Huang *et al.* who demonstrated an almost 7-fold increase in risk in individuals diagnosed with new onset diabetes.²⁶

1.2.1 Development and Subtypes of pancreatic cancer

Pancreatic cancers can arise from either endocrine or exocrine cells. Constituting less than 5% of all pancreatic cancers, endocrine tumours are typically derived from islet cells and can be sub-divided based on cell of origin and hormones produced, namely; gastrinomas, insulinomas and glucagonomas.²⁷ Due to the high levels of hormone produced, often leading to distinctive symptoms (such as hypoglycaemia with insulinomas) these cancers are readily diagnosed.²⁷ For insulinomas, metastatic behaviour is rarely observed (6% of all insulinomas), and as such, patients are typically considered cured after surgical resection.²⁸ In a retrospective study of patients with benign or malignant (defined by distant metastases, direct or lymphovascular invasion and T4 tumour stage) insulinomas, five-year survival following surgical resection was found to be 95.4% and 66.8%, respectively.²⁹ Conversely, 60-90% of gastrinomas are malignant, whilst surgical resection can result in 15 year disease free survival of up to 98%, distant metastases are the biggest predictor of long-term survival.³⁰ Approximately 60% of glucagonomas are found to be malignant. These are the most rare of the endocrine tumours with an incidence of 0.04-0.12 per million/year.³¹

In contrast, exocrine tumours account for more than 90% of pancreatic malignancies.³² The most common of these is pancreatic ductal adenocarcinoma (PDAC).³³ Arising from ductal epithelial cells, PDAC displays distinctive ductal-like features when examined histologically, and is preceded by one of the following five precursor lesions: pancreatic intraepithelial neoplasms (PanIN), intraductal papillary mucinous neoplasms (IPMN), intraductal

tubulopapillary neoplasms (ITPN), intraductal oncolytic papillary neoplasms (IOPN) or mucinous cystic neoplasms (MCN).^{27, 34}

For completeness, it should be noted that there are three non-PDAC pancreatic exocrine tumours, all of which are rare: pancreatic acinar cell carcinoma (ACC), solid pseudopapillary neoplasm (SPN) and pancreatoblastoma. Pancreatic ACC accounts for approximately 1% of all pancreatic cancers.³⁵ Often misdiagnosed as PDAC, ACC demonstrates a well encapsulated tumour (in approximately 60% of cases), has a larger tumour size at presentation and exhibits calcification and central hypodensity.³⁵ Accounting for 0.17-2.7% of pancreatic malignancies, SPN is a low grade tumour, typically seen in young to middle aged women. This slow growing tumour exhibits 95% 5- and 10- year disease specific survival, with only 5-10% of cases metastasising, a stark contrast to the prognosis for PDAC.³⁶ Finally, comprising less than 1% of pancreatic cancers, pancreatoblastoma is a primarily paediatric malignancy. These tumours demonstrate consistently activated Wnt/ β -catenin signalling as well as upregulation of the insulin-like growth factor (IGF)-2 axis. With surgery the only potential curative option, targeting these dysregulated signalling pathways may prove of great therapeutic benefit to this rare cohort.³⁷

1.2.2 PDAC development and progression

The development and progression of PDAC is associated with the acquisition of genetic mutations within key driver genes. These include *KRAS*, *CDKN2A*, *TP53* and *SMAD4*.³⁸ Morphological changes within the pancreas (typically in the form of PanINs) are observed in association with these genetic changes.³⁹

PanINs are characterised as micropapillary, non-invasive lesions, typically less than 5mm.⁴⁰ Owing to their small size, PanINs cannot be detected by any radiological means. Consisting of

columnar and cuboidal epithelial cells, and displaying varying mucin levels, PanINs are graded on the level of cellular and morphological atypia. Low grade PanINs (PanIN-1 or PanIN-2) display mild to moderate atypia of basal nuclei, whilst high grade lesions (PanIN-3) demonstrate loss of cellular polarity, hyperchromasia and increased nucleus to cytoplasm ratio.⁴⁰ Low-grade lesions are relatively common in the general population, particularly in people over the age of fifty, and are found to express MUC5A and MUC6. Conversely, high grade lesions are most commonly identified in association with PDAC and are seen to express MUC1.³⁴

KRAS has been identified as a master regulator of pancreatic cancer initiation and progression.³⁹ Constitutive activation of *KRAS* prevents the hydrolysis of GTP, promoting persistent downstream signalling of multiple pathways including MAPK – MEK and PI3K – AKT – MEK – ERK, as well as activation of transcription factors involved in cell differentiation, proliferation and migration.⁴¹ Oncogenic *KRAS* mutations have been identified in human PanIN lesions, demonstrating increasing frequency with PanIN progression. Thus initial work suggested that it may play a key role in the development of PDAC.⁴² Moreover, development of *KRAS* mutant murine models which resulted in the spontaneous development of invasive, metastatic tumours, recapitulating human disease, clearly revealed the importance of *KRAS* in PDAC progression.⁴³

In addition to oncogenic *KRAS*, mutation of the *CDKN2A* (p16) gene was also found to be associated with higher grade PanINs^{44 45}, playing a key role in the progression from PanIN-1 to PanIN-2.⁴⁶ Furthermore, inactivation of the tumour suppressors *TP53* and *SMAD4* was found to be absent in PanIN-1, but was observed with increasing frequency in PanIN-2 and -3 respectively, suggesting that these mutations may play a key role in the progression to

carcinoma.⁴⁷ This is further supported by the frequent observation of loss of TP53 heterozygosity in the progression from PanIN-3 to metastatic disease.⁴⁸ These key genetic alterations are shown in Figure 1.1.

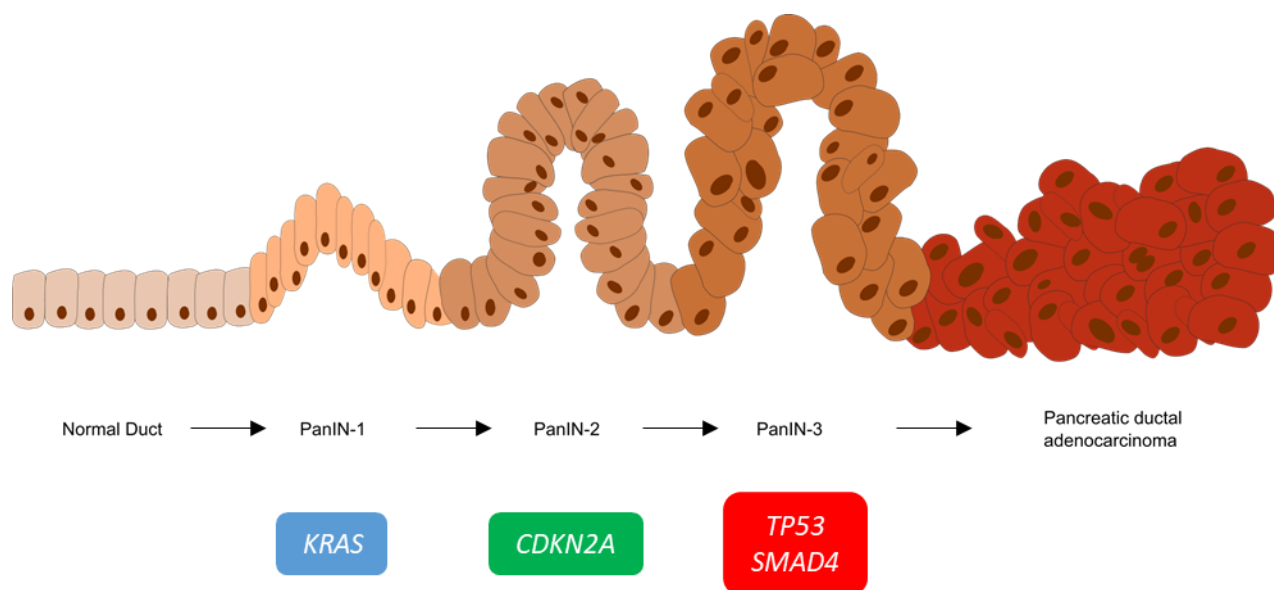


Figure 1.1: Pathogenesis of PDAC development.

The development of PDAC through progressive stages of pancreatic intraepithelial neoplasia. Cellular atypia increases with PanIN progression, with high grade lesions demonstrating loss of cellular polarity and hyperchromasia. Key genetic mutations are shown below each PanIN stage. Oncogenic KRAS initiates the progression from normal duct to neoplasia (PanIN 1). PanIN progression is then further stimulated by the acquisition of a mutation in CDKN2A. Finally, inactivation of the tumour suppressors TP53 and SMAD4 drives progression from PanIN-2 to PanIN-3, and eventually, pancreatic ductal adenocarcinoma. Image created with Inkscape (1.1.2).

In addition to key driver mutations, PDAC is found to be molecularly heterogeneous, expressing multiple mutations throughout the genome, many of which are not found in a recurrent manner.²⁷ Using genomic analysis of PDAC tumours, Bailey *et al.* report that significantly mutated genes were involved in 10 molecular mechanisms including; TGF- β signalling (*SMAD4*, *SMAD3* and *TGFBR1*), the BRCA pathway (*BRCA1*, *BRCA2* and *PALB2*) and WNT signalling (*RNF43*).⁴⁹ Identification of additional mutations may prove to be key to the development of novel treatments for PDAC. This was evidenced through with the identification of *BRCA* mutations. *BRCA* genes are involved in the homologous recombination repair of damaged DNA⁵⁰, thus mutations can result in the accumulation of chromosomal aberrations resulting in genomic instability.^{50, 51} Importantly, mutation of *BRCA* genes results in synthetic lethality to PARP inhibitors⁵², and thus clinical trials have been used to exploit this mutation in *BRCA*-mutated metastatic PDAC patients.^{51 53}

1.2.3 PDAC treatment

For patients who are not eligible for surgical resection, current treatment regimens employ systemic chemotherapy. First-line gemcitabine monotherapy yields poor results, with one- and five-year survival rates of 18% and 2% respectively.³ Combination therapies have demonstrated superior efficacy than their monotherapy counterparts. When treated with FOLFIRINOX (oxaliplatin, irinotecan, 5-fluorouracil and leucovorin), mean overall survival can be extended to 11 months vs 6.8 months in patients treated with gemcitabine alone.⁵⁴ Similarly, gemcitabine in combination with nab-paclitaxel demonstrated superior efficacy than gemcitabine treatment alone (8.5 months vs 6.7 months).⁵⁵ Consequently, these two treatment regimens are now accepted as first-line treatment options in the advanced PDAC setting.³

Failing first-line treatment, options for second-line treatment of PDAC remain unclear. Results from the CONKO 03 study suggest that patients treated with oxaliplatin, folinic acid and 5-fluorouracil had improved median overall survival when compared to those treated with 5-fluorouracil and folinic acid.⁵⁶ This result was not however substantiated by the PANCREOX study which determined that patients receiving treatment containing oxaliplatin, 5-fluorouracil and leucovorin had increased adverse events when compared to those treated with 5-fluorouracil and leucovorin, with no difference in median overall survival.⁵⁷ Finally, results for the NAPOLI trial revealed combination treatment with nano-liposomal irinotecan, 5-fluorouracil and leucovorin to have improved median overall survival than those treated with 5-fluorouracil and leucovorin only (6.1 months vs 4.2 months) in patients previously treated with gemcitabine based chemotherapy.⁵⁷ As such, second-line treatment options include: gemcitabine, gemcitabine + nab-paclitaxel, gemcitabine + cisplatin, nanoliposomal irinotecan + 5-fluorouracil, oxaliplatin + 5-fluorouracil and potentially FOLFIRINOX. Whilst there are many treatment options listed, it should be noted that these are all palliative treatments which extend life for 6 months on average. Thus the desperate need for novel therapeutics is evident.⁵⁷

Immunotherapy has revolutionised treatments for several cancer types including melanoma and non-small cell lung cancer, however its impact in the treatment of PDAC has been underwhelming.⁵⁸ Multiple immune checkpoint inhibitors and several CAR-T cells have now been approved for clinical use, however, to date only one immunotherapy, pembrolizumab, is recommended for PDAC. This is further restricted to patients who exhibit deficient mismatch repair (dMMR) or high microsatellite instability (MSI-H). With only 0.8-2% of PDAC patient expressing these impairments, very few are eligible for immunotherapy.^{58, 59} Data from the phase II KEYNOTE-158 clinical trial revealed that PDAC patients who were treated

with pembrolizumab exhibited median progression free survival of 2.1 months and median overall survival of 4.0 months. However, overall survival for patients with gastric, ovarian, small intestine and endometrial cancers did not reach median overall survival at the end of the study.⁶⁰ This once again highlights the desperate need for improved therapies in the treatment of PDAC.

1.2.4 PDAC Tumour Microenvironment

Characterised by its strong desmoplastic reaction, the PDAC tumour microenvironment plays a crucial role in disease progression.^{61, 62} Primary tumour sites display extensive fibrosis characterised by overexpression of extracellular matrix proteins and activation of fibroblastic cells.⁶² Multiple cell types, both cancer and stromal, are present in the pancreatic tumour microenvironment, including; pancreatic stellate cells (PSCs), myeloid-derived suppressor cells (MDSCs), tumour associated macrophages (TAMs) and regulatory T-cells (Tregs).⁶³ PSCs secrete extracellular matrix proteins (such as laminin, collagen and fibronectin), matrix metalloproteinase and growth factors such as fibroblast growth factor 2 (FGF2), tumour growth factor- β (TGF β) and connective tissue growth factor (CTGF), resulting in the formation of the dense desmoplasia associated with PDAC.^{62, 64} This dense fibrosis results in tumour hypoxia which is exacerbated by the secretion of anti-angiogenic factors (such as endostatin and angiostatin) by pancreatic cancer cells, and has been linked to disease aggressiveness and progression.^{62, 65}

Furthermore, hypoxia has been implicated in chemotherapy resistance in multiple studies. Zhang *et al.* found that hypoxia increased cancer stem cell populations (via the AKT/Notch1 signalling pathway) in pancreatic cancer, resulting in increased resistance to gemcitabine treatment.⁶⁶ Similarly, Wang *et al.*, demonstrated that the miRNA miR-301a-3p, which has

been linked to cancer growth and metastasis, was enriched in exosomes secreted from tumour cells. Moreover, this expression was found to be enhanced by hypoxia. Hypoxia induced secretion of the exosomal miR-301a-3p was also found to catalyse activation of the PTEN/PI3K signalling pathway, resulting in polarisation of M2 macrophages and invasion of pancreatic cancer cells.⁶⁷

As well as playing a key role in chemotherapy resistance, the pancreatic tumour microenvironment is highly immunosuppressive, limiting the efficacy of the immune system on cancer surveillance.^{62, 68} This is characterised by the presence of tumour supporting immune cells and immunosuppressive cells.⁶⁹

1.2.4.1 Myeloid Derived Suppressor Cells

MDSCs are heterogeneous immature myeloid cells which are seen to proliferate in peripheral blood, secondary organs (such as liver and lung) and tumours of cancer patients and modulate anti-tumour immune response to malignancy.^{70, 71} Recent studies have revealed that MDSCs release reactive oxygen/nitrogen species, causing dysregulation of T cell migration, proliferation and fitness within the TME.⁷² In addition, murine models of PDAC have revealed MDSCs induced expression of PD-L1 on tumoural cells through stimulation of the EGFR-MAPK pathways, inhibiting CD8⁺ T cell anti-tumoural activity.⁷³ MDSCs have also been shown to induce the development of Tregs within the TME through the secretion of IL-10 and IFN- γ , further contributing to the immunosuppressive environment.⁷⁴

1.2.4.2 Tumour Associated Macrophages

Tumour associated macrophages are highly abundant in the PDAC TME.⁷⁵ Recently discovered to develop from both monocytic and embryonic origins⁷⁶, TAMs are typically associated with the M2 macrophage phenotype, exhibiting pro-tumoural activity.⁷⁷ Specifically, TAMs have

been found to secrete a range of cytokines and chemokines, which modulate immune cell function.⁷⁸ In murine models of PDAC, TAMs were found to modulate CD8⁺ T cell dependent response to chemotherapy through stimulating IL-12 secretion from dendritic cells.⁷⁹ In addition, NK cell function was found to be reduced by TAMs in a contact- and TGF- β -dependent manner.⁸⁰ Moreover, through secretion of TGF- β , TAMs were found to induced pyruvate kinase M2 (PKM2) translocation in PDAC cells, inducing expression of PD-L1, and thus reducing the efficacy of cytotoxic immune cells.⁸¹

1.2.4.3 *Tregs*

Regulatory T cells are important homeostatic immune cells involved in the regulation of immune tolerance within the body. However, within the tumour microenvironment, Tregs are found to have strong immunosuppressive function, inhibiting anti-tumour immunity.⁸² Specifically, Tregs secrete immunosuppressive cytokines such as interleukin (IL)-10 and TGF β which recruit additional immunosuppressive cells to the tumour microenvironment and stimulate the transition of CD4⁺ T cells to FoxP3⁺ regulatory cells, facilitating immune evasion.^{62, 83} Moreover, Tregs further contribute to an immunosuppressive environment through engaging antigen presenting cells through CTLA-4 and PD-1 receptors, as well as modulating cytotoxic T cell function through upregulation of PD-1 and TIM-3, resulting in decreased anti-tumour activity.⁸⁴

Key components of the PDAC tumour microenvironment are shown in Figure 1.2.

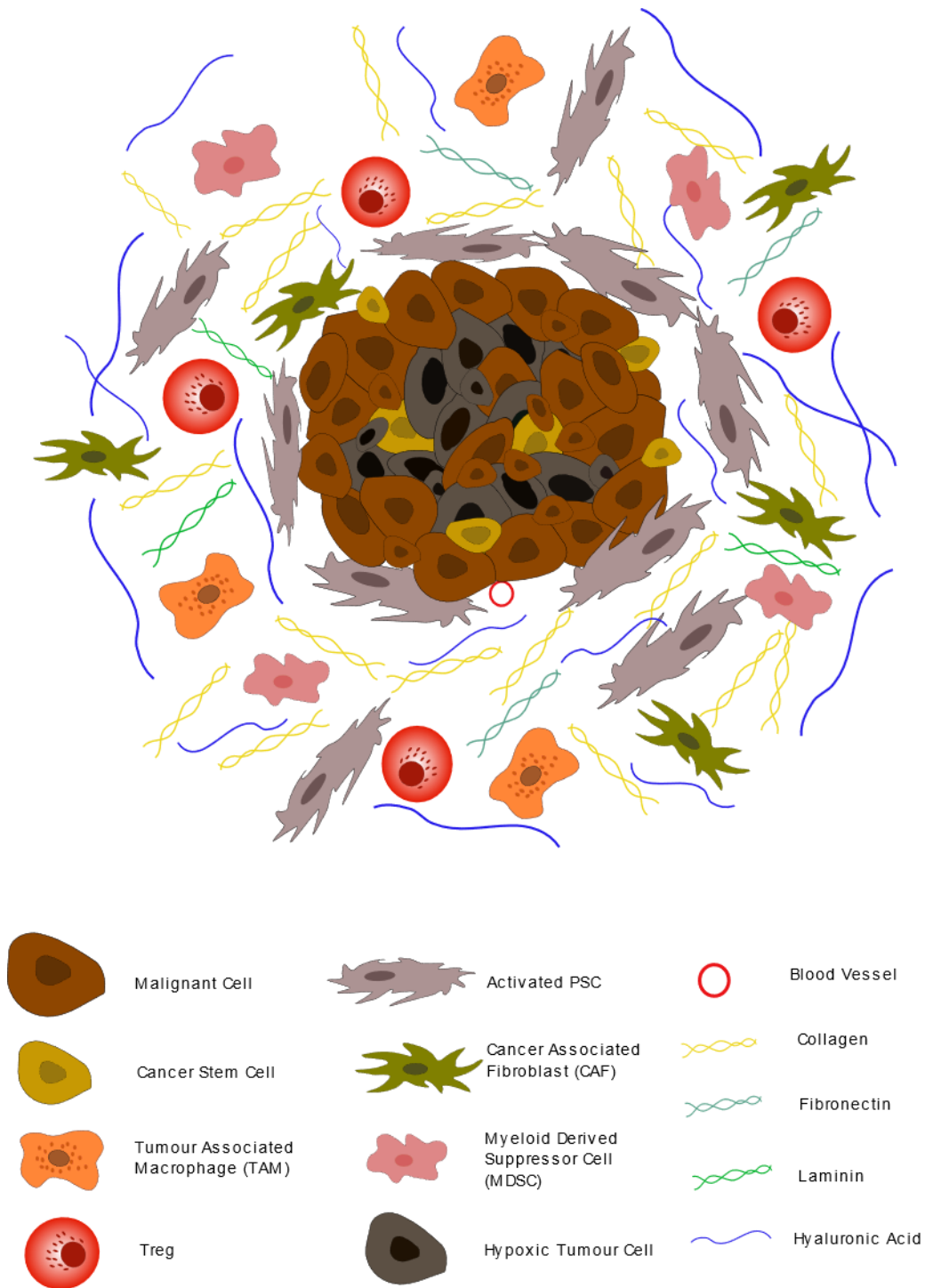


Figure 1.2: The PDAC tumour microenvironment.

Upon activation, pancreatic stellate cells secrete an abundance of extracellular matrix proteins including collagen, fibronectin, laminin and hyaluronic acid, leading to dense desmoplasia. In addition, fibroblastic cells (CAFs) become active and immune suppressive cells (MDSC, Treg and TAMs) are sequestered to the TME. Secretion of anti-angiogenic factors in addition to dense desmoplasia results in the development of a hypoxic tumour. Cancer stem cells are also observed in PDAC.

1.3 Pancreatic Stellate Cells

In the healthy pancreas, pancreatic stellate cells (PSCs) account for 4-7% of the total cell mass and are typically adjacent to pancreatic acinar cells or around small ducts.⁸⁵ PSCs are typically quiescent and non-proliferative in normal tissue, and play a crucial role in supporting epithelial cell function through paracrine signalling, maintaining tissue architecture and injury repair systems.⁸⁵⁻⁸⁸ Moreover, quiescent stellate cells express abundant stores of vitamin A, located in cytoplasmic lipid droplets which surround the nucleus.^{85, 88} Quiescent PSCs are characterised by staining for the stellate cell specific markers; glial fibrillary acidic protein (GFAP), desmin, vimentin and nestin.⁸⁵⁻⁸⁸ Conversely, in malignancy, PSCs switch to an activated state, displaying a myofibroblastic phenotype which can be characterised by the expression of the cytoskeletal marker alpha smooth muscle actin (α -SMA).^{85, 87} Activated stellate cells lose their lipid storing function and exhibit increased proliferation and migration.⁸⁸ Additionally, the function of activated stellate cells differs greatly from that of quiescent cells. Specifically, activated stellate cells express much higher production and deposition of extracellular matrix proteins, such as collagen and fibronectin. Moreover, activated PSCs contribute to extracellular matrix remodelling through the production of hyaluronan, matrix metalloproteinases (MMP) and tissue inhibitors of matrix metalloproteinases (TIMPs).^{85, 87, 88} Once activated, pancreatic stellate cells acquire a capacity for phagocytosis and produce an array of inflammatory cytokines including: interleukin (IL) - 1 β , IL-6, IL-15, TGF β and platelet derived growth factor, which among other functions, may contribute to immune cell trafficking and tumour infiltration.^{61, 85} Finally, PSCs have also been observed to travel to metastatic sites alongside cancer cells. It is hypothesised that this migration may facilitate cancer cell seeding in the metastatic niche, and support cancer cell proliferation and survival.^{89, 90}

1.3.1 PSC signalling pathways

Activated pancreatic stellate cells employ multiple autocrine and endocrine signalling pathways and are key orchestrators of stromal-epithelial interactions (Figure 1.3).⁹¹ PSCs secrete large volumes of inflammatory signals, such as IL-6, which facilitate the progression of PDAC. Recent evidence has demonstrated that IL-6 activates downstream JAK/STAT signalling which, in turn, stimulates the transition of PanIN to carcinoma.⁹¹ In addition, Wu *et al.* identified that activation of the IL-6/STAT pathway resulted in nuclear factor erythroid 2 (Nrf2) mediated epithelial to mesenchymal transition (EMT) of pancreatic cancer cells, a crucial process in the metastatic cascade.⁹² Moreover, this transition was reversed upon IL-6 inhibition and cancer cell propensity for migration and invasion was reduced.⁹² Similarly, Huang *et al.* found that IL-6/STAT3 signalling resulted in the methylation of suppressor of cytokine signalling 3 (SOCS3) (a key negative regulator of the IL-6/STAT3 pathway) via DNA methyltransferase 1 (DNMT1). This methylation led to the downregulation of SOCS3 and resulted in tumour growth and metastasis.^{93, 94}

PSCs have also been shown to facilitate perineural invasion, a key route for pancreatic metastasis.⁹⁵ Specifically, PSCs, but not pancreatic cancer cells, were found to secrete hepatocyte growth factor (HGF), leading to the activation of the HGF/c-Met pathway. Furthermore, secretion of HGF resulted in increased expression of nerve growth factor (NGF) and metalloproteinase 9 (MMP-9). Activation of this pathway lead to the migration and invasion of pancreatic cancer cells via perineural routes.⁹⁵

PSCs also play a crucial role in chemokine signalling. C-X-C motif chemokine receptor 4 (CXCR4) and its ligand C-X-C motif ligand 12 (CXCL12) play a prominent role in the progression of pancreatic cancer, facilitating its development, invasion and metastasis.^{96, 97} CXCL12 is

released in a paracrine fashion from PSCs and binds to its receptor, CXCR4, on the pancreatic cancer cell surface.⁹⁷ Activation of CXCR4 by CXCL12 leads to upregulation of EGFR, activating ERK, AKT and Wnt via PI3K and Ras signalling. Wnt activation promotes transcription of nuclear Wnt target genes, and increases expression of β -catenin, whilst activation of AKT and ERK phosphorylates and degrades $\text{I}\kappa\text{B}-\alpha$, leading to the accumulation of $\text{NF}\kappa\text{B}$, resulting in increased cancer cell proliferation and metastasis, and angiogenesis. Importantly, AKT and ERK also stimulate activation of sonic hedgehog (SHH) which initiates a pro-proliferative feedback loop.^{96, 98, 99} SHH ligand binds to patched (PTCH) on PSCs, this de-suppresses the smoothened (SMO) receptor, leading to a cascade of intracellular signalling. SMO translocates transcription factors to the nucleus and activates GLI family zinc finger transcription factors, modulating expression of downstream genes such as c-myc and VEGF. Ultimately, this signalling cascades potentiates the activation of PSCs and release of CXCL12 and facilitates the continued deposition of extracellular matrix.^{61, 91, 96, 100, 101}

Downstream effects of CXCR4/CXCL12 binding are also seen to play a crucial role in therapeutic resistance. Specifically, ERK activation phosphorylates Bad which subsequently dissociates from Bcl-2. In addition, Bim dissociates from Bcl-2 and Mcl-2 following phosphorylation by ERK. This allows Bcl-2 and Mcl-2 to bind Bax, preventing its pro-apoptotic effects, ultimately conferring resistance to chemotherapeutic strategies such as gemcitabine.^{96, 102}

Recent evidence has also demonstrated that PSCs also orchestrate cell proliferation through fibroblast growth factor (FGF) signalling.¹⁰³ PSCs secrete FGF2 which acts in an autocrine manner to stimulate FGF signalling pathways (MAPK, MEK and ERK).¹⁰⁴ In addition to this classical role, FGF2 and FGFR1 can be targeted to the nucleus where they interact with the

cell cycle regulator cyclin D1, potentiating proliferation of PSCs. Moreover, nuclear translocation of FGF2 and FGFR1 results in increased metastasis and invasion of both PSCs and cancer cells.^{103, 105} Nuclear FGFR1 has also been shown to activate the *FGF2* promoter via cyclic AMP and protein kinase C (PKC) dependent pathways, further driving PSC proliferation.¹⁰³

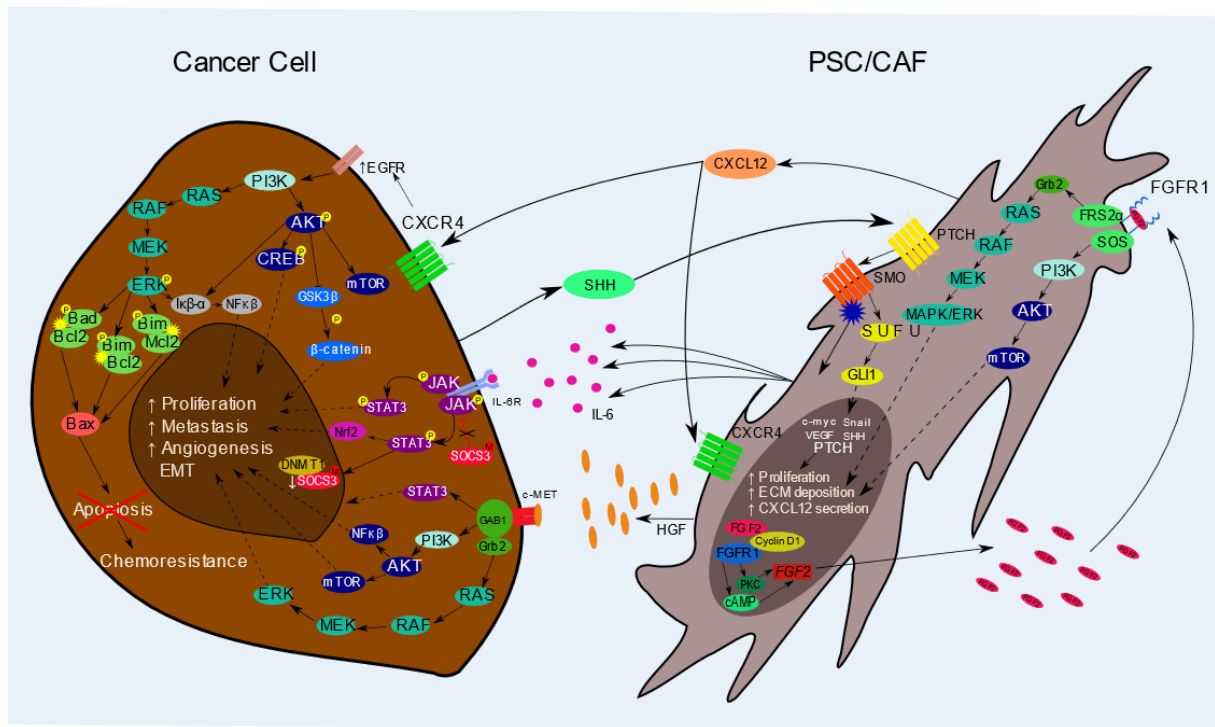


Figure 1.3: Autocrine and paracrine PSC signalling pathways in PDAC.

Release of inflammatory cytokines such as IL-6 activate the JAK/STAT signalling pathway. This results in EMT and increases tumour cell proliferation and metastasis through activation of Nrf2 and SOCS3. AKT and ERK are activated by HGF binding to c-MET, resulting in migration and invasion of tumour cells. CXCL12 Binds to CXCR4 in both paracrine and autocrine fashion. This activates downstream ERK, AKT and Wnt signalling pathways leading to tumour cell proliferation, angiogenesis, metastasis and chemoresistance. ERK and AKT activation stimulate sonic hedgehog release from tumour cells. This binds to PTCH on PSCs leading to the de-repression of SMO and subsequent activation of suppressor of fused (SUFU) and GLI1 zinc finger. This cascade potentiates PSC proliferation and deposition of extracellular matrix proteins. FGF2 binding to FGFR1 stimulates activation of the MAPK, ERK and AKT signalling pathways. FGF2 and FGFR1 are also translocated to the nucleus where they interact with cyclin D1, modulating the cell cycle and resulting in PSC proliferation. Nuclear FGFR1 activates the FGFR2 promoter via cyclic AMP and PKC signalling pathways.

1.3.2 PSC interaction with stromal cells

In addition to their interaction with cancer cells, PSCs display intricate cross-talk with many other stromal cells (Figure 1.4).¹⁰⁶

1.3.2.1 PSC interaction with endothelial cells

PSCs are potent producers of pro-angiogenic factors including periostin, angiopoietin-1 and vascular endothelial growth factor (VEGF), resulting in endothelial proliferation and angiogenic tube formation.¹⁰⁷⁻¹⁰⁹ Interestingly, when treated with all trans retinoic acid (ATRA), which renders stellate cells quiescent, the angiogenic potential of PSCs was abrogated.¹⁰⁷ Moreover, in aortic ring angiogenesis assays, PSCs were found to enhance angiogenic sprouting, an effect inhibited by cancer cells. Importantly however, the number of angiogenic sprouts decreased as collagen concentrations (used for tissue embedding) increased, suggesting that the dense desmoplastic stroma may inhibit angiogenesis.¹⁰⁷ Conversely, PSCs also secrete vasohibin-1¹¹⁰ and stimulate PCC secretion of endostatin¹¹¹, known angiostatic factors which inhibit angiogenesis, highlighting the intricacy of PSC-endothelial interactions.¹⁰⁶

1.3.2.2 PSCs and Immune cells

Much evidence suggests that PSCs may play a role in the characteristic immune evasion of PDAC. PSCs have been found to sequester immune cells in the panstromal compartment, preventing juxtatumoural infiltration. Ene-Obong *et al.* found that infiltrates of CD8⁺ (cytotoxic T cells), FoxP3⁺ (Tregs), CD20⁺ (B cells) and CD56⁺ (natural killer) cells were significantly lower in the juxtatumoural compartment of PDAC tissues when compared to panstroma.⁶¹ In addition, immune cells, particularly CD8⁺ T cells were found to preferentially migrate towards activated PSCs. This preferential chemotaxis was found to be CXCL12

dependent and was negated in quiescent PSCs, suggesting that the activation of PSCs is essential for the orchestration of an immune privileged tumour microenvironment.⁶¹

In contrast to the work of Ene-Obong *et al.*, some evidence has suggested that PSCs may induce B cell tumour infiltration in a CXCL13 dependent manner. However, the role of B cell infiltrates in PDAC remain unclear, with several studies demonstrating a capacity to both stimulate and inhibit T cell response to malignancy.¹¹²

Development of an immunosuppressive tumour microenvironment has also been attributed to PSC-immune cell interactions. PSCs are seen to sequester myeloid derived suppressor cells (MDSCs) and Tregs within the TME.¹¹³ These cells contribute to immunosuppression through conversion of macrophages from an antitumorigenic M1 to a tumour promoting M2 phenotype, suppression of CD4⁺ and CD8⁺ T cells and reduction in the number of NK and NKT cells in tumoural tissue. Li *et al.* found that PSCs drove the expansion of both monocytic-MDSCs (M-MDSCs) and granulocytic-MDSCs (G-MDSCs) in bone marrow, spleen, and tumour tissue in murine models of pancreatic cancer; an effect that was proposed to be IL-6 dependent.¹¹³ Orthotopic models of PDAC also revealed increased numbers of Tregs within tumour tissues, leading to the development of an increasingly immunosuppressive tumour microenvironment.¹¹³ Additionally, PSC dependent galectin-1 production was found to increase CD4⁺ and CD8⁺ T cell apoptosis, and thus depletion of T cells may contribute to PSC mediate immune evasion in PDAC.¹¹⁴

Tregs can also be recruited intratumourally by the chemokine IP-10 (CXCL10) which is secreted by PSCs in response to pancreatic cancer cells. IP-10 acts as a chemoattractant and was found to result in a 16-fold increase in FoxP3⁺ T cells in tumour tissue (when compared to normal tissues).¹¹⁵ Interestingly, through PCR analysis of leukocyte markers in PDAC tissue

samples, Lunardi *et al.* found a two-fold decrease in perforin 1 (pore forming protein 1, PRF1), a key regulator of the cytolytic ability of both NK and T cells. Suggesting that IP-10 may reduce the cytotoxic capacity of these cells in PDAC.¹¹⁵

1.3.2.3 PSC interaction with additional stromal cell types

PSCs have been evidenced to stimulate mast cell activation, resulting in the production of IL-13 and tryptase which stimulates both cancer and stellate cell proliferation.^{106, 116}

Additionally, complex crosstalk between adipocytes, PSCs and tumour associated neutrophils has been demonstrated. Dysfunctional adipocytes secrete increased levels of IL-6, TNF- α , CXCL1 and particularly, IL- β , stimulating PSC proliferation. Concurrently, activated PSCs secrete additional IL-1 β leading to the recruitment of tumour associated neutrophils into the PDAC tumour microenvironment. This crosstalk results in a positive feedback loop, potentiating IL-1 β secretion, PSC proliferation and TAN recruitment.¹¹⁷

In addition to the metastatic routes generated through perineural invasion, PSC interaction with pancreatic nerve cells (via NGF and SHH signalling pathways) plays a crucial role in the generation of abdominal pain associated with pancreatic cancer. Through upregulation of the cation channel transient receptor potential vanilloid 1 (TRPV1), and the neuropeptides, calcitonin gene-related peptide (CGRP) and substance P, PSCs induce neuropathic pain in pancreatic neurones and dorsal root ganglia.¹¹⁸

Finally, PSCs have been shown to interact with islet cells within the pancreas, with activated PSCs being identified in fibrotic islet tissues. Co-culture studies have also revealed that exposure to PSC secretions results in reduced insulin production, suggesting PSC induced β cell dysfunction.¹¹⁹ Moreover, PSCs were found to induce β cell apoptosis via caspase-3 and caspase-9 cleavage and loss of mitochondrial membrane potential.¹¹⁹

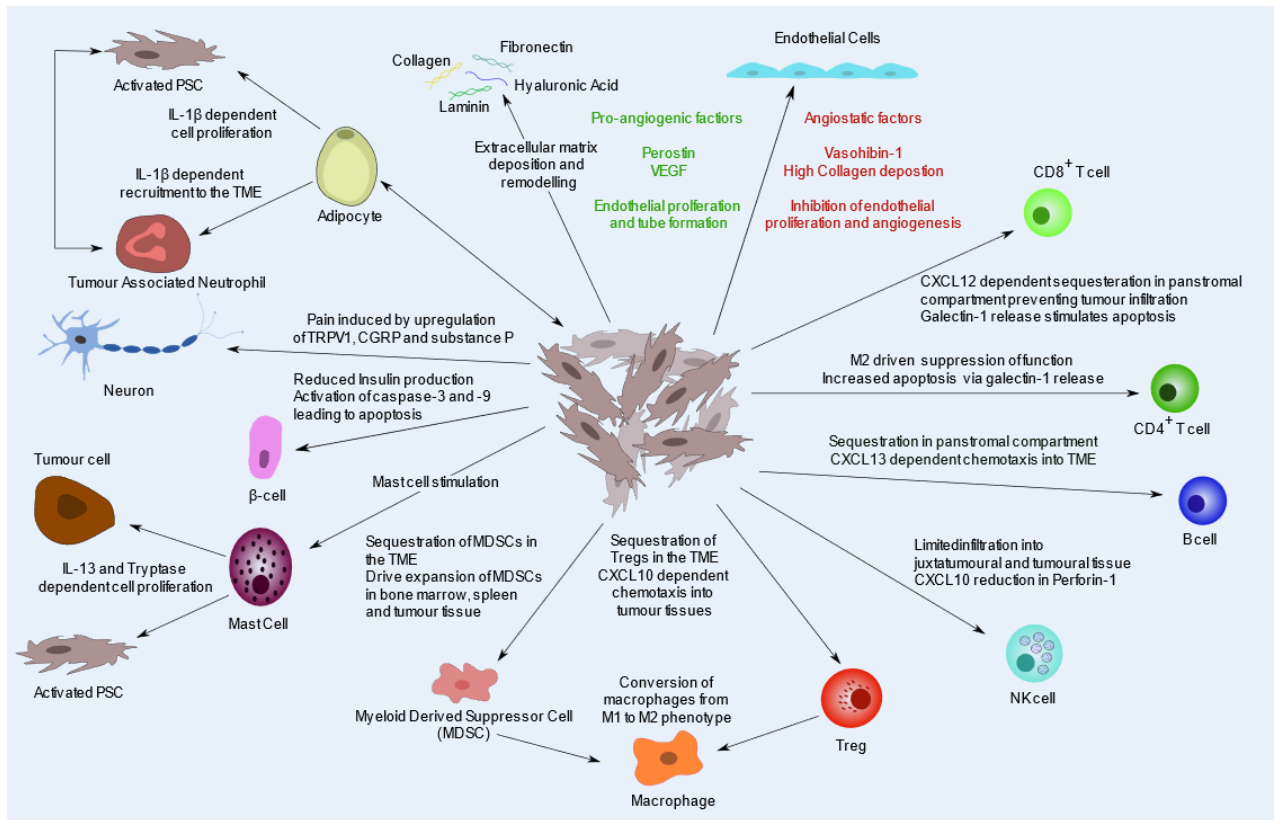


Figure 1.4: PSC interaction with stromal cells.

PSCs intricately regulate multiple stromal cell types. Activated PSCs orchestrate ECM remodelling and prolific deposition of extracellular matrix proteins. Both pro- and anti-angiogenic factors are secreted by PSCs, intricately regulating endothelial cell proliferation. $CD4^+$, $CD8^+$ and NK cells are sequestered in the panstromal tumour compartment, preventing immune destruction of tumour cells whilst MDSC and Tregs are retained within the TME, stimulating macrophage phenotypic conversion from M1 to M2 and generating an immunosuppressive environment. B cells may be sequestered in the panstromal tumour compartment or trafficked into the TME via CXCL13 signalling. Stimulation of mast cells potentiates tumour cell proliferation and perpetuates activation of PSCs. Normal function of β -cells is downregulated by PSCs, and their apoptosis stimulated by activation of caspase cascades. Upregulation of calcium channels and neuropeptides TRPV1, CGRP and substance P generate neuropathic pain in pancreatic neurons. Crosstalk between PSCs, TANs and adipocytes potentiates PSC proliferation. Figure created with Inkscape 1.1.2.

PSCs can be seen to be key orchestrators of the tumour microenvironment, interacting with both pancreatic cancer and stromal cells. The interactions and complex signalling cascades observed in PDAC reveal the complexity of the disease and begin to present novel therapeutic targets which must be explored to improve the dismal prognosis of pancreatic cancer patients.¹⁰⁶

Whilst the relationship between PSCs and CD8⁺ T cells is well established, research to date has only skimmed the surface of the impact of and interaction between PSCs and the cytotoxic immune effector, natural killer cells. With the potential to be an effective therapeutic target in PDAC, natural killer cells demonstrate potent efficacy in malignancy and, in contrast to T cells, do not require pre-sensitisation via antigen presentation for cytolytic activity, a process often exploited in cancer immune evasion.¹²⁰⁻¹²² Consequently, since both NK and PSCs may be key players in malignancy and demonstrate vast therapeutic potential, further research is required to elucidate the relationship between these two players.

1.4 Fibroblasts

Fibroblasts are spindle-shaped mesenchymal cells which exhibit key functions in both the development and maintenance of the pancreas.^{123, 124} In health, fibroblast are seen to play a crucial role in the wound healing response.¹²⁵ Typically, two days after injury fibroblasts migrate towards the wound where they become the most abundant cell type, a process regulated by the tissue growth factors; platelet derived growth factor (PDGF), basic fibroblast growth factor (bFGF) and TGFβ.¹²⁵ Within this process, these cells function to maintain the tissue microenvironment, form extracellular matrix, and sustain cell growth. Moreover, in the final stages of wound healing, fibroblasts substitute type III for type I collagen, remodel the

ECM through the production of matrix metalloproteinases, and are involved in wound contraction.¹²⁵ Thus, demonstrating their crucial role in tissue homeostasis.

1.4.1 Cancer Associated Fibroblasts

Due to similarities identified between wounds and the tumour microenvironment, carcinomas have classically been described as ‘wounds that do not heal’, a comparison clearly evidenced by the dense desmoplastic reaction observed in PDAC.¹²⁴ Cancer associated fibroblasts (CAFs) are prominent within the PDAC stroma and are a major contributor to the characteristic desmoplasia observed within the disease.^{124, 126} Interestingly, recent evidence has suggested that CAFs may exert both tumour promoting and tumour suppressive roles in PDAC.¹²⁶

CAFs are seen to promote tumour growth by providing metabolic support via multiple pathways including the production of alanine. This stromal alanine facilitates lipid and non-essential amino acid synthesis in the nutrient poor tumour microenvironment.^{126, 127} Moreover, the deposition of collagen within the TME provides a source of amino acids, particularly proline, which facilitates tumour cell proliferation.¹²⁶ In addition to this metabolic support, CAFs have been shown to secrete lipids within the TME, facilitating PDAC growth.¹²⁸ Moreover, paracrine metabolite transfer through CAF derived exosomes has also been illustrated.¹²⁶ Several studies have also revealed that CAFs aid PDAC progression through the paracrine activation of pro-survival pathways such as IL-6 induction of the JAK/STAT3 cascade.^{126, 129} In addition to its role in stimulating STAT3, IL-6, alongside other secreted factors (CXCL12 and β ig-h3), facilitates the development of an immune privilege tumour microenvironment through exclusion of crucial effector cells, such as CD8⁺ T cells.¹²⁹⁻¹³¹

Conversely, several studies have indicated that CAFs may hold a tumour suppressive role in pancreatic cancer. Using *Ptf1a*^{cre/+};*LSL-Kras*^{G12D/+};*Tgfb β 2*^{fl α /fl α} (PKT) mice crossed with α SMA-tk transgenic mice, Özdemir *et al.* identified that both early and late myofibroblast depletion led to more invasive, necrotic and undifferentiated PDAC tumours. Moreover, this was found to result in the increased frequency of pulmonary emboli which was suggested to contribute to reduced overall survival.¹³² Similarly, Rhim *et al.*, targeted PDAC stroma through the sonic hedgehog signalling pathway. It was found that tumours in Shh depleted mice expressed reduced stromal content, whilst tumour development was observed to be earlier and more aggressive resulting in reduced overall survival (when compared to Shh containing mice).¹³³ These findings were replicated by Lee *et al.*, who demonstrate the pro-tumorigenic impact of Shh deletion in three murine models of PDAC.¹³⁴ Moreover, Lee *et al.*, also determine that pharmacological blockade of the Hedgehog signaling pathway using vismodegib, a Shh antagonist, resulted in significantly increased tumour volumes and a significant reduction in survival when compared to vehicle control.¹³⁴ Targeting of the Hedgehog pathway has been carried out in several clinical trials, however no increase in overall survival was observed. Furthermore, one trial was halted early due to a shorted median overall survival in the experimental arm.^{135, 136} Consequently, it can be seen that CAFs may play a role in regulating tumour aggressiveness and growth, however more work is needed to fully understand the complex interactions between cancer associated fibroblast and tumour cells in PDAC.

1.4.2 CAF cells of origin

As the implications of CAF heterogeneity are beginning to come to light, increasing interest in the cellular origins of CAFs is evident.¹³⁷ Multiple cell types have been ascribed as sources of CAFs in pancreatic cancer including; pericytes, epithelial cells, adipocytes, smooth muscle cells, fibrocytes and mesothelial cells, however the most commonly described precursors are

pancreatic stellate cells (PSC), tumour infiltrating mesenchymal stem cells and resident fibroblasts (Figure 1.5).^{137, 138} Despite this breadth, pancreatic stellate cells have long been considered the primary source of CAFs in PDAC.^{129, 138-140} Upon activation, pancreatic stellate cells acquire a contractile and secretory phenotype, exhibit myofibroblastic characteristics such as high alpha SMA expression and secrete an abundance of ECM products, features also ascribed to cancer associated fibroblasts.¹³⁹ As such, much of the *in vitro* work to date has utilized PSCs as a source of CAFs.¹⁴¹ However, through development of a murine model in which pancreatic stellate cells can be traced using GFP expression, Helms *et al.*, showed that when stained for the CAF specific marker podoplanin, only approximately 10-15% of these cells originated from GFP⁺ PSCs. Interestingly, PSC-derived CAF ablation revealed that, whilst minor, this subset of CAF cells was found to play a significant role in regulating the stromal microenvironment which may also be associated with tumour aggressiveness.¹⁴² Consequently, further work is needed to assess the cellular origins of CAFs in PDAC and determine their impact on CAF heterogeneity.

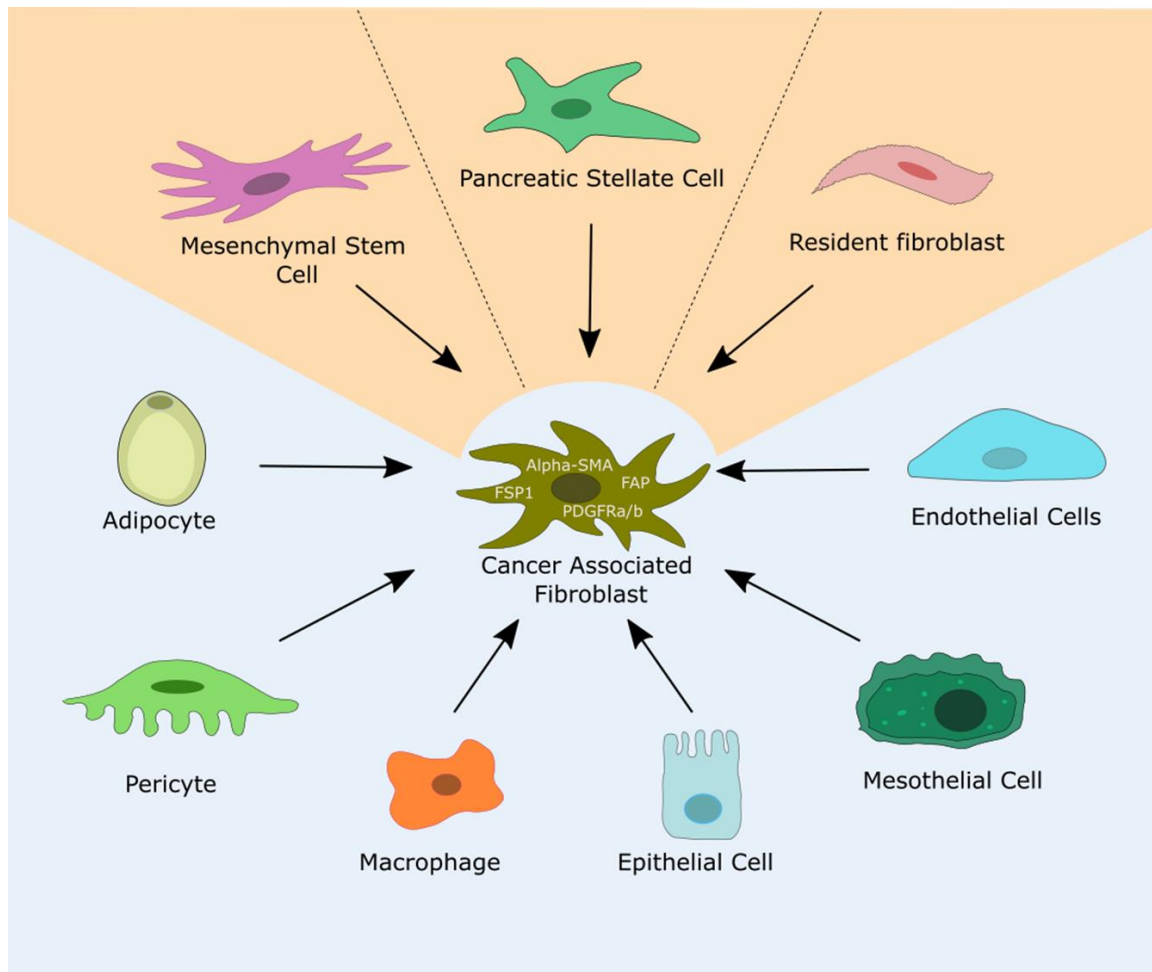


Figure 1.5: CAF cells of origin

Cancer associated fibroblasts arise from a wide variety of precursor cells, the most commonly attributed cells of origin include pancreatic stellate cells, mesenchymal stem cells and resident fibroblasts (highlighted orange). However, lineage tracing experiments have suggested that PSCs may account for as little as 10-15% of CAFs. When activated, CAFs express a range of cellular markers including fibroblast activation protein (FAP), fibroblast specific protein-1 (FSP1), platelet derived growth factor receptor (PDGFR) and alpha smooth muscle actin (α -SMA).¹³⁹

1.4.3 CAF Heterogeneity in PDAC

Due to the crucial role CAFs play in the development of PDAC, much interest has arisen into the potential heterogeneity that may exist within CAF populations. Several studies have investigated these subtypes, identifying multiple, distinct populations of CAFs both within and between patients (Figure 1.6).

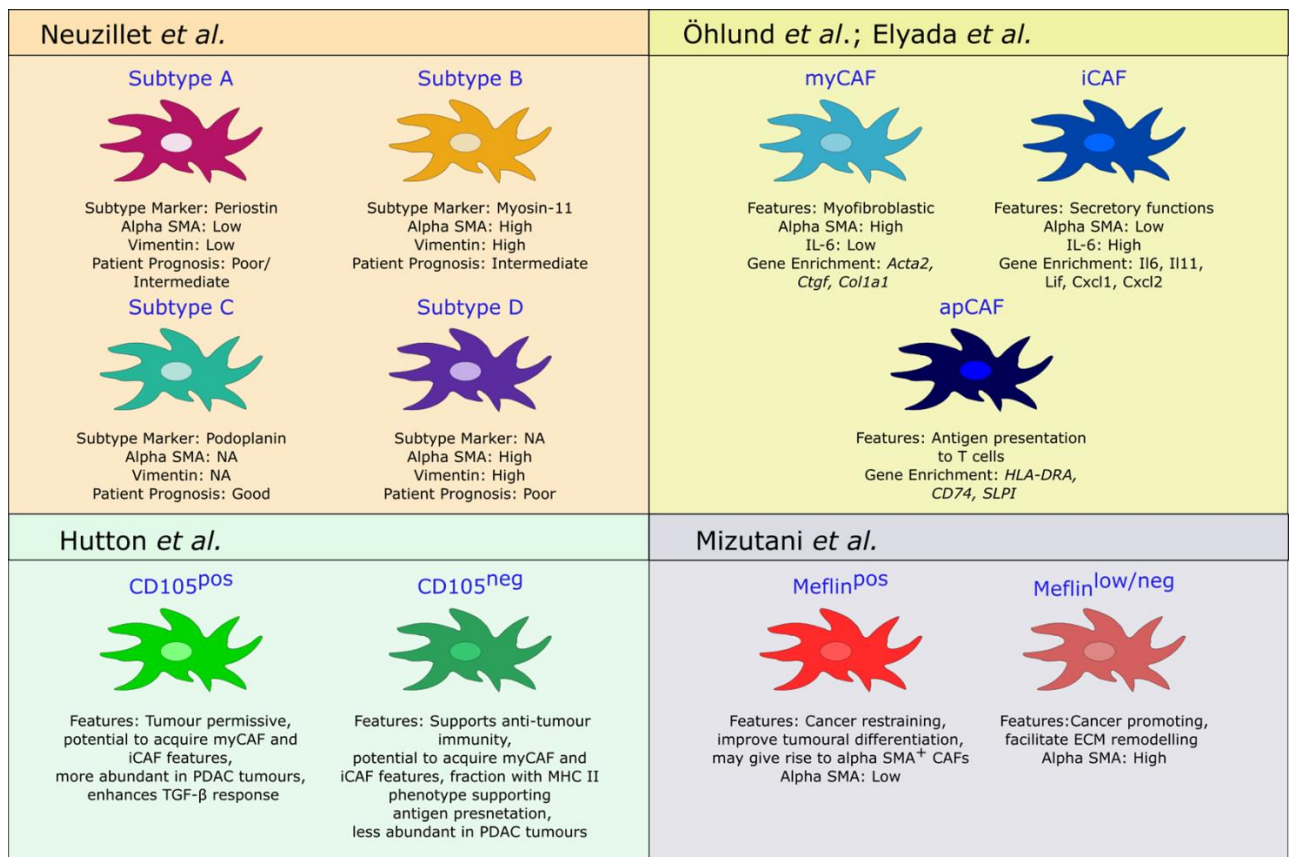


Figure 1.6: CAF heterogeneity in PDAC

Schematic summary diagram of the main cancer associated fibroblast subtypes identified in PDAC.

Using three-dimension co-culture models, Öhlund *et al.*, identified two spatially and phenotypically distinct populations of CAFs in PDAC. Through immunofluorescent and immunohistochemical analysis, fibroblast activation protein (FAP)⁺, alpha SMA^{high} CAFs were identified. This cell subset was found to exhibit a distinct myofibroblastic phenotype and as such was denoted as myofibroblastic CAFs (myCAF_s).¹²⁹ Subsequent secretome analysis revealed a subset of CAFs which exhibited high levels of IL-6 secretion, a known regulator of cell proliferation and survival, and modulator of immune suppression. Moreover, these CAFs demonstrated low levels of alpha SMA and thus were classified as alpha SMA^{low}IL-6^{high} inflammatory CAFs (iCAF_s).¹²⁹

The presence of these two CAF populations was verified by Elyada *et al.*, who identified distinct gene signatures for each population via single cell RNA-seq analysis of six human PDAC samples. Specifically, myCAF markers were found to include; alpha SMA (*ACTA2*), transgelin (*TAGLN*), myosin light chain 9 (*MYL9*), periostin (*PSTN*), matrix metalloproteinase 11 (*MMP11*) and tropomyosins 1 and 2 (*TPM1* and *TPM2*).¹⁴³ Conversely, iCAF_s were found to have enriched expression of the chemokines CXCL1, CXCL2, CCL2 and CXCL12 as well as interleukins 6 and 8. This finding supports the inflammatory phenotype of iCAF_s previously observed.¹²⁹,¹⁴³ iCAF_s were also found to express hyaluronan synthases (*HAS1* and *HAS2*) and angiotensin II receptor type 1 (*AT1*).¹⁴³

Interestingly, gene set enrichment analysis revealed distinct enrichment of differential pathways between myCAF_s and iCAF_s. myCAF_s were found to upregulate pathways involved in extracellular matrix organisation, focal adhesion and smooth muscle contraction, whilst iCAF_s were found to upregulate the complement pathway, IFN- γ response and IL6-JAK-STAT3 inflammatory pathways.¹⁴³

Analysis of KPC mouse tumours also revealed similar gene expression patterns, suggesting that murine models of PDAC may also express both myCAF and iCAF populations, recapitulating human disease.¹⁴³

A third subset of CAFs were also identified in murine tumours. These cells demonstrated gene enrichment in the Major Histocompatibility Complex Class II family (including CD74 and histocompatibility 2 class II antigen A α and β 1 (H2-Aa and H2-Ab1)) as well as Secretory Leukocyte Peptidase Inhibitor (Slpi) and serum amyloid A3 (Saa3). As a result of the enriched expression of the MHC class II genes, this subset was termed antigen presenting CAFs (apCAFs).¹⁴³ Retrospective analysis and immunofluorescent staining also demonstrated the presence of apCAFs in human PDAC samples.¹⁴³

In addition to the CAF classification proposed by Öhlund and Elyada, several other groups have identified subtypes of cancer associated fibroblasts in PDAC. Through *in situ* hybridization analysis, Mizutani *et al.* determined that patients with high infiltration of Meflin⁺ CAFs had better overall survival than did those with low infiltration. Moreover, depletion of Meflin⁺ CAFs in murine models of PDAC was demonstrated to correlate with disease progression and poor tumoural differentiation. Interestingly, CAFs highly positive for Meflin were found to have a low alpha SMA expression. Thus it was suggested that Meflin has the ability to suppress myofibroblastic features of CAFs.¹⁴⁴

Of particular note for the current project, are the subtypes previously established by the Kocher lab. Neuzillet *et al.*, identified four distinct subtypes of cancer associated fibroblasts in patient derived primary CAF cultures using both functional and molecular analysis. Distinct mRNA profiles were associated with each subtype and were validated through analysis of TCGA datasets.¹⁴⁰ Clear intra- and inter-tumoural CAF heterogeneity was observed in PDAC.

Moreover, each subtype was found to convey prognostic significance. Patients expressing high levels of periostin (subtype A) were found to have poor/intermediate prognosis. Similarly, patients with subtype B-like staining (MYH11 ± Periostin) exhibited intermediate overall survival, whilst those with subtype C like CAFs (PDPN ± PSTN) were found to have good prognosis.¹⁴⁰ Patients with subtype D CAFs exhibited the worst survival outcome.¹⁴⁰ Thus, the heterogeneity of CAFs is seen to have a tangible impact on clinical outcome for PDAC patients. Harnessing this information could allow successful stratification of PDAC patients, leading to increasingly personalized therapies.

Whilst the breadth of CAF subtypes identified are indicative of the cellular heterogeneity within the context of PDAC, there is a clear lack of consensus across the literature. For example, Meflin⁺ CAFs are seen to express high levels of α -SMA and may therefore also fit into the myCAF classification identified by Öhlund *et al.*^{129, 144} Similarly, CD105⁺ CAFs were shown to express high levels of periostin compared to CD105⁺ cells, suggesting their potential inclusion within the Subtype A category outlined by Neuzillet *et al.*^{140, 145} The use of different experimental techniques may begin to explain these differences, with data arising from *in situ* hybridization, IHC/IF, bulk RNA-Seq, single-cell RNA-Seq and imaging mass cytometry.^{129, 140, 143, 144} Further work is needed to establish clearly defined CAF subtypes to facilitate our understanding of the PDAC tumour microenvironment in order to effectively exploit potential therapeutic targets.¹⁴⁶

1.5 Natural Killer Cells

Natural killer (NK) cells are large granular lymphocytes which are key components of the innate immune system. Derived from bone marrow and secondary lymphoid organs, NK cells comprise between 5-15% of mononuclear cells¹⁴⁷ and are the first line of defence against

virally infected and malignant cells.^{120, 148} NK cells can be classified as CD56⁺CD3⁻ immune (CD45⁺) cells. This classification can be further sub-divided into two main effector populations: CD56^{bright}CD16⁻ and CD56^{dim}CD16⁺.¹⁴⁹ CD56^{bright}CD16⁻ NK cells are largely immunomodulatory effector units, executing their function through cytokine release, specifically, interferon gamma (IFN- γ). Conversely, CD56^{dim}CD16⁺ NK cells are predominantly cytotoxic effector units.¹⁴⁸ Activation of NK cells relies on the balance of signals received from target cells by inhibitory and activating cell surface receptors (Figure 1.7).¹²⁰ Comprised of killer cell immunoglobulin-like receptors (KIRs) and the c-lectin receptor, natural killer group (NKG) 2A, inhibitory receptors bind to major histocompatibility complex (MHC) class 1 molecules. These ligands are highly expressed on non-transformed 'self' cells and consequently prevent the activation of NK cells. Conversely, malignant cells often downregulate expression of surface MHC-1 molecules to evade detection by T cells, this 'missing self' signal prevents inhibition of the NK cells, resulting in cytotoxic efficacy.^{120, 148} NK cells may also be negatively regulated by checkpoint proteins such as programme death 1 (PD-1) which binds to its' ligands programme death ligand 1 and 2 (PD-L1, PD-L2).¹²⁰ Activating receptors include the type 1 transmembrane natural cytotoxicity receptors (NCRs) NKp46, NKp30 and NKp44, the C-type lectin like receptors NKG2C and NKG2D, activating KIRs and DNAX accessory molecule 1 (DNAM1).^{120, 148, 150} Ligands for the activating KIR receptors include the HLA-C2 and HLA-A ligands, however the interaction between ligand and receptor is less well understood for activating KIRs compared to their inhibitory counterparts.¹⁵¹ NKG2D receptors recognise stress induced proteins on transformed and virally infected cells. These include the MHC class 1 related genes MICA and MICB and UL-16 binding proteins (ULBP).¹⁵¹ Whilst recognising nectin adhesion molecule and the poliovirus receptor, DNAM1 also interacts with the β 2 integrin leukocyte function-associated antigen 1 (LFA-1) which is

involved in the formation of the immunological synapse.¹⁵⁰ It is important to note that in addition to independent activation, specific combinations of activating receptors are synergistic, increasing the overall signal received by the effector cell and consequently, increasing its cytotoxic response.¹⁵²

It should also be noted that in addition to direct receptor-ligand binding, CD16 positive NK cells express a propensity to carry out antibody dependent cellular cytotoxicity (ADCC) and are considered key mediators of this form of cellular cytotoxicity.¹⁵³ CD16 (FcγRIII) is a transmembrane receptor which can bind the Fc region of IgG₁ and IgG₃ antibodies, enabling NK cells to kill immunoglobulin labelled cells.¹⁵¹ This is a crucial concept for monoclonal antibody based therapies.¹²⁰

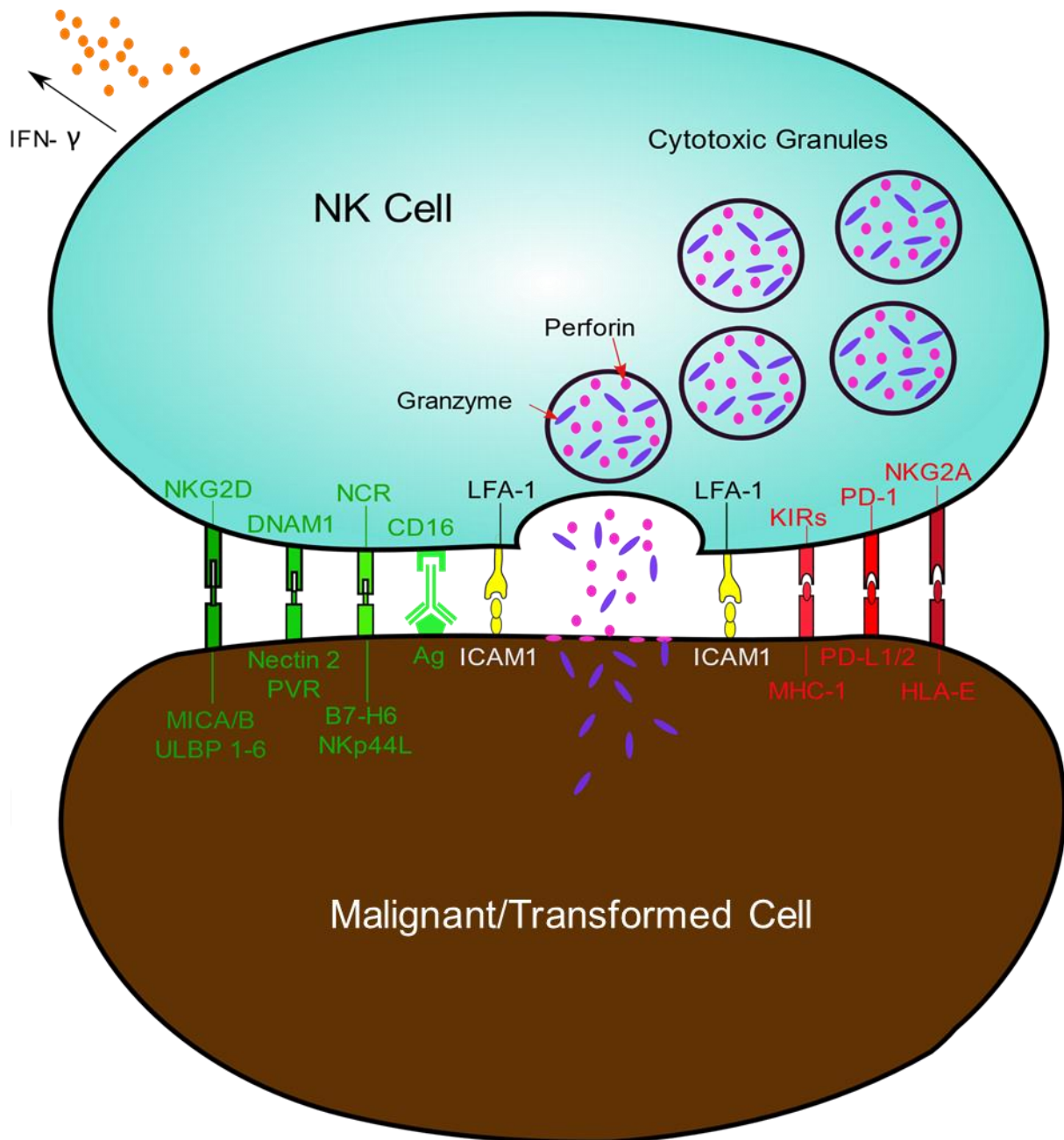


Figure 1.7: Activation and inhibition of NK cells.

NK cells recognise a multitude of ligands on both healthy and transformed cells. Inhibitory receptors (red) recognise 'self-antigens' on healthy tissue preventing activation. However, these molecules are lost on aberrant cells as a result of viral transformation or malignancy ('missing-self') leading to NK cell activation. Alternatively, NK cells may become active through engagement of activating receptors (green) via stress ligands expressed on transformed cells. NK cells can also execute antibody dependent cellular cytotoxicity (ADCC) through Fc engagement of the CD16 receptor. Upon activation NK cells release cytotoxic granules which contain perforin and granzymes to initiate target cell death via necrotic or apoptotic pathways. Binding of LFA-1 to ICAM1 stabilises the immunological synapse between the NK and target cells and ensures effective cytotoxicity. Finally, NK cells secrete cytokines, such as IFN- γ , facilitating crosstalk between the adaptive and innate immune system, resulting in dendritic and T cell recruitment. Figure created with Inkscape 1.1.2.

1.5.1 NK cell receptors

The expression of NK cell receptors has been shown to be intricately linked with NK maturation, with key receptors being acquired at different development stages.^{147, 154} NK cells do not express T-cell receptors (TCR) or natural killer T (NKT) receptors as do their adaptive immune system counterparts, but exert their functions through a wide range of activating and inhibitory receptors.¹⁵⁴ Key activating and inhibitory receptors include NKG2D, NKp30, NKp46, NKG2A, TIM-3 and LAG-3.¹⁵⁵

1.5.1.1 NKG2D

NKG2D is an activating cell surface receptor which is encoded by the gene, *Klrk1*. Whilst not specific to NK cells, NKG2D plays a crucial role in cytotoxic immune cell function.¹⁵⁶ Comprised of two disulphide-linked type II transmembrane proteins, NKG2D forms a homodimer, differing from its NKG2 family counterparts which typically heterodimerise with CD94. Moreover, whilst the NKG2 family largely recognises HLA-E, NKG2D recognises a range of stress induced ligands, including MICA/B.¹⁵⁷ Murine studies have revealed two isoforms of NKG2D generated through alternative splicing; NKG2D-L (long) which interacts with DAP10, and NKG2D-S short which can bind to both DAP10 and DAP12. However, in humans only NKG2D-L has been identified. Thus, NKG2D signal transduction (initiated by receptor-ligand binding) is carried out through the engagement of DAP10.¹⁵⁸ This, in turn, recruits PI3K and GRB2, activating their downstream signalling pathways. Engagement of PI3K results in activation of the Rac1/PAK/c-RAF/MEK/ ERK pathway, inducing NK cytotoxicity and the release of cytotoxic granzymes and perforin, as well as cytokine release. Alternatively, GRB2 activation involves activation of VAV-1 which induces PLC- γ and IP3 resulting in activation of the NF κ B and nuclear factor of activated T cell (NFAT) pathways.¹⁵⁸

MICA/B are expressed on the surface of tumour cells in response to cellular stress, particularly as a result of genomic damage and activation of DNA sensing and replicative stress pathways.¹⁵⁹ These ligands play a crucial role in NK cell activation via the NKG2D pathway and consequently are often shed or downregulated by malignant cells as a method of immune evasion.^{159, 160} Thus, this interaction has received much interest as a potential therapeutic target in multiple cancer types and has resulted in the development of several clinical trials.¹⁶¹

1.5.1.2 *NKp30*

A member of the natural cytotoxicity receptors (NCR) family, NKp30 is a 30kDa protein which acts as an immunoglobulin like activating receptor in NK cells.^{162, 163} NKp30 consists of a single N-terminal Ig-like domain, with a 15 amino acid stalk region which was found to be crucial for ligand binding.^{162, 164} Interestingly, NKp30 lacks its own intracellular signalling domain, relying on the adaptor molecules CD3 ζ or Fc ϵ R1 γ which contain ITAMs.¹⁶⁵ Ligands for NKp30 include B7-H6 and BAG6, which upon engagement result in NK-induced cellular lysis. Importantly, as with NKG2D ligands, malignant cells are able to shed these stress induced ligands, and evade immune surveillance.^{166, 167} Moreover, as with soluble MICA, both soluble B7-H6 and BAG6 were found to affect NK cell mediated killing of target cells.^{166, 168} It is perhaps prudent to note, that although NKp30 is widely regarded as an activating receptor, several isoforms of the receptor have been identified, isoforms A, B and C. Whilst NKp30A and NKp30B mediate cellular cytotoxicity and cytokine release respectively, NKp30c was found to induce release of IL-10, resulting in immunosuppression.^{169, 170}

1.5.1.3 *NKp46*

Encoded by the *NCR1* gene, NKp46 is a highly conserved receptor across mammalian species. Also a member of the NCR family, NKp46 is comprised of two extracellular C2-type Ig-like

domains, and a cytoplasmic chain of 30 amino acids. Similarly to NKp30, NKp46 does not contain a tyrosine based activating motif and as such, signal transduction is mediated through its association with CD3 ζ and Fc ϵ R γ , which become phosphorylated upon receptor engagement.^{171, 172} Ligands for NKp46 include viral components, hemagglutinin and heparin sulfate proteoglycan, however specific cell surface ligands for NKp46 remain to be elucidated.¹⁷³ Previously thought to be expressed solely on NK cells, NKp46 has received attention as a pan-NK marker,¹⁷⁴ however more recent evidence has demonstrated its expression on NKT cells, $\gamma\delta$ T-cells as well as innate lymphocyte subsets.¹⁷⁵⁻¹⁷⁷

1.5.1.4 NKG2A

Similarly to NKG2D, NKG2A is a member of the C-type lectin superfamily, NKG2.¹⁷⁸ Structurally, NKG2A is a type II integral membrane glycoprotein which contains extracellular lectin-like domains, as well as transmembrane and cytoplasmic regions. Unlike some members of the NCR family, NKG2A contains two ITAM regions within the cytoplasmic domain, facilitating signal transduction.¹⁷⁸ NKG2A forms a heterodimer with CD94 and functions as an inhibitory receptor on both NK and T cells.^{179, 180} NKG2A binds to the HLA class I molecule, HLA-E, which stimulates NK production of immunosuppressive cytokines such as IL-10. This results in the modulation of NK cell functional efficacy, preventing NK-induced lysis of target cells.^{181, 182} Importantly, HLA-E, is upregulated on tumour cells in response to IFN- γ stimulation. Furthermore, blockade of the NKG2A receptor has been demonstrated to improve the outcome of immunotherapy and consequently, NKG2A is considered as an NK checkpoint.¹⁸⁰ Moreover, high NKG2A expression has also been associated with NK cell exhaustion.^{183 184}

1.5.1.5 TIM-3

A member of the T cell immunoglobulin and mucin domain-containing (TIM) protein family, TIM-3 is encoded by the *HAVCR2* gene in humans.¹⁸⁵ TIM-3 is a type I transmembrane protein, whilst it contains five tyrosine molecules within its cytoplasmic tail, no defined signalling motifs have been identified within this domain.^{185, 186} TIM-3 has been shown to be expressed on a range of lymphocytes including T-cells, dendritic cells and NK cells.¹⁸⁷ Whilst TIM-3 has been found to be associated with and used as a marker of T-cell exhaustion, its role in NK cells remains unclear. Several studies have reported TIM-3 to be a negative regulator of NK cell function and suggest that, similarly to T-cells, it may be used as a marker of NK cell exhaustion.¹⁸⁸⁻¹⁹⁰ However, work by Gleason *et al.* suggested that TIM-3 may act as an important co-receptor on NK cells, enhancing IFN- γ production.¹⁹¹ Recent work by So *et al.* suggest that the role of TIM-3 on NK cells is variable and may depend on the stimuli of TIM-3 induction, suggesting a multifaceted role of TIM-3 on innate immune cell function.¹⁸⁷

1.5.1.6 LAG3

LAG3 is a member of the immunoglobulin superfamily which binds MHC class II molecules. Similar in structure to CD4, LAG3 exhibits four extracellular IgG domains.¹⁹² Cytoplasmically, LAG3 exhibits three domains; a serine phosphorylation site, a conserved KIEELE motif and a glutamic acid-proline repeat sequence. These domains in turn mediate intracellular signal transduction.¹⁹³ Similarly to TIM-3, the role of LAG3 in NK cells has not been fully elucidated. Early studies revealed that mice deficient in the *lag3* gene exhibited reduced lysis of target cells¹⁹⁴, however this modulation was not observed in human cell lines.¹⁹⁵ More recently, murine studies have revealed that immature NK populations expressing high levels of co-inhibitory molecules, including LAG3, limited NK control of metastases in lung cancer. This finding suggests that LAG-3 may function as a negative regulator of NK cell activity.¹⁹⁶ This

finding is supported by the work of Narayanan *et al.* (preprint) which demonstrates that LAG-3 is a crucial negative regulator of NK cytokine release.¹⁹⁷

1.5.2 NK Cytotoxicity

Following initial interactions between activating and inhibitory receptors and their ligands on target cells, the balance of signals received by the NK cell determines its activation status. If activated, NK cells must form an immunological synapse with the target cell. Formation of this synapse enables stable adhesion, polarization of cytotoxic granules and subsequent lysis of the target cell. This is achieved through binding of the $\beta 2$ integrin, LFA-1.¹⁵² Consisting of two chains, α_L and β_2 , LFA-1 is a heterodimer whose reactivity to its ligands (ICAM family members) can be modified via conformational changes. Specifically, a bent conformation exhibits a low affinity for its ligands, intermediate affinity can be achieved through a closed/extended conformation, whilst an open/extended conformation results in high affinity binding (Figure 1.8).^{152, 198, 199}

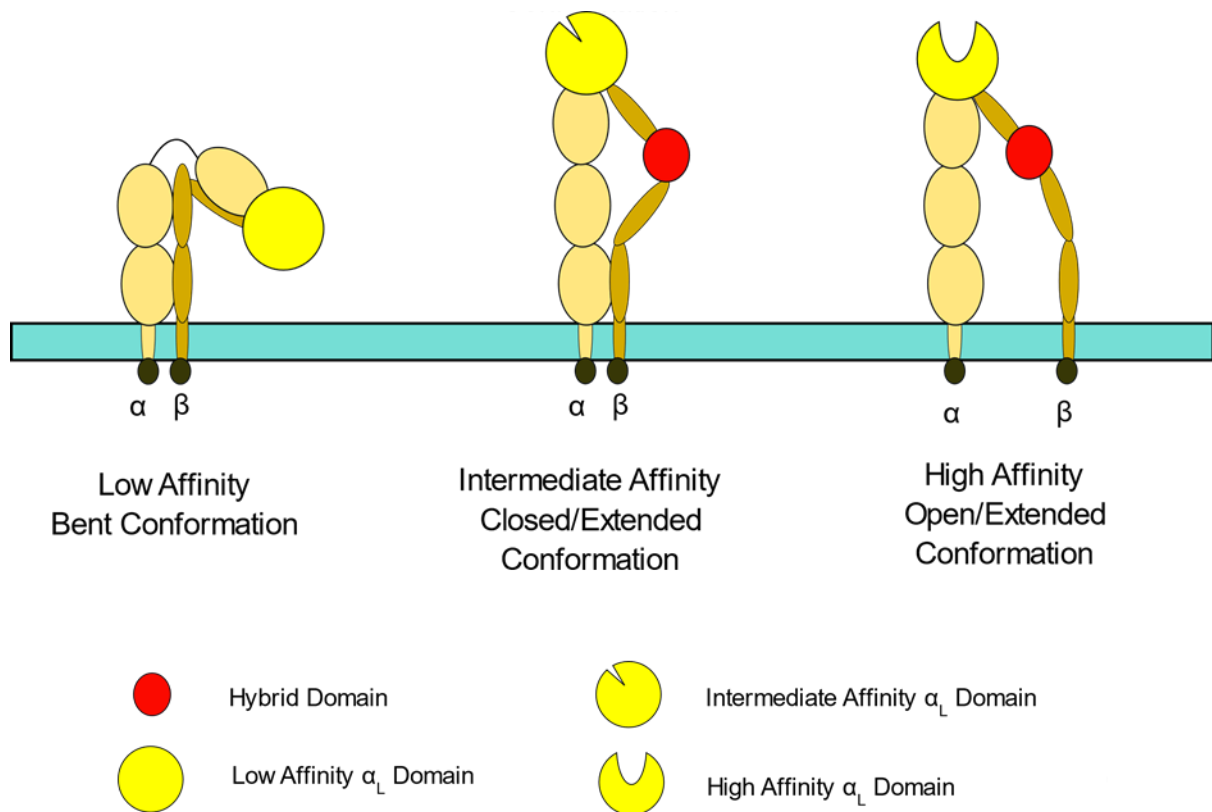


Figure 1.8: LFA-1 conformation.

LFA-1 affinity can be altered by its conformation. When bent, LFA-1 exhibits low affinity for its ligand, ICAM1. Intermediate affinity is achieved through a closed/extended conformation, whilst an open/extended conformation results in high affinity binding to ICAM1 and generation of an effective, stable immunological synapse. Image created with Inkscape (1.1.2).

In contrast to T cells, NK cells do not require inside-out signals (such as chemokines and T cell receptor activation) to stimulate LFA-1 binding, and can signal autonomously.^{150, 200} Following integrin activation, a signalling network is employed to facilitate the convergence of cytotoxic granules to the microtubule organising centre (MTOC) which is subsequently polarised to the target cell, facilitating degranulation (Figure 1.9).²⁰⁰⁻²⁰⁵ Actin remodelling is also carried out at the immunological synapse in response to NK cell activation, facilitating docking of cytolytic granules.²⁰⁶ Integrin-linked kinase (ILK), paxillin, Pyk2 and Rho guanine nucleotide exchange factor 7 (RhoGEF7) signalling cascades are employed for the polarisation of MTOC, with Cdc42, CLIP-170, Par6 and APC components of this signalling cascade being key for granule polarisation.^{200, 207} During this process, mitochondria and golgi have also been shown to polarise towards the immunological synapse.^{208, 209}

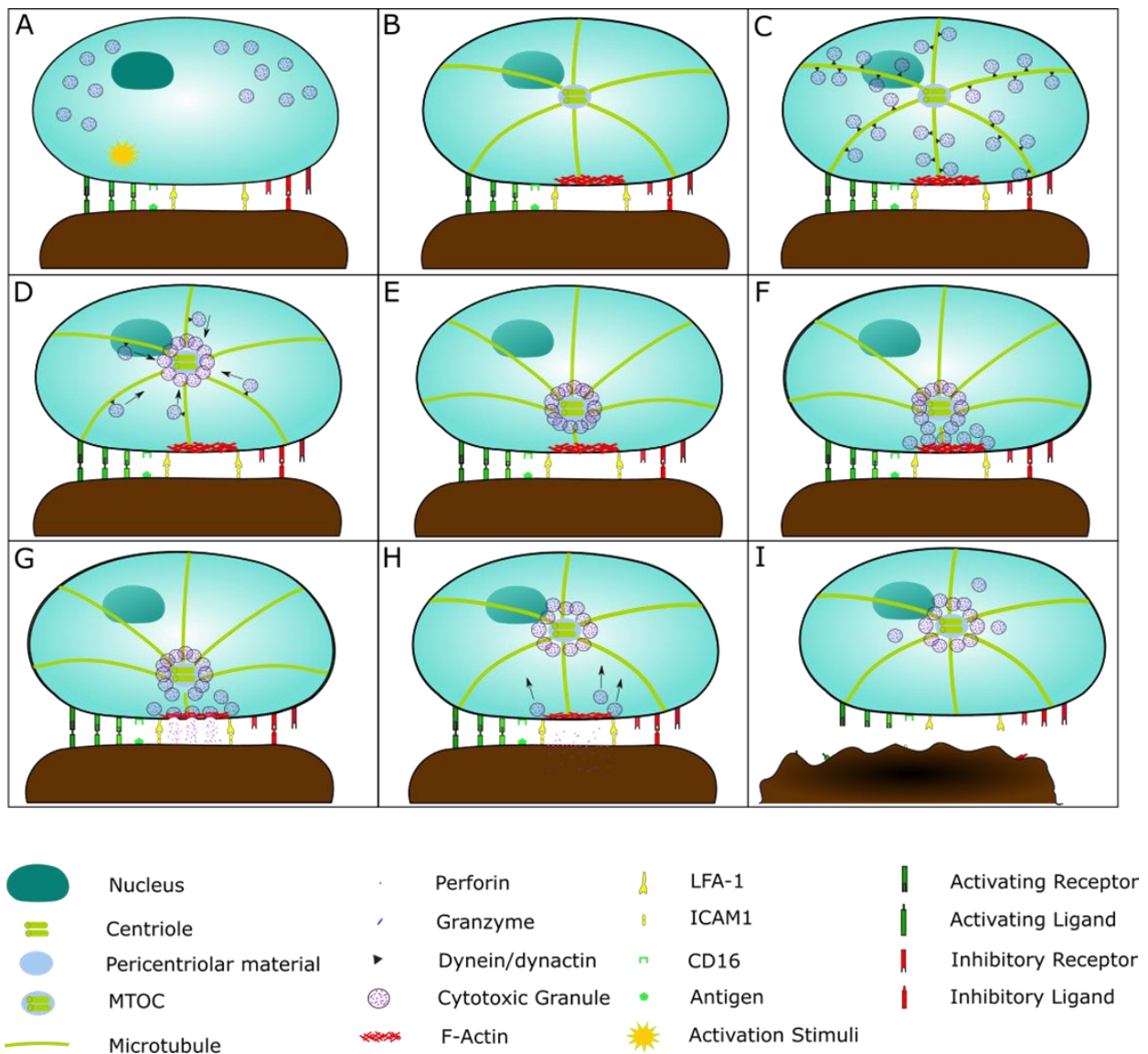


Figure 1.9: Cytotoxic granule convergence and MTOC polarisation.

Following receptor stimulation leading to NK cell activation, LFA-1 engages with its ligand ICAM1 on the malignant cell, forming a stable immunological synapse (A). F-actin accumulates and polymerises at the immune synapse, forming a filamentous mesh which modulates the release of cytolytic granules. Tubulin microtubules then form from the microtubule organising centre (MTOC) (B). Cytotoxic granules converge on the microtubules (C) and are polarised towards the MTOC where they converge (D). This granule movement is dependent on dynein/dynactin motor function. Dynamic rearrangement of the microtubules facilitates polarisation of MTOC towards the immunological synapse (E). This polarisation is stimulated via ILK, paxillin, Pyk2 and RhoGEF7 signalling. Following polarisation to the immunological synapse, a subsection of cytotoxic granules fuse with the plasma membrane (F) (a process largely regulated by Munc 13-4 and Rab27a) and undergo degranulation (G). Cytotoxic granules which do not degranulate are recycled and are hypothesised to remain converged at the MTOC to facilitate serial NK cell killing. Granules which undergo incomplete fusion are rapidly recycled through clathrin mediated endocytosis of granule membrane proteins, further facilitating serial killing (H). Finally, the malignant cell undergoes perforin induced necrosis or granule dependent apoptosis. NK cells detach from the malignant cell and move on to the next target (I).

Following polarisation, cytotoxic granules can be exocytosed by two methods: complete or incomplete fusion (Figure 1.10). In complete fusion, the granule fuses with the plasma membrane and completely discharges its cytolytic components. It is thought that this method facilitates swift degradation, recycling and reuse of the granule. Conversely, incomplete fusion is characterised by the formation of a transient fusion pore at the plasma membrane, and facilitates release of some, but not all of the cytolytic granule contents. Clathrin mediated endocytosis of granule membrane proteins allows rapid recycling of these granules, facilitating serial NK cell killing.^{207, 210}

Cytolytic granules contain the pore-forming protein, perforin, and granzymes which are serine proteases. Following release from the immunological synapse, perforin forms holes in the plasma membrane of the target cell. If the target cells cannot repair the damage caused by perforin, the cell will undergo necrosis via rapid swelling and lysis. Failing perforin induced necrosis, granzymes, which enter the cytosol of target cells via perforin formed membrane gaps, initiate caspase cascades, leading to caspase-dependent apoptosis. Thus, cytotoxic granule release is seen to facilitate target cell destruction via two distinct pathways.²¹¹

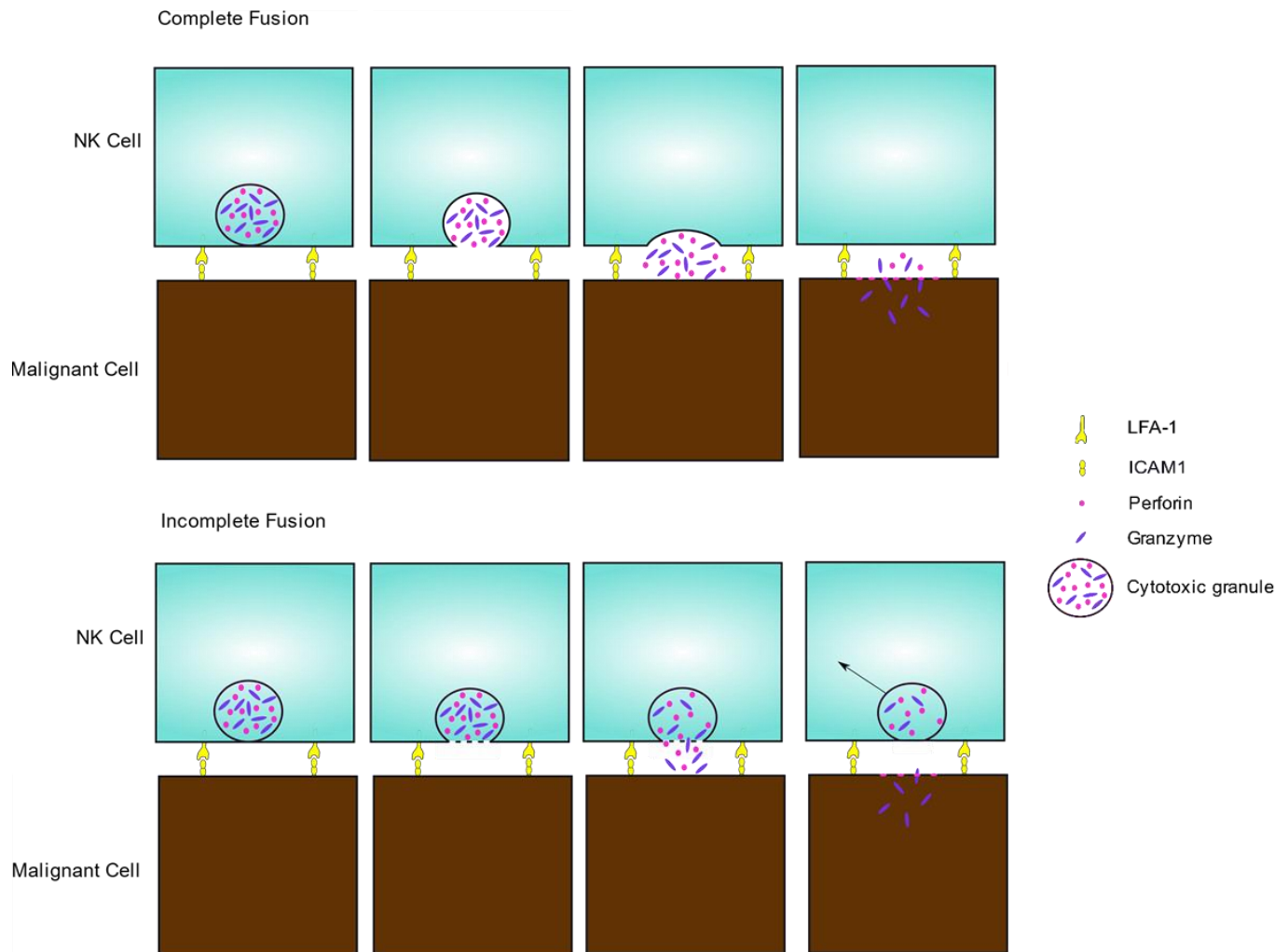


Figure 1.10: Complete and incomplete fusion of lytic granules.

A) Complete fusion. Cytotoxic granules fuse with the plasma membrane and completely discharge their contents into the immunological synapse. B) Incomplete fusion. Cytotoxic granules partially discharge their contents through the formation of transient pores in the plasma membrane. Following partial release of their cytotoxic content, clathrin mediated endocytosis of granule membrane proteins is carried out, allowing the recycling and reuse of these granules, facilitating destruction of multiple target cells. Figure created with Inkscape (1.1.1).

In addition, NK cells can carry out cytotoxicity via non-granule dependent mechanisms. Binding of death ligands such as TNF-related apoptosis inducing ligand (TRAIL) and Fas ligand (FasL) to their receptor on target cells result in extrinsic apoptosis via caspase-8 activation.²¹²

Finally, NK cells can induce target cell death through the release of cytokines such as interferon- γ (IFN- γ).¹²⁰ This cytokine release is multi-functional, conveying widespread anti-cancer activity. Specifically, IFN- γ orchestrates crosstalk between both innate and adaptive immune effector cells and leads to the recruitment of dendritic cells and T cells to the tumour site, facilitating effective effector response to malignancy. Moreover, IFN- γ induces the expression of MHC and ICAM-1 on target cells, enabling engagement and activation of effector cells. Finally, IFN- γ also inhibits angiogenesis and cell proliferation in tumour tissue, adding to a global anti-tumour response.^{213, 214}

1.5.3 NK in Cancer

NK cells are seen to play a vital role in tumour immunosurveillance. Multiple studies have demonstrated favourable outcomes in patients with increased NK cell tumour infiltration in a range of malignancies including, squamous cell lung, colorectal and gastric cancers as well as haematological disease.^{120, 147} In a study on non-small cell lung cancer, Tenuta *et al.* reported that patients with disease control exhibit higher basal NK cell levels than do those with progressive disease. Moreover, high basal NK cell levels were also found to be indicative of longer overall survival.²¹⁵ Similarly, NK cells were found to play a prognostic role in primary central nervous system lymphoma (PCNSL). Treatment responders were found to have a higher median NK cell count and proportion than did non-responders. Additionally, newly diagnosed patients with high NK cell count were found to have longer overall survival (vs low NK cell count). It is perhaps prudent to note that although NK cell numbers were found to be

prognostic, the functional efficacy of NK cells in newly diagnosed patients was found to be impaired when compared to patients in complete remission/healthy donors.²¹⁶ Consistently, low NK cell numbers were found to correlate with reduced relapse-free survival in patients with advanced gastric cancer. Moreover, patients expressing high HLA-E status and low NK cell number were found to have the worse relapse free survival overall.²¹⁷ Interestingly, however, Thacker *et al.* suggest that not all NK cells exhibit the same prognostic benefit. Murine models of triple negative breast cancer revealed a sub-cluster of Socs3^{high}CD11b⁻CD27⁻ immature NK cells which were found to correlate with worse prognosis. Moreover, these cells were associated with reduced cytotoxic granzyme signature and were seen to activate cancer stem cells via the Wnt pathway.²¹⁸

1.5.4 NK cells in PDAC

NK cells have been found to play a crucial role in PDAC and prove to be an attractive therapeutic target.^{219, 220}

Hoshikawa *et al.* investigated the prognostic implication of NK cell number both pre- and post-surgery. It was found that the percentage of NK cells both in the blood and within tumour tissue correlated to progression free survival, with patients who exhibited high NK levels expressing later disease recurrence. Interestingly, percentage of CD8⁺ T cells was not found to be correlated to progression free survival. Moreover, NK cell frequency was found to be the only favourable prognostic factor in patients undergoing curative surgery.²¹⁹ Similarly, Davis *et al.*, identified that absolute numbers of NK cells positively correlated with overall survival in treatment naïve PDAC patients.²²¹ Whilst Jun *et al.* found that impairment of NK cell function correlated to progression of pancreatic cancer, suggesting that functional NK cells may prove to be a positive prognostic marker in PDAC.²²²

As a result of their evident cytotoxic capacity, NK cells have received much attention as a potential immunotherapeutic tool in the treatment of PDAC. Hu *et al.* found that adoptive transfer of NK cells significantly delayed tumour growth in murine models of PDAC. Furthermore, these effector cells were shown to exhibit a greater cytotoxic propensity and higher IFN- γ production than spleen derived NK cells.²²⁰ Similarly, Lin *et al.* demonstrated that allogenic NK cell transfer in combination with irreversible electroporation significantly increased median progression free and overall survival in stage III PDAC patients, and increased median overall survival in stage IV patients. Moreover, multiple allogenic transfers correlated with better prognosis in stage III patients.²²³ Taken together, these results highlight the therapeutic potential of NK cell-based therapies.

Importantly, despite the known cytotoxic capabilities of NK cells in malignancy, multiple studies have revealed significant cellular dysfunction and exclusion of NK cells from tumour tissues, suggesting that NK cells can be educated by the tumour microenvironment and stromal cells.^{224, 225}

Ene-Obong *et al.* demonstrated that NK cells preferentially migrate towards active pancreatic stellate cells and are consequently sequestered in the panstromal compartment of the tumour microenvironment, preventing NK induced cancer cell death.⁶¹ Similarly, Lim *et al.* report that frequencies of NK cells in PDAC tissue are very low at <0.5%. This low infiltration was attributed to reduced expression of the CXCR2 receptor on NK cells which resulted in poor chemotaxis into tumour tissues. Furthermore, the hypoxic tumour microenvironment associated with PDAC was found to limit NK cell proliferation and cytotoxic effector function. Importantly, NK cell dysfunction was found to be negated via *ex vivo* stimulation.²²⁶

NK cell function is also seen to be significantly impacted by tumour derived extracellular vesicles from PDAC cells, specifically those containing large numbers of immune regulatory factors including TGF- β , nectin-2 and PVR, which lead to immune modulation of tumour tissue. When co-cultured with extracellular vesicles, the expression of multiple NK cell receptors and cytokines were downregulated, specifically, IFN- γ , TNF- α , CD107a and NKG2D, resulting in gross cytotoxic impairment. This NK cell dysfunction was found to be a result of activation of the TGF- β -Smad3/4 signalling pathway.²²⁷

It should also be noted that NK cell dysfunction is heavily regulated by the soluble factors and cytokines secreted by both tumoural and stromal cells in PDAC. Release of TGF- β , Indolamine 2, 3 dioxygenase (IDO), matrix metalloproteinases (MMPs) and interleukins was found to be largely responsible for this impairment.^{226, 228-231} These interactions are summarised in Figure 1.11.

It is perhaps prudent to note that in contrast to the beneficial role of NK cells in PDAC previously demonstrated, Yang *et al.*, report that patients with a high density of NK cell infiltration expressed decreased overall survival. Moreover, high NK cell number was associated with decreased levels of IFN- γ , IL-2 and TNF- α suggesting NK cell dysfunction and anergy.²²⁵

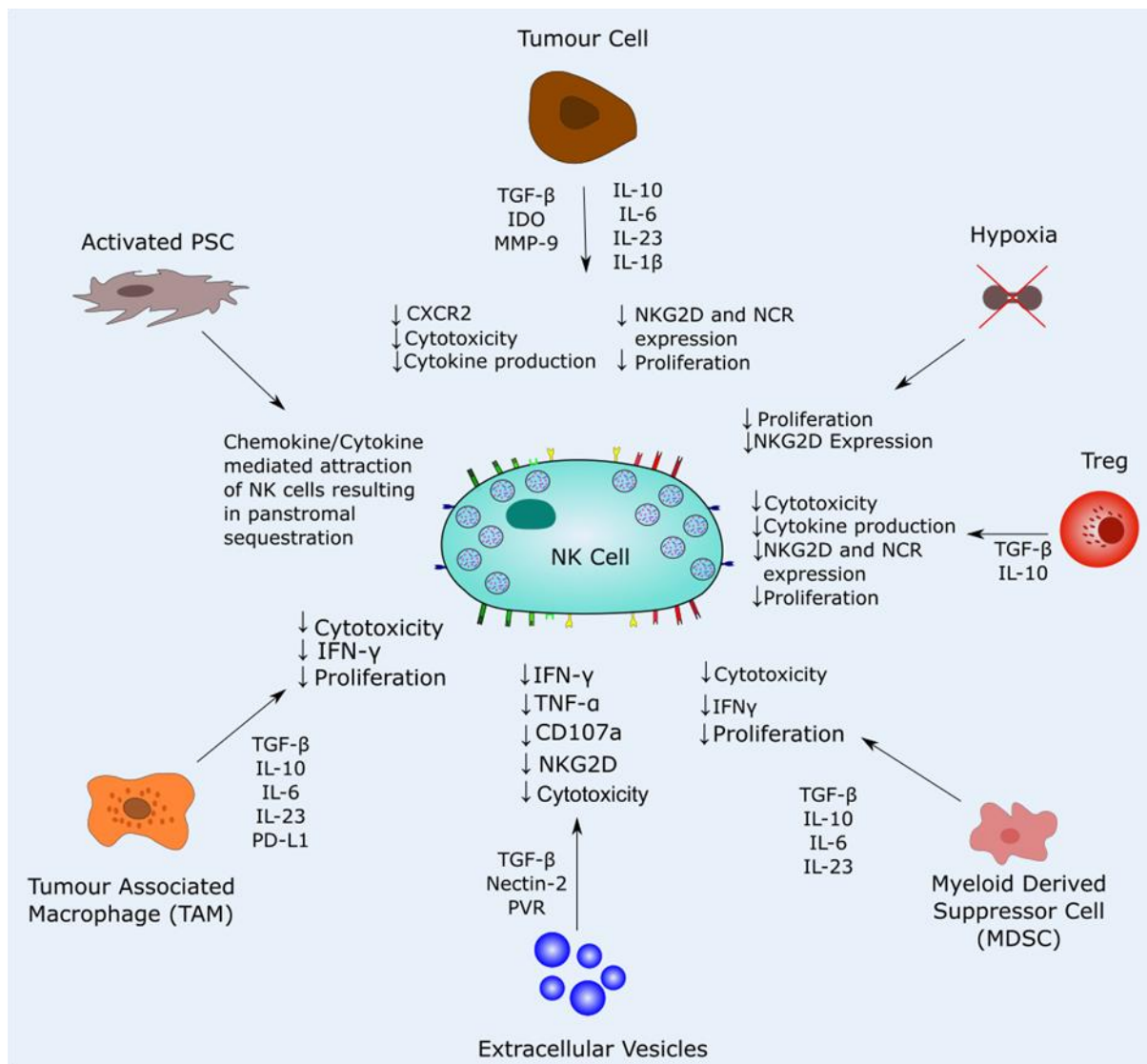


Figure 1.11: NK cell dysfunction caused by tumoural and stromal cells in PDAC.

NK cell interaction with stromal and tumour cells significantly impacts their cytotoxic efficacy in PDAC. Tumour cells, Tregs, MDSCs, TAMs and extracellular vesicles secrete TGF-β, IL-10, IL-6, IL-23 and IL-1β. These factors significantly dampen NK cell cytotoxicity and function and inhibit intratumoural proliferation of NK cells. NK cell mediated cytokine release is also inhibited within the immunosuppressive tumour microenvironment. Finally, chemokine release may also sequester NK cells in the panstromal compartment, preventing engagement with tumour cells. Figure created with Inkscape (1.1.2).

1.6 NK cells and Pancreatic Stellate cells

Despite increasing interest in stromal targeting and NK cell-based therapeutics in PDAC, little remains known about the relationship between these two key players. To date, only two studies have superficially investigated the interaction between NK cells and PSCs in PDAC.

Van Audenaerde *et al.* demonstrated that NK cells killed both pancreatic cancer cells and pancreatic stellate cells (9-35% and 20-50%, respectively) at multiple effector: target ratios in *in vitro* models. Moreover, it was shown that NK cells stimulated by IL-15 had a greater propensity for both cancer and stellate cell cytotoxicity than did unstimulated NK cells. It was also evidenced that PSCs express the NKG2D ligands MICA, MICB and ULBP, confirming possible interaction between these two cell types. Van Audenaerde *et al.*, also report that, in addition to the cell lines tested, patient derived stellate and NK cells displayed the same interaction, with IL-15 stimulated NK cells demonstrating 23.8-52.9% cytotoxic efficacy against PSCs.²³² This work demonstrates a clear propensity for NK cell cytotoxicity towards PSCs and suggests potential therapeutic efficacy in PDAC.

Conversely, Huang *et al.* report a significant decrease in CD107a⁺, IFN- γ ⁺ and granzyme B⁺ NK cells in tissue infiltrating lymphocytes when compared to PBMCs, suggesting that NK cells may be educated by the tumour microenvironment. Furthermore, co-culture studies revealed that NK cell production of these function associated proteins (CD107a, IFN- γ and granzyme B) decreased dramatically when co-cultured with tumour derived activated PSCs when compared to normal PSCs, or NK cells alone.²³³ These data suggest that NK cell function can be heavily influenced by PSC education.

Consequently, further research is required to consolidate the knowledge acquired to date and to provide novel mechanistic insight into the relationship between these two key players in the PDAC tumour microenvironment.

1.7 Project Aims and Hypotheses

As pancreatic stellate cells are known orchestrators of the tumour microenvironment and crucial contributors to the chemoresistance associated with PDAC, further work is needed to identify potential therapeutic strategies to challenge the poor prognostic implications of pancreatic stellate cell activity. Moreover, with NK cells demonstrating strong efficacy against malignant cells but poor chemotaxis into target tumours, the poorly understood interactions between NK cells, the tumour microenvironment and its' orchestrators require illumination. Thus, this project aims to investigate the intricate relationship between pancreatic stellate cells and NK cells in the context of PDAC. Through further unravelling this interaction we aim to provide novel functional and mechanistic insights into the interaction between these two crucial effector units, and in so doing, uncover previously unknown therapeutic targets which can be harnessed to work towards new treatment regimens for this dismal prognosis disease.

Thus, the main objectives of this study are:

- To assess the cytotoxic capacity of naïve NK cells towards PSC (activated versus quiescent).
- To assess the impact of co-culture with PSC (activated versus quiescent) on the cytotoxic capacity of NK cells towards cancer cells.
- To assess the impact of co-culture of PSC and NK cells on CAF subtype determination.
- To identify if co-culture of PSCs and NK cells affects NK phenotypic expression.
- To elucidate downstream signalling pathways involved in NK and PSC interaction.

- To determine the location of, and interaction between, NK cells and PSCs/CAFs in PDAC tissues.

Our objectives have led to the generation of several hypotheses:

- If NK cells encounter activated PSCs, then their immune-modulatory phenotype would be altered because of this interaction.
- If NK cells encounter activated PSCs, then their cytotoxic capacity towards tumour cells would be reduced because of the alteration of NK phenotype.
- If PSCs can be modulated to become quiescent, then NK cells may demonstrate better cytotoxic ability towards tumour cells due to retention of an activated phenotype.
- If naïve NK cells encounter activated PSCs, they will demonstrate initial cytotoxicity towards these cells because of their innate activation state.
- If PSC/CAF encounter NK cells, this interaction may modulate CAF subtype.
- If NK cells encounter activated PSC/CAF, then their location within the tumour micro-environment will be altered because of PSC induced sequestration.

Chapter 2 - Materials and Methods

In Vitro Optimisations

2.1 Cell Culture

Cell line characteristics are delineated in Table 2.1. Cells were cultured and maintained as per standard laboratory practice.^{103, 140} Briefly, adherent cell lines were cultured in T75 (CLS430641, Sigma-Aldrich) and T175 (CLS431085, Sigma-Aldrich) cell culture flasks. Upon reaching 70% confluency, culture media was aspirated from the flasks, and the cells were detached using Trypsin-EDTA (10x) (15400054, Gibco), (5 min, 37°C). Fresh media was added to each flask (containing FBS) to inhibit the action of trypsin, and the culture flasks washed. Cells were transferred to 50mL falcon tubes (CLS430829-500EA, Sigma-Aldrich) and centrifuged for 3 minutes at 1200rpm. The supernatant was aspirated, and the cell pellet resuspended in fresh media. Cells were counted using a haemocytometer and trypan blue (T8154-20ML, Sigma Aldrich) and seeded as necessary.

Non-adherent cells were cultured in T25 (CLS430168, Sigma-Aldrich) and T75 cell culture flasks and passaged every 2-3 days. Cells were aspirated from culture flasks, transferred to 50mL centrifuge tubes and centrifuged for 5 minutes at 250g. The supernatant was aspirated, and the cell pellet resuspended in 1-3mL of fresh media. Cells were counted using a haemocytometer and trypan blue and plated at a density of 2×10^5 - 3×10^5 cells/mL. Cultures were supplemented with IL-2 every 2-3 days. All cell lines were incubated at 37°C with 5% CO₂.

All cell lines were regularly tested for mycoplasma and were determined to be negative before experimentation.

Cell Line		Origin	Media
Capan2 (Adherent)	Human PDAC cell line (RRID: CVCL_0026) ²³⁴	Isolated from the pancreas of a 56-year-old male with pancreatic adenocarcinoma	McCoy's 5A Medium (M9309, Sigma- Aldrich) supplemented with 10% foetal bovine serum (FBS) (10500064, Gibco)
MiaPaca2 (Adherent)	Human PDAC cell line (RRID: CVCL_0428) ²³⁵	Isolated from the pancreas of a 65-year-old male with carcinoma	Dulbecco's Modified Eagle's Medium (DMEM) (41966029, Gibco) plus 10% FBS
BxPc3 (Adherent)	Human PDAC cell line (RRID: CVCL_0186) ²³⁶	Isolated from the pancreas of a 61-year-old female with adenocarcinoma	RPMI 1640 (11875093, Gibco) plus 10% FBS
PS1 (Adherent)	Immortalised human pancreatic stellate cell line ²³⁷	Isolated from a donated, healthy pancreas	Dulbecco's Modified Eagle's Medium/Nutrient Mixture F-12 Ham (D8437, Sigma-Aldrich) with 10% FBS
NK92 (Non- adherent)	Human natural killer cell line (RRID: CVCL_2142) ²³⁸	Derived from peripheral blood mononuclear cells isolated from a 50-year- old male with malignant non-Hodgkin's lymphoma	Minimal Essential Medium (MEM) α , no nucleosides (12561056, Gibco) with 0.2mM myo-inositol (87-89-8, Sigma- Aldrich), 0.1mM 2-mercaptoethanol (31350010, Gibco), 0.02mM folic acid (F8758, Sigma-Aldrich), 12.5% Horse Serum (26050088, Gibco) and 12.5% FBS Supplemented with 100 units of interleukin-2 (PHC0026, ThermoFisher) every 2-3 days

Table 2.1: Cell lines utilised within the current project with their required media.

In order to generate robust data and ensure that our results could be reliably extrapolated, we included three pancreatic cancer cell lines for experimentation. Each cell line demonstrates a different differentiation status as well as variation in the key mutations associated with PDAC (Figure 1.1). The phenotypic and genetic profile of each cancer cell line is outlined in Table 2.2.

Pancreatic cancer cell line	Mutation Status				Differentiation Status
	<i>KRAS</i>	<i>TP53</i>	<i>CDKN2A</i>	<i>SMAD4</i>	
BxPc3	Wild Type ²³⁹	220 cys ²³⁹	Wild Type ²³⁹ /homozygous deletion ²⁴⁰	Homozygous deletion ²⁴¹	Moderate-poor ²⁴²
Capan2	12 val ²³⁹	Wild Type ²³⁹ , 200 bp deletion ^{242, 243}	Wild Type ²³⁹ /base pair insertion ²⁴⁰	Wild Type ²³⁹	Well ²⁴²
Miapaca2	12 cys ²⁴⁴	248 Trp ²⁴⁴	Homozygous deletion ²⁴⁴	Wild Type ²⁴⁴	Poor ²⁴²

Table 2.2: Mutational and differentiation status of pancreatic cancer cell lines used within this project.

2.2 Media co-culture experiments

NK92 and PS1 cells were seeded at a density of 100,000 and 20,000 cells/well, respectively (24 well plates). Cells were cultured in five media conditions (Table 2.3) for 72h to determine optimal media conditions for co-culture experiments. Cell viability assessment was carried out at 24, 48 and 72h via cell counts (haemocytometer) using trypan blue. Representative images of each condition were acquired using the Axiovert 135 liteview microscope (Zeiss) (magnification x10).

Media Condition	Media Ratio for NK92 Cells	Media Ratio for PS1 Cells
100%	1:0 – NK92 Media:PS1 Media	1:0 – PS1 Media:NK92 Media
75%	3:1 – NK92 Media:PS1 Media	3:1 – PS1 Media:NK92 Media
50%	1:1 – NK92 Media:PS1 Media	1:1 – PS1 Media:NK92 Media
25%	1:3 – NK92 Media:PS1 Media	1:3 – PS1 Media:NK92 Media
0%	0:1 – NK92 Media:PS1 Media	0:1 – PS1 Media:NK92 Media

Table 2.3: Media conditions trialled to determine optimal co-culture conditions for NK92 and PS1 cells.

NK92 media: Alpha MEM plus 12.5% Horse Serum, 12.5% FBS, 0.2mM myo-inositol, 0.1mM 2-mercaptoethanol, 0.02mM folic acid; PS1 Media: DMEM/Hams F12 Plus 10% FBS.

2.3 WST-1 validation of media co-culture experiments

WST-1, 2-(4-iodophenyl)-3-(4-nitrophenyl)-5-(2,4-disulfophenyl)-2H-tetrazolium, is a tetrazolium salt, which, when reduced by mitochondrial dehydrogenase, results in the production of a formazan dye. The amount of dye produced is indicative of proliferating cells.

NK92 and PS1 cells were seeded in triplicate (96 well plates (3599, Corning)) at a density of 100,000 and 2,000 cells/well, respectively, in 100µL of one of five media conditions (Table 2.3). Following 0, 24, 48 and 72h culture, 10µL/well of WST-1 reagent (05-015-944-001, Roche) was added. Plates were incubated for 270 minutes and read at 30 min intervals using the Infinite F50 Microtitre plate reader (Tecan). Absorbance was measured at 450nm (reference 620nm) at each time-point. For downstream analysis, the absorbance measured using the reference wavelength (620nm) was subtracted from the test measurement (450nm) for each well to minimise background noise.

2.4 CD107 Degranulation Assay

To determine NK cell cytotoxicity towards pancreatic cancer cell lines the CD107 degranulation assay was employed. The protocol for this assay was kindly provided by the Samson Lab (Appendix 1). Prior to running the assay using educated NK cells (cultured for 24h with either qPSC or aPSC) a trial assay was carried out. NK cells were cultured with MiaPaca2 cells at effector to target ratios of 1:1, 5:1 and 10:1. Briefly, MiaPaca2 and NK92 cells were passaged as described and resuspended in RPMI + 10% FBS. 250,000 MiaPaca2 cells were seeded in 5mL round bottom FACS tubes (352058, Corning Life Sciences). NK92 cells were then added to the tubes at the desired effector to target ratios. Tubes were covered with parafilm and incubated for 1h at 37°C, 5% CO₂. A mastermix of Brefeldin A (420601,

Biolegend) (1:1000), BD Pharmingen™ FITC Mouse Anti-Human CD107a (555800, BD Pharmingen, clone H4A3), BD Pharmingen™ FITC Mouse Anti-Human CD107b (555804, BD Pharmingen, clone H4B4) and PE/Cyanine7 anti-human CD56 (NCAM) (362510, Biolegend, clone 5.1H11) were added to the tubes (diluted in complete RPMI) and mixed by vortexing. Tubes were then incubated for a further three hours. 2mL of FACs buffer (420201, Biolegend) was added to each tube before centrifugation (400g, 5 min). Cells were then fixed in True-Nuclear Transcription Factor fixation buffer (424401, Biolegend) for 20 min, RT. Cells were washed (FACs Buffer, 400g, 5 min) and resuspended in FACs buffer and stored at 4°C until acquisition of the BD LSRFortessa (BD Biosciences).

2.5 CD107 Troubleshooting

Initial CD107 staining yielded poor results, with very low expression of the marker being observed in both unstimulated and stimulated cells. As such, a series of troubleshooting and optimisation experiments were carried out.

2.5.1 Alternative staining protocol – CD56 incubation

To determine if the addition of CD56 during incubation was hindering CD107a/b binding, the assay was repeated with CD56 staining following CD107 incubation. Briefly, NK cells were stained with CD107a/b as described. Following incubation with CD107a/b, cells were washed (FACs buffer) and stained with the cell surface marker CD56 for 30min, 4°C. Cells were then washed and fixed as described before resuspending in FACs buffer. Tubes were maintained at 4°C until sample acquisition. Three target cell lines were used in this experiment: BxPc3, MiaPaca2 and Capan2. NK cells were added at an effector: target ratio of 5:1 (500,000 NK cells to 100,000 cancer cells). NK cells stimulated with PMA (2.5µg/mL) (P1585, Sigma-Aldrich)

and Ionomycin (0.5µg/mL) (I0634, Sigma-Aldrich) were used as a positive control. Samples were acquired on the BD LSRFortessa and analysed using FlowJo (8.0) and GraphPad (9.0) software.

2.5.2 24-hour Degranulation Assay

To determine if the incubation time between NK cells and cancer cells was too short to generate a functional response in the NK cells a 24h assay was undertaken. NK cells were cultured with BxPc3, MiaPaca2 and Capan2 cell lines at effector to target ratios of 1:1 (100,000: 100,000), 5:1 (500,000: 100, 0000) and 10:1 (1,000,000: 1,000,0000). After 1h incubation, CD107a, CD107b and brefeldin A were added to the culture as described. Cells were incubated for a further 23h. Following culture, cells were stained for CD56. NK cells stimulated with PMA (2.5µg/mL) and Ionomycin (0.5µg/mL) were used as a positive control. Samples were acquired on the BD LSRFortessa and analysed using FlowJo and GraphPad software.

2.5.3 Primary NK cell degranulation assay

NK cells were isolated from PBMCs from a single healthy donor (kindly provided by Dr. Lauren Cutmore; ethics reference QMERC2014/61) by the EasySep™ Human NK Cell Isolation Kit (17955, Stem Cell Technologies) according to the manufacturer's guidelines. Briefly, PBMCs were prepared using density gradient centrifugation. T cells were removed from the sample and the remaining cells resuspended in PBS + 2% FBS and 1mM EDTA at a concentration of 5×10^7 cells/mL. Cells were transferred to a 5mL round bottom tube and 50µL/mL of EasySep™ Human NK Cell isolation cocktail (17955C, Stem Cell Technologies) was added to the sample. Cells were incubated for 5 min at RT. EasySep™ Dextran RapidSpheres™ (50103, Stem Cell

Technologies) were vortexed for 30 seconds and 50µL/mL added to the sample. Total sample volume was made up to 2.5mL by the addition of PBS + 2% FBS and 1mM EDTA, and the sample mixed. The sample was placed into an EasySep™ Magnet (18000, Stem Cell technologies) for 3 min. The enriched cell suspension was then transferred into a new tube and was ready for experimentation.

Primary NK cells were then cultured with Capan2 cells (1:1) or stimulated with PMA/ionomycin. Naïve, unstimulated primary cells were used as an unstained control. Cells were then cultured and stained as described and the samples acquired on the BD LSRFortessa. The data were analysed using FlowJo (8.0) software.

It is perhaps prudent to note that this was the only experiment to use primary NK cells. All other experiments were conducted using the natural killer cell line, NK92.

2.5.4 CD107 Degranulation assay alternative staining protocol

Consistent identification of CD107⁺ cells could not be achieved using the protocol outlined above. As such, a different protocol was sought, and new reagents obtained (this coincided with the beginning of attachment in Singapore).

NK cells were stimulated with PMA and Ionomycin generating positive controls. BV786 anti-human CD107a (563869, BD Biosciences) and BV786 anti-human CD107b (565304, BD Biosciences) were then titrated (Section 2.9.2) and the optimal antibody dilution identified. Following titration, naïve NK cells were cultured with three cancer cell lines; BxPc3, Capan2 and MiaPaca2 cells and stained with CD107a/b to determine assay efficacy. Initial trials included effector (NK) to target (cancer cell) ratios of 1:1, 5:1 and 10:1. Briefly, cancer cells were seeded in 24 well plates (32024, SPL Life Sciences) at densities of 200,000, 40,000 and

20,000 cells/well in triplicate, and incubated overnight to adhere. Following overnight incubation, NK cells were passaged and resuspended in complete RPMI at a density of 200,000 cells/140 μ L. NK cells were co-cultured with cancer cell lines and incubated for 1h, 37°C, 5% CO₂. A mastermix of BV786 anti-human CD107a, BV786 anti-human CD107b, monensin (00-4505-51, eBioscience™) and brefeldin A (00-4506-51, eBioscience™) was diluted in complete RPMI. For conditions without CD107a/b, a mastermix of monensin and brefeldin A was created. 10 μ L of antibody mix was added to each well (total staining volume of 150 μ L/well) and incubated for a further three/five hours, resulting in a total incubation time of 4h/6h. Following CD107 incubation, cells were transferred to a 96-well V-bottom plate and centrifuged at 300g for 5 min at 4°C. Cells were washed with PBS and centrifuged a second time before staining with Zombie NIR viability dye (10 min). Cells were then washed with PBS and stained with Pacific Orange anti-human CD45 (MHCD4530, Life Technologies) BV711 anti-human CD56 (318336, Biolegend) and PE/Cy7 anti-human CD57 (359624, Biolegend) for 30 min, 4°C. All antibodies were diluted in FACs buffer (PBS (20012-027, Gibco, + 2% FBS and 2mM EDTA (AM9260G, Invitrogen))). Cells were then washed with PBS and fixed in 100 μ L BD Cytofix Fixation buffer (554655, BD Biosciences) for 20 min 4°C. Cells were washed in PBS at 600g (5 min) before resuspending in 100 μ L PBS and transferring to prelabelled cluster tubes (4401, Corning costar). Fluorescence minus one (FMO) and reference controls were created. For FMO controls, NK cells were cultured and stimulated with PMA and ionomycin as described. These cells were then stained with all the markers included in the panel, bar one. For example, the CD45 FMO was stained using CD56, CD57, CD107a/b and Live/Dead viability dye. An FMO was created for each fluorochrome. For reference controls, cells were stained with a single marker. Following staining, 50 μ L of the single stain was transferred to a prelabelled cluster tube. 50 μ L of unstained cells was also transferred to the same cluster tube,

generating a truly negative population. UltraComp eBeads (01-2222-42, Invitrogen) were used to create positive controls for each fluorochrome as per the manufacturer's guidelines. Briefly, UltraComp eBeads were inverted 10 times to mix. One drop of the compensation beads was added to a pre-labelled FACs tube before the addition of 1µL of antibody per fluor. Tubes were vortexed to mix and incubated at 4°C in the dark for 25-30 min. 1mL/tube of FACs buffer was then added and the beads centrifuged at 600g for 5 min. The supernatant was discarded, and the beads resuspended in 100µL of PBS before transferring to pre-labelled cluster tubes. NK cells stimulated with PMA/Ionomycin were used as a positive control for NK cell degranulation. All samples were maintained at 4°C until sample acquisition. Samples were acquired on the Cytex Aurora 5-Laser Spectral Cytometer (Cytex Biosciences, USA).

2.5.5 Post-Acquisition analysis

Once acquired, samples were compensated using SpectroFlo software (3.0.3). Briefly, NxN plots were created for every fluorochrome in the panel. The distribution of cells within the plot was adjusted manually using the compensation tool (this facilitated 'dragging' of misaligned populations) until positive and negative populations appeared in a linear manner. This was completed for each marker and the compensation matrix reviewed before applying to all samples. Compensated FACs files were then saved and imported into FlowJo (10.8.1) (BD Biosciences) for gating. Cells were gated based on the population of interest, followed by single cells (side scatter area (SSC-A) vs side scatter height (SSC-H)). Live cells were then isolated. From this population gates were drawn for CD45⁺ cells, CD45⁺CD56⁺ Cells and CD45⁺CD56⁺CD57⁺ cells. CD107 expression was gated as a percentage of both CD45⁺CD56⁺ cells and CD45⁺CD56⁺CD57⁺ cells to identify if mature NK cells express differing levels of CD107. The percentages of CD107⁺ cells were then exported to GraphPad Prism for statistical analysis.

Due to low cell numbers of CD45⁺CD56⁺CD57⁺ cells, further downstream analysis was not conducted.

2.5.6 Full effector to target ratio experiments

To identify the best effector to target ratio for NK cell degranulation studies, the CD107 degranulation assay was repeated with additional effector to target ratios of 1:5 and 1:10. In order to accommodate this increased range, cancer cells were cultured in 12 well plates at densities of 500,000, 250,000, 50,000, 10,000 or 5,000 cells/well. 50,000 NK cells/well were then added in 190µL to achieve the desired effector to target ratios. Staining was then carried out as described (total staining volume 200µL/well) and the samples acquired on the Cytex Aurora. Samples were compensated using SpectroFlo software and analysed using FlowJo and GraphPad Prism.

2.6 Cytotoxicity Assays

2.6.1 WST-1 Cytotoxicity Assays

2.6.1.1 *Cancer cell number and WST-1 incubation optimisation*

Optimum seeding densities for NK cell cytotoxicity assays were assessed prior to experimentation. MiaPaca2, Capan2 and BxPc3 cells were seeded at densities of 2,500, 5,000, 10,000, 15,000 and 20,000 cells/well in triplicate (96 well plates) (Figure 2.1). Cells were incubated overnight (37°C, 5% CO₂) prior to culture with NK cells to allow adhesion. NK cells were centrifuged, resuspended in fresh media, and counted (as described). For each cancer cell density, NK cells were prepared and incubated at effector: target ratios of 1:1 or 10:1. Cells were co-cultured for 4h (37°C, 5% CO₂). NK cells were removed via washing with media three times. Cancer cells were then incubated with WST-1 (pre-diluted in media (10µL WST-1

per 100 μ L media)) for 4h. Absorbance was measured hourly (450nm; reference 620nm) using the Infinite F50 Microtitre plate reader (Tecan).

	1	2	3	4	5	6	7	8	9	10	11	12
A	Target cells No WST-1	Target cells No WST-1	Target cells No WST-1	Target cells No WST-1	Target cells No WST-1	Target cells No WST-1	Target cells No WST-1	Target cells No WST-1	Target cells No WST-1	Target cells No WST-1	Target cells No WST-1	Target cells No WST-1
B	Target cells only	Target cells only	Target cells only	Target cells only	Target cells only	Target cells only	Target cells only	Target cells only	Target cells only	Target cells only	Target cells only	Target cells only
C	Target 1:1 NK Cells	Target 1:1 NK Cells	Target 1:1 NK Cells	Target 1:1 NK Cells	Target 1:1 NK Cells	Target 1:1 NK Cells	Target 1:1 NK Cells	Target 1:1 NK Cells	Target 1:1 NK Cells	Target 1:1 NK Cells	Target 1:1 NK Cells	Target 1:1 NK Cells
D	Target 1:10 NK Cells	Target 1:10 NK Cells	Target 1:10 NK Cells	Target 1:10 NK Cells	Target 1:10 NK Cells	Target 1:10 NK Cells	Target 1:10 NK Cells	Target 1:10 NK Cells	Target 1:10 NK Cells	Target 1:10 NK Cells	Target 1:10 NK Cells	Target 1:10 NK Cells
E	Target cells No WST-1	Target cells No WST-1	Target cells No WST-1									
F	Target cells only	Target cells only	Target cells only									
G	Target 1:1 NK Cells	Target 1:1 NK Cells	Target 1:1 NK Cells									
H	Target 1:10 NK Cells	Target 1:10 NK Cells	Target 1:10 NK Cells									

	2,500 Cells
	5,000 Cells
	10,000 Cells
	15,000 Cells
	20,000 Cells

Figure 2.1: A schematic representation of the plate layout used for each cancer cell line during WST-1 optimisation.

2.6.1.2 *WST-1 Troubleshooting*

To address confounder identified in the WST-1 cytotoxicity assays, several protocol modifications and additional experimental conditions were employed. These are delineated in Table 2.4.

Protocol Step	Original Assays	Troubleshooting alternative
Seeding cancer cells	Cells were seeded using a single channel pipette	Seeding of cancer cells using a multichannel pipette
NK cell conditions tested	<ul style="list-style-type: none"> • NK cells cultured alone • NK cells cultured with qPSC • NK cells cultured with aPSC 	<ul style="list-style-type: none"> • NK cells cultured alone • NK cells cultured with qPSC • NK cells cultured with aPSC • NK cells cultured with IL-2 (100units/mL) for 24h and washed prior to plating • NK cells cultured with IL-2 (100units/mL) for 24h and plated with IL-2 (0.1 unit/mL)
Washing	Cells were washed five times via media aspiration of individual wells	Cells were washed three times by expelling the media into a waste bucket and tapping the plate on tissue to absorb excess liquid
Incubation length	Cancer cells incubated for 4h with NK cells	Cancer cells incubated for 4h and 24h with NK cells

Table 2.4: Protocol modifications used to troubleshoot confounder identified in WST-1 Cytotoxicity Assays.

2.6.1.3 WST-1 troubleshooting - IncuCyte Images

Images of each experimental condition tested in the cytotoxicity assay were taken after 24h incubation (following two washes) to observe any interaction between Capan2 and NK cells which may be contributing to the confounder identified. Images of each well were taken using the IncuCyte S3 (Sartorius) (magnification x4) and processed using EssenBio IncuCyte software and Image J.

2.6.2 Calcein AM Cytotoxicity Assays

2.6.2.1 Calcein AM dye optimisation

To ensure adequate staining of target cells, the staining concentration of Calcein AM was trialled. PSCs were seeded in 96-well (black, chimney) flat-bottomed plates (Greiner Bio-One), and incubated for 24h, 37°C, 5% CO₂ to allow cell adhesion. Calcein AM (C1420, Invitrogen) was removed from -20°C and allow to warm to room temperature. Several rounds of optimisations were carried out in which working solutions of 10nM, 100nM, 1µM, 5µM and 10µM of Calcein AM (diluted in serum free RPMI) were created. Cells were incubated for 30min/1h at 37°C, 5%, CO₂. Calcein AM containing media was aspirated and the cells washed in serum free media (1 rinse, 1x 5 min wash on a plate shaker). Cells were then incubated with 100µL complete RPMI (to measure spontaneous release) or RPMI + 2% Triton X-100 (85111, ThermoFisher/TB0198, BioBasic) (to measure maximum release). Cells were incubated for 4h at 37°C, 5% CO₂. Plates were then imaged on the Tecan M200 Microplate reader (excitation: 494nm, emission 517nm and 530nm) (Tecan Group Ltd., Männedorf, Switzerland). Plates were centrifuged and 75µL of cell culture supernatant transferred to a fresh plate. The culture supernatant was then imaged as described.

2.7 Flow Antibody Titration

Ahead of co-culture experiments flow cytometry antibodies (Table 2.5) were titrated (Table 2.6).

Antibody	Conjugated fluorophore	Company
Anti-human CD56 (NCAM)	PE-Cy7	362509, Biolegend
Anti-Human CD314 (NKG2D)	Brilliant Violet 421	320821, Biolegend
Human NKG2A/CD159a	PerCP	FAB1059C-025, R&D Systems
Anti-GFAP Monoclonal antibody (GA5)	AlexaFluor 488	53-9892-80, eBiosciences
Anti-Human alpha smooth muscle actin	PE	IC1420P, R&D Systems

Table 2.5: Antibodies used for flow cytometry staining.

CD56	NKG2D	NKG2A	Alpha SMA	GFAP
1:20	1:10	1:5	1:5	1:50
1:50	1:20	1:10	1:10	1:100
1:100	1:50	1:25	1:25	1:500
	1:100	1:50	1:50	

Table 2.6: Antibody dilution for initial flow cytometry antibody titration.

The following protocols were used for surface and intracellular staining of NK92 and PS1 cells, respectively. For surface staining of NK cells, NK92 cells were seeded at a density of 500,000 cells/tube in 500µL PBS. Cells were then centrifuged (1500rpm, 5 min at 4°C) and the supernatant discarded. Samples were incubated with Zombie NIR viability dye (1µL/sample) for 10min (4°C) before washing (1500rpm, 5min, 4°C in PBS). Human TrueStain FcX block (422301, Biolegend) was added (1:100) and incubated for 10min (4°C). Surface antibodies were prepared in FACs buffer at the dilutions stated and incubated for 30min (4°C). Samples were washed with FACs Buffer and fixed in 400µL of True-Nuclear Fixation buffer for 20min, RT. Following fixation, samples were washed, resuspended in 500µL FACs buffer and stored at 4°C until flow cytometric assessment. For intracellular staining of PSCs, PS1 cells were seeded at a density of 500,000 cells/tube in 500µL PBS. Cells were centrifuged (1500rpm, 5 min at 4°C) and the supernatant discarded. 1µL/sample of Zombie NIR viability dye was added, and the cells incubated for 10min at 4°C. Cells were washed twice (1500rpm, 5min, 4°C), once in PBS and once in FACs buffer. Samples were then fixed in 400µL fixation buffer and incubated at RT for 20 min in the dark. Cells were washed twice in permeabilisation buffer (424401, Biolegend) (1500rpm, 5min, 4°C) before incubating with intracellular stains (30 min, RT). Cells were washed again in permeabilisation buffer, resuspended in FACs buffer, and stored at 4°C until flow cytometric assessment. Samples were run on the BD Fortessa using FACS Diva Software. Ten thousand events were recorded for each sample. Analysis was carried out using FlowJo version 10 (BD biosciences).

2.7.1 NKG2A Antibody Troubleshooting

2.7.1.1 *Western Blot Analysis*

Following poor staining results achieved during antibody titration, Western blot analysis was carried out to determine if NKG2A was expressed by NK92 cells. MiaPaca2, BxPc3, Capan2 and PS1 cells were used as negative controls. Briefly, cells were lysed using cell lysis buffer (50mM Tris-Cl pH7.5, 150mM NaCl, 1mM EDTA, 1% Triton) with protease and phosphatase inhibitors (539131 and 524625, Millipore). Non-adherent cells were centrifuged whilst adherent cells were mechanically dissociated using a cell scraper before resuspension in lysis buffer. Cells were maintained in lysis buffer at 4°C for 30min, vortexing at 5 min intervals. Cells were then centrifuged (12,000rpm, 20min at 4°C) to pellet cell debris. Supernatants were removed and protein quantified using the Bio-Rad DC Protein Assay Kit (reagent A; 5000113; reagent B 5000114; reagent S 500-0115) according to manufacturer's instructions. Samples were added to sample buffer (Novex), boiled for 5 min at 95°C and loaded onto a 10% SDS-PAGE gel. Gels were run for 1h 40min at 100V before being transferred onto 0.45µm nitrocellulose membrane (10600003, GC Healthcare) (120V, 1h). Efficient protein transfer was visualised using Ponceau S solution (P7170, Sigma). Membranes were blocked in 5% Milk (70166, Sigma) diluted in Tris Buffered Saline (20-6400-10, Severn Biotech Ltd) + 0.05% Tween 20 (500-018-3, MPbio) for 30min. NKG2A (ab96319, abcam) and HSC70 (Merck) primary antibodies were diluted 1:5000 and 1:10000, respectively and incubated overnight at 4°C. Horse-Radish Peroxidase conjugated secondary antibodies were diluted 1:5000 (in milk) and incubated for 1h (RT). Membranes were washed (3x 5min in TBST) and proteins visualised using Immobilon Forte Western HRP substrate (WBLUF0500, Millipore) and the GE Amersham Imaging system.

2.7.1.2 Primary and Secondary NKG2A Antibody Staining

Following validation of the presence of NKG2A in NK92 cells it was decided that the primary antibody used for Western blot would be trialled for Flow cytometry (alongside the conjugated antibody) using both surface and intracellular protocols (Table 2.7).

Protocol step	Conjugated Antibody – Surface Staining	Abcam NKG2A antibody - Surface Staining	Conjugated Antibody – Intracellular Staining	Abcam NKG2A antibody – Intracellular Staining
Antibody dilution	Antibody diluted 1:10	Primary antibody – 1:100 Secondary antibody (Goat anti-Rabbit AF488) - 1:200	Antibody diluted 1:10	Primary antibody – 1:100 Secondary antibody (Goat anti-Rabbit AF488) - 1:200
Antibody incubation	30 min, 4°C	Primary antibody - 30 min, 4°C Wash with cell staining buffer (1500rpm, 5min, 4°C) Secondary antibody - 30 min, RT	30 min, 4°C	Primary antibody - 30 min, RT Wash with permeabilization buffer (1500rpm, 5min, 4°C) Secondary antibody - 30 min, RT
Antibody Diluent	Cell Staining Buffer	Cell Staining Buffer	Permeabilization buffer	Permeabilization buffer
Washing	Cells washed at 1500rpm, 5min 4°C in Cell Staining Buffer	Cells washed at 1500rpm, 5min 4°C in Cell Staining Buffer	Cells washed at 1500rpm, 5min 4°C in Permeabilization Buffer	Cells washed at 1500rpm, 5min 4°C in Permeabilization Buffer
Fixation	Cell Fixed using True-Nuclear Transcription Factor Fixation buffer (45min, RT) after staining	Cell Fixed using True-Nuclear Transcription Factor Fixation buffer (45min, RT) after staining	Cell Fixed using True-Nuclear Transcription Factor Fixation buffer (45min, RT) before staining	Cell Fixed using True-Nuclear Transcription Factor Fixation buffer (45min, RT) before staining

Table 2.7: Key protocol steps involved in NKG2A troubleshooting

2.7.1.3 Validation of positive NKG2A staining

Primary and secondary antibody staining of NK92 cells using an intracellular staining protocol yielded positive results. To validate this finding, staining was repeated using MiaPaca2 cells as a negative control. In parallel to intracellular staining, both NK92 and MiaPaca2 cells were fixed (45 min, RT) prior to carrying out surface staining (as described) to assess if epitope fixation improved antibody-antigen binding.

2.7.1.4 NKG2A APC Conjugated antibody trial

An APC conjugated NKG2A antibody was obtained (130-114-089, Miltenyi) to streamline the flow cytometry protocol. NK92 cells were fixed either before or after staining and stained using the surface marker protocol as described. All data output was analysed using FlowJo (version 10) software.

2.8 Receptor expression and phenotype analysis

The experimental timeline for flow-based analysis of receptor or phenotype expression is delineated in Figure 2.2.

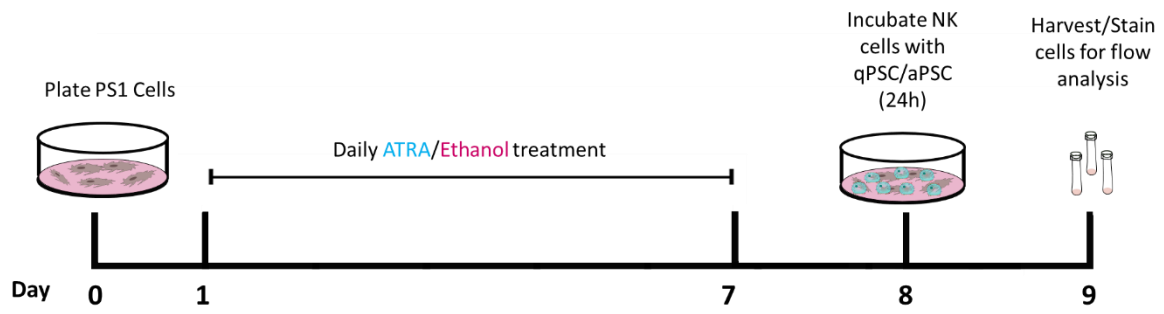


Figure 2.2: Experimental workflow of co-culture experiments for flow cytometric analysis of receptor and phenotype expression.

PS1 cells were seeded in 15cm dishes and treated daily with ATRA/EtOH in subdued light for 7 days. On day 8 NK cells were incubated with qPSC, aPSC or alone for 24h. Dishes of qPSC and aPSC alone were also maintained for 24h in fresh media. On day 9, cells were harvested for flow cytometric analysis.

PS1 cells were treated daily with either ATRA or ETOH for 7 days in subdued light. NK92 cells were incubated at a 1:1 ratio with either qPSC or aPSC or cultured alone for 24h. qPSC alone and aPSC alone were also maintained for 24h for phenotypic evaluation. NK92 cells were aspirated, centrifuged (250g, 5min) and resuspended in PBS. Cells from each condition were divided between two round bottom, 5ml FACs tubes. One sample from each condition was stained with CD56 (1:100), NKG2A (1:50) and NKG2D (1:10). Each condition was run alongside an unstained control. Similarly, PS1 cells were trypsinised, centrifuged (1200rpm, 3 min) and resuspended in PBS. Cells were transferred to FACs tubes and stained with Alpha SMA (1:50), GFAP (1:500) and CD56 (1:100). Surface (NK92) and intracellular (PS1) staining was carried out as described. All data analysis was carried out using FlowJo (8.0) software.

2.9 Flow cytometry Panel design - Cytex Aurora (Cytex biosciences)

A comprehensive panel of NK cell and PSC markers was designed for spectral flow cytometry. Panel design was based on the seminal work of Park *et al.* who developed a 40-colour panel for the 5-laser Cytex Aurora (Cytex Biosciences).²⁴⁵ Fluorochrome intensities were matched to marker abundance to ensure even sample staining. Cytex Biosciences spectral viewer was used to ensure equal distribution of fluorophores across lasers and panel complexity was assessed using the Cytex Biosciences spectral viewer to ensure that effective spectral unmixing and compensation could be carried out.

2.9.1 Development of an 18-colour panel for full spectrum flow cytometry

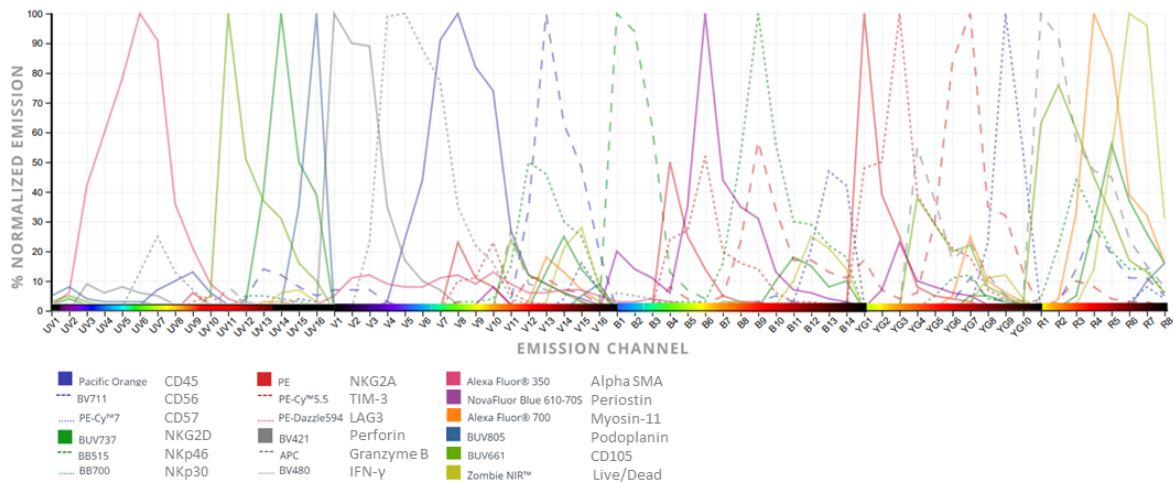
To further investigate the impact of PSC education on NK cells, an 18-colour panel was developed to assess receptor expression and functional markers in NK cells and PSC phenotype following co-culture (Table 2.8, Figure 2.3).

Approximate Emission wavelength (nm)	Peak Channel					UV	Violet	Blue	Yellow-Green	Red
395	UV2									
420		V1					Perforin - BV421			
440		V2								
450	UV6	V3				AlexaFluor350 - α SMA				
480		V5					IFN γ - BV480			
500	UV7		B1					NKp46 - BB515		
520		V6	B2							
550		V8	B3				CD45 - Pacific Orange			
570	UV9	V8		YG1					Alpha SMA- PE NKG2A - PE	
580				YG1						
600	UV19	V10		YG3				Periostin - NovaFluor Blue 610/70s	LAG3 - PE/Dazzle594	
660	UV11	V11		YG4	R1	CD105 - BUV661				Granzyme B - APC
680			B8	YG5					NKG2D - PE-Cy5	
690			B9					NKp30 - BB700		
700		V13	B10	YG7			CD56 - BV711		TIM-3 - PE-Cy5.5	Myosin-11 - AlexaFluor 700
730	UV14					NKG2D - BUV737				
750		V14								Zombie NIR
780		V15		YG9	R7		CD107a/b - BV786		CD57 - Pe-Cy7	
800	UV16				R8	Podoplanin - BUV805				

Table 2.8: Flow cytometric panel design.

The distribution of markers across all detectors and lasers based on the Cytex Aurora five laser cytometer. Coloured squares indicated marker category: Green - NK activating receptor; Red - NK inhibitory receptor; Blue - NK lineage Marker; Pink – alpha SMA, Purple – periostin, Orange – Myosin-11; Teal – Podoplanin; Lime – CD105.

A



B

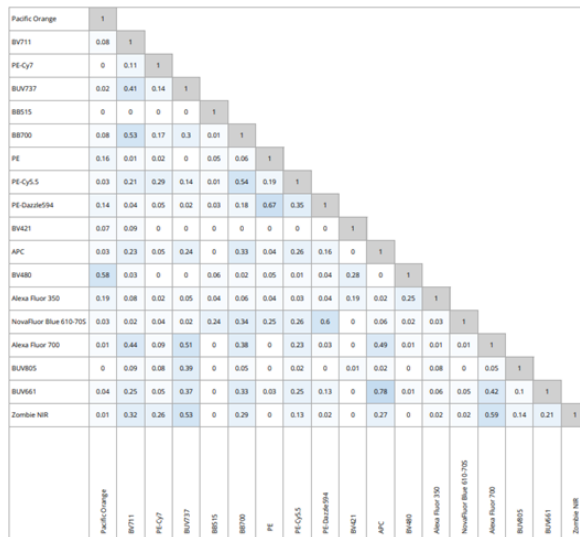


Figure 2.3: Spectral emission of the 18-marker flow cytometry panel.

A) Spectral emissions for each chosen fluorochrome are shown based on the 5 laser Cytek aurora. B) Complexity index matrix. This matrix demonstrates the similarities between fluorophores and delineates how complex a panel is. Squares with darker blue colouration depict fluorophores which have a great spectral overlap. Figure generated using CytekBio's Full Spectrum Viewer.

Following optimisations, no positive signal could be determined for NKG2D or alpha SMA. As such, antibodies with different fluorescent markers were chosen. To ensure separation between marker positivity and PSC autofluorescence the PE fluorophore was selected for alpha SMA. Consequently, to facilitate the use of two PE antibodies (alpha SMA and NKG2A), it was decided that separate flow cytometric staining panels would be used for each cell type (NK/PSC). The individual spectral emission profiles and complexity indices are shown in Figure 2.4 and Figure 2.5.

2.9.2 Antibody titration

Antibodies were titrated through serial dilution, with initial concentrations twice that recommended by the manufacturer. Antibody and titration details are outlined in

Table **2.9**.

Marker	Fluorochrome	Clone	Company	Catalogue Number	Recommended dilution	Titration concentrations			
CD45	Pacific Orange	HI30	Life Tech/ Invitrogen	MHCD4530	Assay- dependent	1:50	1:100	1:200	1:400
CD56	BV711	HCD56	Biolegend	318336	1:20	1:10	1:20	1:40	1:80
CD57	PE-Cy7	HNK-1	Biolegend	359624	1:20	1:10	1:20	1:40	1:80
NKG2D	BUV737 PE/Cy5	1D11	BD Biosciences/ Biolegend	748426 320844	Assay Dependent 1:20	1:10	1:20	1:40	1:80
NKp46	BB515	9E2	BD Biosciences	564536	1:20	1:10	1:20	1:40	1:80
NKp30	BB700	p30-15	BD Biosciences	745937	Assay Dependent	1:10	1:20	1:40	1:80
NKG2A	PE	REA110	Miltenyi Biotech	130-113-566	1:50	1:25	1:50	1:100	1:200
TIM-3	PE-Cy5.5	F38-2E2	ThermoFisher	35-3109-42	1:20	1:10	1:20	1:40	1:80
LAG-3	PE/Dazzle	11C3C65	Biolegend	369332	1:20	1:10	1:20	1:40	1:80
CD107a	BV786	H4A3	BD Biosciences	563869	1:20	1:10	1:20	1:40	1:80
CD107b	BV786	H4A4	BD Biosciences	565304	1:20	1:10	1:20	1:40	1:80
IFN-γ	BV480	B27	BD Biosciences	566100	1:20	1:10	1:20	1:40	1:80
Perforin	BV421	dG9	Biolegend	308122	1:20	1:10	1:20	1:40	1:80
Granzyme B	APC	REA226	Miltenyi Biotech	130-120-703	1:50	1:25	1:50	1:100	1:200
aSMA	AF350 PE	1A4	R&D Systems	IC1420U IC1420P	0.25- 1ug/million cells	1:10	1:20	1:40	1:80
Periostin	NovaFluor Blue 610/70S	JA63-40	ThermoFisher	MA5-32701	1:50-1:100	1:25	1:50	1:100	1:200
Myosin-11	AF700	ID8	Novus Biologicals	NPB2- 47899AF700	Assay dependent	1:25	1:50	1:100	1:200
Podoplanin	BUV805	LpMab-23	BD Biosciences	749716	Assay dependent	1:10	1:20	1:40	1:80
CD105	BUV661	266	BD Biosciences	750036	Assay dependent	1:10	1:20	1:40	1:80

Table 2.9: Antibody and titration details for Spectral Flow Cytometric Staining.

2.9.3 Staining Protocol

Cells were passaged as per standard laboratory protocol and resuspended in RPMI + 10% FBS at a density of 250,000 cells/100 μ L. Cells were transferred to pre-labelled 96-well v-bottom plates and centrifuged for 5 min at 300g (4°C) to pellet the cells. Culture supernatant was discarded by flicking, and the cells washed (100 μ L PBS followed by centrifugation 300g, 5min). Surface antibodies were prepared according to the required dilutions (Table 2.9) in FACs buffer (PBS +2mM EDTA + 2% FBS) to achieve a final staining volume of 50 μ L/well. Wash supernatant was discarded and 50 μ L/well of antibody dilution added to each well. Plates were incubated in the dark for 30 minutes at 4°C. Unstained controls were incubated in FACs buffer alone. Cells were then washed and fixed using 100 μ L/well of either BD Cytofix fixation buffer (surface stains) or BD Cytofix/Cytoperm fixation and permeabilisation solution (51-2090KZ, BD biosciences) (intracellular stains) and incubated in the dark for 20 min at 4°C. Following fixation, cells stained for surface markers were washed with 100 μ L PBS and centrifuged for 5 minutes at 600g (4°C). Cells were then resuspended in 100 μ L PBS and transferred to pre-labelled cluster tubes. For intracellular markers, cells were washed twice with BD Perm/Wash buffer (diluted to 1x with distilled water) (51-2091KZ, BD biosciences), centrifuging at 600g, for 5 minutes at 4°C. Intracellular antibodies were diluted to the desired dilutions in BD Perm/Wash buffer, in a total staining volume of 50 μ L/well. Antibodies were added and plates incubated for 45 min in the dark, 4°C. Unstained cells were incubated with Perm/Wash buffer alone. Following incubation, cells were washed twice with BD Perm/Wash buffer and resuspended in 100 μ L PBS. Cells were transferred to prelabelled cluster tubes and stored in the dark at 4°C until sample acquisition.

2.9.4 Sample Acquisition

Samples were acquired on the 5-laser Cytex Aurora (Cytex bioscience). For each antibody, a reference control containing stained (50%) and unstained (50%) cells was included to allow clear visualisation of positive and negative populations. In addition, UltraComp compensation beads were stained with 1µL of antibody (as described) to be used as a positive control for each fluorophore. 10,000 events were collected for reference controls and 500,000 events for experimental samples (to ensure the whole sample was acquired).

2.9.5 Spectral unmixing

Adequate visualisation of the cell population within the cytometric dot plot was achieved through manipulation of the forward/side scatter values. Running of the unstained control at low speed facilitated this optimisation. Reference samples were then placed on the sample probe and acquired according to the experimental set up. Once all reference controls were acquired, spectral unmixing was completed. Briefly, the 'unmix' option was chosen from the experiment options. This launched the unmixing pane. All markers were automatically loaded into list form. For each marker, either single stained cells or beads were chosen as the reference control (depending on separation between positively and negatively stained populations); where possible, cells were used for spectral unmixing. Autofluorescence was also chosen as a separate fluorophore. The 'next' option was chosen generating dot and spectral plots for each marker. Care was taken to ensure each fluorophore was detected by the correct channel, if erroneous, the ranged gates displayed on the spectral plot were 'dragged and dropped' into the correct location.²⁴⁵ For each marker, a gate was drawn around the NK/PSC population within the dot plot. This modified a preset histogram which displayed the positive and negative populations. Ranged gates were then drawn around the most

extreme values of both the positive and negative populations and the spectral profile of the fluorophore checked. The option to undertake 'live unmixing' was then selected, and the samples spectrally unmixed. Following unmixing, the remaining samples were acquired. Individual FACS files, as well as the experiment, were exported for post-acquisition analysis.

2.9.6 Post-Acquisition analysis

Samples were gated using FlowJo (version 10.8.1) software. Gating strategies were based on single stain reference controls (highest antibody concentration). Briefly, a polygon gate was drawn around the population of interest. From this population, doublets were excluded from the sample through the plotting of side scatter area (SSC-A) versus side scatter height (SSC-H) and selecting the single cells. A new dot plot was raised from the single cell population and the axis were altered to display the marker of interest. Gates were then drawn around both the positive and negative populations. This gating strategy was applied to all titration conditions. This gating was maintained for the highest concentration of each antibody. All remaining gates were then adjusted to achieve the same percent positive population as the highest antibody concentration. Fluorochromes were determined to be no longer effective when the positive and negative populations could not be distinguished. The lowest antibody concentration which demonstrated clear separation between positive and negative cells was chosen for full panel experimentation, thus minimising spillover between fluorochromes in neighbouring channels.

2.9.7 Marker troubleshooting

Clear positive populations for NKG2D on NK cells and alpha SMA on PSCs could not be identified after initial titration. As such, titrations were repeated several times. To test

whether stained populations were expressing low fluorescence intensity (preventing separation of positive and negative populations), both NK and PSC cells were included in the titrations to generate truly negative populations. Additionally, double staining for NKG2D and Myosin-11, and CD56 with alpha SMA was carried out to ensure that the PSC and NK cell populations could be identified, respectively. It was hoped that this would allow the demarcation of the negative, and by consequence, positive cells. This however was not the case, and no positive cells could be identified using these fluorophores. It was hypothesised that the spectral emission for the alpha SMA antibody was too similar to PSC autofluorescence and as such, positive cells were not able to be identified. Similarly, no truly positive cells could be identified for NKG2D. As such, new antibodies were sourced for these two markers (NKG2D: 320844, Biolegend; alpha SMA: IC1420P, R&D Systems). To ensure no further confound was incurred due to autofluorescence, alpha SMA was assigned to the PE fluor. As such, staining of NK and PSCs was separated to allow the inclusion of two PE fluorophores and streamline experiment compensation. Antibodies were titrated as described and the optimal dilutions determined.

2.9.8 Full Panel Trial

Once all antibodies were optimised, full panel trials for both PSCs and NK cells were carried. Briefly, PSCs were passaged as per standard laboratory protocol and resuspended in complete RPMI at a density of 250,000 cells/50µL. Cells were transferred to 96-well v-bottom plates and centrifuged to pellet cells (300g, 5min, 4°C). Cells were then stained with Zombie NIR viability dye (1:1000 in PBS) for 10 min in the dark (4°C). During this time, a surface antibody mastermix was created. PSCs were stained with the surface stain markers CD105 (1:80) and podoplanin (1:40). FMO controls and single stains were also prepared in this time. All surface

markers were diluted in FACs buffer at a total staining volume of 50µL/well. Following live/dead staining, cells were washed and centrifuged as described. Cells were then stained with the surface stain mastermix and incubated for 30 min in the dark at 4°C. Unstained cells were incubated with FACs buffer alone. Cells were then washed and fixed with 100µL/well of BD Cytofix/Cytoperm fixation buffer for 20min, 4°C. During this time, a mastermix for intracellular stains (diluted in Perm/Wash buffer) was created. PSCs were stained for alpha SMA (1:20), periostin (1:50) and myosin-11 (1:100) (final staining volume of 50µL/well). FMO and single stain controls were also created. Cells were then centrifuged (600g, 5 min) and washed twice with BD Perm/Wash solution. Cells were incubated with intracellular stains for 45 min in the dark at 4°C. During this incubation, cluster tubes were prelabelled. Cells were then washed in Perm/Wash buffer, resuspended in 100µL PBS and transferred to the cluster tubes. Reference controls were created as previously described. Cells were stored at 4°C until sample acquisition.

This staining process was repeated for NK cells with the following antibodies. Surface stains: CD45 (1:200), CD56 (1:80), CD57 (1:80), NKG2D (1:40), NKp30 (1:20), NKp46 (1:40), NKG2A (1:200), LAG3 (1:40) and TIM-3 (1:20). Cells were stained intracellularly for perforin (1:40), IFN-γ (1:40) and Granzyme B (1:50).

2.10 Characterisation of Cancer Cell lines

Cancer cells were grown on coverslips (15,000 cells/well in 12-well plates) to 70% confluency. Cells were then fixed in 10% Neutral Buffered Formalin (BAF-0010-25A, Cellpath Plc) for 10 min, RT and permeabilised with Methanol (10675112, Fisher Scientific), 10 min, -20°C to allow intracellular staining. Non-specific staining was then blocked by incubating coverslips with 5% goat serum + 0.3% TritonTMX-100 (T8787, Sigma-Aldrich) in PBS for 1h, RT. Primary antibodies

(Anti-Cytokeratin (Z0622, DAKO) 1:100, Rabbit IgG (SAB5500149, Sigma-Aldrich) 1:100) were diluted in 1% bovine serum albumin ((BSA) A8022, Sigma-Aldrich) + 0.3% TritonTMX-100 in PBS, added to the coverslips and incubated overnight (4°C). Coverslips were washed 3x in PBS (5 min/wash) and incubated with secondary antibodies (goat anti-rabbit AlexaFluor 488 (1:500)) for 1h (RT) in the dark. Cells were counterstained and coverslips mounted using ProLong Gold Antifade mountant with DAPI (P36941, Invitrogen). Slides were then imaged using the LSM710 Laser Scanning Confocal Microscope (Carl Zeiss).

2.11 Characterisation of PS1 Cells

Stellate cells were similarly stained for specific markers. α -SMA (M085101-2, Dako) (1:250), desmin (D1033, Sigma Aldrich) (1:100) and Mouse IgG (X0931, DAKO) (1:10) were stained as previously described. For vimentin (HPA 001762, Sigma Aldrich) (1:100) and rabbit IgG (1:100) several modifications were made to the staining protocol. Briefly, for permeabilisation, cells were incubated with PBS + 0.2% Triton X-100 for 5 min. Blocking was carried out using PBS + 0.1% Triton X-100 + 5% BSA for 30 min. Primary antibodies were diluted in PBS + 0.1% Triton X-100 + 5% BSA. An additional anti-mouse AlexaFluor488 (1:500) secondary antibody was used in this staining protocol to allow visualise vimentin staining as the primary antibody was raised in mouse. All slides were imaged on the LSM710 Laser Scanning Confocal Microscope (Carl Zeiss).

2.12 PSC-Educated NK cell WST-1 Cytotoxicity Assays

The following experiment time course was used for PSC-Educated NK cell WST-1 cytotoxicity Assays (Figure 2.6).

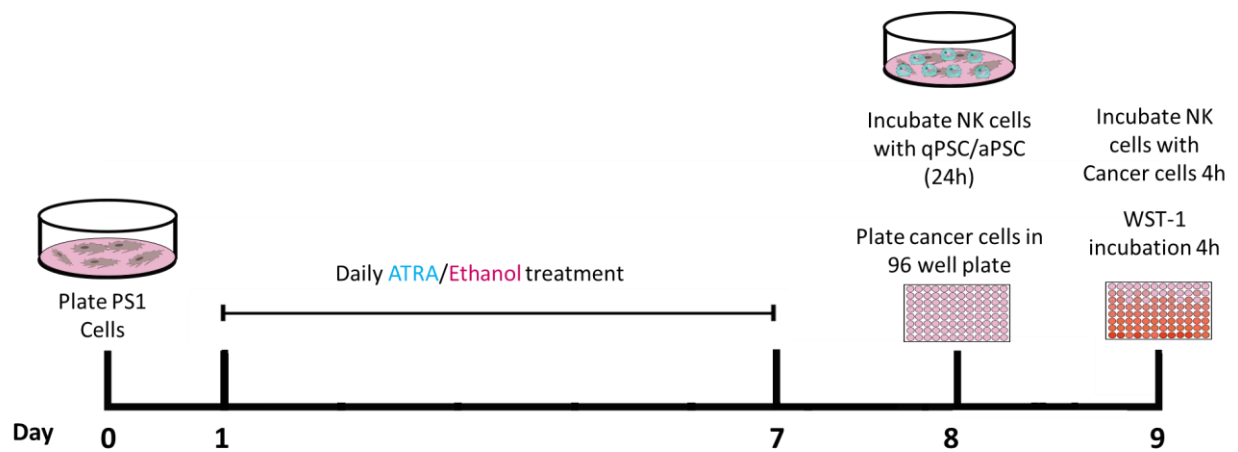


Figure 2.6: Schematic representation of the WST-1 Cytotoxicity assay time-course.

On day 0, PSCs were seeded in 15cm dishes and treated daily with ATRA/EtOH for 7 days in subdued light. On day 8, cancer cells were seeded in 96-well plates, and NK cells co-cultured with qPSC/aPSCs. On day 9, educated NK cells were incubated with cancer cells for 4h. Cells were then washed, and cancer cells stained with WST-1 for 4h. WST-1 absorbance was measured at 450nm.

PS1 cells were seeded in 15cm dishes (430599, Corning) and treated daily with either ATRA (1 μ M) or ethanol for 7 days in subdued light. On day 8, one representative plate from each condition was counted (as described) to determine approximate cell numbers. NK cells were centrifuged, resuspended in fresh media, counted and added to qPSC/aPSCs at a 1:1 ratio. Dishes of NK cells alone were also plated. Cells were incubated for 24h (37°C, 5% CO₂). Cancer cell lines were also seeded in triplicate at optimised densities in a 96 well plate (at least 12h prior to incubation with NK cells). Following co-culture with PSCs, NK cells were aspirated, centrifuged and resuspended in fresh media. NK cells were then incubated with cancer cell lines at an effector: target ratio of 1:1, 5:1, or 10:1 for 4h (37°C, 5% CO₂). Plates were washed in media five times and 100 μ L of media containing WST-1 (ab65475, Abcam) was added to each well. Plates were incubated and absorbance measured as described (section 2.6). Cytotoxicity (delineated by % proliferation) was calculated as = (absorbance of effector treated target cells/absorbance of target cells alone)*100.

2.13 Degranulation Assay against PSC

PSCs were seeded in 24 well plates and treated daily with ATRA/ethanol for 7 days in subdued light. On day 8, NK cells were added at a 1:1 (E:T) ratio and incubated for 1h. Cytotoxic granule recycling was prevented through the addition of Brefeldin A and monensin.²⁴⁶ Cells were incubated with BV786 anti-human CD107a and BV786 anti-human CD107b for 5h. Live/dead staining was carried out using Zombie NIR viability dye (10min, 4°C, 1:1000) (423106, Biolegend). NK cells were then stained for the cell surface lineage markers CD45 and CD56 (30 minutes, 4°C) before fixation. Samples were stored at 4°C and acquired on the Cytex Aurora 5-Laser Spectra Analyser (Cytex Biosciences, Fremont, California). Fluorescence minus one (FMO) and single stain controls were created for each marker using both PMA/ionomycin

stimulated NK cells and compensation beads (according to manufacturer's guidelines). Post-acquisition processing and analysis was completed using SpectroFlo (3.0.3) (Cytek Biosciences) and FlowJo (10.8.1) (BD Biosciences) software (Figure 2.7).

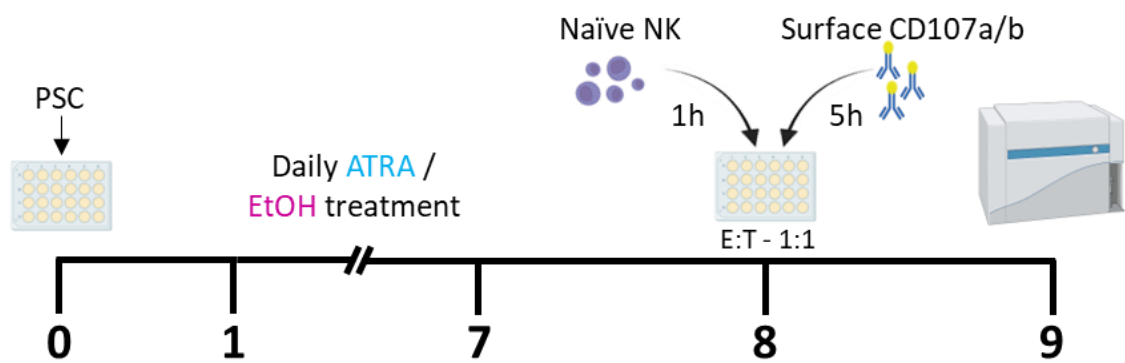


Figure 2.7: Schematic workflow of CD107 degranulation Assay.

PSCs were seeded in 24 well plates and treated daily with ATRA/EtOH for seven days in subdued light. On day 8, NK cells were added at a 1:1 effector: target ratio and stained for CD107a/b. Cells were incubated for a total of 6h. On day 9, samples were acquired on the Cytek Aurora Spectra Analyser.

2.14 Educated Degranulation Assay

Following optimisation, an effector: target ratio of 1:5 was chosen for the educated degranulation assay. On day 0, PSCs were seeded at a density of 400,000 or 100,000 cells/dish in 15cm cell culture plates and treated daily (in subdued light) with 1 μ M ATRA or EtOH, respectively, for seven days (days 1-7). On day 7, NK cells were passaged as per standard laboratory protocol. On day 8, BxPC3, Capan2 and MiaPaca2 cells were seeded at a density of 250,000 cells/well in 24 well plates and incubated overnight at 37°C, 5% CO₂ to allow adherence. Concomitantly, NK cells were incubated with qPSCs or aPSCs at a ratio of 1:1 (seeding densities of 1,200,000 or 1,700,000 cells per dish, respectively). NK cells alone were seeded at a density of 1,700,000 cells/plate, controlling for any stimulation incurred as a result of increased NK cell density. PSC and NK cells were co-cultured in complete NK92 media +100 units IL-2 per mL and incubated for 24h at 37°C, 5% CO₂.

Following 24h incubation, NK cells were aspirated and centrifuged for 5 min at 250g. Culture media was aspirated, and the NK cells resuspended in complete RPMI. Cells were counted using a haemocytometer and trypan blue and resuspended at a density of 50,000 cells/140 μ L. Culture supernatant was aspirated from target (cancer) cells and the cells washed once in complete RPMI. The media wash was aspirated and 140 μ L/well of NK92 culture added to the cancer cell lines. Controls for each NK cell culture condition were also seeded. For stimulated controls, an aliquot of counted NK cells was transferred to a fresh falcon tube and stimulated with PMA and Ionomycin. Following stimulation, cells were transferred to a 24-well plate and the cells stained as previously described (Figure 2.8).

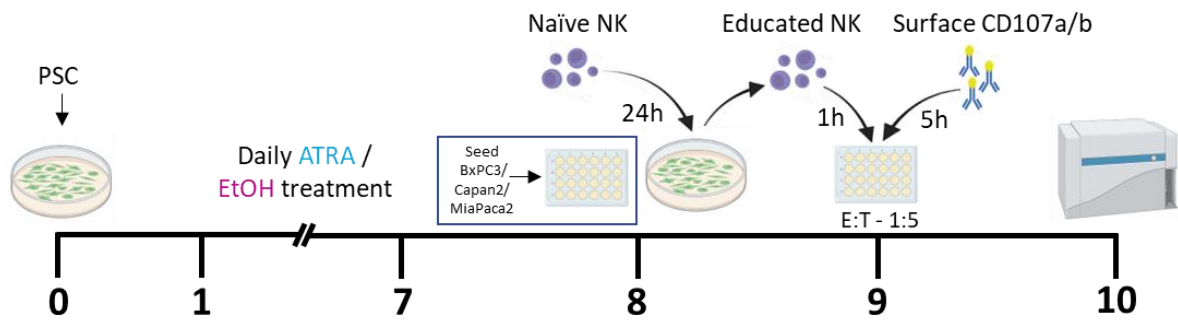


Figure 2.8: Experiment workflow of Educated NK cell degranulation assay.

PSCs were seeded in 15cm dishes and treated daily for 7 days with ATRA/EtOH in subdued light. On day 8, NK cells were incubated at a 1:1 ratio with either quiescent or activated PSCs, or alone. On day 9, educated NK cells were co-cultured with cancer cells at a 1:5 effector to target ratio and stained for CD107a/b. Samples were acquired on the Cytex Aurora on day 10.

2.15 Calcein AM Cytotoxicity Assays against PSC

Briefly, PSCs were seeded in 96-well plates and treated for daily 7 days with ATRA/ethanol (in subdued light). On day 8, PSCs were stained with 10 μ M (titrated for optimal difference between maximum and spontaneous release)²⁴⁷ of Calcein AM cell permeable dye (diluted in serum free RPMI) for 1h at 37°C. Cells were then washed twice with complete RPMI before incubating with naïve NK cells at effector: target ratios of 5:1, 1:1, 1:5 and 1:10 for 6h. Fluorescent dye release was measured using the Tecan M200 microplate reader (Tecan Trading AG, Switzerland); excitation 494nm, emission 530nm. To establish maximum and baseline release controls, respectively, cells were treated with media containing 2% Triton X-100 (TB0198, BioBasic) or complete media only. Percent cell lysis was calculated as follows:

Percent cell lysis = [(test release – spontaneous release)/ (maximum release – spontaneous release)] x 100.²⁴⁸ A schematic representation of the workflow is shown in Figure 2.9.

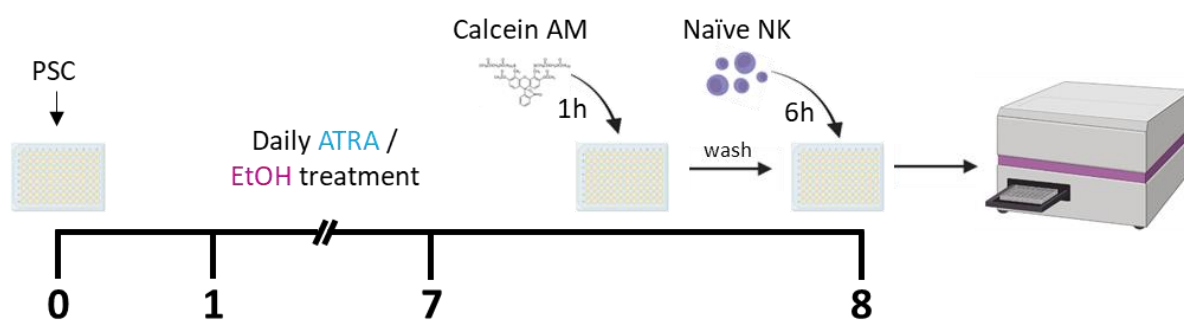


Figure 2.9: Experimental workflow of Calcein AM cytotoxicity assays against quiescent and activated PSCs.

PS1 cells were seeded in 96 well plates and treated daily for 7 days with ATRA/EtOH in subdued light. On day 8, cells were stained for 1h with 10 μ M Calcein AM before incubating with NK cells at 5:1, 1:1, 1:5 and 1:10 effector to target ratios. Fluorescence intensity was measured at excitation 494nm, emission 530nm.

2.16 Educated NK cytotoxicity assay

For educated NK cytotoxicity assays, PSCs were seeded in 15cm dishes and treated daily with ATRA or ethanol for 7 days. Naïve NK cells were incubated either alone or with qPSC/aPSC at a 1: 1 ratio for 24h. On the same day, MiaPaca2, BxPc3 and Capan2 cells were seeded in 96-well plates and allowed to adhere overnight. Following adherence, cancer cells were stained with 10 μ M Calcein AM dye for 1h (as above). Educated NK cells were then incubated with cancer cell lines at effector: target ratios of 5:1, 1:1, 1:5 and 1:10 for 6h. Plates were read and percent lysis calculated as above. Figure 2.10 demonstrates a schematic workflow of the educated degranulation assay.

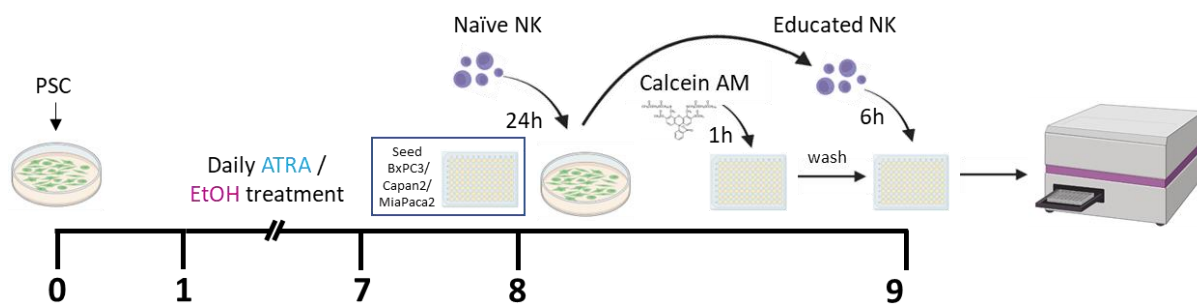


Figure 2.10: Schematic workflow of educated NK cell cytotoxicity assays against cancer cell lines.

PSCs were seeded in 15cm dishes and treated daily with ATRA/EtOH (in subdued light) for 7 days. On day 8, NK cells were co-cultured with qPSC/aPSCs or alone for 24h. On day 9, cancer cell lines were stained for 1h with 10 μ M Calcein AM before being incubated with educated or naïve NK cells at multiple E:T ratios for 6h. Fluorescence intensity was measured at excitation 494nm, emission 530nm.

2.17 Receptor/Phenotype Expression Assay

In order to determine the impact of co-culture on PSC and NK phenotype a receptor/phenotypic expression assay was carried out. An overview of the flow cytometry workflow is outlined in Figure 2.11.

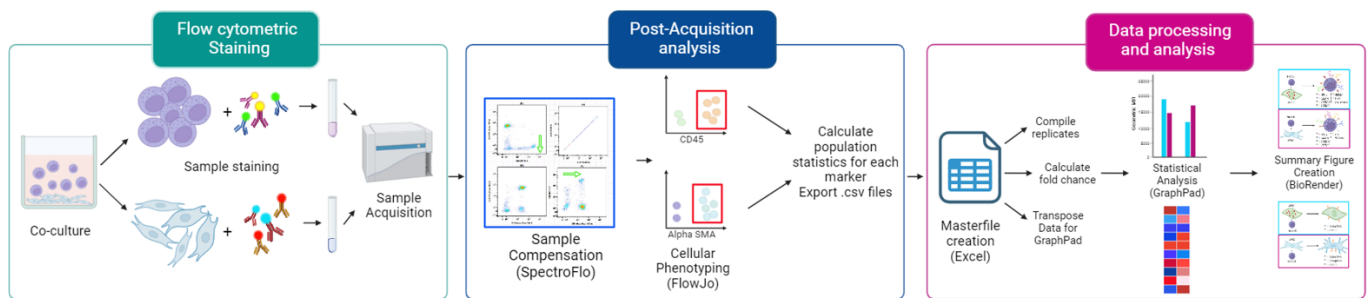


Figure 2.11: Flow cytometry workflow.

NK cells and PSCs were co-cultured according to experimental need. Following culture, cells were stained with surface and intracellular antibodies and samples acquired on the Cytex Aurora (Cytex Biosciences). Samples were then compensated using SpectroFlo software. Cellular phenotypes were explored for each population, with gating strategies established using fluorescence minus one and reference controls. Population statistics including percentage of parental population and Geometric Mean Fluorescence intensity were calculated for each marker of interest and the data tables exported as .csv files. These data were then used to create a Masterfile by combining replicate data, calculating receptor fold change and preparing the data for transfer to the statistical analysis software, GraphPad. Data were then statistically analysed and represented graphically. Finally, summary figures were created (using BioRender) to provide an overview of the changes/interactions observed.

2.17.1 Direct Contact and Transwell™ Experiments

Briefly, PSCs were seeded at densities of 16,000 cells/well or 2,000 cells/well for ATRA and ethanol treatment, respectively, yielding approximately 50,000 cells/well. For PSC controls, cells were seeded at a density of 7,000 cells/well. Cells were treated daily with ATRA/EtOH or media alone for 7 days in subdued lighting. On day 7, NK92 cells were passaged in preparation for co-culture experiments. On day 8, NK92 cells were passaged as standard and resuspended at a density of 50,000 cells in either 100µL (stock A), 250µL (stock B) or 600µL (stock C) of complete NK92 media + 100 units IL-2 per mL.

For direct contact experiments (Figure 2.12), the supernatant was aspirated from each well and the cells washed with 200µL of complete NK92 media to remove any traces of ATRA/ethanol. 600µL of stock C was then added directly to each co-culture well. For conditions without NK92 cells, 600uL of complete NK92 media +IL-2 was added per well. Cells were incubated for 24h at 37°C, 5% CO₂.

For Transwell™ experiments (Figure 2.13) the media from each well containing PSCs was aspirated and the cells were washed as described. 600µL of complete NK92 media plus 100 units IL-2/mL was then added to the lower compartment of the Transwell™ plate (3413, Costar). Transwell™ inserts were then transferred into position using sterilised forceps. 100µL of stock A was then transferred to the required Transwell™ inserts. For conditions without NK92 cells, 100µL of complete NK92 media +IL-2 was added. Cells were incubated for 24h at 37°C, 5% CO₂.

Following co-culture, all supernatants (for both direct contact and Transwell™) were transferred to 1.5mL Eppendorf tubes. Those containing NK92 cells were centrifuged at 300g for 5 min, the supernatant aspirated and transferred to a fresh Eppendorf tube. Supernatants

were stored short-term at 4°C prior to preparation for Luminex analysis. NK cells were transferred to a pre-labelled v-bottom 96-well plate ready for staining. Concomitantly, PSCs were trypsinised and transferred to a separate pre-labelled v-bottom 96 well plate.

Controls for direct contact assays were prepared by transferring 250µL of stock B to each well of a 24-well plate. Cells were incubated for 24h, 37°C, 5% CO₂. For stimulated NK cell controls, after 20h incubation, plates were removed from the incubator and 1x PMA/Ionomycin, brefeldin A and monensin were added. The plates were mixed by gentle shaking and incubated for a further 4h.

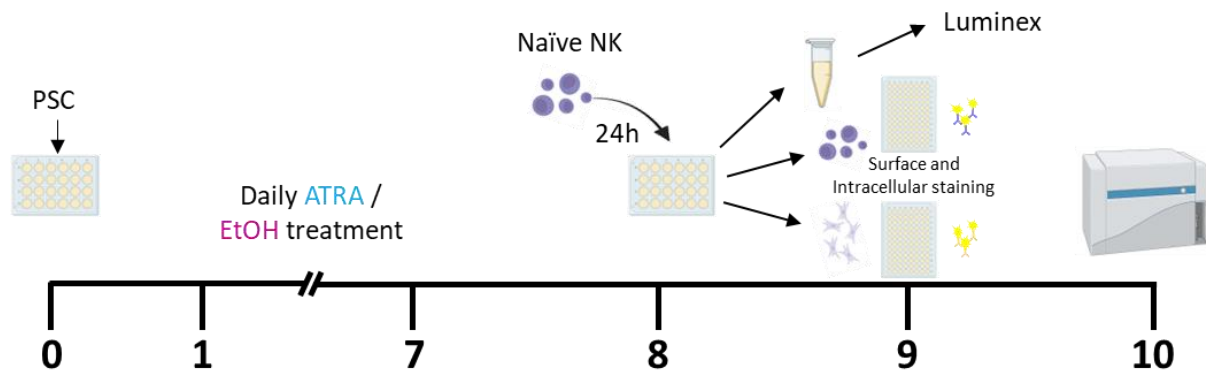


Figure 2.12: Schematic representation of the workflow for direct contact receptor/phenotypic expression assays.

PSCs were seeded in 24 well plates before treating daily with ATRA/EtOH for 7 days in subdued light. On day 8, naïve NK cells were co-cultured with qPSC or aPSCs for 24h at a 1:1 ratio. On day 9, culture supernatant was collected for Luminex analysis and NK cells and PSCs stained for surface and intracellular markers. Samples were acquired on the Cytex Aurora on day 10.

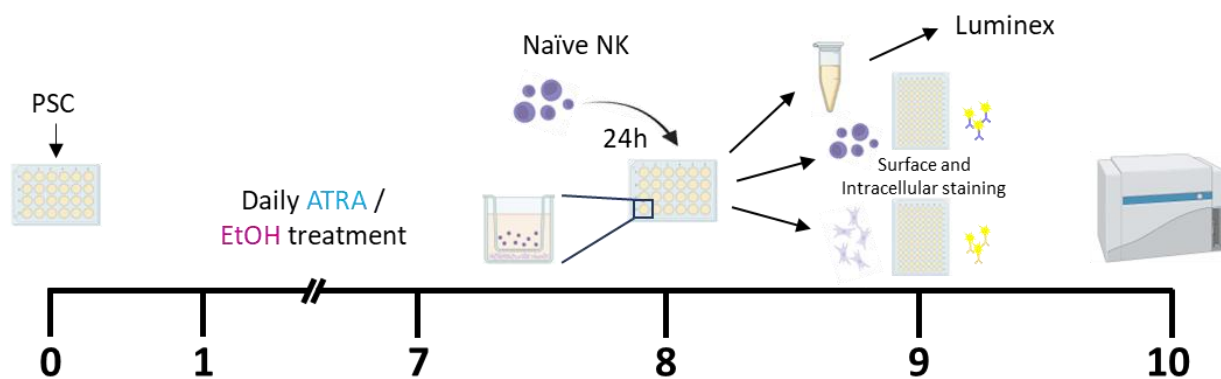


Figure 2.13: Schematic representation of the workflow for Transwell™ receptor/phenotypic expression assays.

PSCs were seeded in 24 well plates before treating daily with ATRA/EtOH in subdued light. On day 8, naïve NK cells were added to 0.4µm Transwell™ inserts and cultured with qPSC or aPSCs. On day 9, culture supernatant was collected for Luminex analysis and NK/PSCs stained for surface and intracellular markers. Samples were acquired on the Cytex Aurora on Day 10.

2.17.2 Conditioned Media Experiments

To investigate the impact of secreted factors on receptor/phenotypic expression in PSCs and NK cells, conditioned media experiments were employed.

Briefly, PSC conditioned media was created by seeding 400,000 and 100,000 PSCs in 15 cm dishes (day 0) and treating cells daily with ATRA/EtOH (day 1-7) in subdued light. On day 8, media was aspirated from qPSC/aPSCs and the cells gently washed with 5mL complete NK92 media. The culture wash was aspirated and 13mL/dish of complete NK92 media containing 100 units IL-2 per mL was added. PSCs were incubated at 37°C for 24h. Conditioned media was aspirated from qPSC/aPSC and transferred to 50mL falcon tubes. The conditioned media was then centrifuged at 600g for 5 minutes to pellet any cells/cellular debris. An aliquot of conditioned media was transferred to a fresh falcon tube (with care taken not to disturb the cell pellet), and 100 units/mL of IL-2 added. For NK conditioned media, on day 8, NK92 cells were seeded at a density of 250,000 cells/mL in 13mL of complete NK92 media (+ 100 units/mL IL-2) in 15 cm dishes. The cells were then incubated at 37°C for 24h. NK cells/conditioned media were then aspirated and prepared as described.

Concomitantly, PSCs were seeded in 24 well plates at a density of 16,000 or 2,000 cells/well (day 1) and treated daily for 7 days with ATRA/EtOH (days 2-8). On day 9, culture media was aspirated and the cells gently washed. 600µL/well of NK conditioned media was then added to each well. For NK cells, 3mL of stock C was transferred to a fresh falcon tube and

centrifuged (300g for 5min). The supernatant was aspirated and 3mL of qPSC conditioned media was added. This was repeated for aPSC conditioned media. For each condition, three wells of conditioned media treated NK cells were seeded in 24-well plates (600µL/well). For NK controls, 600µL of culture from stock C was added to the well. Cells were incubated at 37°C, 5% CO₂, for 24h.

On day 10, NK and PSCs were harvested and prepared for flow cytometric staining as described.

Schematic workflows of conditioned media experiments are shown in Figure 2.14 and Figure 2.15 .

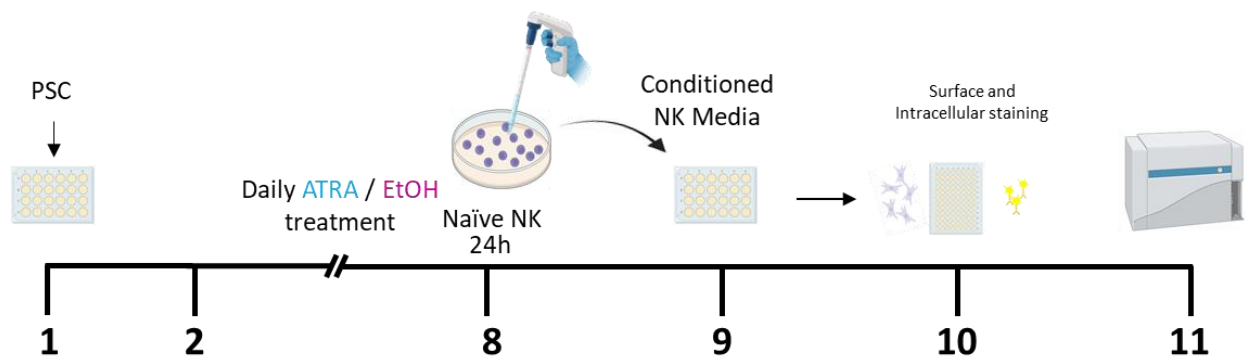


Figure 2.14: Schematic diagram of the experimental workflow for PSCs treated with NK conditioned media.

PSCs were seeded in a 24 well plate and treated daily with ATRA/EtOH for 7 days in subdued light. On day 8, naïve NK cells were cultured in a 15cm dish and incubated for 24h. On day 9, conditioned media was collected from NK cells and transferred to the qPSC/aPSC. Cells were cultured for 24h before completing surface and intracellular flow cytometric staining. Samples were acquired on the Cytek Aurora on day 11.

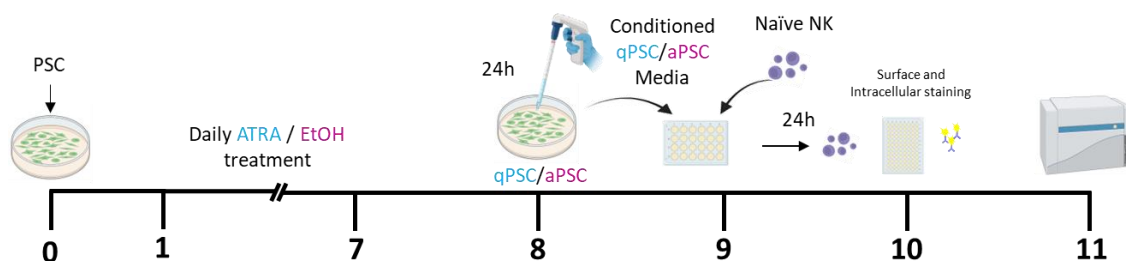


Figure 2.15: Schematic diagram of the experimental workflow for NK cells treated with qPSC/aPSC conditioned media.

PSCs were seeded in 15cm dishes before treating daily with ATRA/EtOH for 7 days in subdued light. On day 8, complete media was added to qPSC and aPSCs and the cells incubated for 24h. On day 9, conditioned media was collected and naïve NK cells seeded in 24 well plates in conditioned media. Cells were incubated for 24h before staining for surface and intracellular markers. Samples were acquired on the Cytek Aurora on day 11.

2.18 Luminex ELISA

Cell culture supernatant was removed from 4°C short term storage (3-5h) and cellular debris removed via centrifugation. Aliquots of culture supernatant were then transferred to fresh Eppendorf tubes. Samples were stored at -20°C until sample acquisition.

Luminex ELISA and analyte concentration calculations were performed by Veonice Au (Institute of Molecular and Cell Biology, A*STAR). Cytokines and chemokines from direct contact and Transwell™ culture supernatants were analysed using the 65-plex Immune Monitoring ProcartaPlex™ Panel (EPX650-10065-901, ThermoFisher). Assays were performed according to the manufacturer's guidelines. Plates were read using Flexmap 3D system (Luminex Corporation) and analysed using Bio-Plex manager v 6.2 (Bio-Rad Laboratories, Hercules, California, USA). A 5-parameter curve-fitting algorithm was applied for standard curve calculations. Logarithmically transformed, averaged analyte concentrations were presented as a heatmap using the R package, ComplexHeatmap²⁴⁹ (R v 4.1).

2.19 Proteomics

To identify differences in protein expression following qPSC/NK and aPSC/NK co-culture global proteomic analysis was carried out. An overview of the proteomic workflow is shown in Figure 2.16. Global Proteomic analysis was conducted in collaboration with Dr Parthiban Periasamy (Institute of Molecular and Cell Biology, A*STAR).

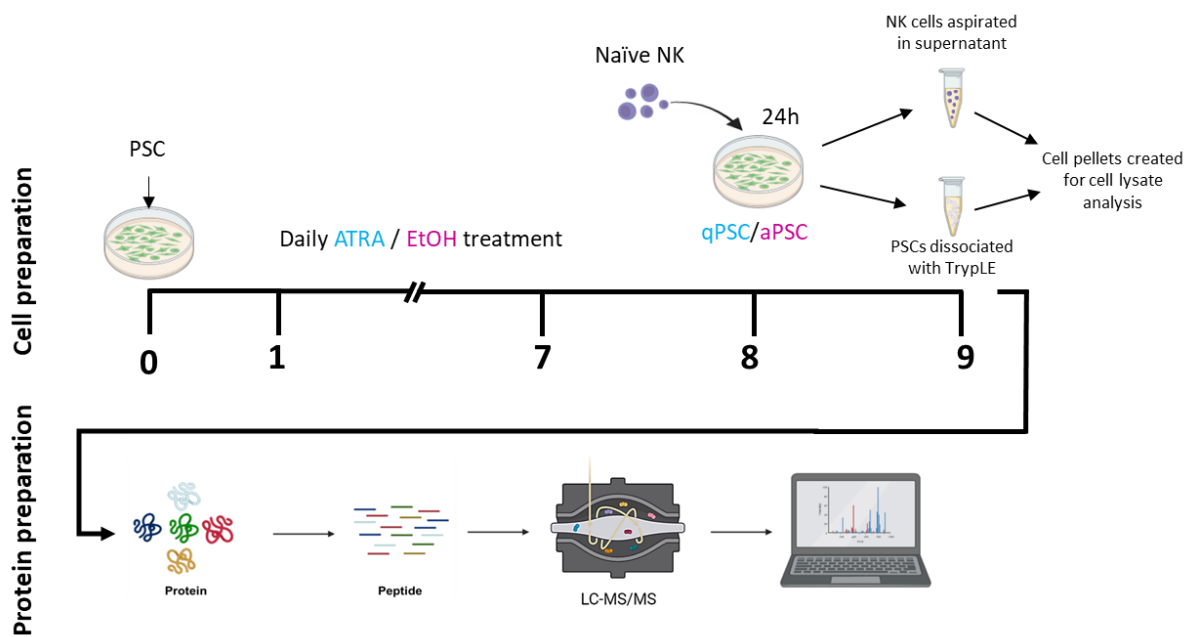


Figure 2.16: Schematic workflow of proteomic sample preparation and acquisition.

PSCs were seeded in 15cm dishes and treated daily with ATRA/EtOH for 7 days in subdued light. On day 8, naïve NK cells were cultured with PSCs at a 1:1 ratio and incubated for 24h. Cell pellets were then created for each cell type on day 9. Cells were lysed and the proteins extracted. The extracted proteins were reduced and linearised into short peptides. Peptides were cleaned, lyophilised and resuspended in 0.1% formic acid before acquisition on the mass spectrometer. Following acquisition, the data was cleaned and post-acquisition analysis conducted.

2.19.1 Cell culture

PSCs were seeded in Nunc™ EasYDish™ 15cm dishes (150468, Nunc) in DMEM/Ham's F12 media with 10% FBS (10082147, Gibco) at densities of 400,000 and 100,000 cells per dish for ATRA and EtOH treatments, respectively. Cells were treated daily with ATRA/EtOH for 7 days in subdued light. On day 8, media was aspirated, and NK cells were added at a 1:1 ratio in complete NK media. Cells were incubated for 24h at 37°C, 5% CO₂. Following incubation NK cells and media were transferred to a fresh 15mL Falcon tube. PSC were detached from the plate using TrypLE dissociation reagent (12604013, Gibco) and were centrifuged for 5 min at 300g. The supernatant was aspirated and the cell pellet washed in 4mL sterile PBS. Cells were then centrifuged for 5 min at 300g, the supernatant aspirated and cell pellets stored at -80°C overnight. Similarly, NK cells were prepared by centrifugation at 300g for 5 min and the supernatant removed. NK cells were washed in PBS and pelleted (300g, 5 min). The supernatant was aspirated and the cell pellet stored at -80°C overnight.

2.19.2 Dead cell exclusion

Dead cells were excluded from proteomic analysis using the EasySep™ Dead Cell Removal (Annexin V) Kit (17899, StemCell Technologies). Cells were processed according to manufacturer guidelines. Briefly, cell pellets were resuspended in 100µL of the recommended buffer (PBS + 2%FBS and 1mM CaCl₂) and samples transferred to 5mL polystyrene round bottom tubes. 5µL of dead cell removal (Annexin V) cocktail was added to each sample. The sample was mixed using a pipette and incubated at RT for 3 min. RapidSpheres were vortexed for 30 sec and 10µL added per sample. The sample was then immediately topped up with recommended media to a total volume of 2.5mL and mixed. Samples were then placed in an EasySep Magnet and incubated for 3 min at RT. The magnet and tube were then inverted and

the enriched cells transferred to a new, pre-labelled 15mL falcon tube. The cells were washed with PBS and the supernatant removed. Cell pellets were stored at -80°C overnight.

2.19.3 Peptide Preparation

To extract cellular proteins, samples were lysed using 10% SDS in 30mM Triethylammonium bicarbonate buffer (TABC) (T7408, Sigma-Aldrich). 150µL or 400µL of lysis buffer was added to NK cell and PSC pellets, respectively. Each sample was vortexed and placed on ice. Samples were then probe sonicated to further aid lysis using the QSonica Sonicator. The sonicating probe was placed at least half-way into the cell suspension. Each sample was subjected to 10x one second pulses. Samples were then maintained on ice for 1h. The protein concentration of each sample was then calculated using the Pierce BCA protein assay kit (23227, ThermoFisher). Samples were prepared in accordance with the manufacturer's guidelines. Briefly, protein standards were reconstituted according to the manufacturer's guidelines in 2% SDS in 30mM TABC. Standards were vortexed and centrifuged for 1 min at 21300g. Samples were then centrifuged for 3 min at 3220g at 4°C. 25µL of protein standards and samples were added to a 96 well plate. A working reagent was created by combining reagents A and B at a 50:1 ratio. 200µL of working solution was added to each well and the plate was incubated for 15 min at 37°C. The plate was cooled at RT for 3 min and the absorbance of each sample was measured at 592nm. A standard curve was created by plotting the absorbance of each standard (background absorbance subtracted) on a scatter plot. The amount of protein per sample was then calculated based on the equation generated from the standard curve. 100µg of protein for each sample was then transferred to a fresh Eppendorf tube (0030 120.086, Eppendorf), and samples were normalised to 200µL in 30mM TABC. Dithiothreitol (DTT) (10708984001, Sigma-Aldrich) was then added to a final concentration of

5mM per sample. Samples were incubated at 60°C, 15 min on a heat shaker, 800rpm. A 0.5M stock of Idoacetamide (IAA) (I1145-25G, Sigma- Aldrich) was then created in 30mM TABC. Following incubation, samples were centrifuged briefly to cool. IAA was then added to a final concentration of 5mM. Samples were vortexed and centrifuged before incubating in the dark for 10 min (RT). 50µg of protein per sample was then transferred to fresh Eppendorf tubes and the samples normalised to 150µL. 1mL of acetonitrile (ACN) (51101, ThermoFisher) was then added to each sample to precipitate the protein. Samples were centrifuged for 3 min at 21300g before incubating for 4h at -20°C. Samples were centrifuged for 2 min, 21300g and stored overnight at -80°C. Following overnight incubation, samples were centrifuged for 30 min, 21300g at 4°C before maintaining at -80°C for a further 1h. Samples were then centrifuged for a further 40 min, 21300g at 4°C. The supernatant was then aspirated and the cell pellet resuspended in 100% ACN. Samples were vortexed and centrifuged for 10 min, 21300g at 4°C. The supernatant was then aspirated and 20µL (2µg) of Platinum grade trypsin (VA9000, Promega) was added to each sample (1:25 trypsin: protein ratio). Samples were vortexed to mix and briefly centrifuged before transferring to a heat shaker and incubating overnight at 37°C at 500rpm. Following overnight incubation, trypsin was inactivated by the addition of 0.1% (final volume) formic acid (85178, ThermoFisher) and the samples incubated for 10 min at 37°C, 500rpm. Samples were then centrifuged and maintained at RT. C18

Peptide Clean-up

In order to remove unwanted salts and large proteins (such as trypsin) from the sample, C18 filter tips were created by cutting 4, 2mm discs of Empore Octadecyl C18 membrane (66883-U, CDS) and placing them inside 200µL pipette tips. The discs were gently compacted within the tip using a blunt end needle. Filter tips were placed inside fresh Eppendorf tubes and were held in place using spin columns. The filter tips were calibrated by the addition of 200µL of

80% acetonitrile in 0.1% formic acid. The tips were centrifuged at 1000g for 1 min. The waste was discarded and 200µL of 0.1% formic acid in MilliQ water was added to each tip. Tips were centrifuged 1000g/1 min. Samples were centrifuged a second time at 1200g, 1 min to elute the remaining buffer. Tips were transferred to new Eppendorf tubes. 180µL of 0.1% formic acid was added to each sample and the samples transferred to the corresponding pre-labelled tip. Samples were centrifuged at 1000g for 1 min 30 sec. Eluted samples were reloaded into the C18 tip and centrifuged at 1000g for 1 min 30 sec. Tips were transferred to fresh Eppendorf vials and the flow through tubes labelled accordingly. 200µL of elution buffer (40% ACN in 0.1% formic acid) was then added to each tip. Samples were centrifuged at 1000g for 2 min 30 sec. Tubes containing the eluted peptides were labelled and the samples lyophilised using a speedvac for 2h. Samples were resuspended in 27µL of 0.1% formic acid and sonicated in a water bath for 10 min, 37°C to improve peptide solubility. Samples were centrifuged and peptide concentration estimated using the NanoDrop™ One (Thermo Scientific).

2.19.5 Peptide Estimation

Protein A205 was selected to analyse peptides using the 31 method. 2µL of 0.1% formic acid was placed onto the NanoDrop™ platform and the arm gently closed. This generated a background level for the samples. The NanoDrop™ reader was cleaned using a Kim wipe. 2µL of sample 1 was loaded onto the NanoDrop™ stage, the arm lowered and the peptide content measured. The arm was raised, and the stage and arm cleaned. This process was repeated for each sample. Following estimation, 2µg of peptide per sample was aliquoted to a new, labelled Eppendorf tube and sample volumes normalised to 5µL. Samples were stored at -20°C until acquisition on the mass spectrometer.

2.19.6 Acquisition on the Mass Spectrometer

Samples were brought to room temperature and centrifuged before transferring to a 96 well plate. 2.5µL of each sample was injected for mass spectrometry. Samples were acquired using the Fourier Transform and Ion Trap method in the following order: NK cells cultured with qPSC (x3), blank, NK cells cultured with aPSC (x3), blank, qPSC cultured with NK cells, blank, aPSC cultured with NK cells. Mass spectrometry was performed by the functional proteomics laboratory of Dr. Radoslaw M. Sobota (Institute of Molecular and Cell Biology, A*STAR).

2.19.7 Post-Acquisition analysis

Post-acquisition peptide alignment and characterisation and data clean-up was carried out by Dr Parthiban Periasamy (Institute of Molecular and Cell Biology, JY Lab, A*STAR). The inverse log of each protein abundance was then calculated. Heatmaps of differential protein expression between culture conditions were plotted using Z-score with the R package, ComplexHeatmap (initial R code provided by Dr Parthiban Periasamy).²⁴⁹ The biological pathways associated with up- and down- regulated proteins were further investigated using ProteoMaps²⁵⁰ (www.proteomaps.net).

2.19.8 RNA- Seq analysis

Proteins identified as significantly up- and down regulated were subsequently investigated in publicly available TCGA and GTEx RNA-Seq databases. Briefly, corresponding genes associated with proteins of interest were input into the online web server GEPIA: Gene Expression Profiling and Interactive Analysis.²⁵¹ Boxplots of the log-fold change in RNA transcripts per million for PDAC and matched controls were then plotted for genes of interest. Significance was established at $p < 0.05$, and Log2 Fold Change cut-off set to 1.

GEPIA software was also used to create Kaplan-Meier survival analysis plots of the proteins of interest. Patients were dichotomised based on high or low RNA expression (transcripts per million), with the dichotomisation threshold set at the third quartile. Significant differences in survival were calculated using the log-rank test.

2.20 Immunofluorescent staining of NK cells in Human spleen tissue

2.20.1 Antibody Titration

To establish optimal immunofluorescent staining conditions, anti-CD56 (ab118291, Abcam), anti-NKG2D (ABIN1027685, antibodies online) and anti-NKG2A (GTX108498, Genetex) antibodies were titrated at dilutions of 1:100, 1:250, 1:500 and 1:1000. Briefly, slides were rehydrated by passing through concentrations of xylene and ethanol: xylene 2x (5 min), 100% ethanol 2x (5 min), 80% ethanol (2 min), 70% ethanol (2 min), 50% ethanol (2 min), distilled water (5 min). Slides were then heated (microwave) for 12 min in citrate buffer (pH 6.0). Following antigen retrieval, slides were blocked with 5% goat serum in PBS-ABC, for 1h (RT). Slides were then incubated with primary antibodies overnight (4°C). Slides were washed 3 times in PBS+0.05% Tween (5 min/wash). Secondary antibodies were then added (Donkey anti-goat AlexaFluor 647 (1:500), Goat anti-mouse AlexaFluor 488 (1:500), Goat anti-rabbit AlexaFluor 546 (1:500)) and incubated for 1h, RT in the dark. Slides were counterstained and mounted with ProLong Gold Antifade mountant with DAPI, and images acquired on the LSM710 laser scanning confocal microscope (Zeiss).

2.20.2 Background troubleshooting

Initial staining demonstrated high background fluorescence. To address this, different blocking agents and secondary antibody dilutions were trialled (Table 2.10).

Blocking Condition	Primary Antibody Dilution	Secondary Antibody Dilution
5% Goat Serum	None	1:400
5% Goat Serum	1:100	1:400
5% Goat Serum		1:1000
3% BSA		1:400
3% BSA		1:1000
Secondary only controls with different blocking agents		
No Blocking	None	Donkey Anti-Goat AlexaFluor647, 1:500 Goat Anti-Rabbit AlexFluor546, 1:1000 Goat Anti-Mouse AlexaFluor488, 1:1000
5% Goat Serum		
5% Horse Serum		
1% BSA		
5% BSA		

Table 2.10: Blocking conditions and secondary antibody dilutions trialled to troubleshoot the high level of background staining observed in human spleen tissue.

Primary and secondary antibody dilutions are indicated for each blocking agent tested. All other protocol steps remained unaltered.

2.20.3 Antibody Titration using a different immunofluorescent staining protocol

Due to persistent high background fluorescence, a different immunofluorescent protocol was trialled. Key differences are highlighted in Table 2.11. Antibodies dilutions are shown in Table 2.12.

Protocol Step	Original Protocol	New Protocol
<i>Antigen retrieval</i>	Microwave, 12 min	Microwave, 20 min
<i>Wash Buffer</i>	PBS + 0.05% Tween	TBS+0.025% Triton X-100
<i>Antibody Diluent</i>	PBS-ABC	TBS+1%BSA
<i>DAPI</i>	ProLong Gold Antifade Mountant with DAPI	DAPI (1:5000)

Table 2.11: Key difference between Immunofluorescent staining protocols trialled.

Anti-CD56	Anti-NKG2D	Anti-NKG2A
1:50	1:100	1:100
1:100	1:200	1:250
1:200	1:500	1:500
Isotype 1:50	Isotype 1:100	Isotype 1:100
Secondary only control 1:500	Secondary only control 1:500	Secondary only control 1:500

Table 2.12: Antibody dilutions tested in spleen and tonsil tissue using a new immunofluorescent protocol.

2.20.4 Immunohistochemical evaluation of antibody signal

Following initial IHC assessment of anti-CD56, anti-NKG2D and anti-NKG2A antibodies gratefully carried out with the help of Dr Andrew Clear (Barts Cancer Institute), further antibody titration was undertaken. Two protocols were used for antibody optimisations. For CD56 (Abcam), NKG2D and NKG2A antibodies slides were dewaxed at 60°C for 20 min. Slides were then passed through the following reagents: xylene (2x 5 min), 100% ethanol (2 min), hydrogen peroxide in methanol (10 min), 100% ethanol (2 min), 80% ethanol (1 min), 70% ethanol (1 min), 50% ethanol (1 min) distilled water (2 min) to facilitate deparaffinization and the blocking of endogenous peroxidases. Slides were then heated in citrate buffer to perform antigen retrieval and washed in TBS + 0.025% Triton X-100. Horse (CD56 and NKG2A) or goat (NKG2D) serum diluted in TBS (1:25) (30 min) was then added to block non-specific antibody binding. Primary antibodies (diluted in TBS + horse/goat serum (1:25)) were incubated overnight (4°C). Slides were washed and secondary antibodies incubated for 40 min at RT. Slides were incubated for 30 min with ABC before staining with DAB for 2 min. Slides were counterstained with Mayer's Haematoxylin (5 min) and dehydrated (reverse xylene and ethanol series, no hydrogen peroxide). For CD56 (DAKO) slides were dewaxed as described before passing through the following reagent series to facilitate deparafinisation and blocking of endogenous peroxidases: xylene (2x 5min), 100% ethanol (2 min), 100% ethanol (2 min), 80% ethanol (2 min), hydrogen peroxide in methanol (10 min), 70% ethanol (2 min), 50% ethanol (2 min), distilled water (2 min). Antigen retrieval was then carried out by heating the slides in citrate buffer (pH 6.0). Slides were washed in TBS+0.05% Tween and blocked with Goat Serum in TBS (1:100) (30 min). Primary antibodies were then diluted in 0.1% sodium azide +5% BSA in PBS and incubated for 40 min at RT. Slides were washed and incubated with secondary antibodies for 30 min (RT). ABC was then applied for 20 min (RT) before incubating

with DAB for 10 min. Slides were counterstained with Mayers haematoxylin for 3 min and dehydrated by passing through the reverse xylene/ethanol series (no hydrogen peroxidase). Antibody details and antigen retrieval methods for each antibody are outlined in Table 2.13 and Table 2.14.

Antibody	Dilution	Antigen retrieval method	Tissue type tested
CD56 (DAKO)	1:50	Microwave and Pressure Cooker	Tonsil
CD56 (Abcam)	1:500	Microwave and Pressure Cooker	Tonsil
	1:750		
	1:1000		
	1:5000		
NKG2D	1:25	Microwave	Spleen and Tonsil
	1:50		
	1:100		
NKG2A	1:100	Microwave	Spleen and Tonsil
	1:500		
	1:1000		

Table 2.13: Dilutions, antigen retrieval method and tissue type used for immunohistochemical analysis of anti-CD56, anti-NKG2D and anti-NKG2A antibodies.

Staining with CD56 DAKO antibody was used as a positive control.

CD56 Antibody Dilution	Antigen retrieval method	Tissue type tested
No Primary Antibody	Microwave and Pressure Cooker	Spleen
1:50		
1:100		
1:200		

Table 2.14: Dilutions, antigen retrieval method and tissue type used for immunohistochemical analysis of the anti-CD56 antibody from DAKO.

2.20.5 IHC antibody optimisations for Multiplex Immunohistochemistry

Prior to carrying out multiplex immunohistochemical staining of pancreatic cancer tissue microarray sections, the following antibodies were optimised using the Leica Bond-Max Autostainer (Leica Biosystems) (Table 2.15).

Antibody	Clone	Catalogue number	Company
Periostin	EPR20806	ab215199	Abcam
Myosin-11	MYH11/923	NBP2-44533	Novus Biologicals
CD105/Endoglin	3A9	14606	Cell Signalling Technology
NKp46	EPR22403-57	ab244703	Abcam
NKG2D	1D11	NB100-65956	Novus Biologicals

Table 2.15: Antibodies optimised prior to mIHC staining.

2.20.6 Slide setup

Slides were set up using the Leica BOND online system. For each titration, a 'case' was created. Within each case, the details of each antibody dilution and epitope retrieval condition (ER1: citrate-based retrieval, pH 6.0 (AR9961, Leica Biosystems); ER2: Tris-EDTA based retrieval, pH 9.0 (AR9640, Leica Biosystems)) were input to create a staining profile for each slide. This generated a unique slide identification number which was subsequently printed onto a label and attached to the corresponding slide. Labelled slides were loaded into slide racks and covered using Leica BOND universal covertiles (S21.4611, Leica Biosystems). Slides were loaded into the autostainer and the slide tags imaged.

2.20.7 Antibody preparation

Antibodies were diluted in 5mL round bottom tubes using DAKO antibody diluent with background reducing components (S3022, DAKO), and inserted into BOND titration containers (OPT9049, Leica Biosystems). Each titration container was scanned, and the volume of the container refilled to 6mL prior to staining using the BOND software (Leica Biosystems). The titration containers were placed into a titration container rack and inserted into the autostainer. The antibody volume in each titration container was estimated by an automated probe to ensure enough antibody was present to complete the staining run. A BOND refine polymer detection kit (DS9800, Leica Biosystems) containing hydrogen peroxide, polymers and DAB was inserted into the autostainer system and the levels of the reagents calculated. Once the level of reagents had been assessed, the staining run was scheduled using the BOND software.

Antibody dilutions and antigen retrieval conditions tested for each antibody are displayed in

Table 2.15. Initial NKG2D titration was carried out by Craig Ryan Joseph (Institute of Molecular and Cell Biology, A*STAR). Details of additional incubation optimisations for NKG2D are shown in Table 2.17.

Antibody	Positive Control Tissue	Dilution	Antigen Retrieval condition
Periostin (ab215199)	Colon/ Placenta/ Stomach	1:500	ER1/ER2
		1:1000	ER1/ER2
		1:1500	ER1/ER2
		1:2000	ER1/ER2
		1:3000	ER1/ER2
	Normal Pancreas	1:1000	ER1
		1:1500	ER1
		1:3000	ER1
Myosin-11 (NBP2-44533)	Breast/ Prostate/ Skeletal Muscle	0.25µg/mL	ER1/ER2
		0.5µg/mL	ER1/ER2
		1µg/mL	ER1/ER2
		1.25µg/mL	ER1/ER2
		1.5µg/mL	ER1/ER2
	Normal Pancreas	1.25µg/mL	ER2
CD105 (14606)	Kidney /Placenta/ Tonsil	1:500	ER1/ER2
		1:1000	ER1/ER2
		1:1250	ER2
		1:1400	ER2
		1:1500	ER1/ER2
		1:2000	ER1/ER2
		1:2500	ER1/ER2
	Normal Pancreas	1:1400	ER2
NKp46 (ab244703)	Spleen	1:100	ER1/ER2
		1:250	ER1/ER2
		1:500	ER1/ER2
		1:1000	ER1/ER2
		1:1500	ER1/ER2

Table 2.16: Positive control tissue, antibody dilutions and antigen retrieval conditions tested for each optimised marker.

Antibody	Positive Control Tissue	Dilution	Antigen Retrieval condition	Incubation length
NKG2D (NB100-65956)	Tonsil	1:75	ER2	20min
				1h
				1h, Block, 1h
				1.5h (2x 45min)
				2h (2x 1h)

Table 2.17: Positive control tissue, antibody dilution, antigen retrieval condition and incubation length tested for NKG2D.

For IHC optimisations, the IHC HEA MAG protocol was selected, and the slides stained according to the pre-set protocol. Briefly, slides were heated to 99°C, before incubation with BOND epitope retrieval solution 1 or epitope retrieval solution 2 for 20 min. Endogenous peroxidases were then blocked using 3-4% (v/v) hydrogen peroxide for 10 min and slides were washed 3 times with BOND wash solution (AR9590, Leica Biosystems). Primary antibodies were then added and incubated for 20 min at room temperature (unless otherwise stated for NKG2D optimisation). Slides were washed as described and a rabbit anti-mouse post-primary linker added (8 min). This enabled the detection of mouse antibodies by the anti-rabbit horseradish peroxidase polymer. Slides were washed three times (2 min per wash) and an anti-rabbit poly-HRP-IgG added for 8 min. Slides were then washed twice with wash solution and once with deionised water. DAB substrate was then added for 10 min. Slides were washed three times with deionised water and counterstained with <0.1% Haematoxylin for 5 min. Slides then underwent three rounds of washing: deionised water, wash solution and deionised water.

2.20.8 Slide Dehydration and Mounting

Once the automated staining protocol had been completed, slides were removed from the autostainer and placed in a slide rack. Slides were then passed through the following concentrations of ethanol and xylene (2 min each) before mounting: 70% ethanol, 95% ethanol, 100% ethanol (three incubations), xylene (three incubations).

Once dehydrated, the slides were mounted with glass coverslips using DPX mounting medium (SEA-1304-00Z, CellPath). Slides were left overnight for the coverslips to adhere before imaging using the Olympus CKX53 inverted light microscope and Olympus EP50 camera. Scale bars were added to each image using ImageJ software.

2.21 Multiplex Immunohistochemistry

An overview to the multiplex immunohistochemical workflow is outlined in Figure 2.17.

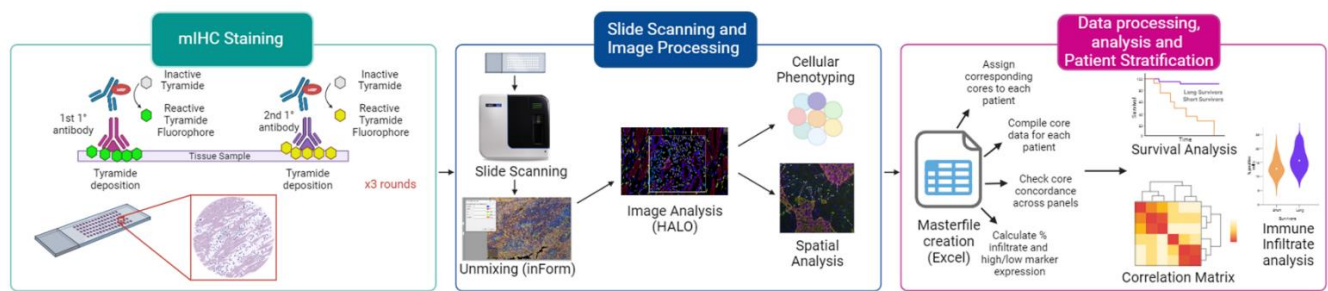


Figure 2.17: Overview of the mIHC workflow.

Tissue Microarray slides containing patient samples underwent three rounds of staining, with each round probing the tissue with two primary antibodies and two OPAL fluorophores. Upon binding of the secondary antibody, horseradish peroxidase catalysed the reaction of inactive tyramide to a reactive tyramide fluorophore. The reactive tyramide then bound covalently to tyrosine residues within the tissue. Antibodies were then stripped and the tissue re-probed with the next primary antibody. On the final round of staining slides were counterstained using spectral DAPI. Slides were then imaged using the Vectra Imaging system and the resultant images spectrally unmixed using inForm software (Akoya Biosciences). Component tif files were uploaded into HALO image analysis software (Indica Labs) for downstream analysis. Cellular phenotypes were identified based on the combination of markers of interest and the total number of cells expressing these phenotypes assessed. Spatial analysis was carried out using HALO's Spatial Analysis module (Indica Labs). All resultant data were exported as .csv files. Masterfiles were created for each panel in which corresponding cores were assigned to each patient. The concordance across cores was verified between panels, removing any cores which were missing in one or more of the panels. Cellular data from the cores of each patient were compiled and the percent positive cells calculated for each marker. This data was then used to dichotomise patients into high and low expression of each marker for survival analysis. Compiled data were then analysed using GraphPad to calculate survival analysis, correlation matrices and the prognostic impact of immune infiltrate.

2.21.1 TMA staining panels

Three panels were designed to investigate the interaction between NK cells and cancer associated fibroblasts (CAFs) in patient TMA sections. The staining order of each panel was determined based on antigen retrieval method and antibody expression, with more precious markers being stained earlier in the panel. The staining details for the markers included in each of the three panels are shown in Table 2.18.

Panel	Marker	Company/Cat Number	ER	Dilution	Positive Control Tissue
1	Alpha SMA	DAKO, M0851	No ER	1:800	Appendix
	Periostin	Abcam, ab215199	ER1	1:1500	Stomach/Colon/Placenta
	Myosin-11	Novus Biologicals, NBP2-44533	ER2	1.25ug/mL	Skeletal Muscle/Prostate/Breast Cancer
	Podoplanin	DAKO, M3619	ER2	1:200	Appendix
	CD105	Cell Signalling Technology, 14606	ER2	1:1400	Kidney/Tonsil/Placenta
	CK/EpCAM	DAKO, M3515 / Biolegend, 324202	ER2	1:200/1:800	Appendix
2	CD45	DAKO, M0701	ER1	1:800	Tonsil
	CD56	Leica (Novacastra), NCL-L-CD56-504	ER2	1:200	Brain
	NKG2D	Novus Biologicals, NB100-65956	ER2	1:75	Tonsil
	NKp46	Abcam, ab244703	ER2	1:1000	Spleen
	Vimentin	DAKO, M0725	ER2	1:200	Tonsil
	CK/EpCAM	DAKO, M3515 / Biolegend, 324202	ER2	1:200/1:800	Appendix
3	CD45	DAKO, M0701	ER1	1:800	Tonsil
	CD56	Leica (Novacastra), NCL-L-CD56-504	ER2	1:200	Brain
	NKG2A	Abcam, ab260035	ER1	1:4000	Tonsil
	LAG-3	Cell Signalling Technology, 15372	ER1	1:800	Tonsil
	Vimentin	DAKO, M0725	ER2	1:200	Tonsil
	CK/EpCAM	DAKO, M3515 / Biolegend, 324202	ER2	1:200/1:800	Appendix

Table 2.18: Multiplex immunohistochemistry staining panels with epitope retrieval conditions (ER), antibody dilutions and positive control tissues.

2.21.2 Preparation of OPAL dyes

OPAL dyes were reconstituted in 75µL of DMSO (DMSO0100UL, Akoya Biosciences), before being diluted (Table 2.19) in 1x plus automation amplification diluent (FP1609, Akoya Biosciences).

OPAL dye	Catalogue Number (Akoya Biosciences)	Dilution
OPAL 520	OP-001001	1:100
OPAL 570	OP-001003	1:100
OPAL 650	OP-001005	1:100
OPAL 540	OP-001002	1:100
OPAL 620	OP-001004	1:100
OPAL 690	OP-001006	1:50

Table 2.19: Dilutions of OPAL dyes

2.21.3 Automated mIHC staining

Prior to the staining of TMA sections, each panel was trialled on normal pancreas and pancreatic cancer sections.

For all mIHC (trial and TMA), three rounds of staining were carried out to achieve 7-plex images. Each round included two primary antibodies and two opal dyes, with the final round also including counterstaining with spectral DAPI. Briefly, slides were set up as described and labels affixed. Slides were heated to 99°C and incubated with epitope retrieval solution for 20 min. Endogenous peroxidases were then blocked with 3-4% (v/v) hydrogen peroxide for 10 min and slides washed (3x). Primary antibodies were incubated for 20 minutes (RT). Slides were washed three times with BOND wash solution and incubated with a rabbit anti-mouse post-primary antibody for 8 minutes. Slides were then washed (3x 2 minutes per wash) and OPAL polymer horseradish peroxidase (HRP) added for 8 minutes. Following another round of washing, the first OPAL fluor was added (10 minutes). Slides were then washed 3 times before being heated to 99°C and incubated with the second round of antigen retrieval (20 min). This removed the first primary antibody to allow re-probing. The second primary antibody of the staining round was then added (20 min, RT). The slides were then washed, linked with post-primary, incubated with HRP and stained with an OPAL dye as described, completing the first round of staining. Slides were then removed from the autostainer and new unique slide identifiers printed and affixed. This staining procedure was repeated a further two times (three rounds in total), without blocking of endogenous peroxidases. Following the final wash step in round three, slides were incubated with Spectral DAPI diluted in 1x TBS-Tween (UA0046, Biobasic) for 5 minutes, before undergoing three final wash steps.

2.21.4 Mounting slides

Prior to mounting, ProLong diamond antifade mountant (P36970, Life Technologies) was heated at 60°C for 10 minutes. Following the final round of staining, slides were removed from the BOND-MAX autostainer and transferred to a slide rack. Slides were placed into distilled water and maintained in the dark until mounting. Slides were individually removed from the distilled water, excess water dried with Kimwipe tissue and 35µL of mountant added to the slide. A glass coverslip was then placed on top of the tissue and pressure applied from the bottom to the top of the slide to remove any bubbles during coverslip adherence. Slides were allowed to dry overnight in the dark before imaging using the Vectra Polaris imaging system (Akoya Biosciences).

2.21.5 Spectral Unmixing

2.21.5.1 Creation of Library Slides

In order to effectively unmix the spectra of the six opal dyes, a library of single stained slides for each OPAL fluor, and one slide for Spectral DAPI, was created. In this instance, pancreas cancer tissue was used to create the slides. Each slide underwent the complete staining cycle (six rounds) as described, but only one OPAL fluor (or Spectral DAPI) was applied per slide. To ensure a strong signal could be observed, vimentin was used as the primary antibody for each OPAL fluor. Following staining, library slides were scanned using the Vectra Polaris Multispectral imaging system (PerkinElmer, Inc), and images exported. Scanned images were then loaded into inForm (Akoya Biosciences) and a new unmixing library created.

2.21.5.2 Unmixing of mIHC slides

Following scanning, all TMA images were uploaded to inForm software, and a selection chosen to test the spectral unmixing algorithm. A reference library (pancreas) was then selected from which mIHC images would be unmixed. Each OPAL fluor was labelled with its

corresponding marker name (primary antibody) and pseudo-colours for each marker chosen. The image was then unmixed using the selected library. The expression of neighbouring OPAL dyes was then evaluated to ensure effective unmixing. Briefly, pseudo-colours were set alternately to red and green for neighbouring OPAL channels. These channels were then switched on and off to visualise any spectral overlap between markers (denoted by the expression of an orange/yellow colour within the image). Once checked, all images were unmixed using the chosen reference library and exported as component tif files.

2.21.6 HALO analysis

To analyse the multiplex images, HALO imaging software (Indica Labs) was used. Images were loaded into a new study file and analysis algorithms created.

2.21.6.1 *View Settings*

To facilitate accurate scoring of individual markers, the view settings of a representative image were adjusted to enhance the image appearance. Briefly, each OPAL dye contained within the panel expressed a fluorescent spectral signature which could be manually adjusted. Background/non-specific staining was reduced by adjusting the 'black in' of the image, whilst image brightness was increased by adjusting the 'white in' settings. The view settings for each marker were adjusted individually and the settings saved. These settings were then exported and applied to all the images within the study. Importantly, altering the view settings does not impact results of the scoring, which is achieved using the raw stain intensities.

2.21.6.2 *Creating an analysis algorithm*

HALO software was navigated to the Analysis Tab. The number of dyes included in the panel (7) was input into the 'number of dyes' field, and a marker assigned to each dye from a drop-down menu (for example; DAPI, alpha SMA, podoplanin, periostin, CD105, myosin-11,

CK/EpCAM). The software was then trained to identify cells within the tissue through adjustment of the nuclear detection parameters. This included adjusting the size range of the nuclei to be detected as well as altering the aggressiveness of nuclear segmentation. This determined how harshly the software dissected compact nuclei. Fill nuclear holes was also set to 'true' to ensure any cells with faint DAPI at the centre of the nucleus were counted as one cell, rather than many.

The number of phenotypes desired for analysis were then assigned to the algorithm and defined (Table 2.20).

Panel 1			Panel 2			Panel 3		
Phenotype	Markers included	Markers excluded	Phenotype	Markers included	Markers excluded	Phenotype	Markers included	Markers excluded
Alpha SMA ⁺ Cells	DAPI / Alpha SMA	CK/EpCAM	CD45 ⁺ Cells	DAPI / CD45	N/A	CD45 ⁺ Cells	DAPI / CD45	N/A
Periostin ⁺ Cells	DAPI / Periostin	CK/EpCAM	CD45 ⁺ CD56 ⁺ Cells	DAPI / CD45 / CD56	N/A	CD45 ⁺ CD56 ⁺ Cells	DAPI / CD45 / CD56	N/A
Myosin-11 ⁺ Cells	DAPI / Myosin-11	CK/EpCAM	CD45 ⁺ CD56 ⁺ NKG2D Cells	DAPI / CD45 / CD56 / NKG2D	NKp46	CD45 ⁺ CD56 ⁺ NKG2A ⁺ Cells	DAPI / CD45 / CD56 / NKG2A	LAG3
Podoplanin ⁺ Cells	DAPI / Podoplanin	CK/EpCAM	CD45 ⁺ CD56 ⁺ NKp46 ⁺ Cells	DAPI / CD45 / CD56 / NKp46	NKG2D	CD45 ⁺ CD56 ⁺ LAG3 ⁺ Cells	DAPI / CD45 / CD56 / LAG3	NKG2A
CD105 ⁺ Cells	DAPI / CD105	CK/EpCAM	CD45 ⁺ CD56 ⁺ NKG2D ⁺ NKp46 Cells	DAPI / CD45 / CD56 / NKG2D / NKp46	N/A	CD45 ⁺ CD56 ⁺ NKG2A ⁺ LAG3 ⁺ Cells	DAPI / CD45 / CD56 / NKG2A / LAG3	N/A
Alpha SMA ⁺ Periostin ⁺ Cells	DAPI / Alpha SMA / Periostin	CK/EpCAM	CD45 ⁺ Vimentin ⁻ Cells	DAPI / CD45	Vimentin	CD45 ⁺ Vimentin ⁻ Cells	DAPI / CD45	Vimentin
Alpha SMA ⁺ Myosin-11 ⁺ Cells	DAPI / Alpha SMA / Myosin-11	CK/EpCAM	CD45 ⁺ CD56 ⁺ Vimentin ⁻ Cells	DAPI / CD45 / CD56	Vimentin	CD45 ⁺ CD56 ⁺ Vimentin ⁻ Cells	DAPI / CD45 / CD56	Vimentin
Alpha SMA ⁺ Podoplanin ⁺ Cells	DAPI / Alpha SMA / Podoplanin	CK/EpCAM	CD45 ⁺ CD56 ⁺ NKG2D ⁺ Vimentin ⁻ Cells	DAPI / CD45 / CD56 / NKG2D	NKp46 / Vimentin	CD45 ⁺ CD56 ⁺ NKG2A ⁺ Vimentin ⁻ Cells	DAPI / CD45 / CD56 / NKG2A	LAG3 / Vimentin
Alpha SMA ⁺ CD105 ⁺ Cells	DAPI / Alpha SMA / CD105	CK/EpCAM	CD45 ⁺ CD56 ⁺ NKp46 ⁺ Vimentin ⁻ Cells	DAPI / CD45 / CD56 / NKp46	NKG2D / Vimentin	CD45 ⁺ CD56 ⁺ LAG3 ⁺ Vimentin ⁻ Cells	DAPI / CD45 / CD56 / LAG3	NKG2A / Vimentin
Alpha SMA ⁺ Periostin ⁺ CD105 ⁺ Cells	DAPI / Alpha SMA / Periostin / CD105	CK/EpCAM	CD45 ⁺ CD56 ⁺ NKG2D ⁺ NKp46 ⁺ Vimentin ⁻ Cells	DAPI / CD45 / CD56 / NKG2D / NKp46	Vimentin	CD45 ⁺ CD56 ⁺ NKG2A ⁺ LAG3 ⁺ Vimentin ⁻ Cells	DAPI / CD45 / CD56 / NKG2A / LAG3	Vimentin
Alpha SMA ⁺ Myosin-11 ⁺ CD105 ⁺ Cells	DAPI / Alpha SMA / Myosin-11 / CD105	CK/EpCAM	Vimentin ⁺ Cells	DAPI / Vimentin	N/A	Vimentin ⁺ Cells	DAPI / Vimentin	N/A
Alpha SMA ⁺ Podoplanin ⁺ CD105 ⁺ Cells	DAPI / Alpha SMA / Podoplanin / CD105	CK/EpCAM	CK/EpCAM ⁺ Cells	DAPI / CK/EpCAM	N/A	CK/ EpCAM ⁺ Cells	DAPI / CK/EpCAM	N/A
CK/ EpCAM ⁺ Cells	DAPI / CK / EpCAM	Alpha SMA / Periostin / Myosin-11 / Podoplanin / CD105	Vimentin ⁺ (Markers Excluded) Cells	DAPI / Vimentin	CD45 / CD56 / NKG2D / NKp46 / CK/EpCAM	Vimentin ⁺ (Markers Excluded) Cells	DAPI / Vimentin	CD45 / CD56 / NKG2A / LAG3 / CK/EpCAM
			CK/EpCAM ⁺ (Markers Excluded) Cells	DAPI / CK/EpCAM	CD45 / CD56 / NKG2D / NKp46 / Vimentin	CK/ EpCAM ⁺ Markers Excluded Cells	DAPI / CK/EpCAM	CD45 / CD56 / NKG2A / LAG3 / Vimentin

Table 2.20: Description of cellular phenotypes assessed in PDAC TMA samples.

Next, the 'nuclear', 'cytoplasm' or 'membrane' detection for each marker was adjusted. Briefly, a real-time tuning window was opened in the software, displaying a scoring mask over the mIHC image. The 'output image' was changed to the marker being scored and the staining threshold adjusted. Thresholds were adjusted so that positively, but not negatively stained cells were shown as positive in the scoring mask. Compartments (nuclear, cytoplasm/membrane) not included in the analysis were set to a default value of -1. Algorithms were created with approximately 90% concordance (underscored), allowing for variation between cores. Each marker was adjusted individually, and the resultant algorithm trialled on 15-20 separate cores. The 'store object data' box was set to true, and the 'Output image' changed to co-localisation. The algorithm was then run on every slide stained within the same batch. Separate algorithms were created for different staining batches. In cases where a single algorithm could not be applied to all batch images, an additional algorithm was created, maintaining as much consistency as possible in marker thresholds between algorithms. Once analysed, the 'Summary Analysis data' was exported, and post-analysis processing carried out using Excel (Microsoft Office) (Figure 2.18). It is perhaps prudent to note that tissue folds were excluded from analysis to prevent erroneous results and any annotations made were copied across panels to maintain consistency.

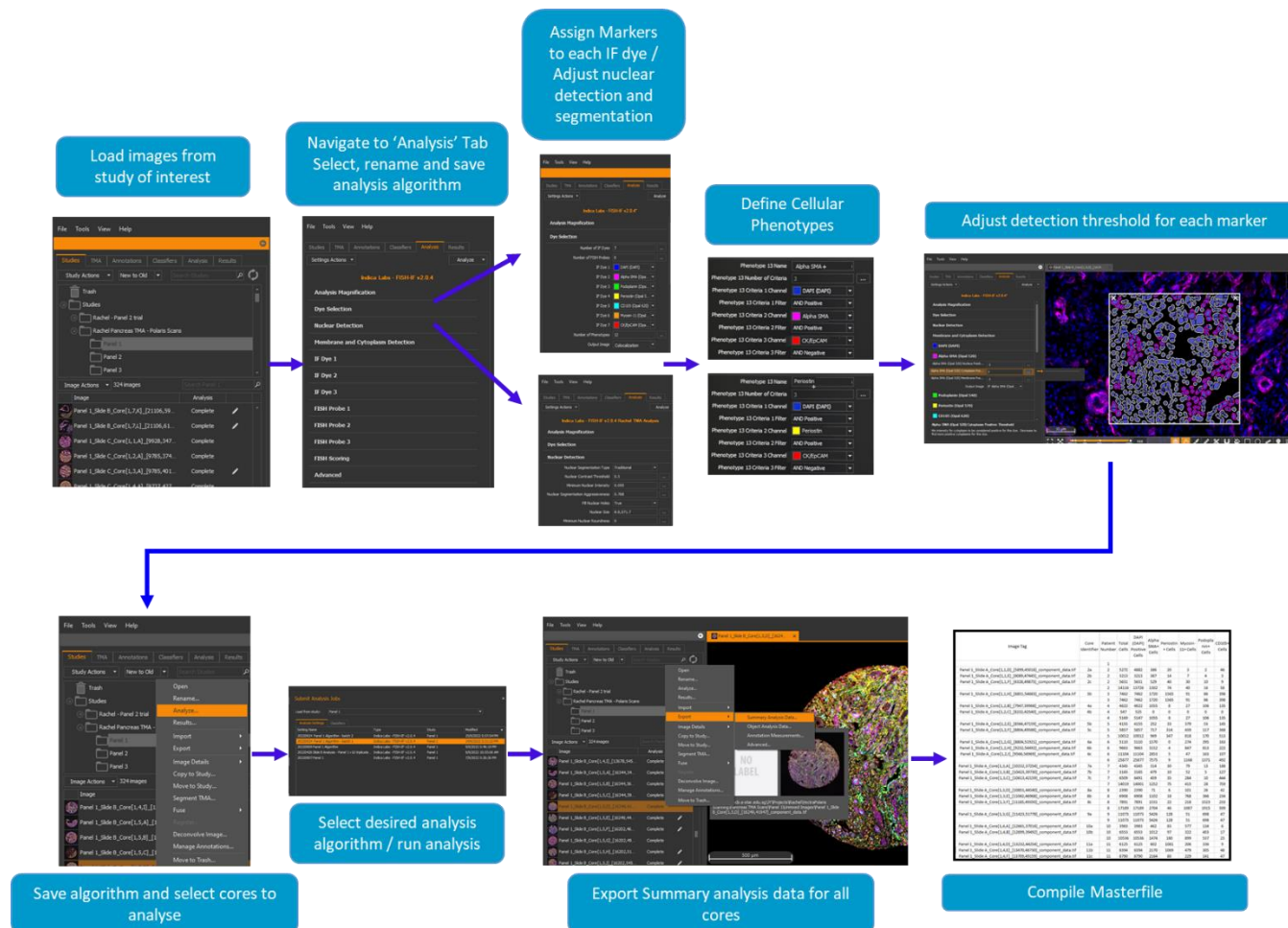


Figure 2.18: Schematic workflow of the major steps involved in the creation, and running of scoring algorithms within HALO software.

Images are selected from the study of interest and loaded into HALO. The user then selects the analysis tab and selects the number of dyes and phenotypes to be included in the scoring algorithm. The nuclear detection settings are then adjusted and phenotypes defined. Positivity thresholds are set for each marker, ensuring approximately 90% concordance between the scoring mask and the underlying image. Once the algorithm has been created, the user selects all images to be analysed and selects the 'analyze' tool. The desired algorithm is selected and run on the chosen images. Summary analysis data is then exported as a .csv file, and the data processed using Excel (Microsoft).

2.21.6.3 Data Processing

Masterfiles were created for data processing. Each TMA core was assigned a unique identifier based on H&E staining and TMA maps. Patient information was then assigned to each core. Core concordance was established across all three panels. In instances where a core was missing from one panel, this data was removed from the remaining panels. For each patient, the data obtained from each core was combined and the tissues treated as a whole. Cellular percentages were calculated from the number of DAPI positive cells. Statistical analysis was carried out using GraphPad Prism (version 9). Survival analysis was completed using the Kaplan Meier method, with significance established using the log-rank test. All instances where patient follow up data were missing were censored.

2.22 Proximity Analysis

Upon scoring, TMA Cores positive for NK cell infiltrate were included for proximity analysis. Briefly, HALO software was navigated to the results pane, and the results from the scoring algorithm selected. In the 'Object data' window, cells were filtered (1= positive; 0 = negative) for markers of interest. These markers were then added to a spatial plot. Within the spatial plot, the spatial analysis option was chosen. The marker of interest (for example CD45⁺CD56⁺) was selected and entered into the 'Measure' parameter. The distance (within) was then set to 50µM and vimentin⁺ added to the 'in proximity of' box. The number of bands was set to 10 to return information on the number of NK cells in each 5µm band from a vimentin⁺ cell. 'Store object (pair) data' was set to true, returning the individual distances between NK cells and vimentin⁺ cells. Once setup was complete, the proximity algorithm was saved (Figure 2.19). This was repeated for each NK cell marker. Once algorithms were created for all

markers, proximity analysis was run on all selected cores. The data were then exported and processed using Excel (Microsoft).

2.23 Statistical Analysis

Statistical analysis was carried out using GraphPad Prism v 8.0-9.3 (GraphPad Software, Dotmatics), and R v 4.1 (The R Project, Vienna, Austria). Unless otherwise stated, non-parametric Mann-Whitney U tests and Kruskal Wallis analysis with Dunn's post hoc tests were used to compare between groups. For *in vitro* assays, unless otherwise stated, three biological replicates were carried out, each with at least three technical replicates. Survival analysis was assessed using the Kaplan Meier method, with significance established using the log-rank test. Results are expressed as median +/- SEM (non-parametric) or mean +/- SEM (parametric). Significance was established at $p < 0.05$ for all tests.

Chapter 3 - Results – *In vitro* Optimisations

3.1 Introduction

Natural killer cells and PSCs have been receiving increasing interest as potential therapeutic targets in the treatment of pancreatic ductal adenocarcinoma.^{220, 222, 252} NK cells are potent cytotoxic lymphocytes which have been linked to improved patient survival in PDAC.²¹⁹ Moreover their innate cytotoxicity prevents the need for antigen pre-sensitisation, thus making them an attractive therapeutic option.²⁵³ Conversely, PSCs have been found to modulate and orchestrate the PDAC tumour microenvironment, creating an immunosuppressive, tumour permissive environment, earmarking these cells as a potential target for new therapies.²⁵⁴ Despite this, little remains known about the interaction between these two players *in vitro*.

CD107 degranulation assays have long been recognised as important indicators of NK activity and an indirect measure of NK cell cytotoxicity.²⁵⁵ Here we optimise this assay for its use against both PSCs and PDAC cell lines. Despite the widespread use of this assay, direct measurement of NK-induced lysis is often used to confirm cytotoxicity.²⁵⁶⁻²⁵⁸ Whilst the chromium-51 release assay is considered the 'gold standard' measure of cellular cytotoxicity, its radioactive nature is often a limitation.²⁵⁹ Here we optimise the Calcein AM release assay for the staining of adherent cells.²⁴⁸ Finally, we developed flow cytometric assays to provide a comprehensive overview of the impact of direct cell-cell contact as well as Transwell™ separation on NK/PSC cellular phenotype.

In this chapter we present the optimisation experiments undertaken to provide a global overview of NK- PSC interactions in the context of PDAC

3.2 NK92 and PS1 media co-culture experiments

To investigate the interaction between NK cells and PSCs *in vitro*, media conditions for co-culture experiments were optimised. As NK cells were reported to have complex media needs (as outlined by ATCC at the time of experimentation), it was important to ensure optimal functional efficacy so as not to mask functional or phenotypic changes induced by co-culture.

Cell count analysis revealed that both NK92 and PS1 cells demonstrate the best proliferation in conditions containing a high ratio of Alpha MEM (NK92 media) to DMEM/Hams F12 (PS1 media) (Figure 3.1). WST-1 proliferation assays demonstrate this conclusively for NK92 cells (Figure 3.2). Thus, it was concluded that co-culture experiments would be carried out in 100% NK92 media (Alpha MEM plus 12.5% Horse Serum, 12.5% FBS, and 0.2mM myo-inositol, 0.1mM 2-mercaptoethanol, 0.02mM folic acid).

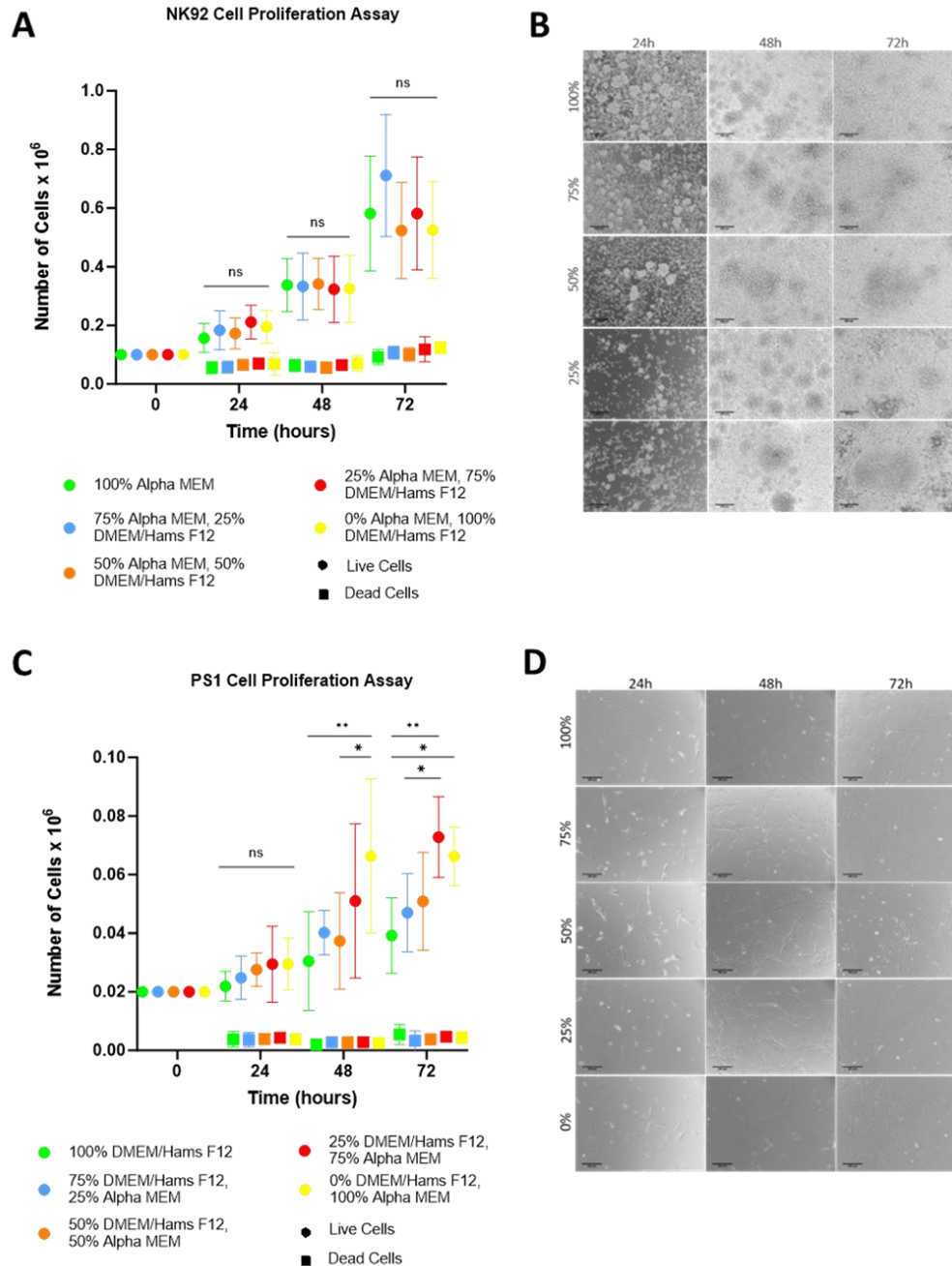


Figure 3.1: NK92 and PS1 cell viability following culture in one of five conditions of Alpha MEM and DMEM Hams/F12.

A) NK92 culture in one of five media conditions; 1:0- NK92 media: PS1 Media, 3:1 - NK92 media: PS1 Media, 1:1 NK92 media: PS1 Media, 1:3 - NK92 media: PS1 Media, 0:1 - NK92 media: PS1 Media. B) Representative images of NK92 cells from each media condition at 24, 48 and 72h. Magnification $\times 10$. C) PS1 culture in one of five media conditions; 1:0- PS1 media: NK92 media, 3:1 - PS1 media: NK92 media, 1:1 PS1 media: NK92 media, 1:3 - PS1 media: NK92 media, 0:1 - PS1 media: NK92 media. D) Representative images of PS1 cells from each media condition at 24, 48 and 72h. Magnification $\times 10$. All data were analysed using a Kruskal-Wallis test with Dunn's post hoc analysis. Summary statistics are represented by the mean \pm SEM. Significance was established at $p < 0.05$. Scale bars = 200 μ m.

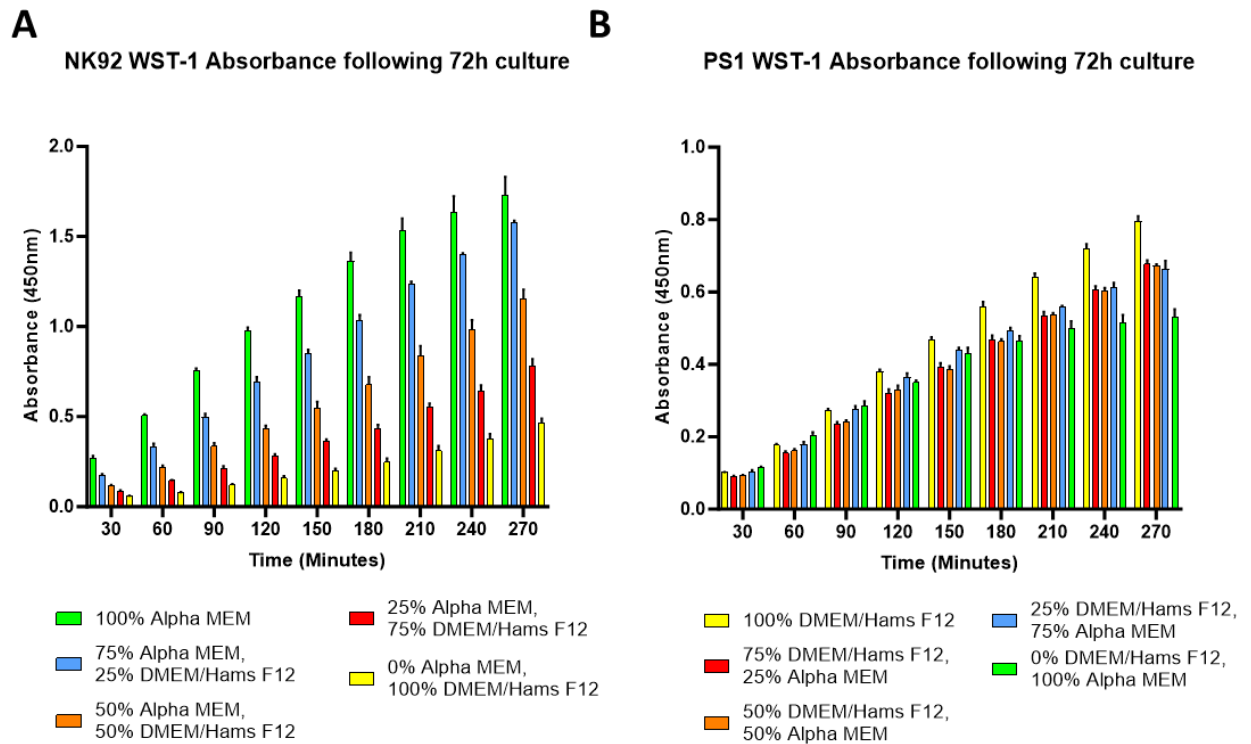


Figure 3.2: NK92 and PS1 WST-1 proliferation assays.

A) NK92 cell proliferation denoted by colourmetric absorbance. Cells were cultured for 72h in one of the following five media conditions; NK92 cells; 1:0- NK92 media: PS1 Media, 3:1 - NK92 media: PS1 Media, 1:1 NK92 media: PS1 Media, 1:3 - NK92 media: PS1 Media, 0:1 - NK92 media: PS1 Media. PS1 cells. Data are from one biological replicate. B) PS1 cell proliferation denoted by colourmetric absorbance following 72h culture in one of five media conditions; 1:0- PS1 media: NK92 media, 3:1 - PS1 media: NK92 media, 1:1 PS1 media: NK92 media, 1:3 - PS1 media: NK92 media, 0:1 - PS1 media: NK92 media. Data are from one biological replicate

3.3 WST-1 incubation and seeding density optimisation for cytotoxicity assays

To measure NK cytotoxicity (following education by quiescent and activated PSCs) against pancreatic cancer cell lines, a proliferation assay using the tetrazolium salt WST-1 was employed. Prior to conducting WST-1 cytotoxicity assays, cell seeding densities were optimised to ensure accurate readouts of the colourmetric assay. All cell lines demonstrate good discrimination between experimental conditions when incubated with WST-1 for four hours. BxPc3 cells demonstrate significant differences in proliferation between cancer cells alone and 10:1 co-culture with NK cells at all seeding densities tested. Similarly, Miapaca2 cells exhibit the best discrimination between cancer cells alone and 10:1 NK cell incubation when seeded at densities of 10,000, 15,000 and 20,000 cells/well. For Capan2 cells, we observe the expected decrease in proliferation (when cultured with NK cells) when seeded at densities of 2,500, 15,000 or 20,000 cells/well, with the greatest difference observed at 15,000 or 20,000 cells/well (Figure 3.3). Consequently, the following seeding densities were established for subsequent cytotoxicity assays: BxPc3, 20,000 cells/well; MiaPaca2, 15,000 cells/well; Capan2, 20,000 cells/well.

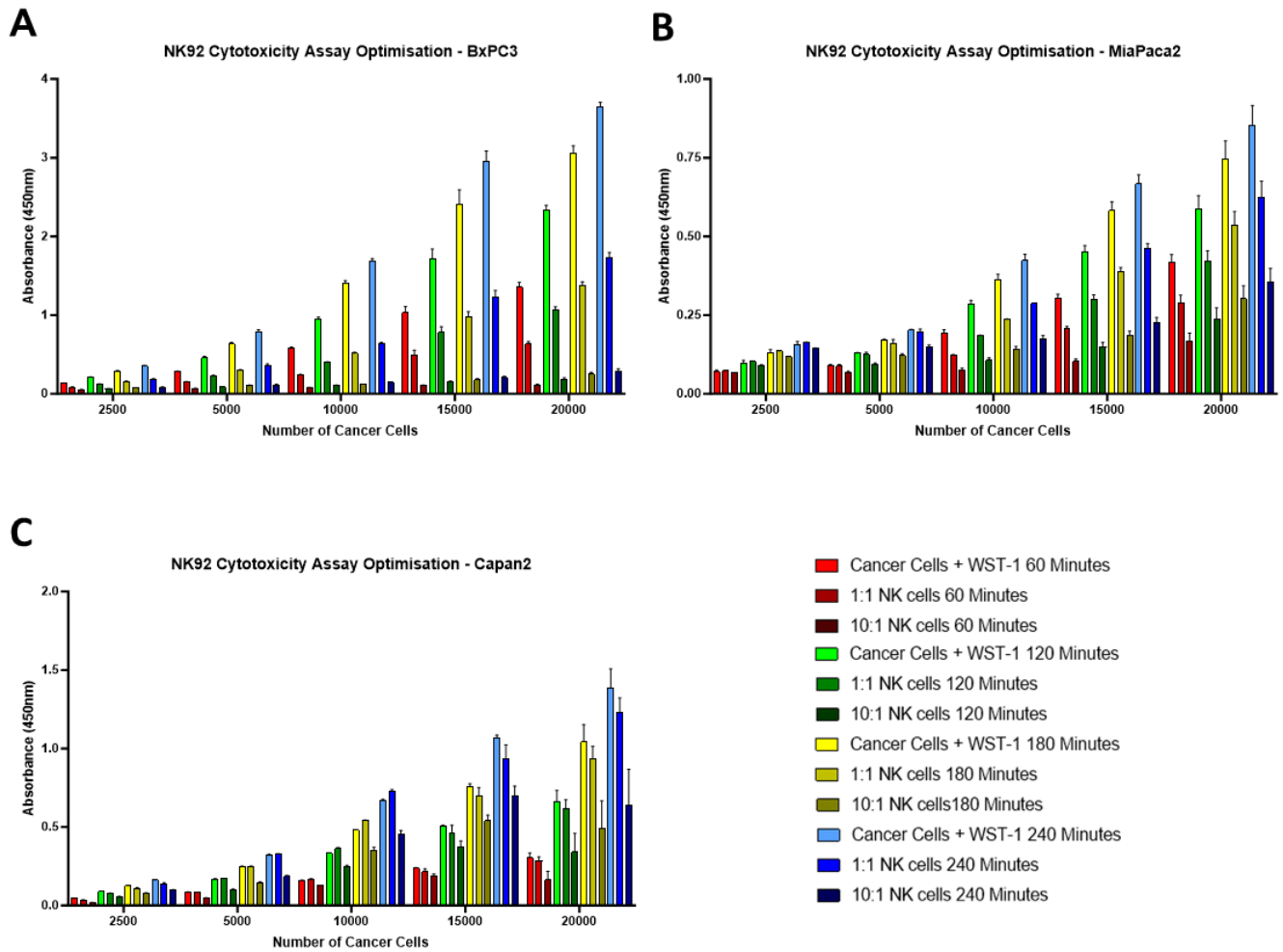


Figure 3.3: WST-1 incubation and seeding density optimisations.

BxPC3 (A), MiaPaca2 (B), and Capan2 (C) cells were seeded at densities of 2,500, 5,000, 10,000, 15,000 and 20,000 cells/well. Cells were cultured alone or with NK92 cells at a ratio of 1:1 or 10:1 for 4h. Data are from one biological replicate

3.4 Initial CD107 Degranulation assay trial

To measure NK functional efficacy against both qPSC/aPSC and pancreatic cancer cell lines, a CD107 degranulation assay was used. Widely recognised as a marker of NK functional activity, the use of CD107a/b expression in *in vitro* assays has been well documented.²⁶⁰ Prior to experimentation, a CD107 degranulation assay protocol was kindly provided by The Samson Lab (Leeds) (Appendix 1).²⁶¹ To ensure this protocol worked in our hands, a trial assay was conducted using naïve NK cells (Figure 3.4).

No observable difference was evident in the percentage of CD56⁺CD107⁺ cells when comparing NK cells cultured alone to those cultured with MiaPaca2 cells at any effector to target ratio trialled.

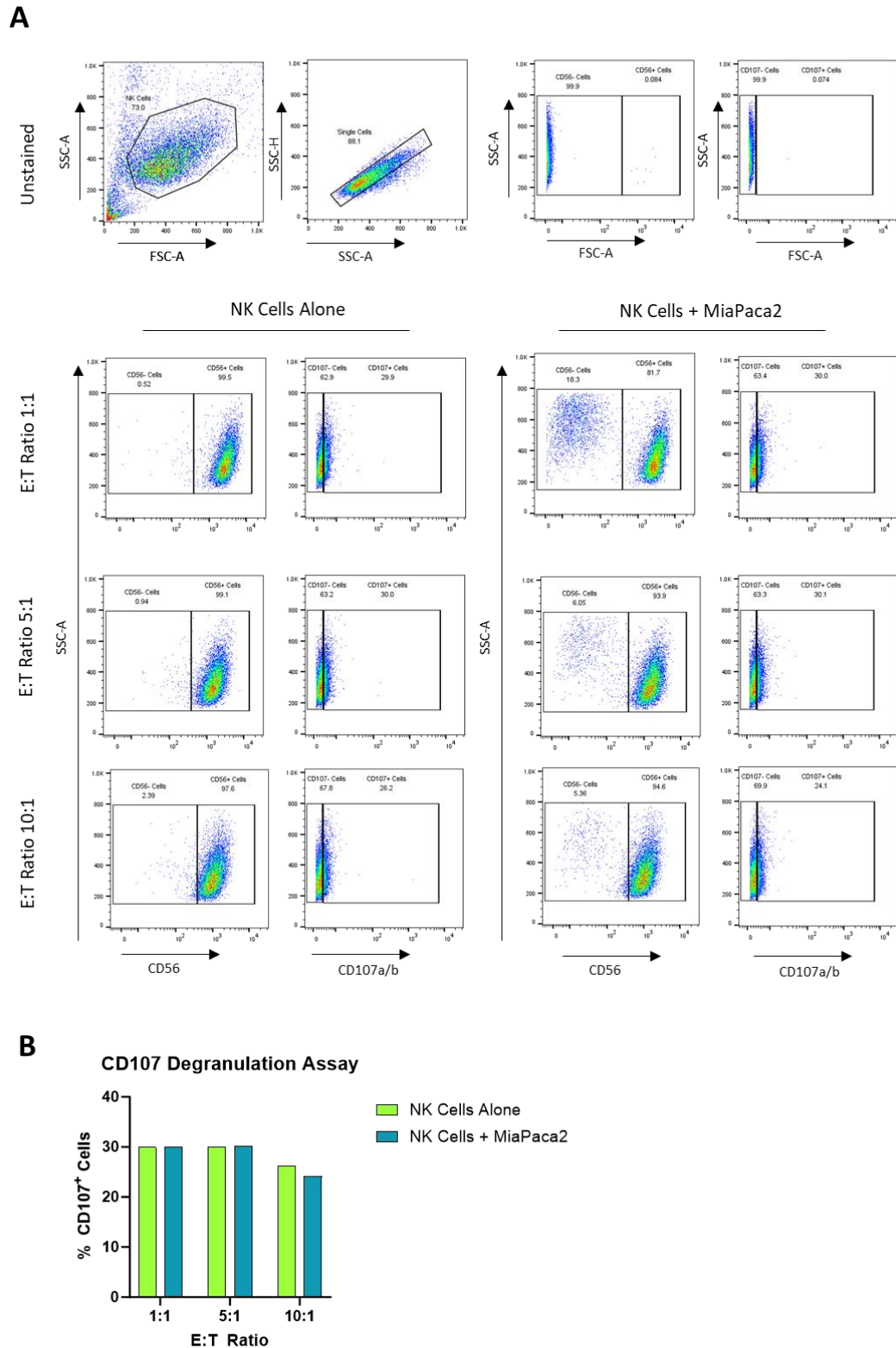


Figure 3.4: Initial CD107 degranulation assay against MiaPaca2 cells

A) FACS plots of CD56⁺ and CD107⁺ Cells at Effector: Target (E:T) ratios 1:1, 5:1 and 10:1. An unstained control is shown in the top panel. Samples were acquired on the LSR Fortessa. Post-acquisition analysis was conducted using FlowJo Version 10.8.1. B) Summary graph of the percentage of CD107⁺ cells in each condition. Data are from one biological replicate.

3.4.1 CD107 Degranulation Assay Optimisations and Troubleshooting

To determine if the addition of the CD56 antibody during CD107 incubation was impeding CD107a/b binding, the assay protocol was modified and CD56 staining conducted after co-culture. Concomitantly, the original staining protocol was run to facilitate comparison between these two methods (Figure 3.5).

A

CD56 added during co-culture

CD56 added after co-culture

Unstained

NK cells +
PMA/Ionomycin

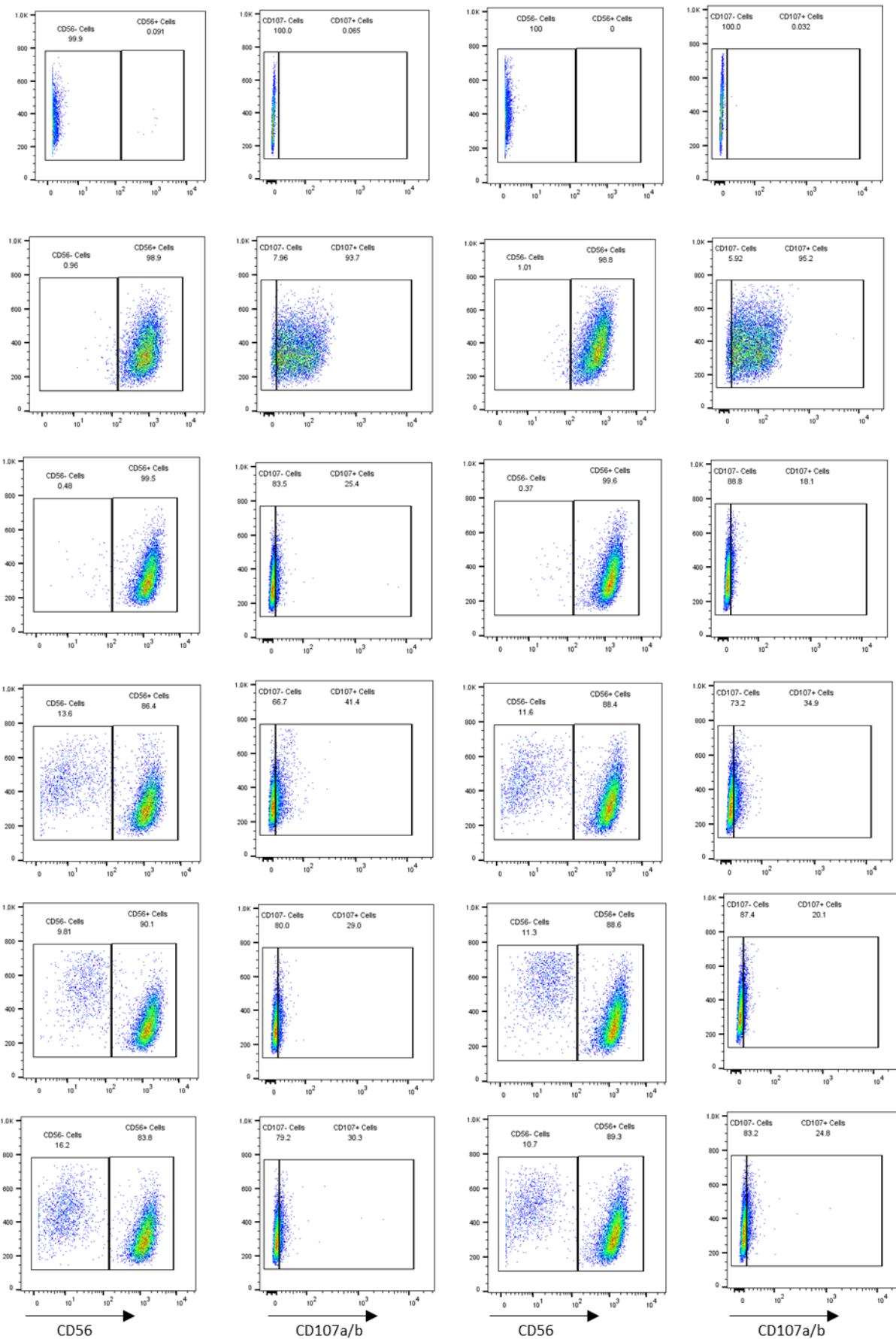
NK cells alone

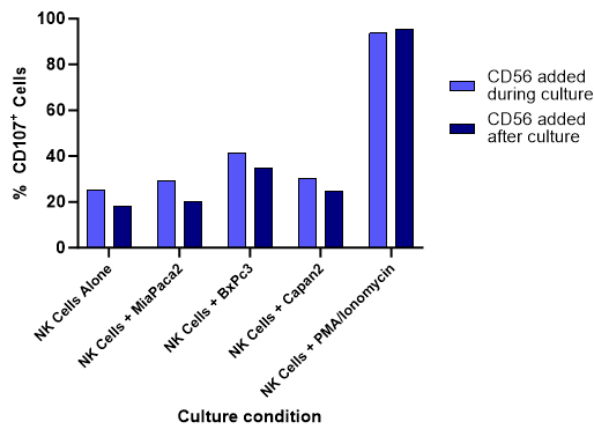
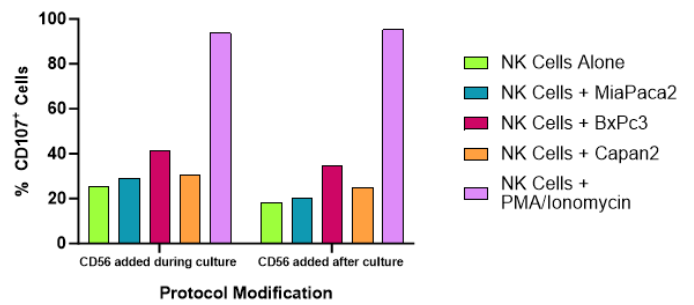
NK: BxPc3 5:1

NK: MiaPaca2 5:1

NK: Capan2 5:1

SSC-A

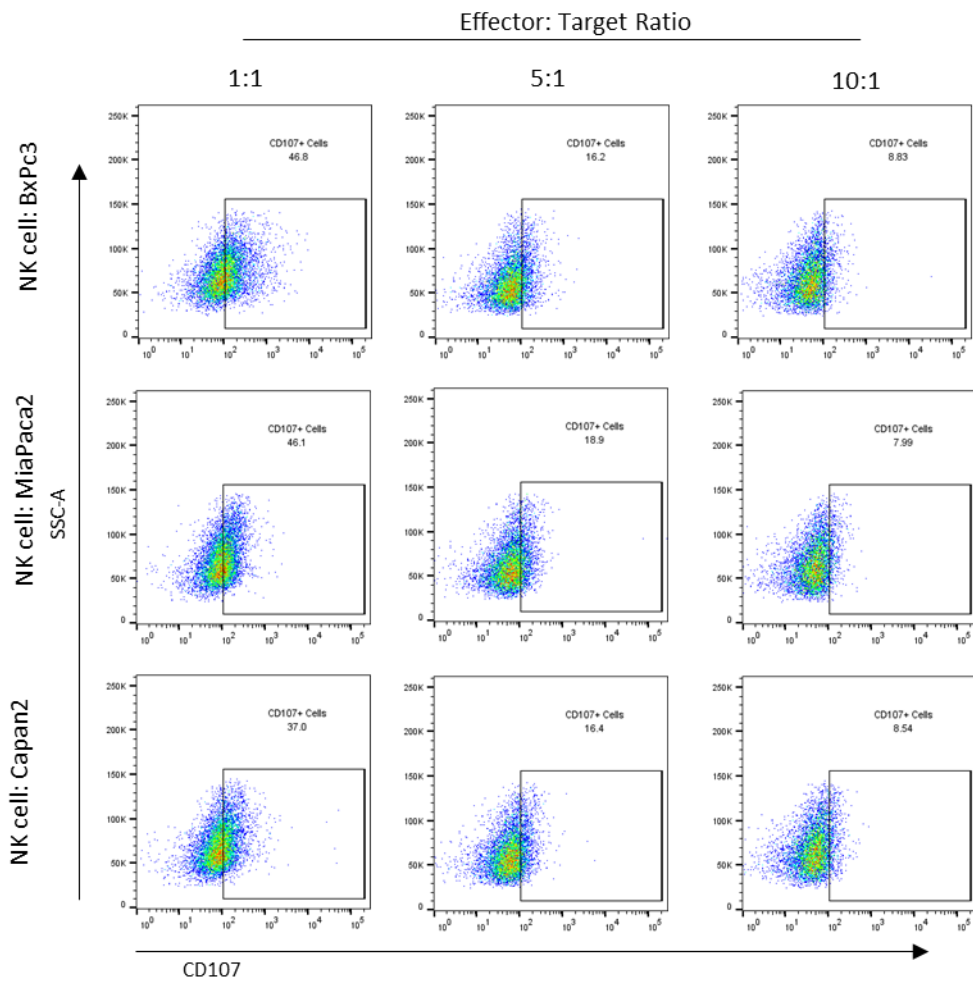
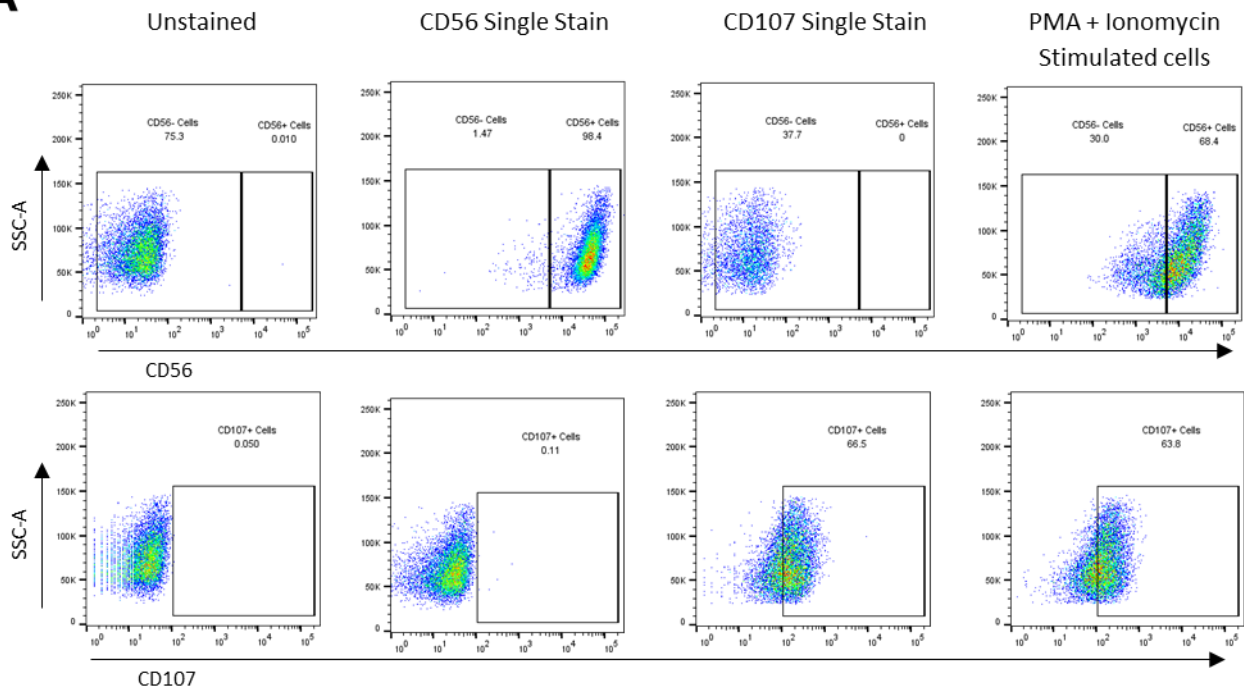


B**CD107 Protocol Optimisation****C****CD107 Degranulation Assay****Figure 3.5: CD107 Degranulation Assay Troubleshooting.**

A) FACS plots of CD56⁺ and CD107⁺ NK cells following culture alone, with target cells (BxPc3, MiaPaca2, Capan2) at a ratio of 5:1 or following PMA/Ionomycin stimulation. Cells were cultured for 4h as previously described. CD56 was either added during CD107 incubation, or after co-culture. Cells were washed in FACS Buffer following staining and fixed for 45min at RT before acquiring on the LSR Fortessa. Post-acquisition analysis was carried out using FlowJo version 10.8.1. B) Graphical representation of the percentage of CD107⁺ cells for each experimental condition with CD56 being added either during or after culture. C) Comparison of CD107⁺ cells in all experimental conditions tested in each protocol modification. Data are from one biological repeat.

No observable difference was seen in the percentage of CD56⁺CD107⁺ cells expressed when comparing addition of CD56 during or after co-culture, suggesting that this was not impeding the assay. Whilst some degranulation was observed within this assay, FACs plots from previous works have demonstrated distinct CD107⁺ subsets.²⁵⁵ Moreover, the fluorescence intensities observed herein remained similar to the unstained sample suggesting that antibody addition may be responsible for the slight population shift observed. As such, a 24h assay was carried out to determine if the results obtained were true staining or a result of antibody addition (Figure 3.6).

A



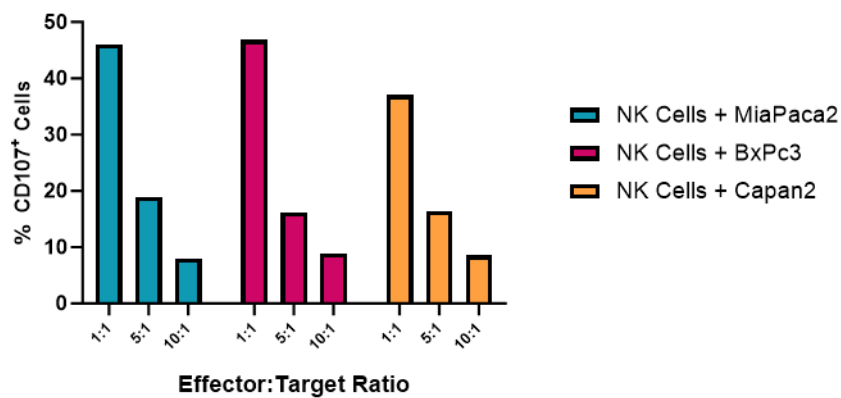
B**CD107 Degranulation Assay**

Figure 3.6: Results of a 24h degranulation assay.

A) FACS plots of CD56⁺CD107⁺ NK cells following 24h co-culture. Samples were acquired on the LSR Fortessa. Analysis was carried out using FlowJo version 10.8.1. B) Percentage of CD107⁺ cells at each E: T ratio for MiaPaca2, BxPc3 and Capan2 cell lines. Data are from one biological replicate.

Figure 3.6 demonstrates a clear inverse relationship between increasing effector: target ratio and degranulation against all three cancer cell lines following 24h incubation. These results also demonstrate assay efficacy; however, the lack of NK cell alone control limits the extent to which these findings can be extrapolated. Moreover, as the typical time-course for this assay is widely reported as 4-6h, further assessment was required.

As such, to validate assay efficacy, degranulation was measured in NK cells freshly isolated from PBMCs from a single healthy donor (Figure 3.7). Notably, this was the only experiment to use primary NK cells. All other experimentation was carried out using the natural killer cell line, NK92.

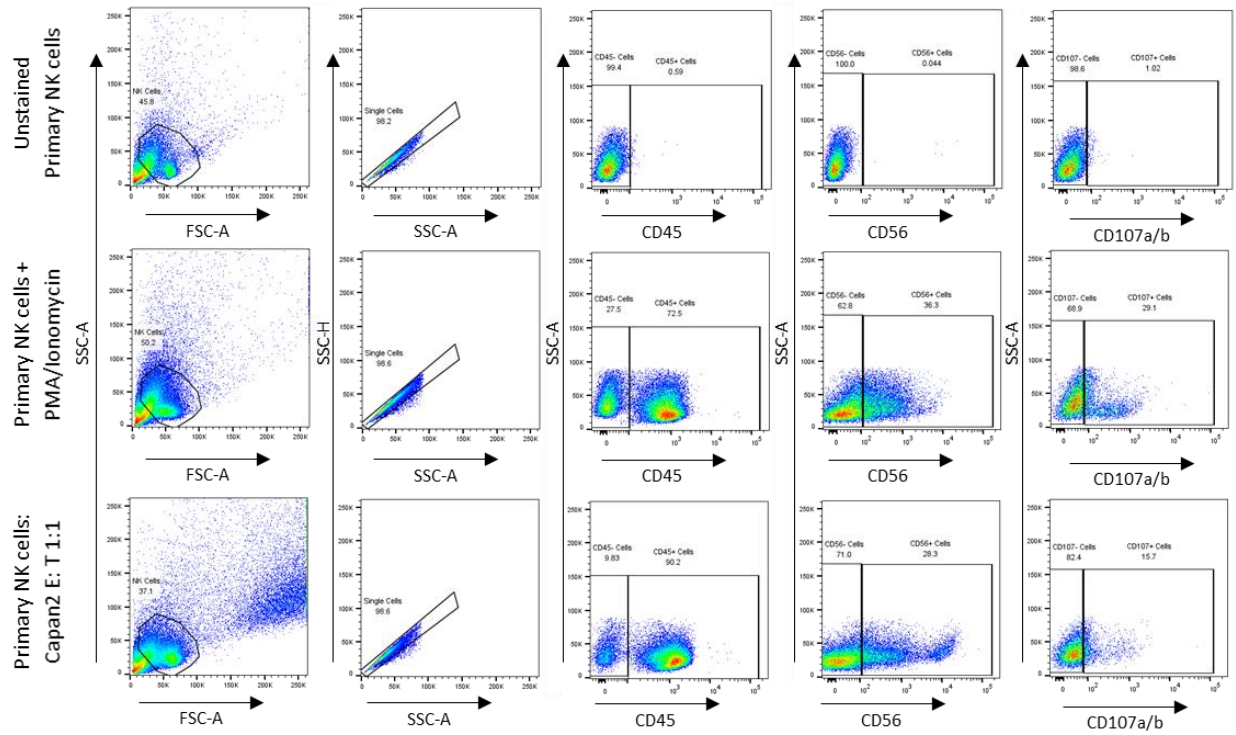


Figure 3.7: Primary NK cell Degranulation Assay

NK cells were isolated from PBMCs from a single healthy donor using an NK cell enrichment kit. Cells were then cultured as previously described either alone, with PMA + Ionomycin or with Capan2 cells at a 1:1 ratio. Samples were acquired on the LSR Fortessa and analysed using FlowJo software (version 10.8.1).

3.5 CD107 Degranulation Assay using the Cytex Aurora Flow cytometry system

Following demonstration of assay efficacy, the CD107 degranulation assay was chosen to be taken forward to assess NK-PSC interactions. However, the introduction of a new spectral flow cytometry system (Cytex Aurora) necessitated the optimisation of new CD107a/b antibodies (Figure 3.8).

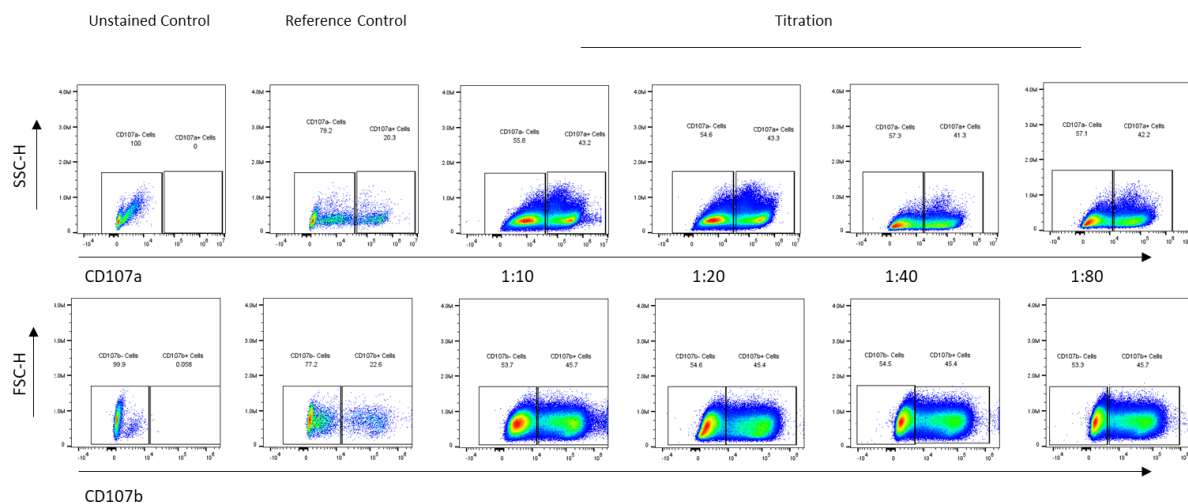


Figure 3.8: CD107a/b antibody titration.

NK92 cells were stimulated with PMA and ionomycin for 4h prior to staining. A separate unstimulated population of NK cells were used as the negative control. Gating was based on the reference and unstained controls. The reference control gate was applied to the highest stain concentration (1:10). Gates for the remaining titrations were adjusted to maintain the same proportion of % positive cells. Antibodies were considered to be no longer efficacious at the point at which positive and negative populations could not be separated. All titrations were run on the Cytex aurora 5 laser cytometer. Data were analysed post-acquisition using FlowJo version 10.8.1.

Antibody dilutions of 1:80 for both CD107a and CD107b were selected for degranulation assays (details of NK lineage marker titrations are shown in Figure 3.19 and Table 3.1). Following successful antibody titrations, a trial degranulation assay was run against all three cancer cell lines using the spectral flow cytometry system to determine assay efficacy (Figure 3.9 and Figure 3.10).

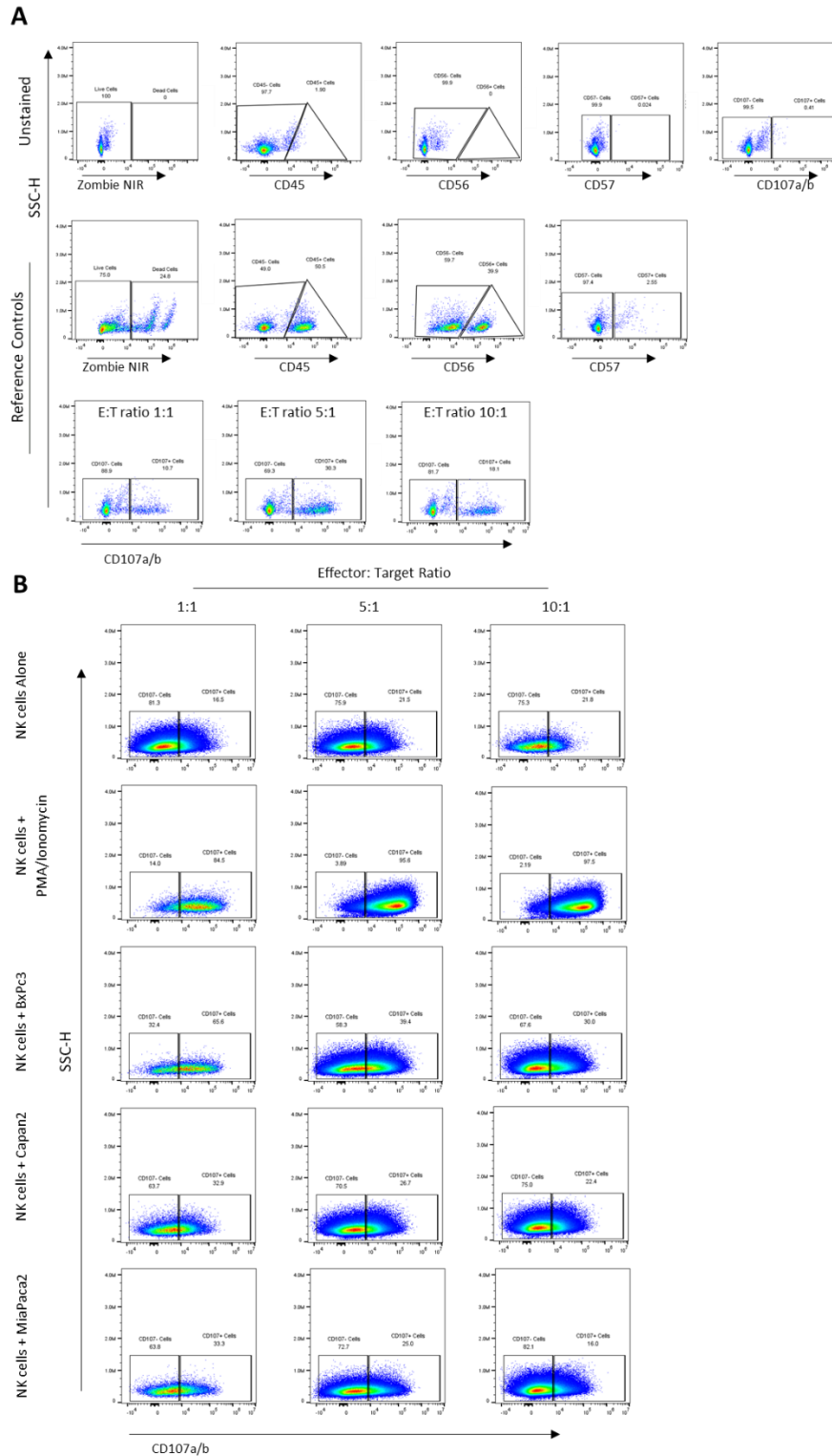


Figure 3.9: CD107 Degranulation Assay using the Cytex Aurora Flow cytometry system.

A) FACs plots of unstained and reference control samples on which the gating strategy was based. B) FACs plots for each experimental condition at Effector: Target Ratios of 1:1, 5:1 and 10:1. Gates display CD45⁺CD56⁺CD107a/b⁺ cells. Samples were acquired on the 5 laser Cytex Aurora using Spectro flow software. Post-acquisition analysis was carried out using FlowJo version 10.8.1

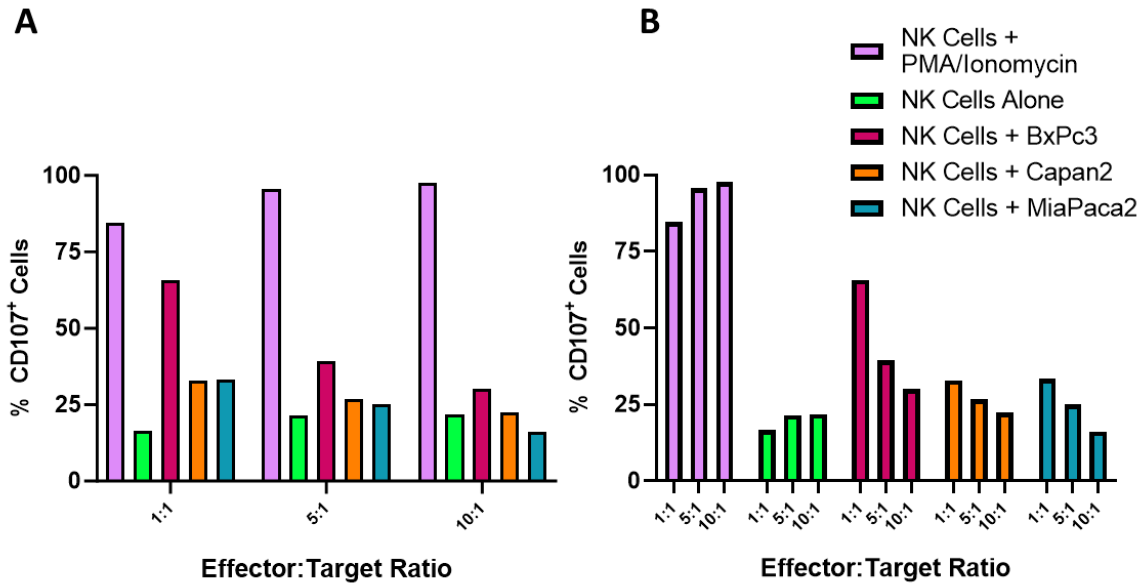


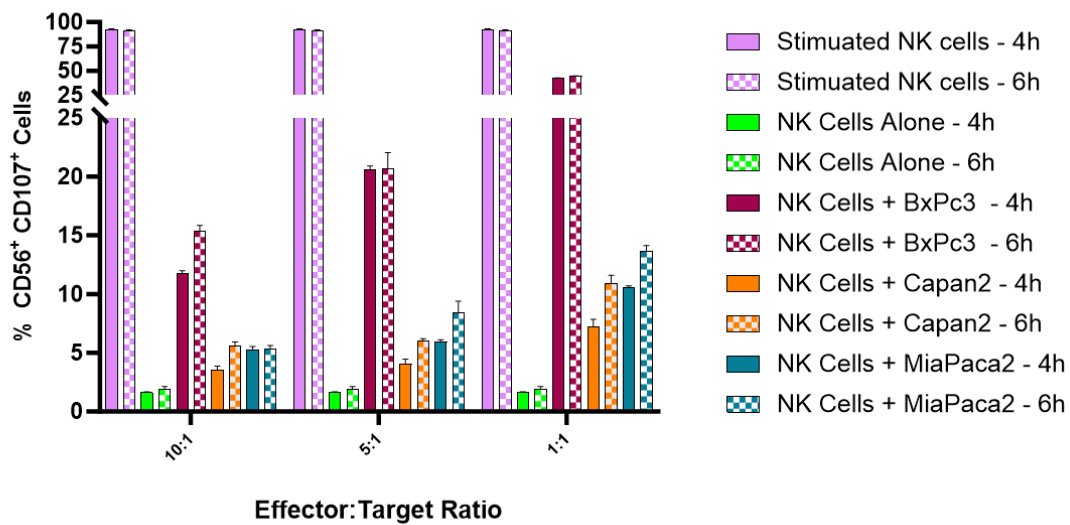
Figure 3.10: Initial comparison CD107 Degranulation assay against PDAC cell lines using the Cytex Aurora flow cytometry system.

A) Comparison between each experimental condition at each Effector: Target ratio. B) Comparison within each experimental group between Effector: Target ratios. Data are from one biological replicate.

We determined the CD107 degranulation assay using the Cytex Aurora to be efficacious against all three cancer cell lines. Next, to ensure optimal data acquisition was achieved, optimisations for CD107 incubation length and effector to target ratios were carried out (Figure 3.11).

Whilst no discernible difference was observed between 4h and 6h incubation, it was decided that NK and target cells would be incubated for 6h, ensuring smaller differences in NK degranulation (as a result of PSC education) could be observed. Furthermore, the greatest NK cell degranulation was observed at effector to target ratios of 1:5 and 1:10. As no significant difference was observed between these two ratios, NK and cancer cells would be seeded at a density of 1:5 for future experiments.

A Percentage of CD56⁺CD107⁺ Cells following 4h/6h Incubation



B

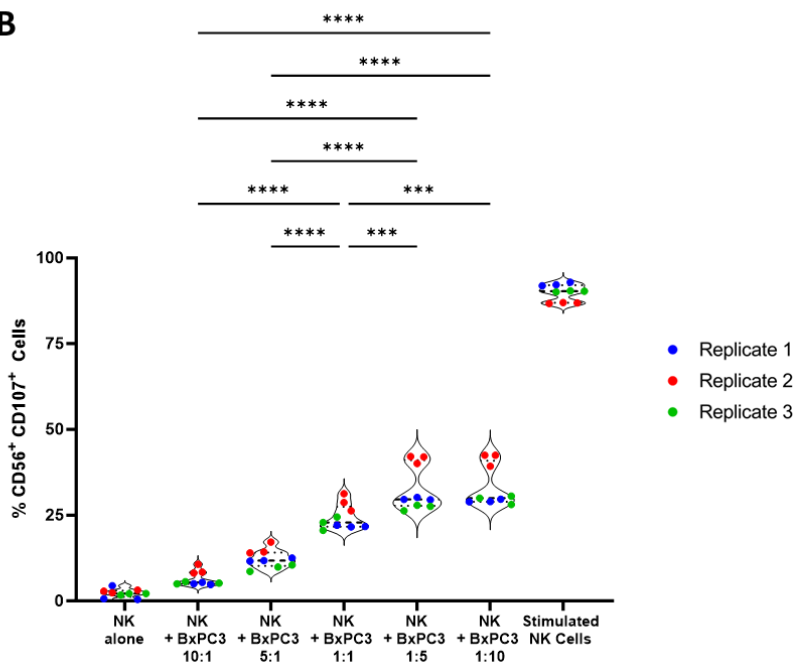


Figure 3.11: CD107 Incubation length and effector to target ratio optimisation.

A) CD107 incubation optimisation. % CD56⁺CD107a/b⁺ cells following 4h/6h incubation with BxPC3, Capan2 and MiaPaca2 cells at effector to target ratios of 10: 1, 5: 1 and 1: 1). Data are from one biological replicate. B) Optimisation of Effector: Target ratios. NK cells were cultured with BxPC3 cells (6h) at multiple effector to target ratios (10:1, 5:1, 1:1, 1:5, 1:10). Samples were acquired on the Cytex Aurora and analysed using SpectroFlo (3.0.3) and FlowJo (10.8.1) software. Data were analysed using a One-Way ANOVA with Šidák's multiple comparisons. * $p < 0.05$, ** $p < 0.01$, *** $p < 0.001$; **** $p < 0.0001$.

3.6 Calcein AM Cytotoxicity Assay optimisation and troubleshooting

To validate the findings of the CD107 degranulation assay, Calcein AM cytotoxicity assays²⁴⁸ (a direct measurement of NK-induced lysis) were utilised. To ensure optimal conditions were used for this experiment, several rounds of optimisations and troubleshooting were completed (Figure 3.12).

Optimisations revealed the 530nm wavelength to be crucial to determine maximal differences between spontaneous and maximum release conditions. Final densities of 10,000 PSCs would be used for Calcein cytotoxicity assays (following 7-day ATRA/EtOH treatment). Whilst some difference was observed in the fluorescence intensity between trypsinised and adherent PSCs, the trend observed was the same. Thus, it was concluded that PSCs would be stained in their adherent state to prevent any phenotypic alterations induced by trypsinisation.

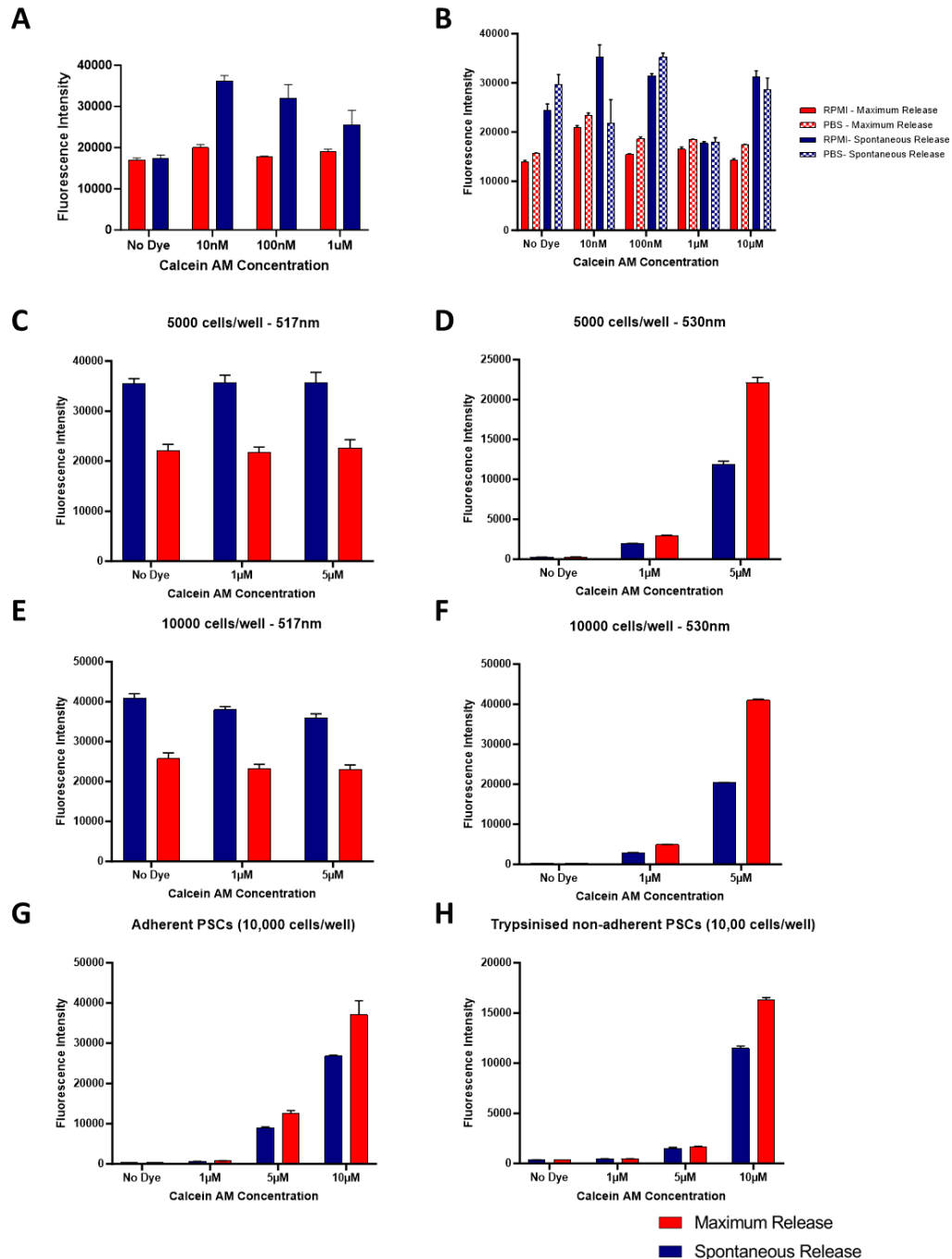


Figure 3.12: Calcein AM optimisation and troubleshooting.

A) Adherent PSCs were stained with 10nM, 100nM or 1μM of dye and incubated for 4h. Plates were centrifuged and 75μL of supernatant transferred to a fresh plate. Plates were read on a microplate reader, 517nm emission. B) Trial of diluent for cytotoxicity assays. Cells were stained with 10nM, 100nM, 1μM or 10μM and then incubated with 2% triton (or no surfactant) diluted in either RPMI or PBS and incubated for 4h. Plates were read at 517nm. C-F) Optimisation of emission wavelength and seeding densities. Cells were seeded at 5,000 (C, D) or 10,000 (E-F) cells/well and treated as described. Plates were then read at 517nm (C, E) or 530nm (D, F). G-H) Final PSC optimisations (10,000 cells/well) in either adherent (G) or Trypsinised (H) PSCs. Plates were read at 530nm. Data for each round of optimisation are from one biological replicate.

3.7 Initial flow cytometric antibody titrations

We next wanted to assess the changes in NK receptor expression and PSC phenotype in response to co-culture. In order to achieve this, a flow cytometric based assay was developed. Ahead of running co-culture experiments, antibodies for the NK cell markers CD56, NKG2D and NKG2A (Figure 3.13), and the stellate cell markers alpha SMA and GFAP (Figure 3.14) were titrated.

Whilst optimal staining dilutions were determined for CD56 (1:100), NKG2D (1:10), alpha SMA (1:50) and GFAP (1:500), no staining was observed for the NK cell inhibitory receptor NKG2A. Thus, further troubleshooting was carried out (Section 3.7.1).

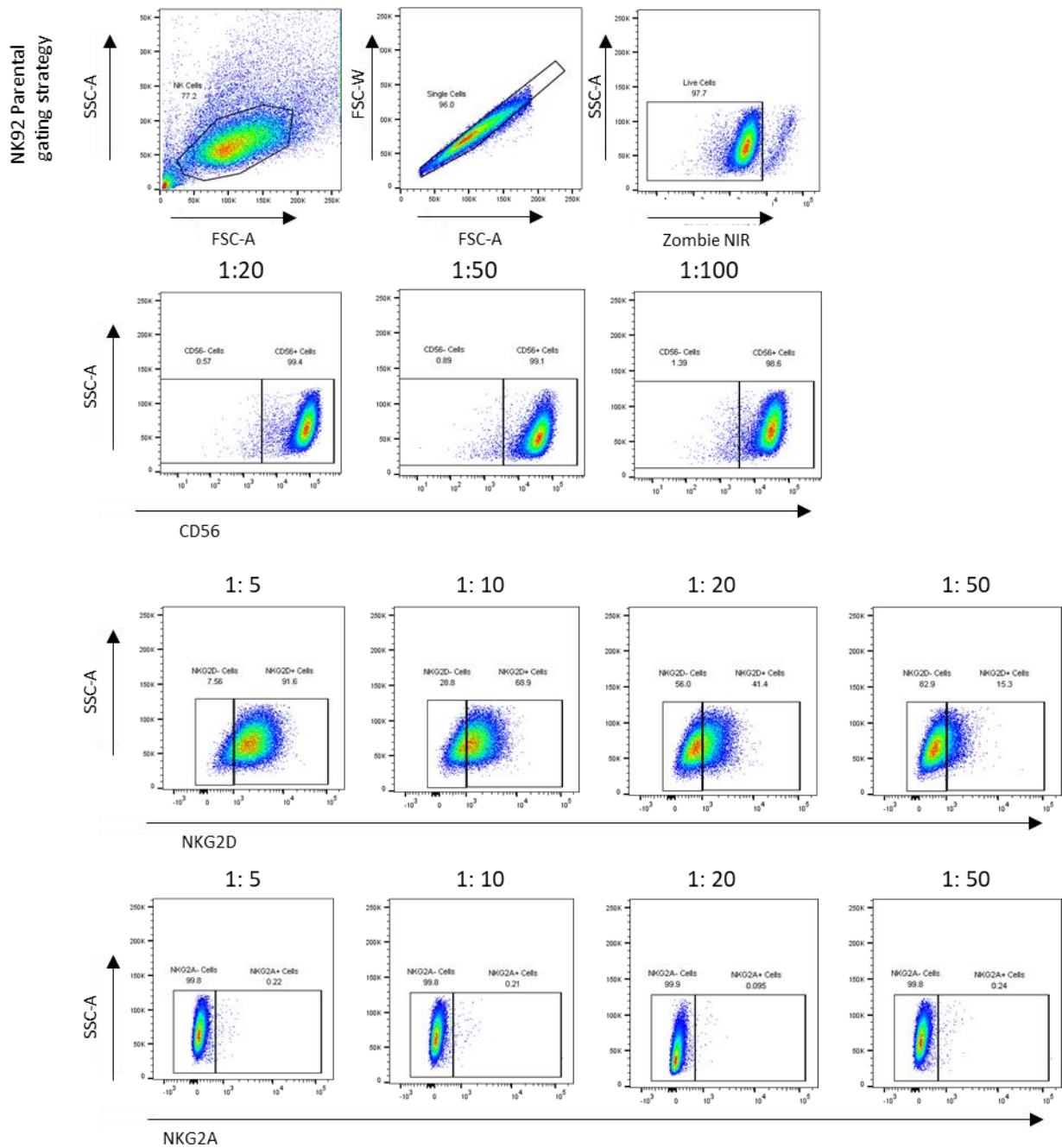


Figure 3.13: NK flow cytometry antibody titration.

Unstimulated NK cells were stained with lineage and receptor markers using the following titration dilutions: CD56- 1:20, 1:50, 1:100; NKG2D – 1:5, 1:10, 1:20, 1:50; NKG2A – 1:5, 1:10, 1:25, 1:50. Gates for positive staining were based on the unstained sample. Samples were acquired on the LSR Fortessa. Post-acquisition analysis was conducted using FlowJo Version 10.8.1.

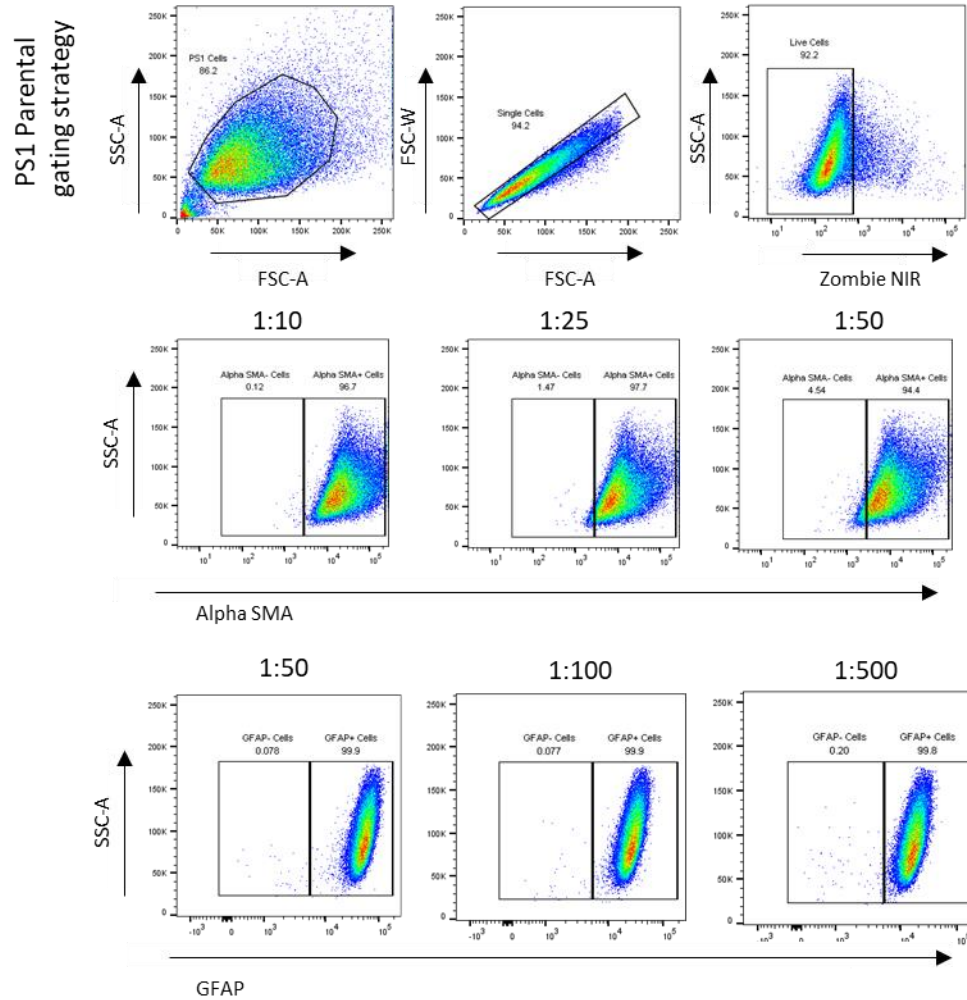


Figure 3.14: PSC flow cytometry antibody titration.

PSC markers were titrated at the following concentrations: Alpha SMA – 1:10, 1:25, 1:50; GFAP – 1:50, 1:100, 1:500. Gates for positive staining were based on the unstained sample. Samples were acquired on the LSR Fortessa. Post-acquisition analysis was conducted using FlowJo Version 10.8.1.

3.7.1 NKG2A Troubleshooting

3.7.1.1 *Western blot analysis*

To ensure the natural killer cell line NK92 expressed the inhibitory receptor NKG2A, western blot analysis was employed. Clear expression of NKG2A in NK92, but not cancer cells or PSCs was observed (Figure 3.15).

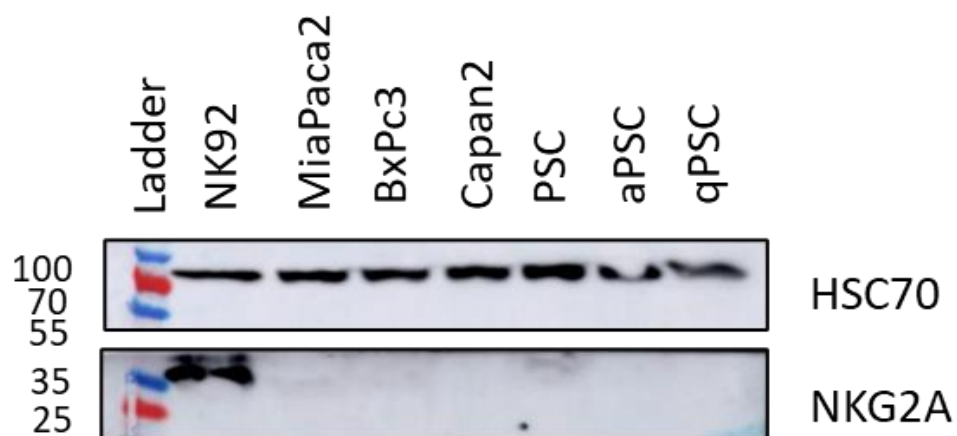


Figure 3.15: Western blot analysis of NKG2A expression.

NK92, MiaPaca2, BxPC3, Capan2, untreated PSC, aPSC and qPSC were loaded into a 10% SDS-PAGE gel and run for 1h 40min. Membranes were stained using a rabbit anti-NKG2A antibody. HSC70 was used as a loading control. Blots were imaged using the ChemiDoc 600.

3.7.1.2 Primary and Secondary antibody staining for NKG2A

To assess if antigen-antibody binding was the cause for the lack of staining observed, staining protocols for single staining (conjugated antibody) and double staining (unconjugated NKG2A primary antibody and fluorescent secondary antibody) were trialled. Surface and intracellular staining protocols were used for each condition.

Intracellular but not surface staining for NKG2A using primary and secondary antibodies was found to yield a positive population (Figure 3.16).

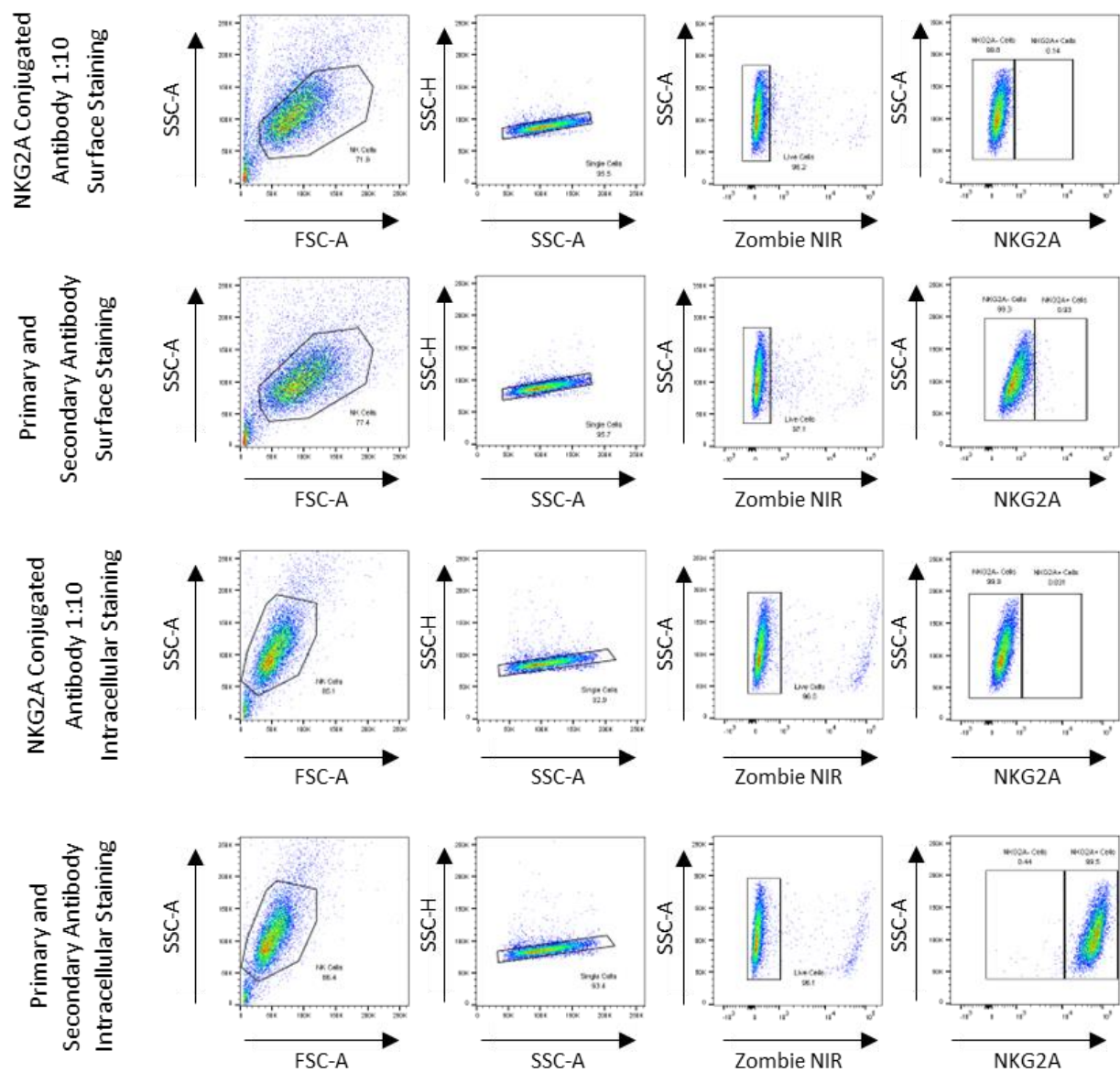


Figure 3.16: NKG2A expression on NK92 cells using surface and intracellular staining protocols.

NKG2A expression on NK92 cells using surface and intracellular staining protocols. Staining was carried out using either a PerCP conjugated antibody, or primary and secondary antibodies. Gating strategies were established from unstained samples. Samples were acquired on the LSR Fortessa. Post-acquisition analysis was conducted using FlowJo Version 10.8.1.

To validate this finding as true staining rather than a population shift as a result of antibody addition, staining was repeated with the inclusion of MiaPaca2 cells as a negative control (Figure 3.17).

Intracellular staining of both NK92 cells and MiaPaca2 cells yielded a population positive for NKG2A. Thus, it was concluded that the positive signal observed previously was a result of a population shift rather than true staining. Conversely, cells fixed before staining demonstrate a distinct population of NKG2A positive NK92 cells (panel 3, Figure 3.17), a population absent in MiaPaca2 cells.

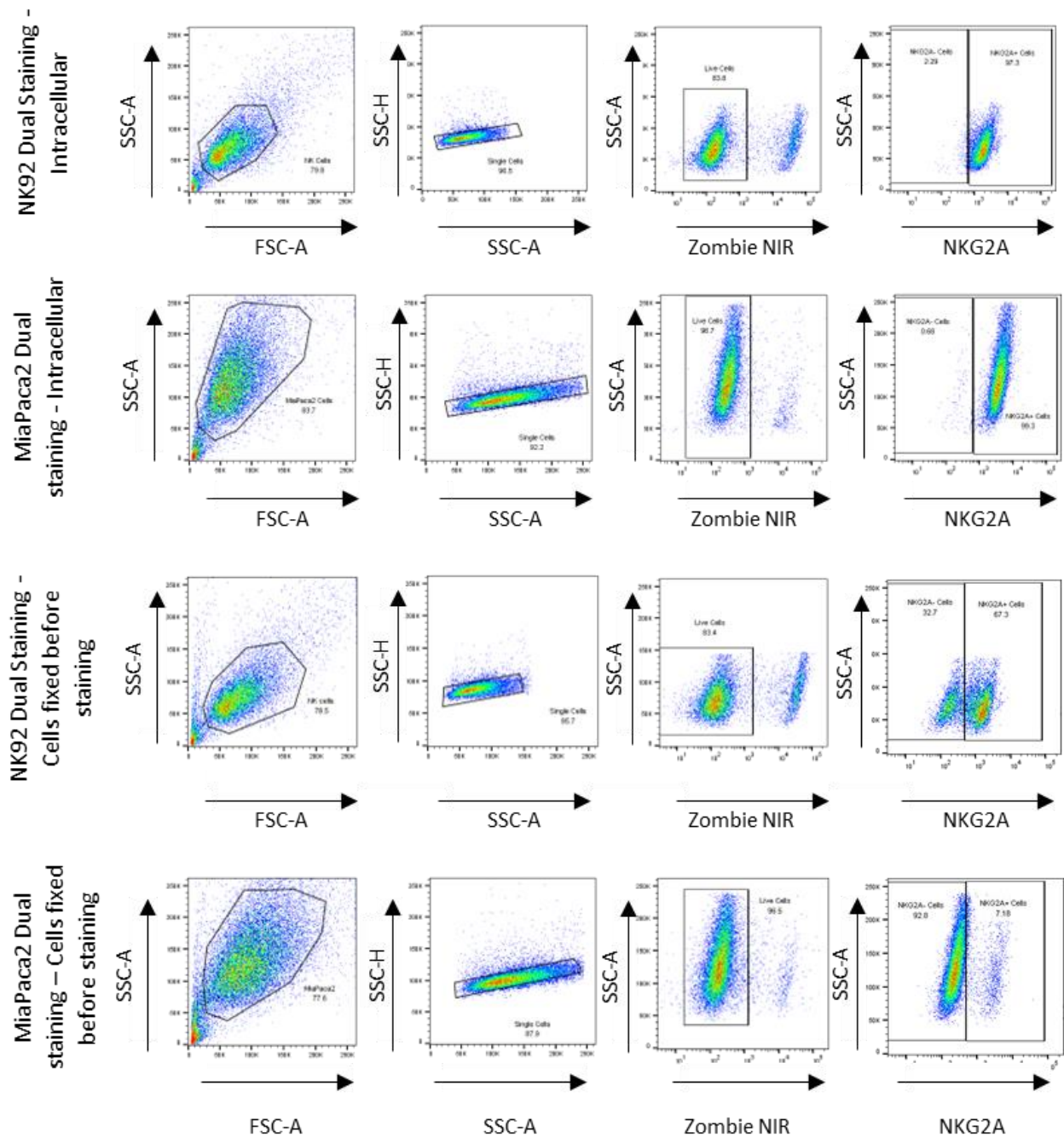


Figure 3.17: NK92A troubleshooting.

NK92 and MiaPaca2 cells were stained using either an intracellular staining protocol or fixing cells before surface staining. Gating strategies were established using unstained samples. Samples were acquired on the LSR Fortessa. Post-acquisition analysis was conducted using FlowJo Version 10.8.1.

3.7.1.3 *APC conjugated NKG2A antibody trial*

We next sought to determine if the antibody fluorochrome conjugate may be responsible for the lack of staining observed. As PerCP has been demonstrated to be a weak fluor²⁶², a trial vial of the NKG2A antibody conjugated to the highly fluorescent APC fluor²⁶² was tested (Figure 3.18).

Staining using an APC conjugated anti-NKG2A antibody was found to yield positive staining (1:50 dilution) using both classical surface staining protocols and fixing the cells before staining (Figure 3.18). Consequently, this antibody was used for subsequent experiments.

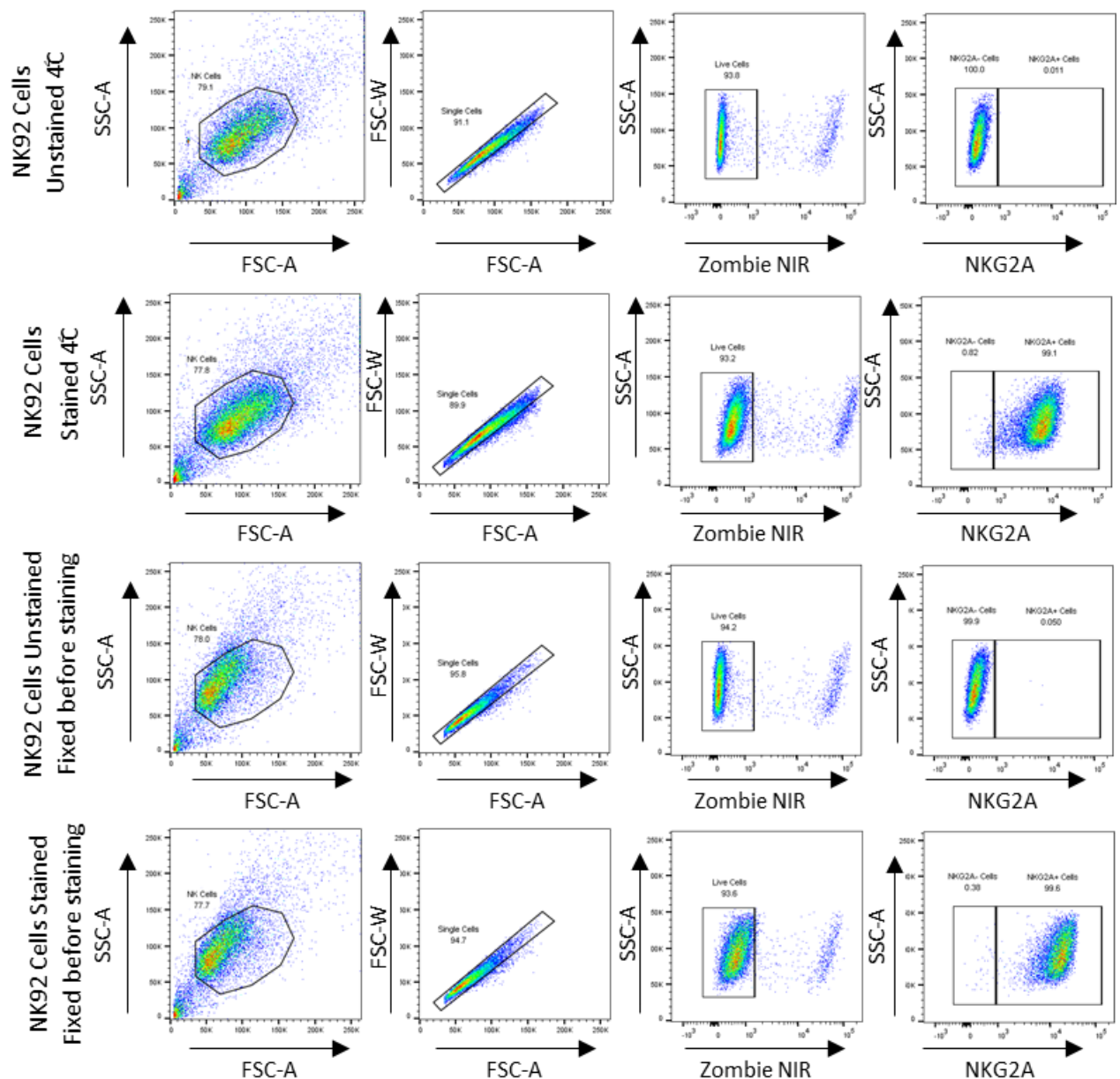


Figure 3.18: Flow cytometry staining of NK92 cells using an APC conjugated anti-NKG2A antibody.

Staining was carried out using either classical surface staining protocols or fixing the cells before staining. Gating strategies were established using unstained samples. Samples were acquired on the LSR Fortessa. Post-acquisition analysis was conducted using FlowJo Version 10.8.1.

3.8 Development of Spectral flow cytometry panels for receptor/phenotypic expression assays

To build on the results of initial receptor/phenotypic expression assays, a more comprehensive spectral flow cytometry panel was developed to assess the impact of co-culture on a range of NK and PSCs functional and phenotypic markers. Antibodies were titrated to determine the optimal staining concentrations, with care taken to maximise fluorescence intensity whilst minimising spectral spill-over (Figure 3.19; Figure 3.20; Figure 3.21 and Figure 3.22).

Alpha SMA and NKG2D antibodies yielded no positive staining in their target populations. This staining was repeated alongside additional cell lines (to establish a truly negative population), however no positive populations could be discerned. As such, additional antibodies were trialled (Figure 3.21). This titration yielded positive results.²⁶¹ Thus, it was concluded that fluors detected in the ultraviolet laser were difficult to extract from cellular autofluorescence. The optimal staining dilutions identified for each marker are shown in Table 3.1.

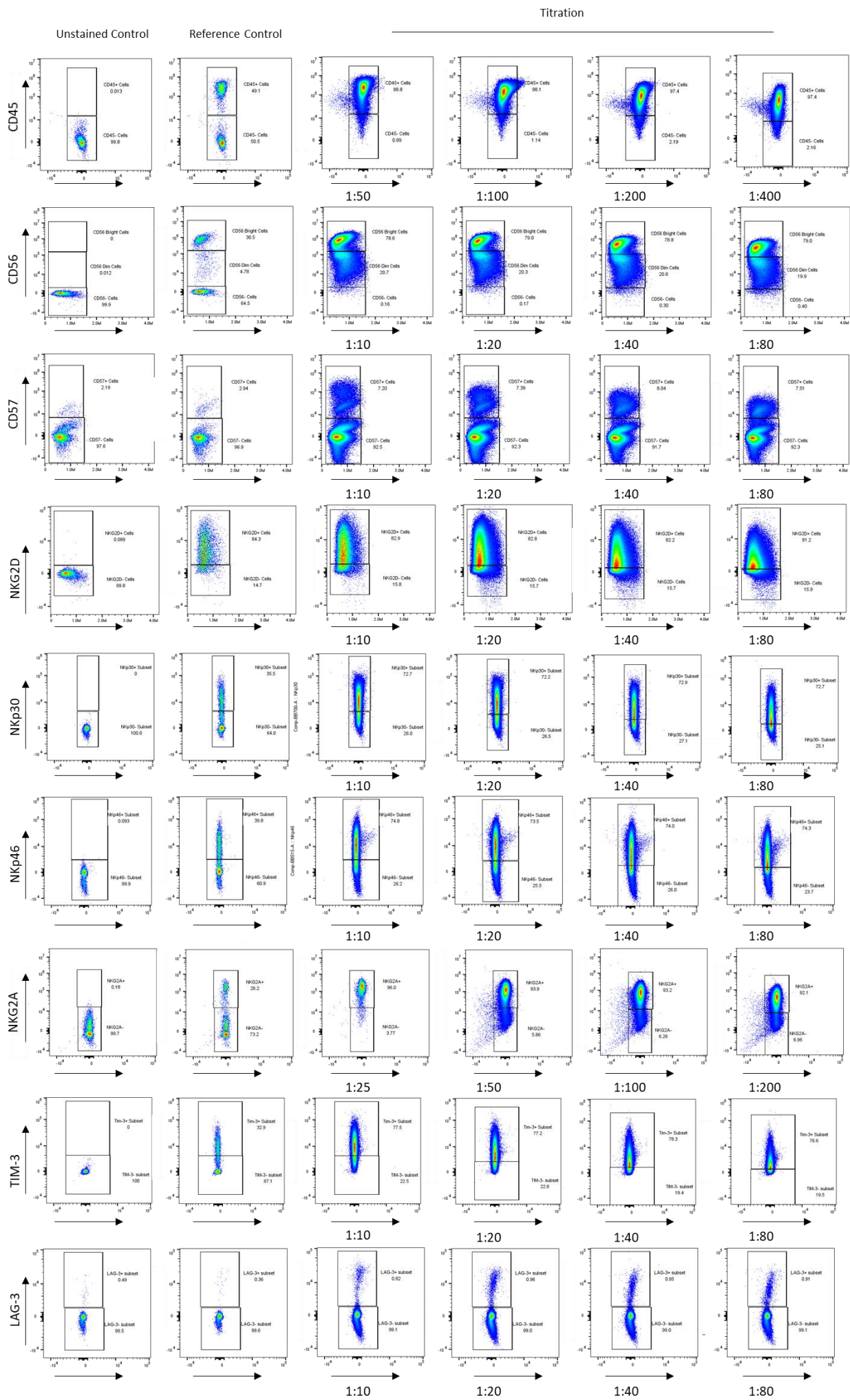


Figure 3.19: NK marker antibody titration results.

Single marker staining of NK92 cells alone. Each marker was titrated one-fold higher and two-folds lower than the manufacturers recommended dilution. Each marker panel displays an unstained sample, a reference control consisting of 50% stained NK cells (stained with the highest antibody concentration) and 50% unstained cells to demonstrate where a true negative population would be found. Gates for the highest dilution were based on the reference and unstained controls. For each dilution thereafter the gates were adjusted to maintain the same percentage of positive and negative cells. Antibodies were considered no longer efficacious at the point at which positive and negative populations could not be separated. All titrations were run on the Cytex aurora 5 laser cytometer. Data were analysed post-acquisition using FlowJo version 10.8.1.

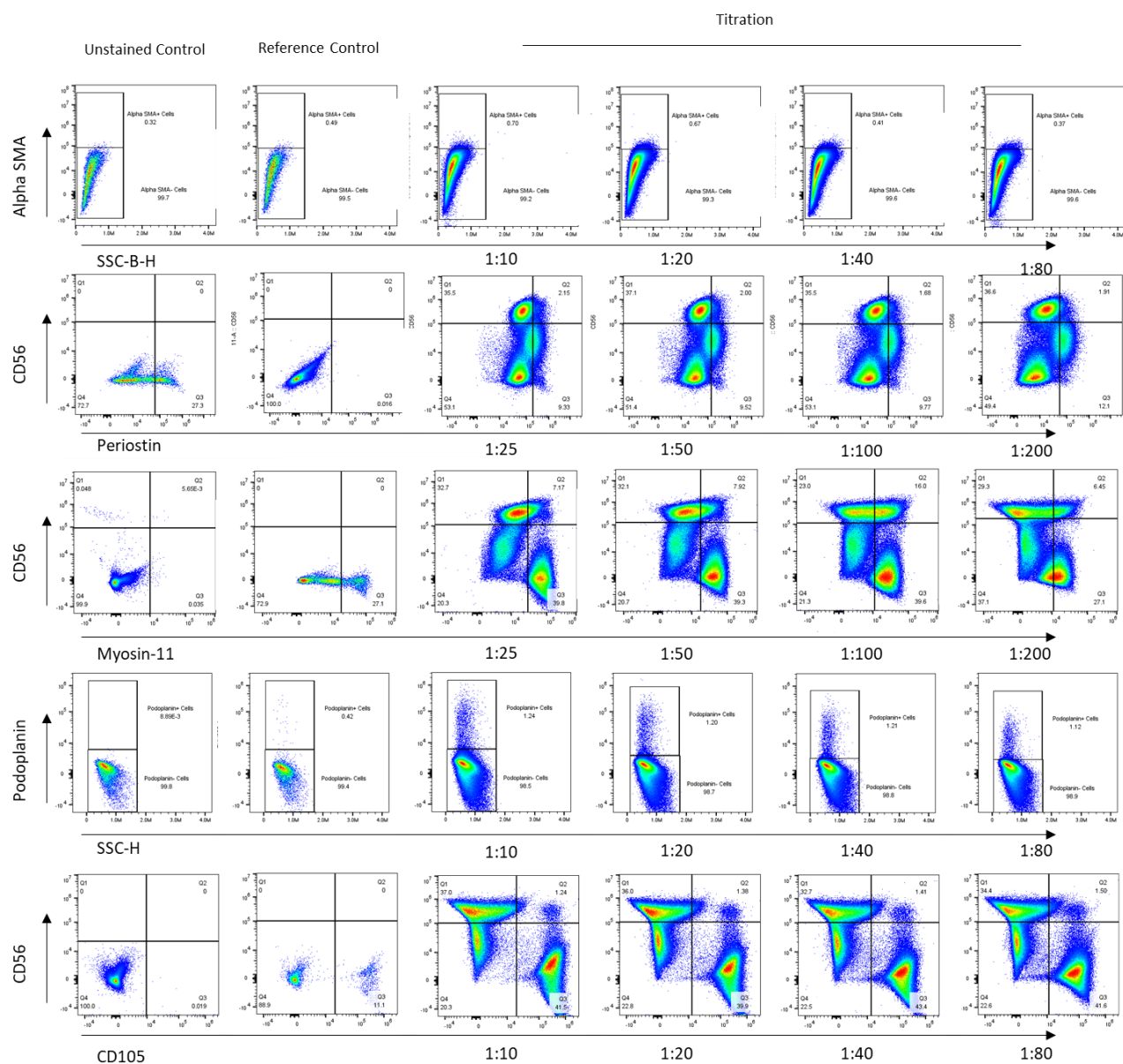


Figure 3.20: PSC Marker Titration.

Due to some difficulty differentiating negative cells during NK92 marker titrations, PS1 cells were stained alongside BxPC3 (alpha SMA and Podoplanin) or NK92 cells (Myosin-11, CD105, Periostin) to ensure truly negative populations were present within the samples. Titrations of Periostin, Myosin-11 and CD105 were double stained for CD56 (1:80). Reference controls were created as described using single stains for the marker of interest. All titrations were run on the Cytex aurora 5 laser cytometer. Data were analysed post-acquisition using FlowJo version 10.8.1.

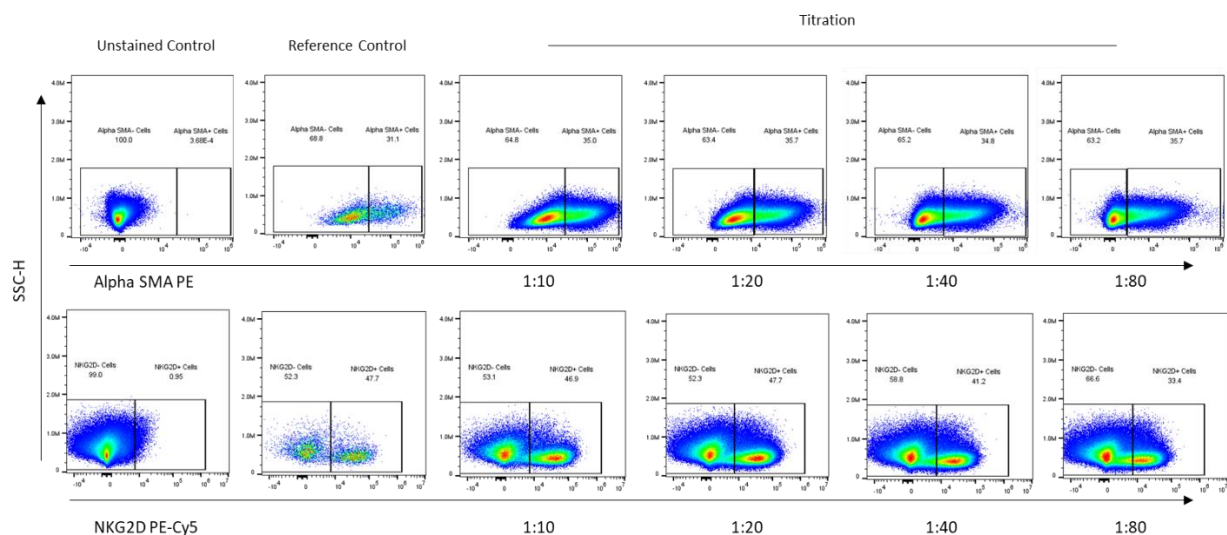


Figure 3.21: Optimisation of re-sourced antibodies for alpha SMA and NKG2D.

Each marker was titrated one-fold higher and two-folds lower than the manufacturers recommended dilution. To ensure truly negative populations were present for each marker, a 1:1 ratio of NK and PSCs were used for each condition. Each marker panel displays an unstained sample, a reference control and each titration condition. All titrations were run on the Cytex aurora 5 laser cytometer. Data were analysed post-acquisition using FlowJo version 10.8.1.

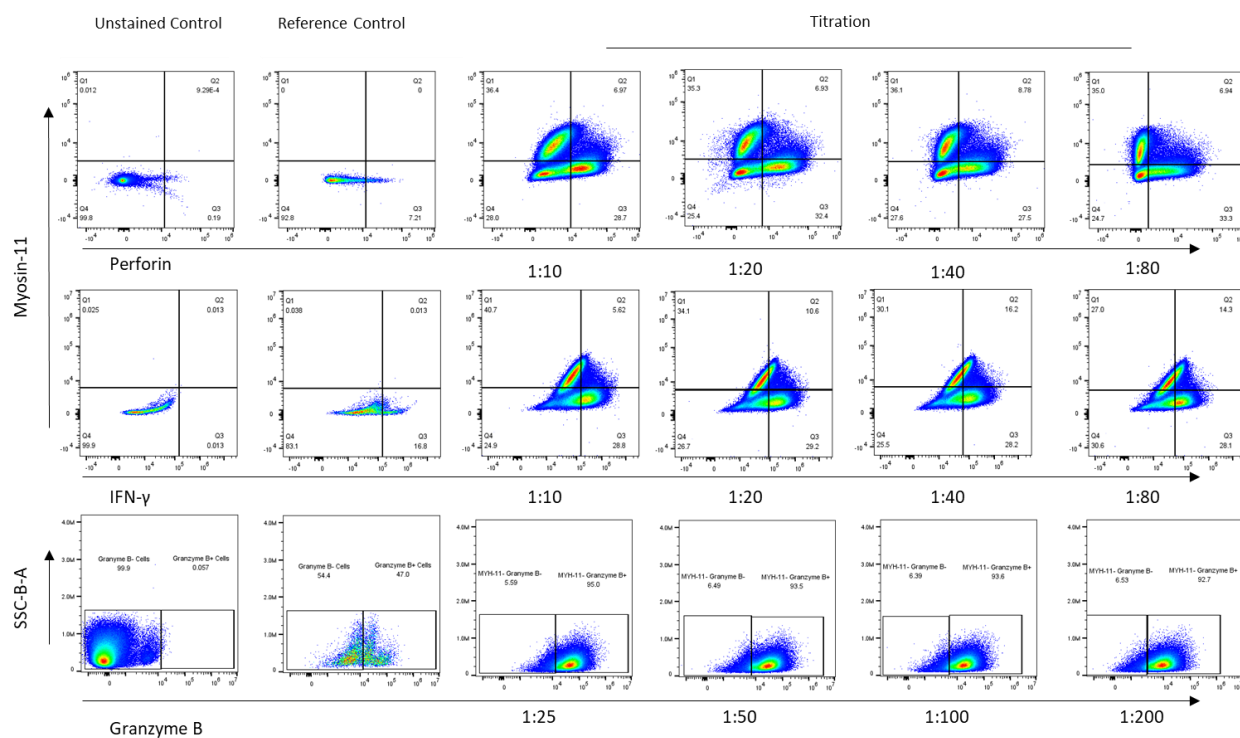


Figure 3.22: NK Cell Functional Marker Titration.

NK92 cells were stained alongside PS1 cells. For Granzyme B and IFN- γ , NK92 cells were stimulated with PMA and ionomycin for 4h prior to staining. Cells were double stained with Myosin-11 to identify positive and negative populations. Granzyme B⁺ cells are gated from the Myosin-11⁺ population. All titrations were run on the Cytex aurora 5 laser cytometer. Data were analysed post-acquisition using FlowJo version 10.8.1.

Staining Panel	Antibody	Dilution
Natural Killer Cells	CD45	1: 200
	CD56	1: 80
	CD57	1: 80
	NKG2D	1: 40
	NKp30	1: 20
	NKp46	1: 40
	NKG2A	1: 200
	TIM3	1: 20
	LAG-3	1: 40
	Granzyme B	1: 50
	Perforin	1: 40
	IFN- γ	1: 40
PSCs	Alpha SMA	1: 20
	Periostin	1: 50
	Myosin-11	1: 100
	Podoplanin	1: 40
	CD105	1:80

Table 3.1: Optimised antibody dilutions for NK and PSC flow cytometric staining.

3.9 Receptor/Phenotypic expression assay trial

To determine if spectral unmixing could be successfully carried out with the designed panels and to identify if compensation was necessary/could be achieved, trial experiments for full panel staining of both NK and PSCs were carried out prior to running co-culture experiments. The results of full panel trials are shown in Figure 3.23 and Figure 3.24.

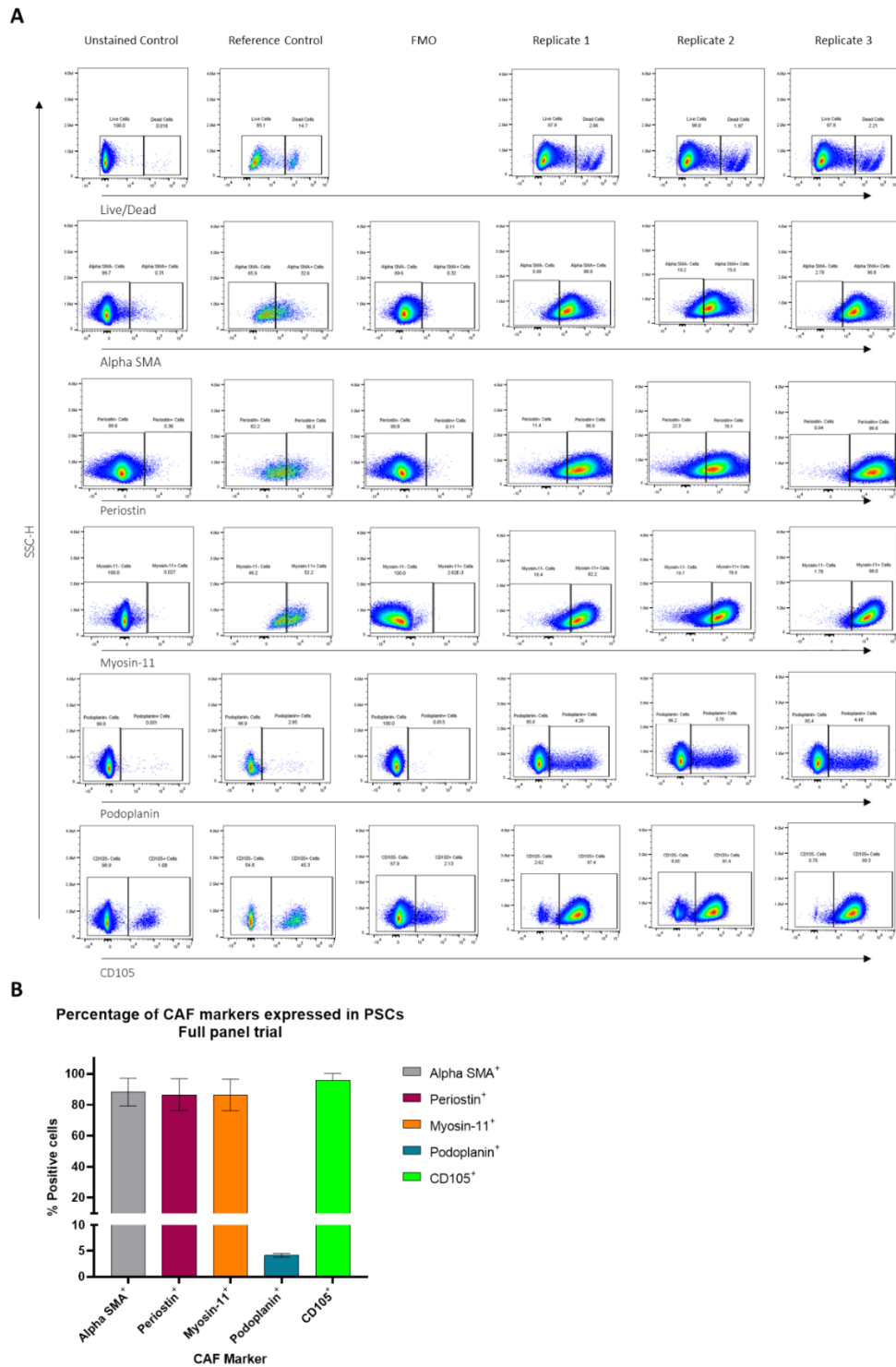
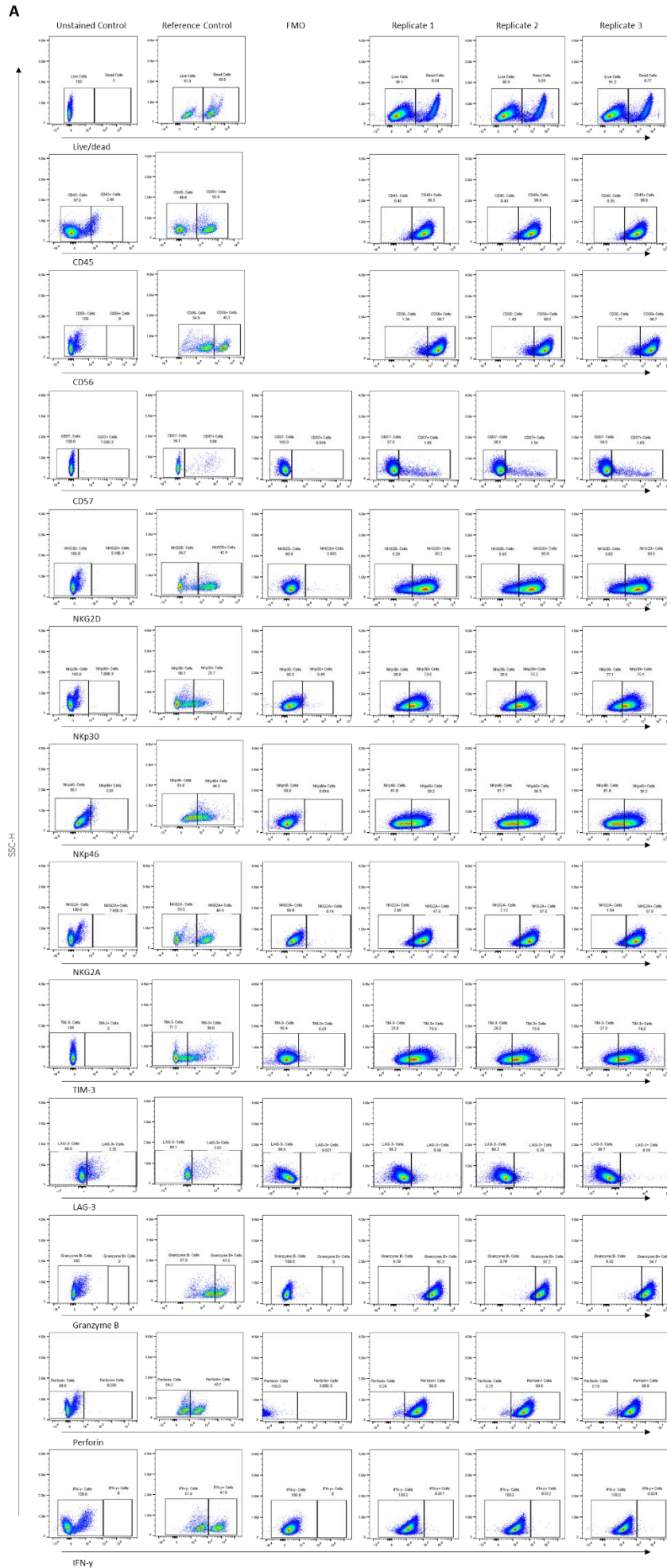


Figure 3.23: PSC full panel trial.

A) Flow cytometry plots of each PSC marker stained in the full panel trial. Gating was based on reference and fluorescence minus one (FMO) controls. Samples were run on the Cytex aurora. Compensation was carried out using SpectroFlo (3.0.3) and data analysed using FlowJo (10.8.1). B) Average percentages of each CAF marker identified in untreated PSCs. Data are from one biological replicate.



B

Percentage of NK Markers expressed by unstimulated NK cells

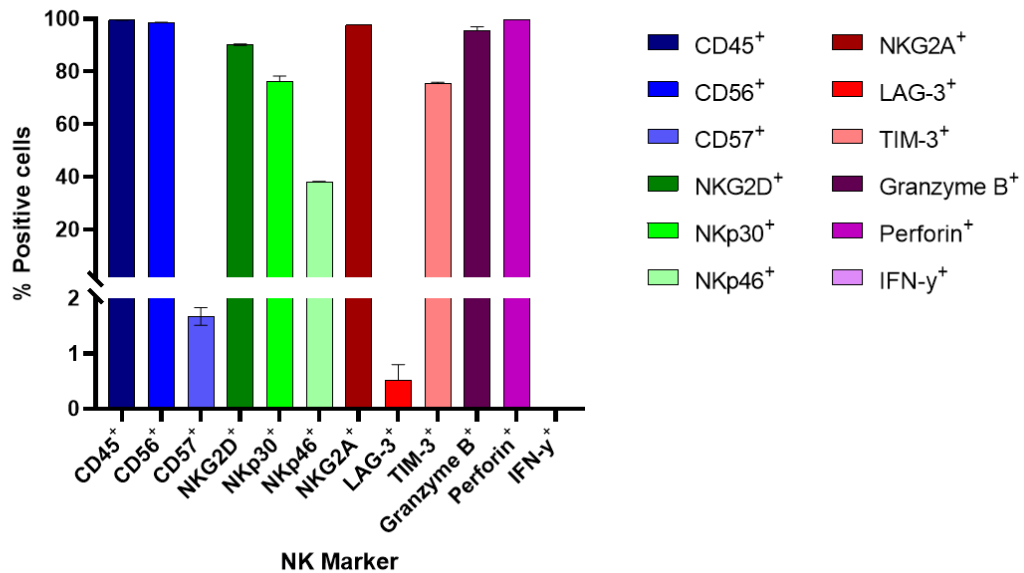


Figure 3.24: NK cell full panel trial.

A) Flow cytometry plots of each NK marker stained in the full panel trial. Gating was based on reference and fluorescence minus one (FMO) controls. Samples were run on the Cytex aurora. Compensation was carried out using SpectroFlo (3.0.3) and data analysed using FlowJo (10.8.1). B) Average percentages of each NK marker identified in naïve NK cells. Data are from one biological replicate.

Chapter 4 - Results 2 – *In Vitro* Experiments

4.1 Introduction

The interaction between NK cells and PSCs remains largely understudied. Previous work has demonstrated NK potential to target and lyse PSC cell lines when stimulated with IL-15. This process was NKG2D dependent, highlighting the importance of direct contact in this interaction.²³² However others have suggested downregulation of crucial NK functional markers, such as CD107a, granzyme B and interferon- γ , in response to co-culture with activated but not 'normal' pancreatic stellate cells.²⁶³ Thus, despite early knowledge, a global perspective of the functional proteomic changes within both cell types in response to cell-cell interaction is lacking.²⁶⁴

Previously we optimised several assays for the investigation of NK-PSC interaction. In this chapter we investigate the bi-directional interaction between NK cells and PSCs *in vitro* through the use of degranulation, cytotoxicity and Luminex assays as well as global proteomic analysis.

4.2 Characterisation of pancreatic stellate cells and pancreatic cancer cell lines

To ensure the cell lines used within our experiments retained their classic phenotype in culture, immunofluorescent staining was carried out. PSCs were stained for the stellate specific markers alpha SMA, vimentin and desmin, whilst the pancreatic cancer cell lines BxPC3, Capan2 and MiaPaca2 were stained for cytokeratin (Figure 4.1 and Figure 4.2). We determined positive staining for each cell specific marker, demonstrating a stable cellular phenotype prior to experimentation.

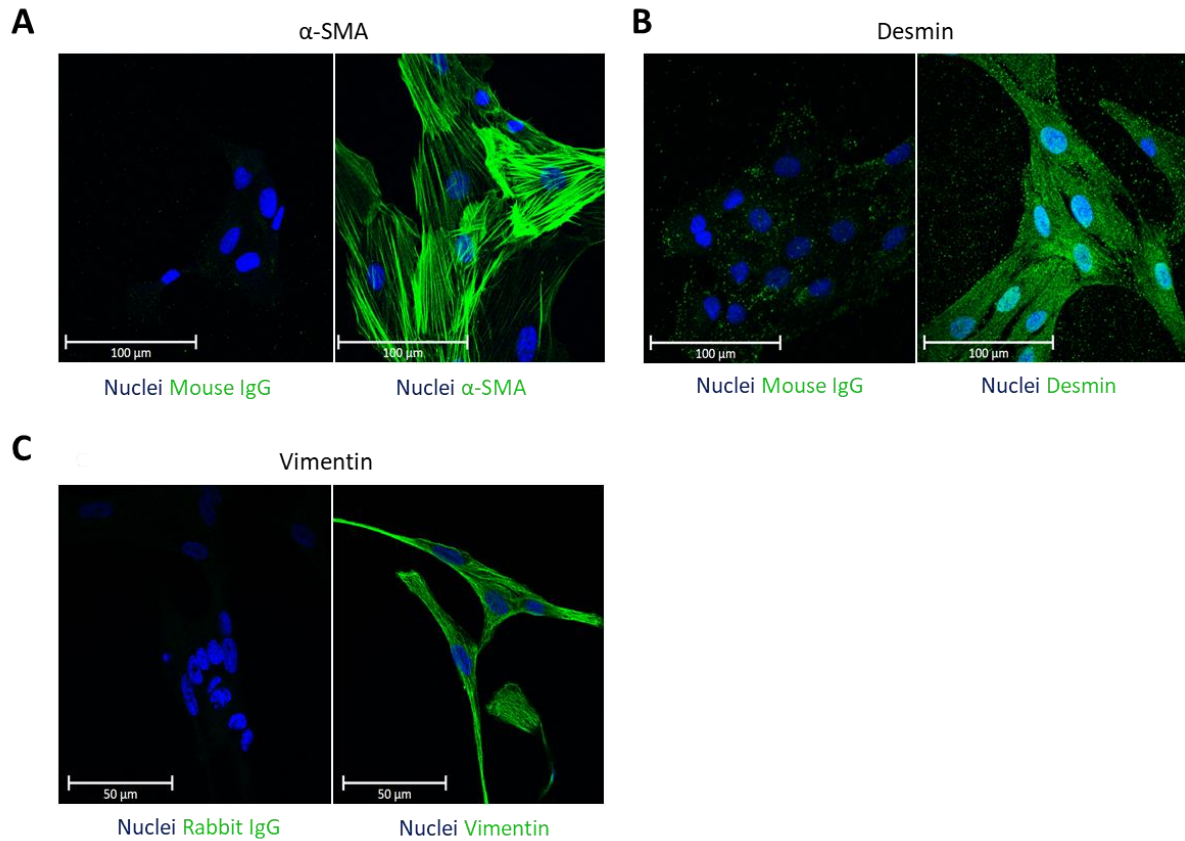


Figure 4.1: Characterisation of PS1 cells.

A) α -SMA (magnification x40) B) Desmin (magnification x40) C) Vimentin (magnification x63) staining of PS1 cells. Each marker is depicted next to an IgG control (left). Images A and B were acquired on the LSM710 Laser scanning confocal microscope (Zeiss). Image C was acquired on the LSM880 Laser scanning confocal microscope (Zeiss). Scale Bars A, B = 100 μ m, C = 50 μ m.

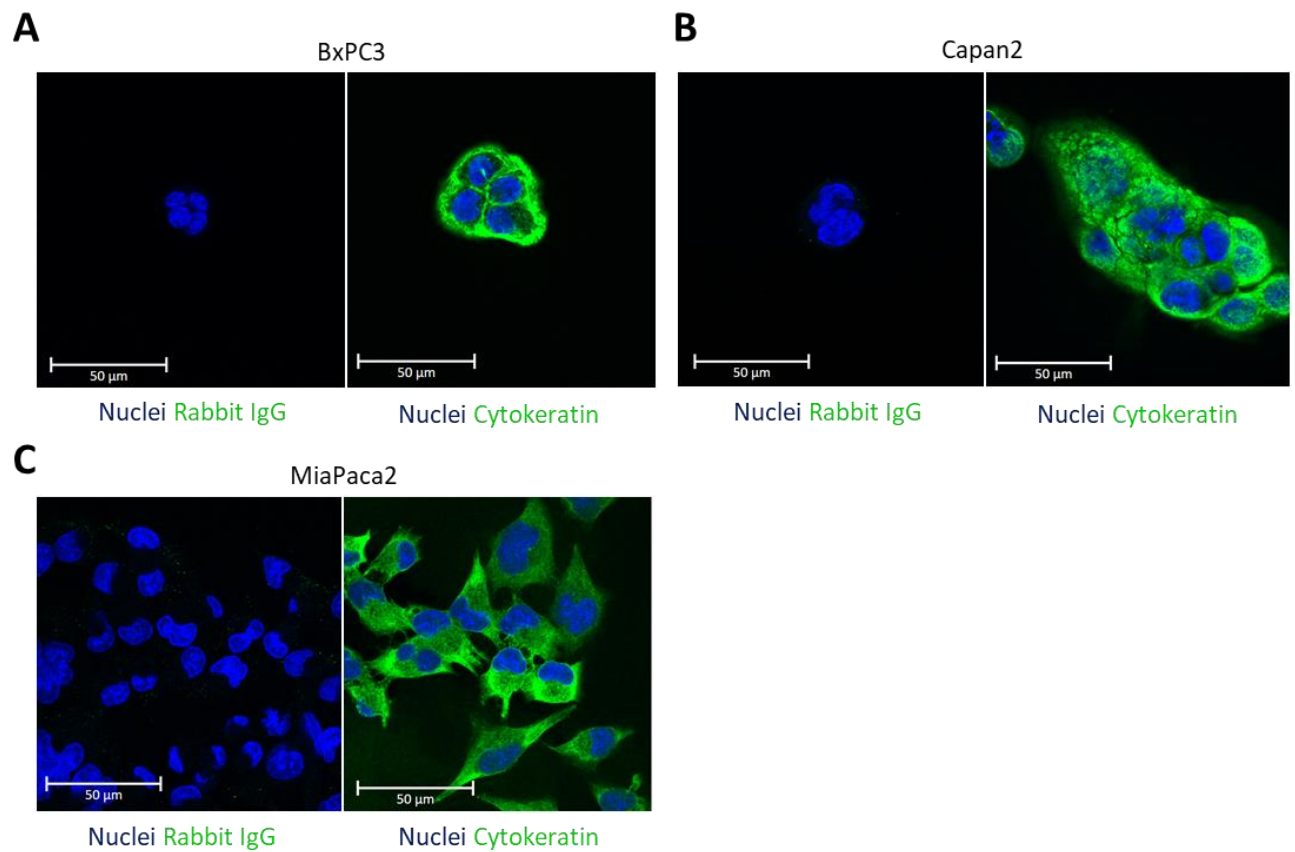


Figure 4.2: Characterisation of pancreatic cancer cell lines.

A) BxPC3, B) Capan2 and C) MiaPaca2 cells stained with isotype control (left) or the epithelial marker cytokeratin (right). Cells were counterstained with DAPI. All images were acquired on the LSM710 laser scanning confocal microscope. Magnification x63. Scale bars = 50μm.

4.3 WST-1 Cytotoxicity Assays

To determine if education (24h co-culture at a 1:1 ratio) by quiescent pancreatic stellate cells (qPSC) and/or activated pancreatic stellate cells (aPSC) impacted NK cell cytotoxic capabilities, a WST-1 cytotoxicity assay was employed.²⁶⁵

Incubation with naïve, qPSC educated or aPSC educated NK cells did not yield a significant decrease in proliferation for BxPc3, MiaPaca2 or Capan2 cells at any effector to target ratio tested (Figure 4.3). Moreover, for both MiaPaca2 and Capan2, proliferation significantly increased when cultured with qPSC or aPSC educated NK cells (versus target cells alone).

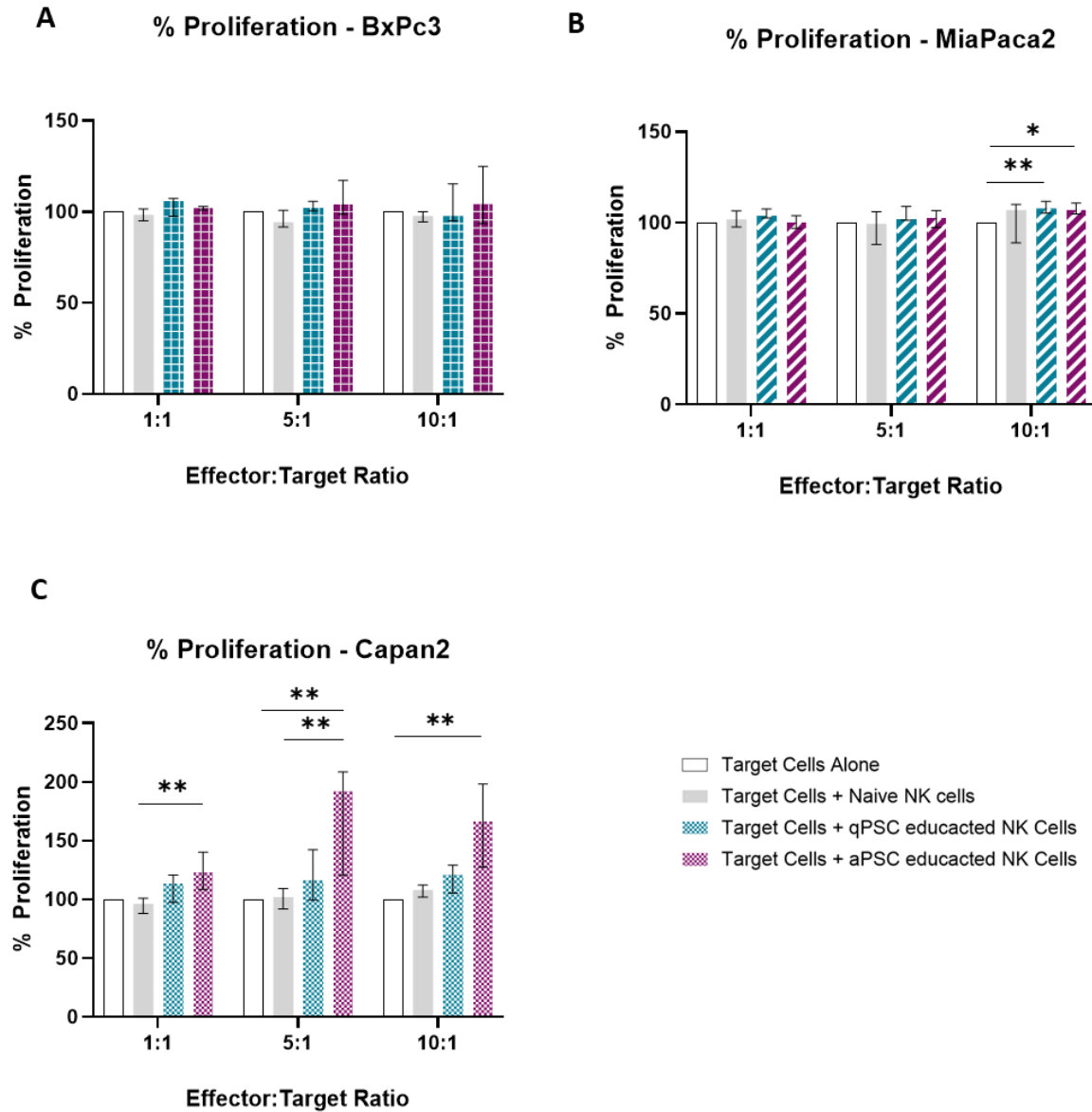


Figure 4.3: WST-1 cytotoxicity assays

BxPC3 (A), MiaPaca2 (B) and Capan2 (C) cells were cultured either alone or with NK92 cells at effector: target ratios of 1:1, 5:1 or 10:1. Cell were incubated for 4h prior to addition of WST-1. All data were analysed using Kruskal Wallis with Dunn's post hoc analysis. Summary statistics are represented as median+/-IQR. Significance was established if $p < 0.05$.

The lack of cytotoxicity observed was suggested to be a result of; IL-2 starvation resulting in modulation of NK function^{266 267}, insufficient washing leading to the viability of residual NK cells being assessed, or synapse formation between NK and PSCs resulting in cellular transfer of PSCs to experimental plates, increasing the total number of cells analysed. Consequently, two further cytotoxicity assays were carried out to address these areas of potential confounder.

Following 4h incubation, NK cells do not decrease Capan2 proliferation in any condition tested, suggesting that IL-2 starvation may not be the cause for the confound observed at this time point (Figure 4.4A). Conversely, 24h incubation with NK92 cells plated with IL-2 demonstrates a clear decrease in Capan2 proliferation, proving NK functional efficacy (Figure 4.4B).

Despite controlling for washing inaccuracies, Capan2 cells incubated with NK cells cultured with both qPSCs and aPSCs at 4h and 24h demonstrate dramatically elevated proliferation versus target cells alone, suggesting that additional factors may be responsible for the confounder observed (Figure 4.4).

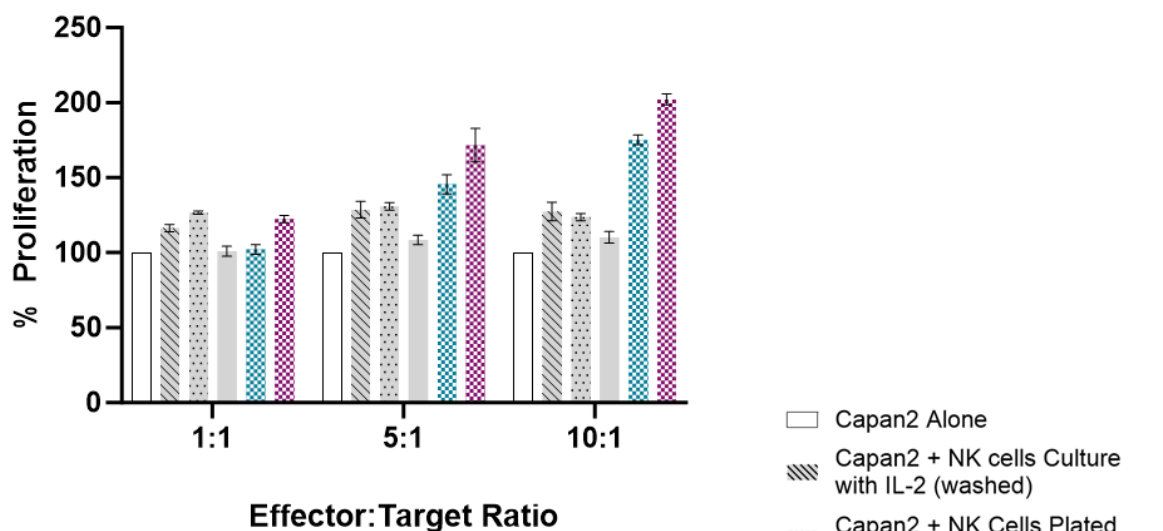
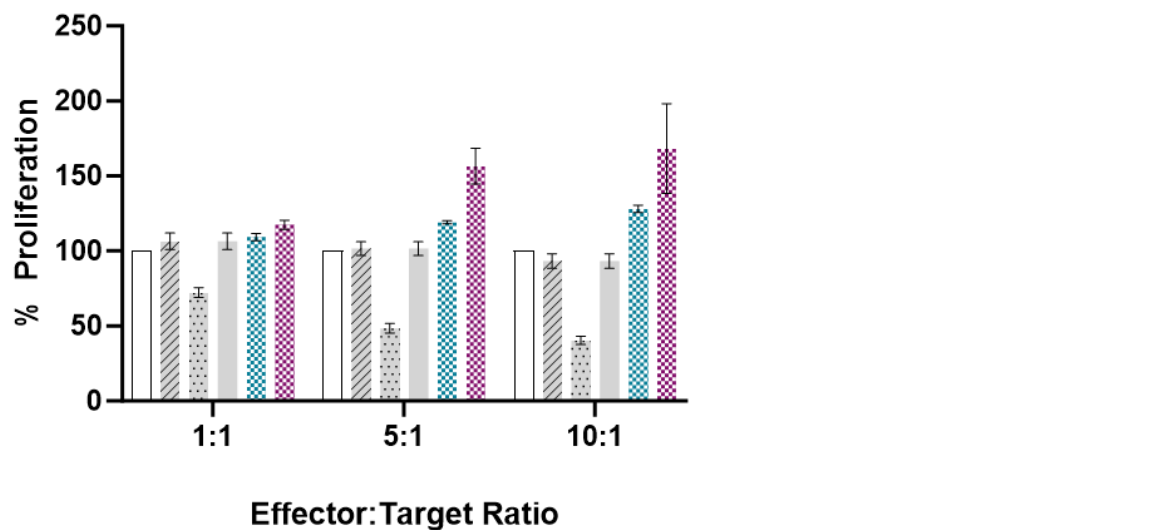
A**% Proliferation - 4h Incubation****B****% Proliferation - 24h Incubation**

Figure 4.4: WST-1 cytotoxicity assay troubleshooting.

Capan2 cells were cultured for either 4h (A) or 24h (B) in one of the following five conditions: cultured alone, with NK cells treated with IL-2 prior to plating, with NK cells cultured and plated with IL-2, with naïve NK cells, with qPSC educated NK cells or aPSC educated NK cells. Data are from one biological repeat.

To further investigate the cause of the increased proliferation observed, cells were plated as described and incubated for 24h. Following incubation, plates were imaged to visualise cell-cell interactions. Incucyte images reveal the presence of PSCs within the cytotoxicity assay. It is likely that some PSCs were aspirated and transferred alongside the NK cells and may account for the increased proliferation observed. Moreover, co-cultured NK cells, specifically those cultured with aPSCs, appear to display a more adhesive phenotype, making the cells less easily removed during washing steps, vastly increasing cell number within the well (Figure 4.5).

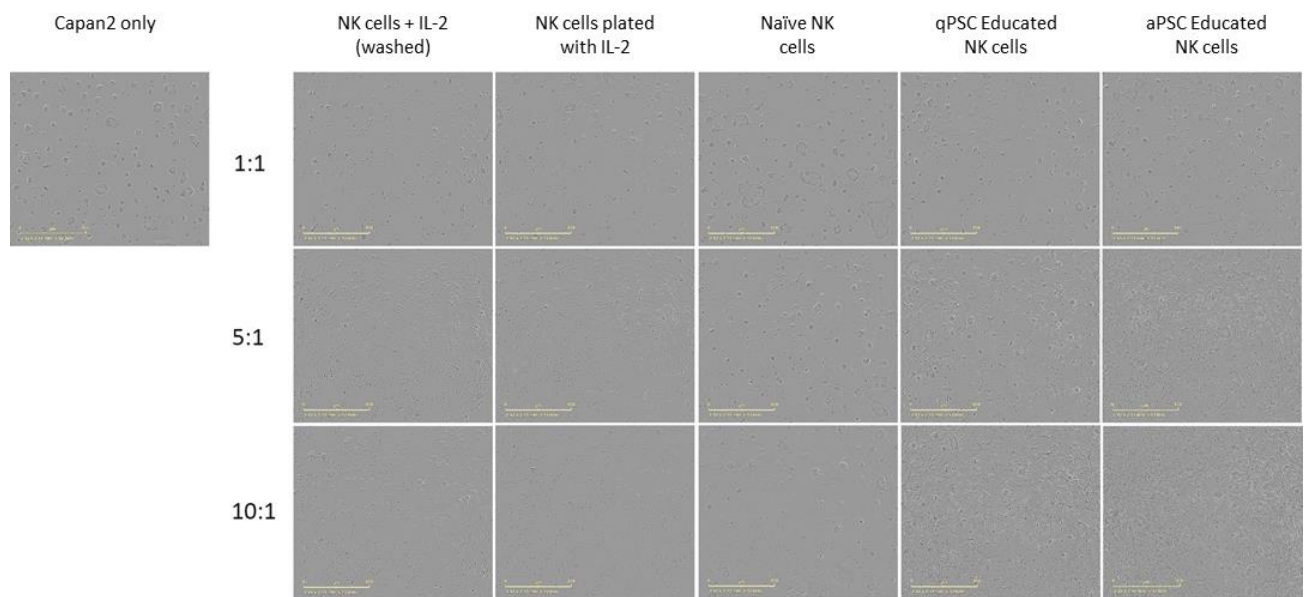


Figure 4.5: Incucyte images of Capan2 cells following 24h incubation with NK92 cells

Capan2 cells were cultured in one of the following five conditions: cultured alone, with NK cells treated with IL-2 prior to plating, with NK cells cultured and plated with IL-2, with naïve NK cells, with qPSC educated NK cells or with aPSC educated NK cells. Effector: Target ratios are shown to the left of each panel. Magnification x4. Scale Bar=800µm.

4.4 CD107 Degranulation Assays

As previous work remains inconclusive as to the interaction between NK and PSCs in regards to NK functional efficacy, we used the CD107 degranulation assay to assess the functional efficacy of naïve and educated NK cells against qPSCs/aPSCs and pancreatic cancer cell lines, respectively (Appendix 2).²⁵⁵

We identify NK cell degranulation in response to co-culture with both qPSC and aPSC at 1:1 and 5:1 ratios (Figure 4.6A, B), demonstrating NK cell activity against PSCs. Additionally, as previous work suggested that PSC education may modulate NK functional proteins, we hypothesised that education of NK cells by either qPSCs or aPSCs for 24h, may variably affect NK-mediated cancer cell cytotoxicity. Using three cancer cell lines (BxPC3, Capan2, MiaPaca2) with distinct properties we identified a reduction in the percentage of NK cells demonstrating surface expression of CD107a/b upon education by qPSC compared to those cultured with aPSC or in their naïve state at a 1:5 ratio (Figure 4.6C). This suggests a reduction in NK cell functional efficacy in qPSC-, but not aPSC-, educated NK cells.

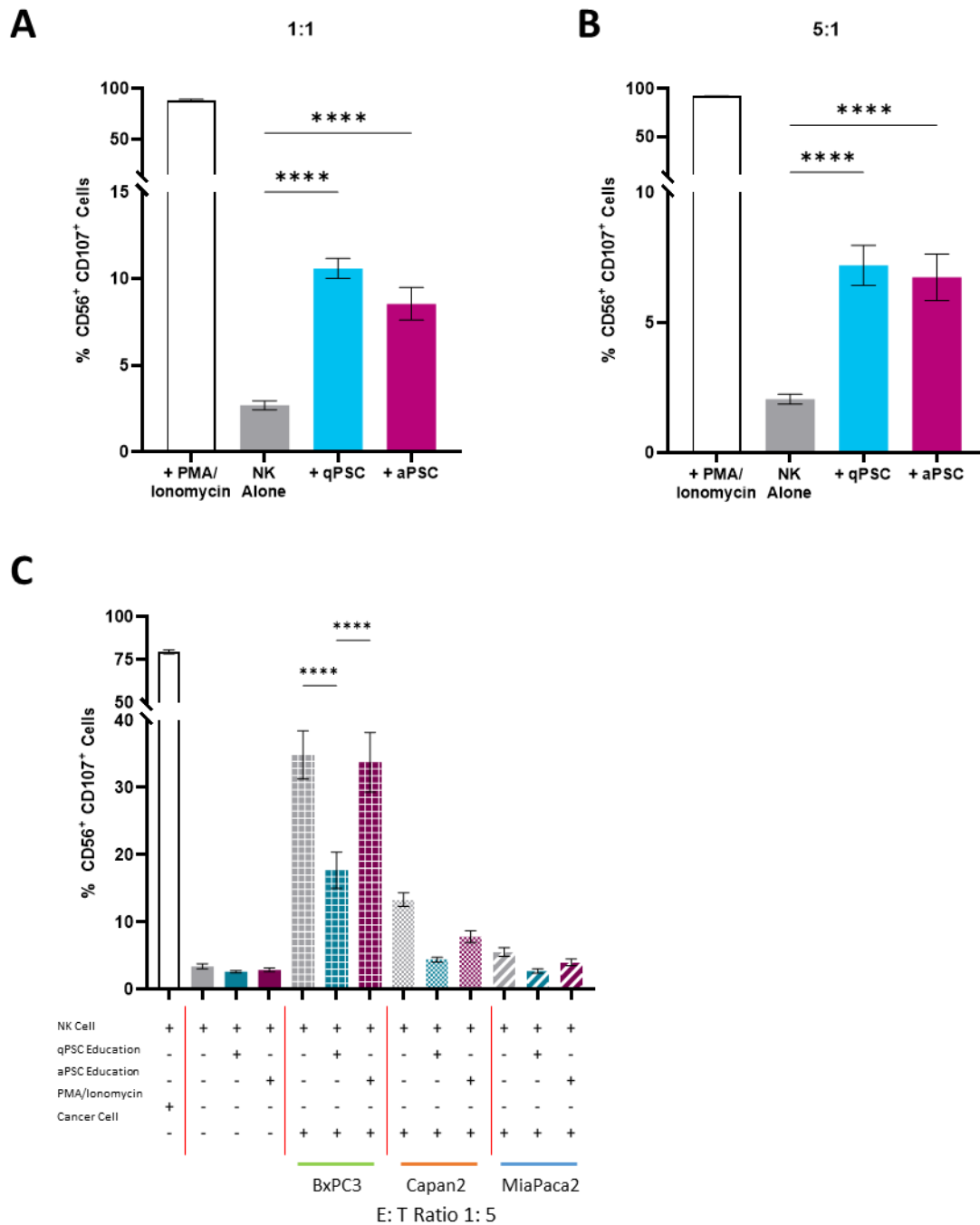


Figure 4.6: NK cell degranulation against PSCs and the impact of PSC education on NK functional efficacy.

A-B) CD107a/b expression in NK cells following 6h co-culture at a 1:1 (a) or 5:1 (B) effector: target ratio with quiescent or activated PSCs. Expression is delineated by % positive cells. Data were analysed using One-Way ANOVA with Šidák's post hoc tests. C) Naïve/educated NK cell expression of CD107a/b following co-culture with pancreatic cancer cell lines. Educated NK cells were cultured for 24h (1:1) with either qPSC or aPSC before 6h incubation with cancer cell lines (effector: target ratio 1:5). One-Way ANOVA results show significant variation in CD107a/b expression between naïve and educated NK cells cultured with BxPC3 cells (Šidák's multiple comparisons) **** $p < 0.0001$.

4.5 Calcein AM Cytotoxicity Assays

We next sought to validate our findings using a direct measure of NK cell-induced lysis. Whilst WST-1 cytotoxicity assays have proved effective in the screening of cytotoxic compounds,^{265, 268, 269} due to the cell transference observed during initial assays (Figure 4.5) we opted to use the Calcein AM cytotoxicity assay²⁴⁸ to confirm our findings.

Calcein AM cytotoxicity assays²⁴⁸ demonstrate PSC lysis in response to NK cell co-culture in a dose dependent manner within six hours. This effect was more pronounced on qPSCs (Figure 4.7A), suggesting that PSC activation may lead to protection from NK cell lysis. Moreover, qPSC education of NK cells is seen to reduce NK-induced cell lysis of cancer cells in a dose dependent manner when compared to aPSC educated or naive NK cells (Figure 4.7B-D). Some variation across cancer cell lines is observed. Taken together, our data build on the previous information^{232, 233} and demonstrate that whilst qPSC are more vulnerable to NK induced lysis (Figure 4.6A, B; Figure 4.7A) their education of NK cells results in decreased NK-mediated cancer cell cytotoxicity when compared to education by aPSCs (Figure 4.6C and Figure 4.7B-D).

Interestingly, of the three pancreatic cancer cell lines, BxPc3 cells demonstrate the greatest susceptibility to NK cell lysis (Figure 4.7B), whilst Capan2 cells were the least susceptible. This may be due to the variation in differentiation and mutational status of the cell lines (Table 2.2). Previous work in colorectal cancer has highlighted the importance of cancer differentiation status in NK-induced lysis²⁷⁰, however further work is needed to validate this hypothesis in PDAC and to determine the impact of mutational status on NK efficacy.

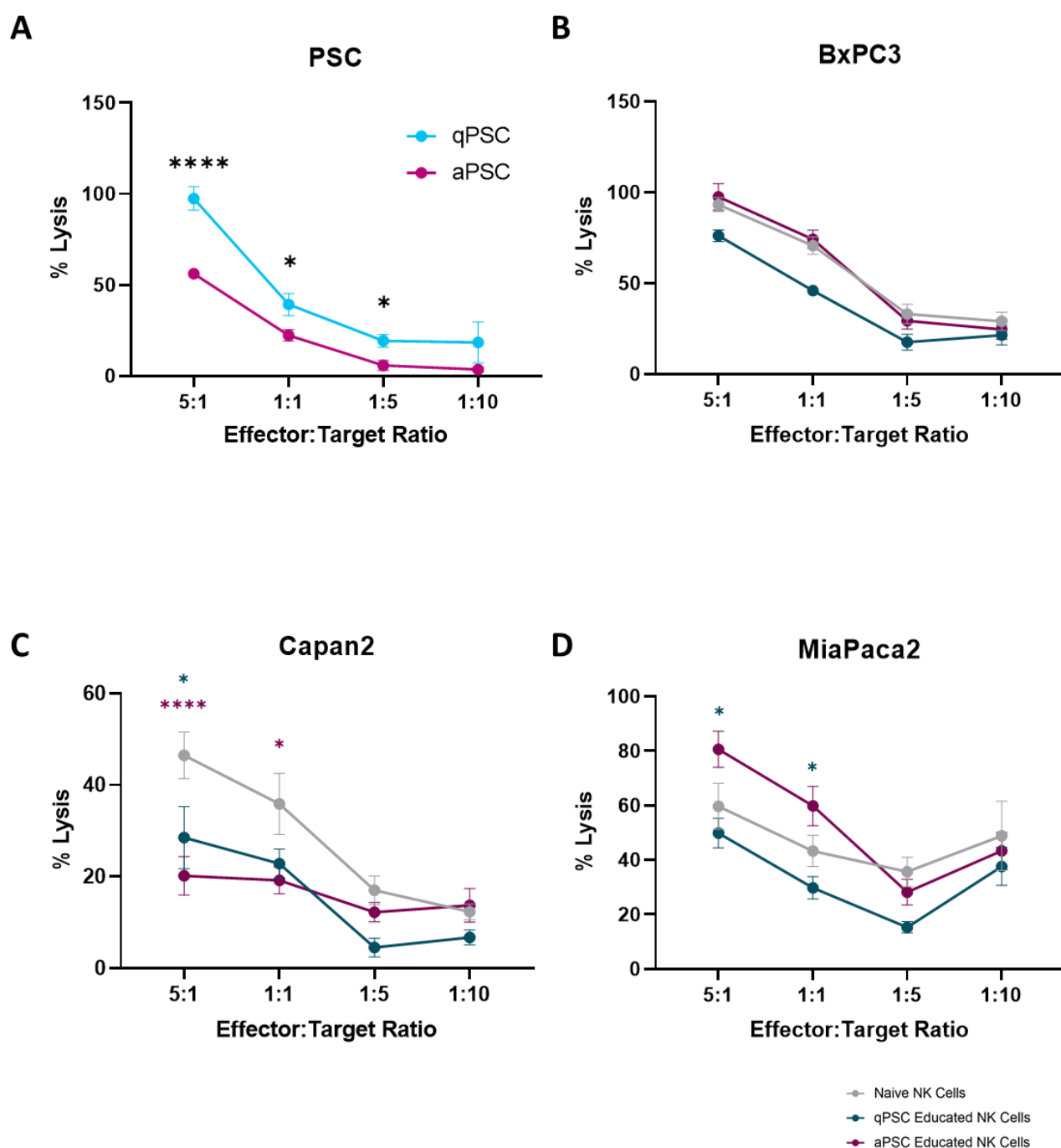


Figure 4.7: Calcein AM Cytotoxicity assays.

A) Percent lysis of quiescent and activated PSCs following 6h incubation with naïve NK cells at multiple effector to target ratios. Percent lysis = (test value – spontaneous release)/ (maximum release - spontaneous release) *100.²⁴⁸ Data were analysed using multiple unpaired t-tests (Welch correction) with Holm-Šidák post hoc analysis. B-D) Percent lysis of BxPC3 (B), Capan2 (C) and MiaPaca2 (D) cells following 6h incubation with naïve or educated NK cells. Percent lysis was calculated as described. Data were analysed using Kruskal-Wallis analysis with Dunn's post hoc tests (BxPC3) or One-Way ANOVA (Capan2; MiaPaca2) with Šidák's Post hoc analysis. * $p < 0.05$; ** $p < 0.01$; *** $p < 0.001$; **** $p < 0.0001$.

4.6 Receptor/Phenotypic Expression Assays

As we demonstrated clear modulation of NK functional efficacy in response to PSC education, we next wanted to determine if co-culture affects the phenotypic or receptor expression in NK and qPSC/aPSC.

4.6.1 Initial NK cell receptor expression experiment

Initial studies revealed that NK cells express a trend towards increased NKG2D receptor expression when cultured with either qPSC or aPSC when compared to NK cells cultured alone (Figure 4.8; Figure 4.9). Conversely, NKG2A positive cell populations remain comparable between culture conditions, however Geometric MFI is seen to increase (although not significantly so), suggesting that the number of receptors per cell may increase in response to co-culture (Figure 4.9).

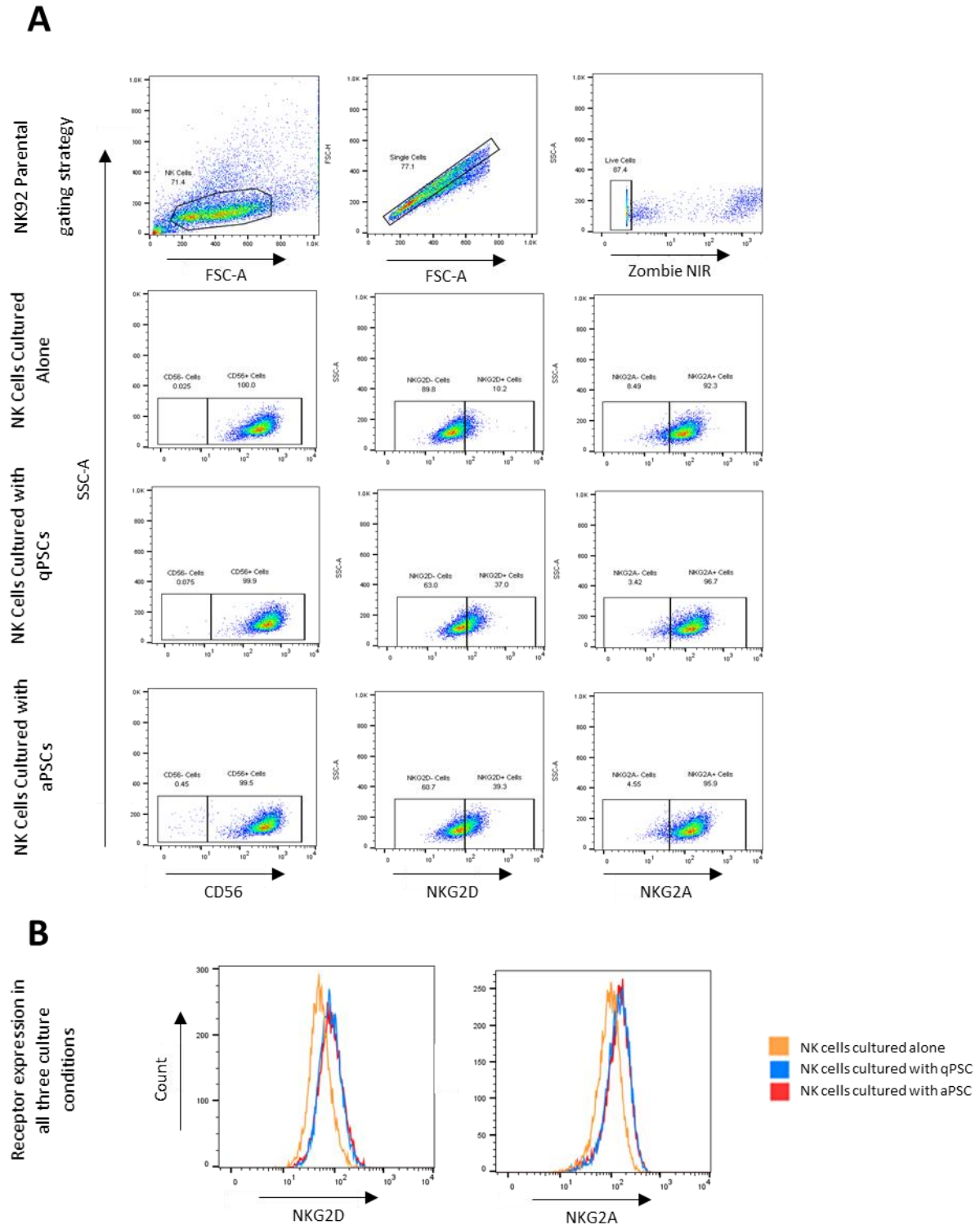


Figure 4.8: Representative plots of NK92 receptor expression following co-culture with qPSC or aPSC.

A) Representative FACS plots of each culture condition. B) Overlaid histograms demonstrating the population shift between culture conditions. Samples were acquired on the LSR Foretessa and analysed using FlowJo 10.8.1.

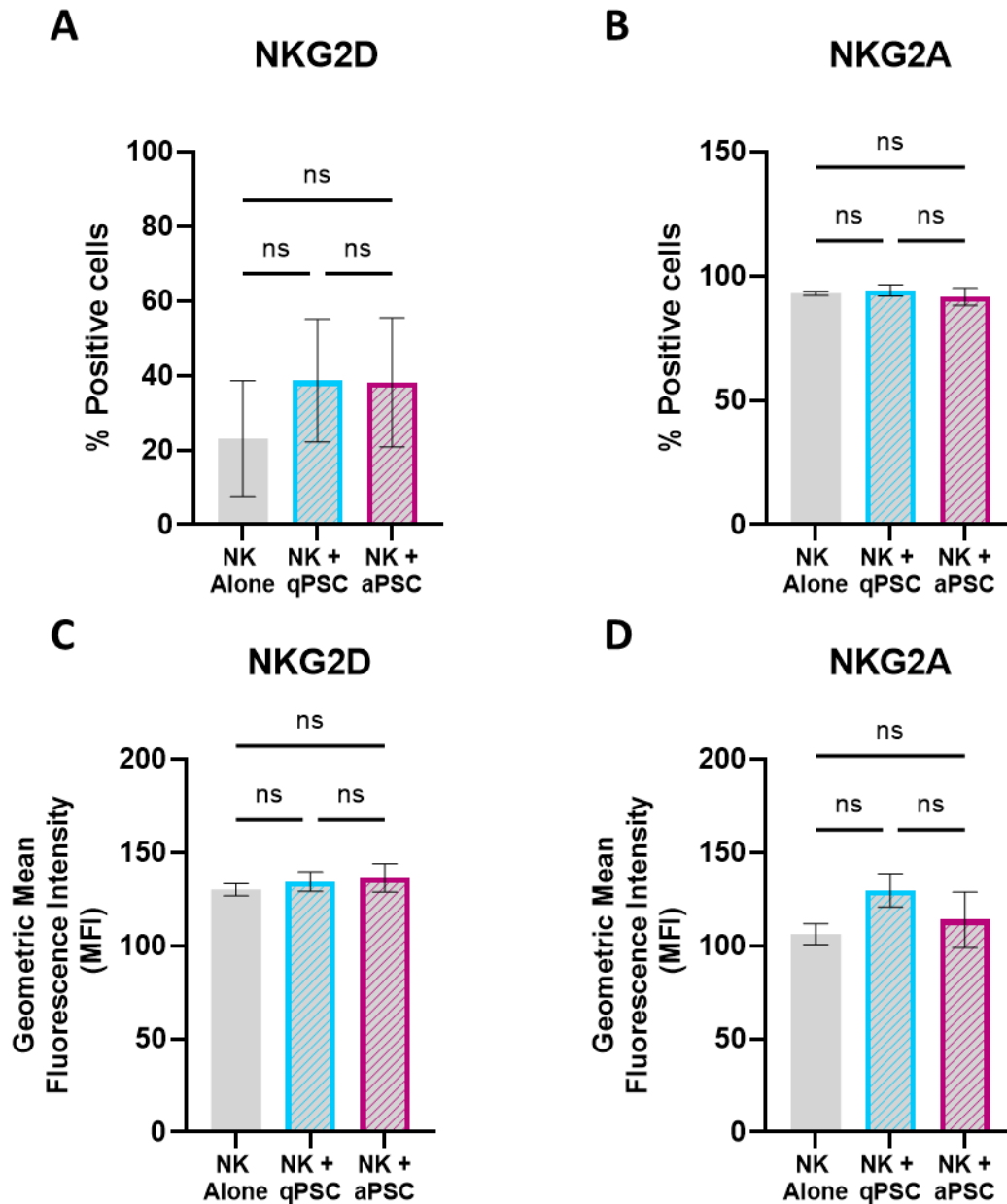


Figure 4.9: Percent positive and Geometric Mean Fluorescence intensity of NKG2D and NKG2A in mono- and co-culture conditions.

A-D) Percent positive cells and Geometric Mean Fluorescence Intensity (MFI) of NKG2D (A, C) and NKG2A (B, D) in NK cells cultured alone or with qPSC/aPSC. Samples were acquired on the LSR Fortessa and gated using FlowJo (10.8.1). Data were analysed using One-Way ANOVA with Šídák's Post Hoc analysis (GraphPad (9.0.0)). Each biological replicate consisted of one technical replicate for each culture condition.

4.6.2 Initial PSC Phenotypic Expression

Forward versus side scatter analysis neatly demonstrates the impact of ATRA and ethanol treatment on PS1 cells; ATRA treated cells present with a large surface area, whilst ethanol treated cells are much smaller, suggesting a more myofibroblastic phenotype (Figure 4.10).

We observe an upregulation of alpha SMA⁺ cells in aPSCs cultured with NK cells when compared to aPSC alone (Figure 4.11). Moreover, the distribution of alpha SMA positive cells is seen to shift in response to co-culture, with greater variation in the size of alpha SMA positive cells being evidenced (Figure 4.10). No significant variation in geometric MFI was observed between culture conditions for alpha SMA or GFAP (Figure 4.11C-D).

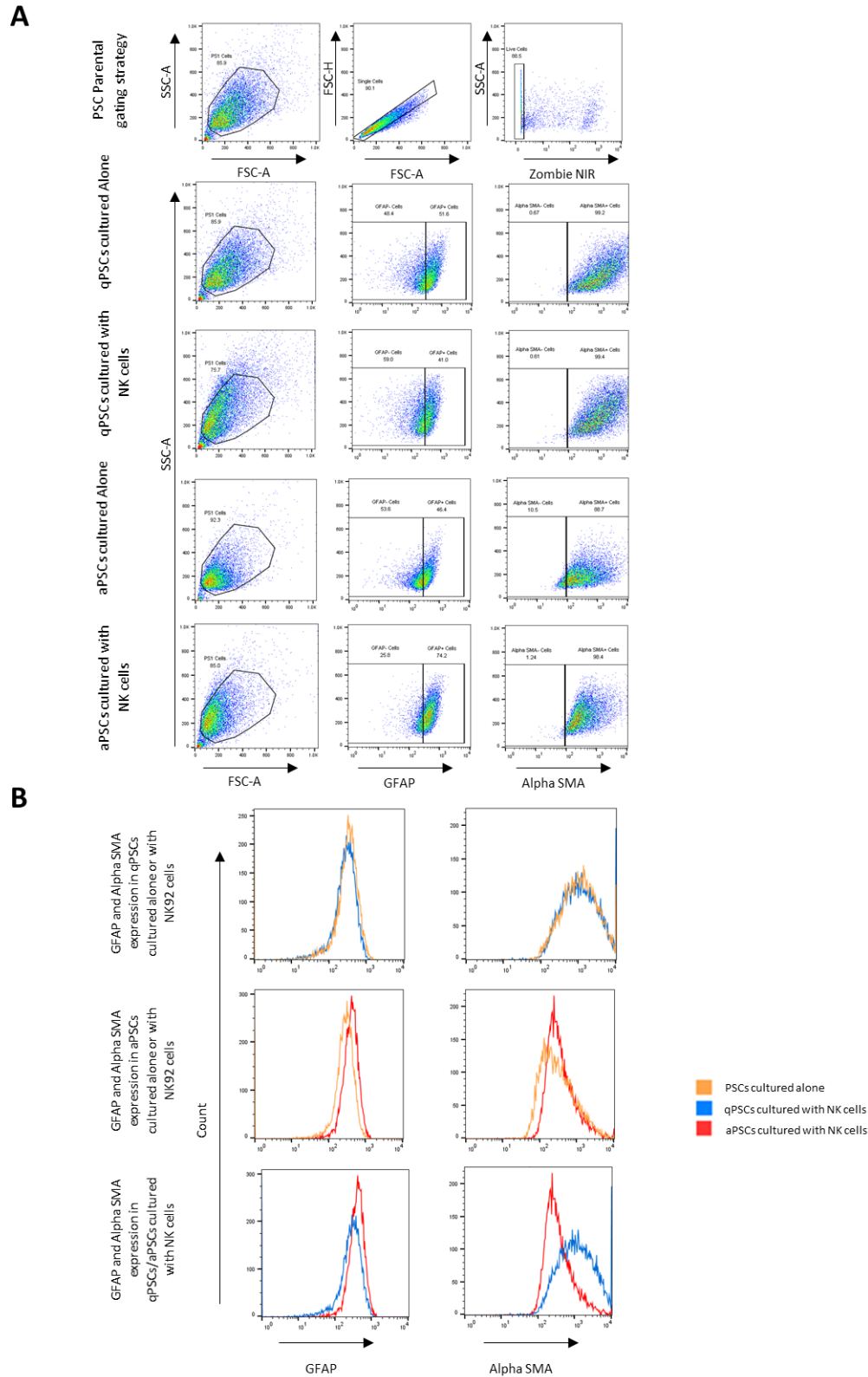


Figure 4.10: Representative plots of phenotypic markers in qPSC and aPSC following co-culture with NK92 cells.

A) Representative FACS plots of each culture condition. B) Overlaid histograms demonstrating the population shift between culture conditions. Samples were acquired on the LSR Fortessa and analysed using FlowJo 10.8.1.

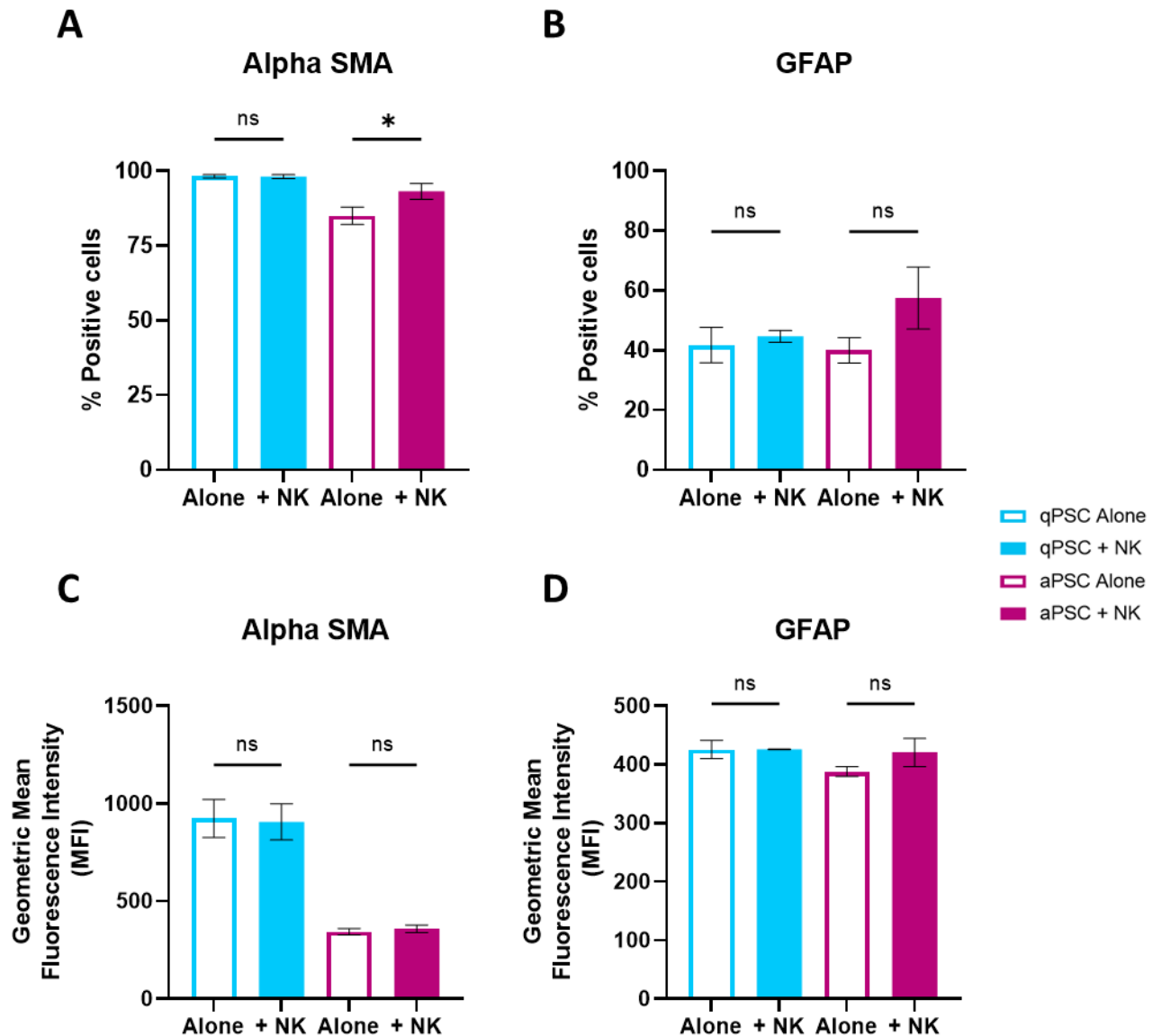


Figure 4.11: Percent positive and Geometric Mean Fluorescence intensity of alpha SMA and GFAP in mono- and co-culture conditions.

A-D) Percent positive cells and Geometric Mean Fluorescence Intensity (MFI) of alpha SMA (A, C) and GFAP (B, D) in quiescent and activated PSCs when cultured alone (empty bars) or in direct contact (filled bars) with NK cells. Samples were acquired on the LSR Fortessa and analysed using FlowJo (10.8.1) and GraphPad (9.0.0). Statistical analysis was carried out using One-Way ANOVA with Šídák's Post Hoc analysis; * $p < 0.05$. Each biological replicate consisted of one technical replicate for each culture condition.

Taken together these results suggest a dynamic interplay between these two cell types and necessitate further investigation into their interaction.

4.6.3 Spectral Flow cytometry

Initial receptor/phenotypic assay results suggested a dynamic interplay between NK cells and PSCs. To further explore this interaction, we employed spectral flow cytometry. The development of spectral flow cytometry has provided a flexibility that conventional flow cytometry does not, allowing the development of multicolour panels as well as the assessment of rare populations within small sample sizes. Moreover, with Full Spectrum Flow cytometry (FSFC) systems using avalanche photo diodes to capture narrower bandwidths, electronic noise is reduced, generating high resolution between cellular populations.²⁷¹ Thus, we assessed multi-fluor panels using the FSFC Cytex Aurora 5-Laser system (Cytex Biosciences) to facilitate greater characterisation of the changes induced in NK/PSCs by co-culture conditions.

4.6.3.1 PSC phenotypic changes in response to co-culture

To comprehensively assess phenotypic changes in PSC in response to NK cell co-culture, we contemporaneously used direct co-culture (Figure 4.12) alongside co-culture separated by 0.4µM Transwell™ inserts to prevent heterotypic cell-cell contact (Figure 4.13). We also utilised NK conditioned media onto aPSC/qPSC (Figure 4.14) (Appendix 3).

We demonstrate stellate cell polarisation to a myofibroblastic activation state⁸⁸ in response to direct contact with NK cells (Figure 4.12A), as assessed by alpha SMA abundance (geometric MFI), irrespective of previous activation status (aPSC or qPSC), a fact not observed in Transwell™ separated co-culture (Figure 4.13A) or conditioned media (Figure 4.14A). Similarly, only the NK cells' direct co-culture was found to induce global upregulation of

CD105 expression in PSCs (Figure 4.12B) but not the other conditions (Figure 4.13B, Figure 4.14B). Finally, aPSCs but not qPSCs demonstrate an increase in podoplanin expression in response to direct co-culture with NK cells (Figure 4.12E), but not in other conditions (Figure 4.13E, Figure 4.14E). These phenotypic changes are summarised in Figure 4.15.

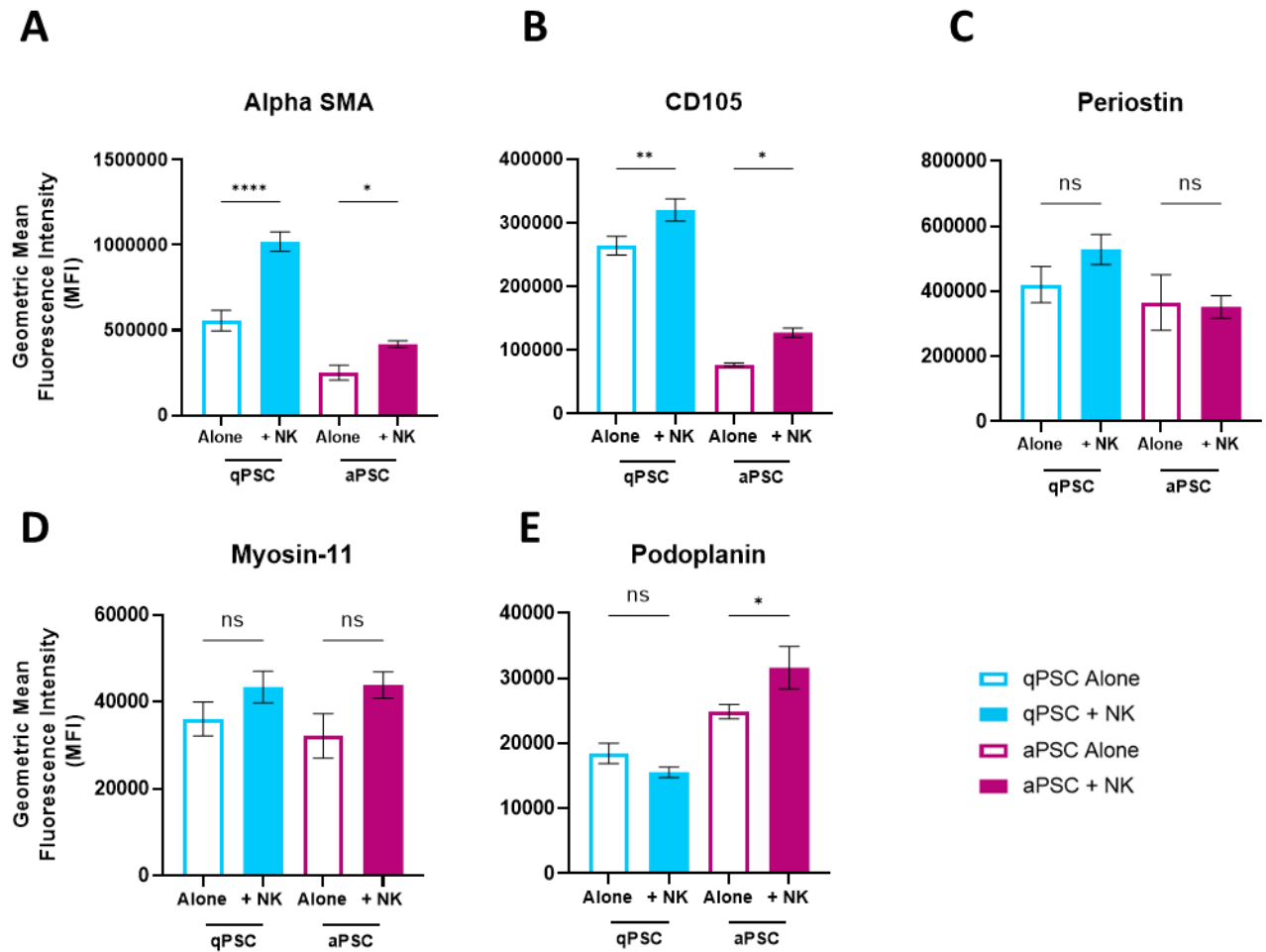


Figure 4.12: The presence of NK cells encourages a myofibroblastic phenotype in both quiescent and activated PSCs.

A-E) Geometric Mean Fluorescence Intensity (MFI) of alpha SMA (A), CD105 (B), Periostin (C), Myosin-11 (D), and Podoplanin (E) in quiescent and activated PSCs when cultured alone (empty bars) or in direct contact (filled bars) with NK cells. Data were analysed using One-Way ANOVA with Šídák's multiple comparisons analysis. Parametric data are displayed as Mean \pm SEM. ns- non-significant; * $p < 0.05$; ** $p < 0.01$; **** $p < 0.0001$.

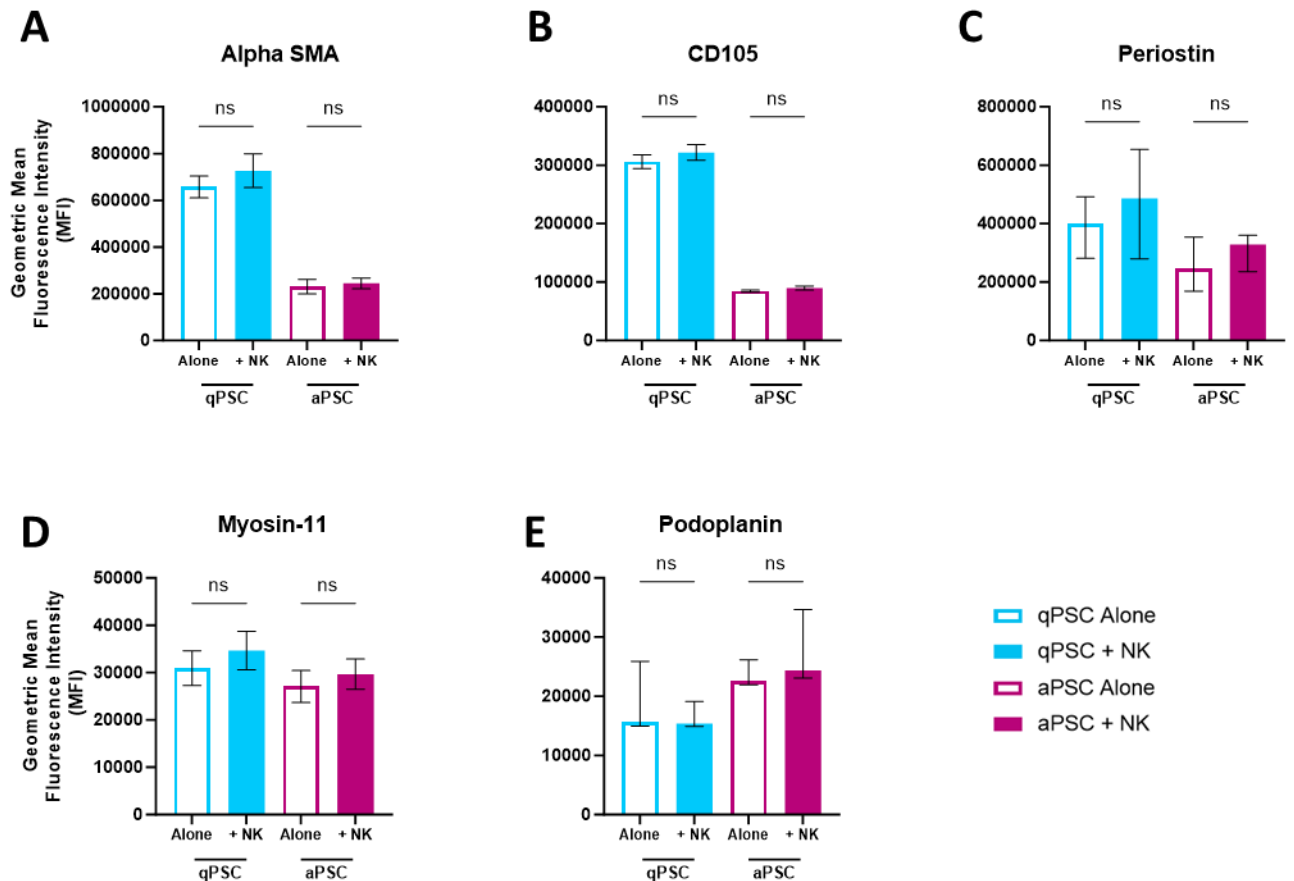


Figure 4.13: PSC marker expression following 24h culture with NK cells separated by 0.4µm Transwell inserts.

A-E) Geometric Mean Fluorescence Intensity of alpha SMA (A), CD105 (B), Periostin (C), Myosin-11 (D), and Podoplanin (E) expression in PSCs cultured alone (empty bars) or with NK cells separated by a 0.4µm Transwell insert (filled bars). Data were analysed using One-Way ANOVA with Šídák's multiple comparisons (A, B, D) or Kruskal-Wallis analysis with Dunn's post hoc (C, E). Parametric data are displayed as Mean +/- SEM whilst non-parametric data are represented via media +/- inter-quartile range. * $p < 0.05$; ** $p < 0.01$; *** $p < 0.001$; **** $p < 0.0001$.

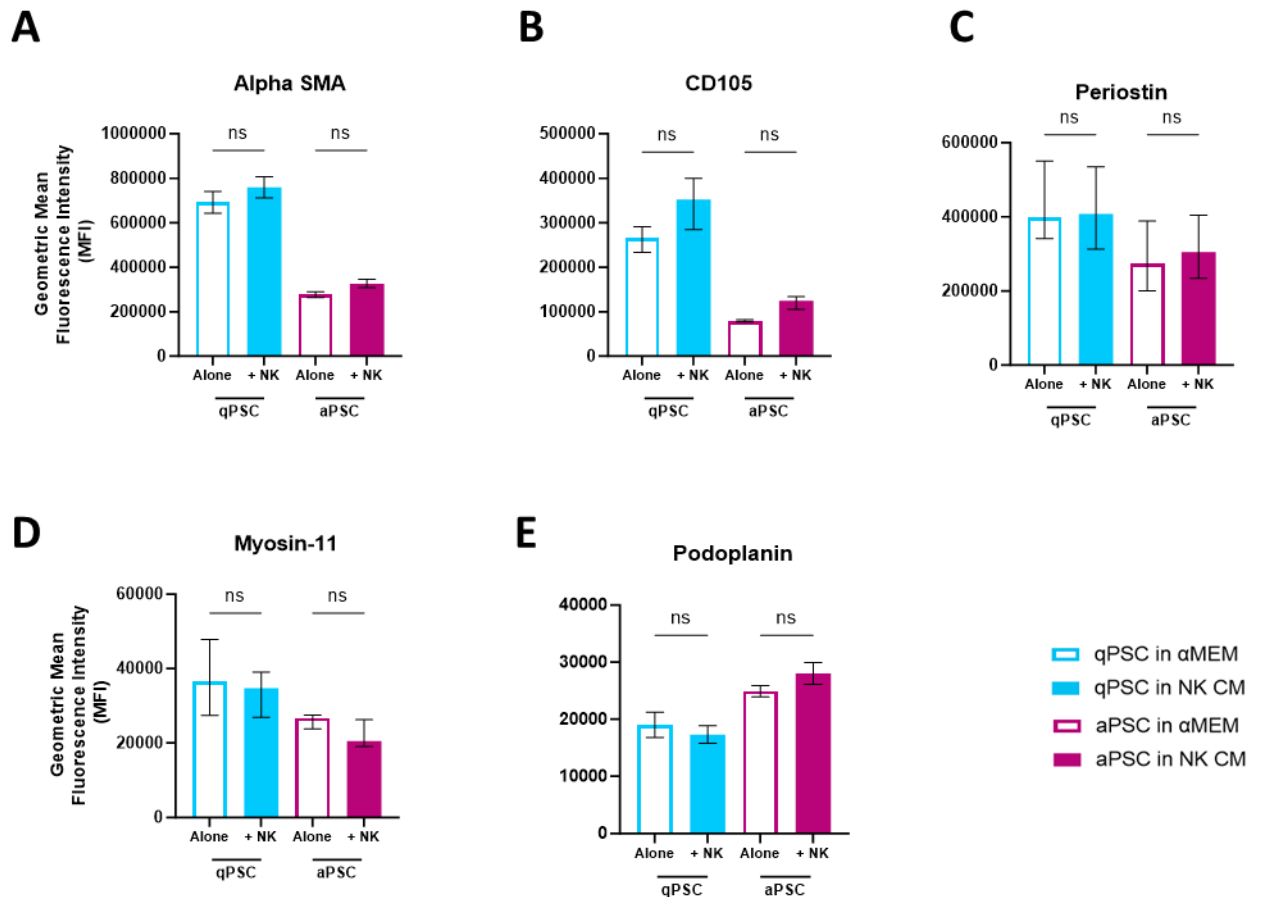


Figure 4.14: PSC marker expression following 24h culture in NK conditioned media.

A-E) Geometric Mean Fluorescence Intensity of alpha SMA (A), CD105 (B), Periostin (C), Myosin-11 (D), and Podoplanin (E) expression in PSCs cultured in alpha MEM (empty bars), or NK conditioned media (filled bars). Data were analysed using One-Way ANOVA with Šídák's multiple comparisons (A, E) or Kruskal-Wallis analysis with Dunn's post hoc (B-D). ns- non-significant. CM – Conditioned Media.

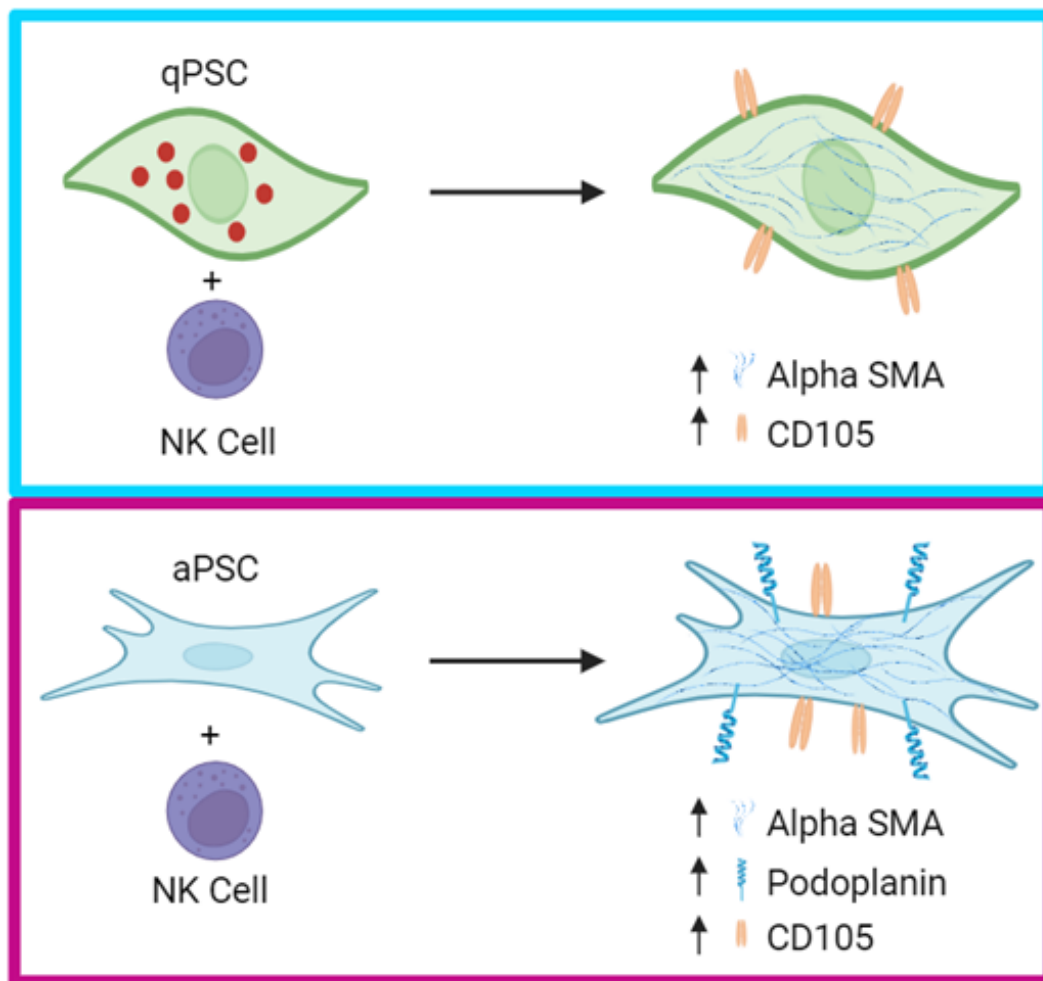


Figure 4.15: Schematic summary of the changes in qPSCs and aPSCs invoked by direct co-culture with NK cells.

Quiescent PSCs demonstrate upregulation of alpha SMA and CD105, whilst activated PSCs demonstrate an increase in both podoplanin and CD105 expression, as well as an increase in alpha SMA fibres.

4.6.3.2 *NK Receptor and functional marker expression in response to co-culture*

We next looked to assess changes in surface NK cell receptor expression (Figure 4.16) (Appendix 4) in response to PSC direct co-culture, Transwell™ separated co-culture and PSC conditioned media. Upon PSC education we demonstrate upregulation of TIM3 in response to co-culture with both qPSC and aPSCs (receptor per cell (geometric MFI) and at the population level (% positive)), but a differential increase in NKG2A expression per cell in response to qPSC but not aPSC (Figure 4.16A, Figure 4.17A). Other activating/ inhibitory receptor abundance remains unchanged. This trend in TIM3 expression is also observed in Transwell™ co-culture conditions as well as conditioned media (Figure 4.16B, C). Thus, it is likely that TIM3, but not NKG2A expression is regulated by PSC secreted factors such as IL-12/15/18 as previously described.²⁷² It is noteworthy that whilst NKG2D expression does not increase on a per cell basis in response to direct co-culture (although an upregulation is observed at the population level (Figure 4.17B)), an increase is observed in Transwell™ separated culture and conditioned media, thus this may also be due to cytokine stimulation.²⁷³ Though NK cells exhibit reduced degranulation following qPSC education (Figure 4.6C), intracellular staining reveals an upregulation of granzyme B in qPSC educated NK cells suggesting that, although not efficacious, NK cells may be primed for cytotoxicity in response to PSCs education (Figure 4.16A). Furthermore, a significant upregulation in perforin expression is evident in aPSC educated NK cells (direct co-culture; Figure 4.16A) as well as in response to qPSC conditioned media (Figure 4.16C), further suggesting NK cell priming.²⁷⁴

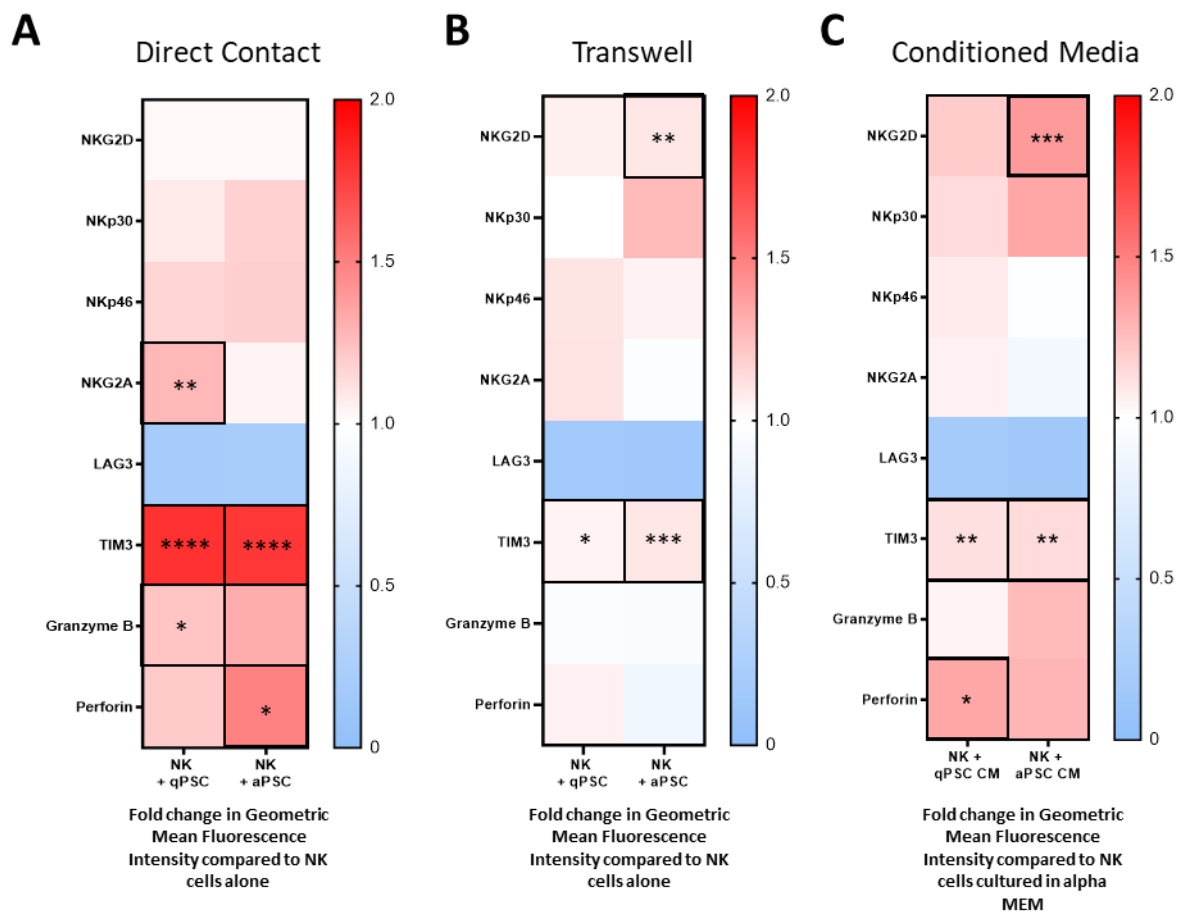


Figure 4.16: PSCs influence receptor expression on natural killer cells.

A) Fold change in geometric mean fluorescence intensity in NK cells + qPSCs/aPSCs vs NK cells alone following 24h co-culture. Data were analysed using One-Way ANOVA with Šídák's multiple comparisons (NKG2D, NKp30, NKp46, NKG2A, LAG3, TIM3, Granzyme B) or Kruskal-Wallis analysis with Dunn's post hoc (Perforin). B) Fold change in geometric mean fluorescence intensity in NK cells + qPSCs/aPSCs vs NK cells alone following 24h culture separated by Transwell™ inserts. Data were analysed using One-Way ANOVA with Šídák's multiple comparisons (NKG2D, NKp30, NKp46, NKG2A, TIM3, Granzyme B, Perforin) or Kruskal-Wallis analysis with Dunn's post hoc (LAG3). C) Fold change in geometric mean fluorescence intensity in NK cells cultured in qPSCs/aPSCs conditioned media vs NK cells cultured in alpha MEM (24h). Data were analysed using One-Way ANOVA with Šídák's multiple comparisons (NKG2D, NKp30, NKp46, NKG2A, TIM3, Granzyme B, Perforin) or Kruskal-Wallis analysis with Dunn's post hoc (LAG3). * $p < 0.05$; ** $p < 0.01$; *** $p < 0.001$; **** $p < 0.0001$.

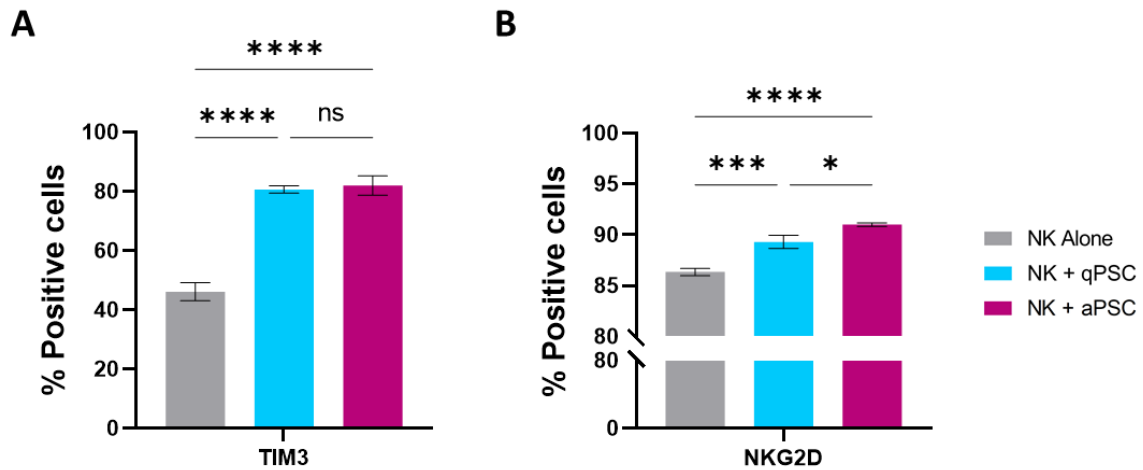


Figure 4.17: NK marker expression at the population level in response to direct culture.

A) TIM3 expression on NK cells (% positive) in response to direct culture with qPSC/aPSC. Data were analysed using One-Way ANOVA with Šídák's multiple comparisons B) NKG2D expression on NK cells (% positive) in response to direct culture with qPSC/aPSC. Data were analysed using One-Way ANOVA with Šídák's multiple comparisons. * $p < 0.05$; *** $p < 0.001$; **** $p < 0.0001$.

4.6.4 Luminex Analysis

To investigate if there were any changes in the secretome in response to direct/Transwell™ NK-PSC co-culture we utilised the Luminex 65-plex Immune Monitoring ProcartaPlex™ Panel (ThermoFisher Scientific, Inc.; conducted by Veonice Au, Institute of Molecular and Cell Biology, A*STAR).

We identified upregulation of IFN- γ , CXCL9, CXCL10 and CXCL11, amongst others, in both quiescent and activated PSCs in direct co-culture with NK cells (Figure 4.18A; Appendix 5, Appendix 6, Appendix 7), but to a much-reduced extent in Transwell™ separated co-culture (Figure 4.18B), highlighting the importance of proximity in NK-PSC interactions.

Taken together our results demonstrate a reciprocal interaction between NK cells and activated/quiescent PSC in terms of phenotypic changes in both PSC and NK cells, as well as functional changes within NK cells which may, in turn, influence NK cell mediated cancer cell cytotoxicity (Figure 4.6, Figure 4.7). These direct-contact induced changes are represented schematically in Figure 4.19.

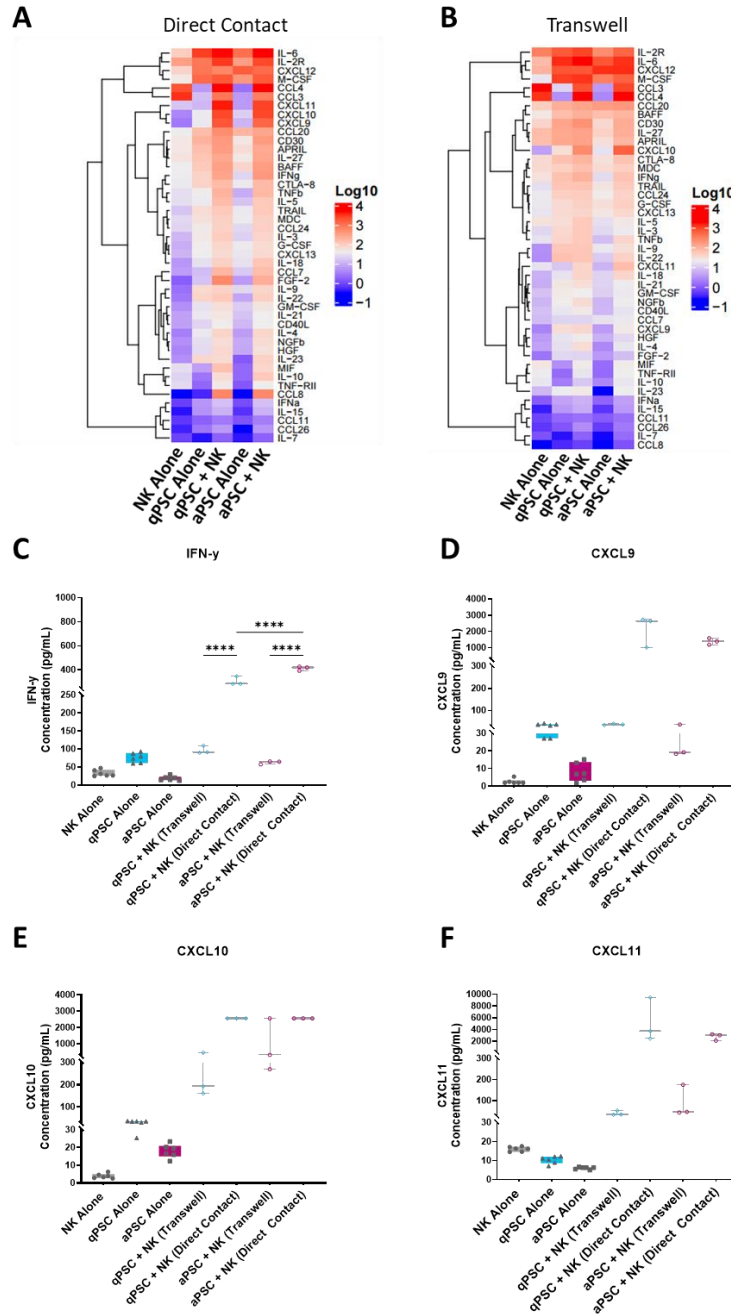


Figure 4.18: Chemokines and Cytokines up and down regulated in response to Direct and Transwell™ culture.

A) Heatmap of cytokines and chemokines of interest observed in direct co-culture conditions. Analytes were measured using 65-plex Luminex assay. Observed values were Log10 + 1 transformed and heatmaps created using R (4.0). Highly abundant analytes are displayed in red, whilst those with lesser abundance are displayed in blue. B) Heatmap of cytokines and chemokines of interest observed in Transwell™ conditions. Analytes were measured and presented as above. C-F) Abundance of Interferon- γ (C), CXCL9 (D), CXCL10 (E) and CXCL11 (F) secreted in mono- and co-culture of NK and PSCs in direct contact and Transwell™ conditions. Analyte concentrations are displayed as picograms per mL. Data were analysed using One-Way ANOVA with Šidák's multiple comparisons analysis (C) or Kruskal-Wallis analysis with Dunn's Post Hoc tests (D-F). For each biological replicate, one of three technical replicates was analysed. The Luminex ELISA assay was conducted by Veonice Au.

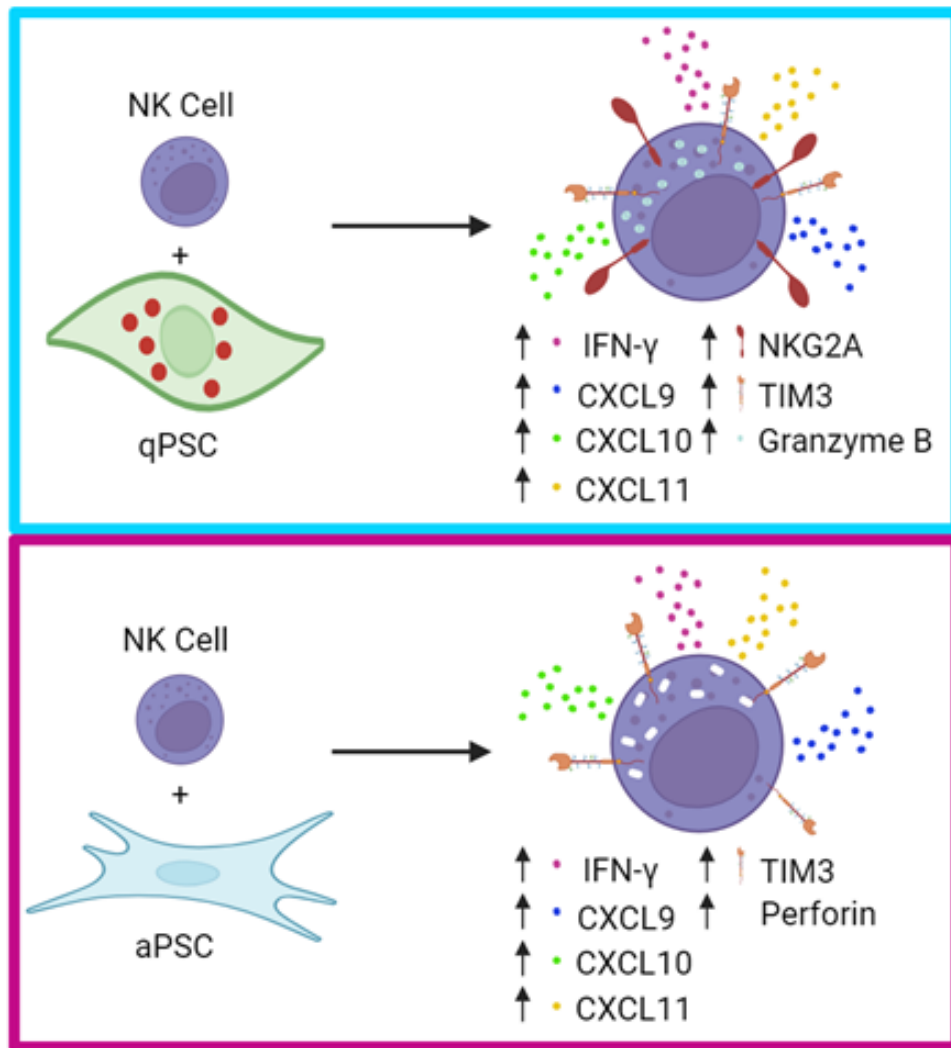


Figure 4.19: Schematic summary of the changes in NK cells invoked by qPSC/ aPSCs direct co-culture.

Direct contact with quiescent PSCs results in upregulation of IFN- γ , CXCL9, CXCL10 and CXCL11 cytokines/chemokines, as well as an increase in TIM3, NKG2A and perforin, whilst NK cells cultured with aPSCs demonstrate upregulation of IFN- γ and related chemokines, TIM3 and granzyme B.

4.7 Proteomics

Since we demonstrated distinct changes in NK/PSC phenotype in response to direct co-culture, we next wanted to determine if this interaction regulated intracellular protein expression and/or invoked modulation of biological pathways in both NK cells and PSCs. In order to achieve this, we utilised cell-type specific mass spectrometry. Following 24h direct co-culture, NK cells, qPSCs and aPSCs were prepared (cells lysed, proteins extracted and peptides created and linearised) and maintained separately, allowing assessment of the distinct proteomic landscape of each cell type following co-culture. As mono-cultures of naïve NK, qPSC and aPSC were not included in the experiment, down- and up- regulated proteins (Figure 4.20C, D) and alterations in biological pathways (Figure 4.21; Figure 4.22) are displayed as ‘diseased’ (aPSC) vs ‘healthy’ (qPSC) conditions.

Significant differences in protein expression were observed in both qPSCs, aPSCs and NK cells in response to co-culture (Figure 4.20; Appendix 8). Moreover, activated PSCs were found to induce differential protein expression in NK cells when compared to qPSC. These changes involved multiple cellular pathways including biosynthesis, protein folding, sorting and vesicular transport (Figure 4.21). Reciprocally, NK cells induced differential protein changes in activated versus quiescent PSCs such that changes in key pathways, including lipid and steroid metabolism, glycolysis and spliceosome function were altered (Figure 4.22A, D). We explored this further by looking at specific gene expression changes between normal pancreatic tissue and pancreatic ductal adenocarcinoma. Importantly, we identify similar down/upregulation in corresponding genes such as PSAT1 (SERC) and HNRNPK (HNRPK) (Figure 4.22B, E) which has a prognostic impact (Figure 4.22F, G).²⁷⁵

Taken together these results highlight a significant bi-directional relationship between NK cells and PSCs in the context of PDAC and provide a firm platform on which further mechanistic studies can be based.

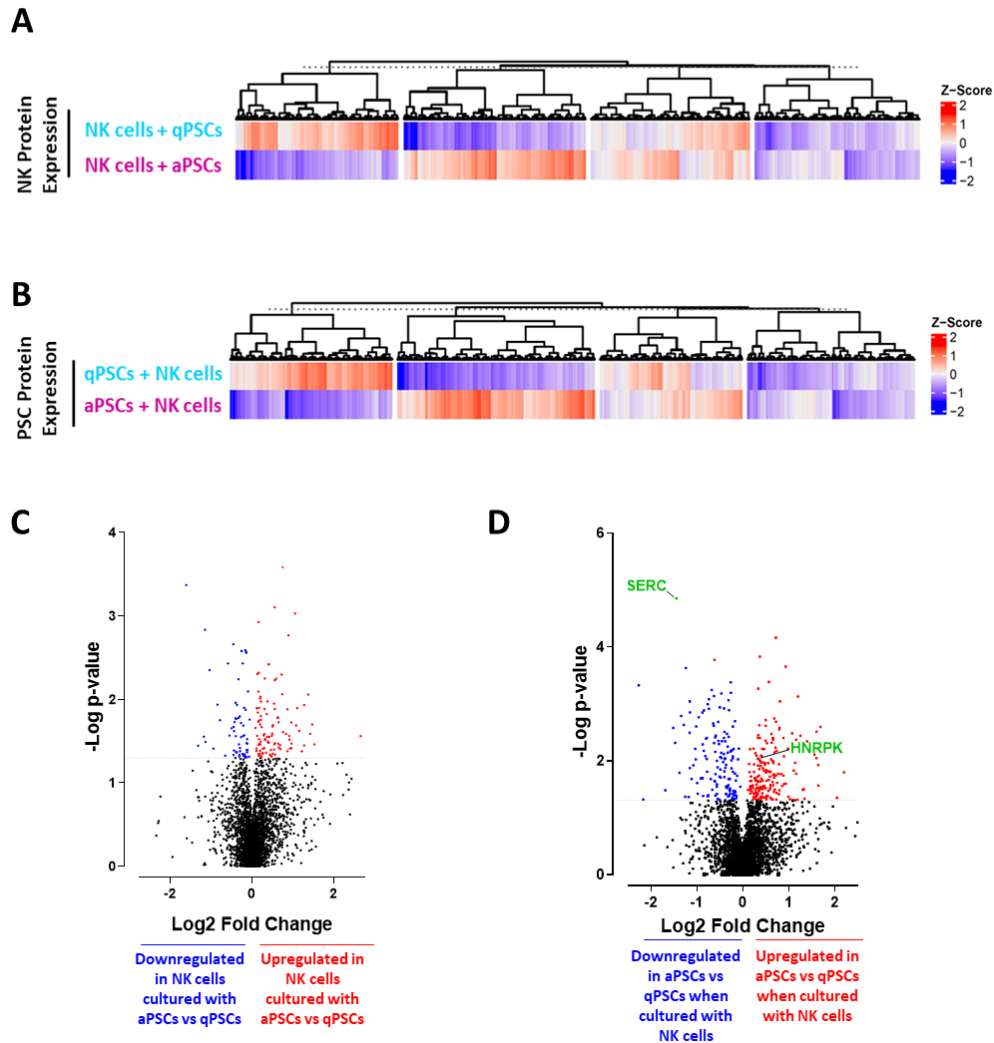
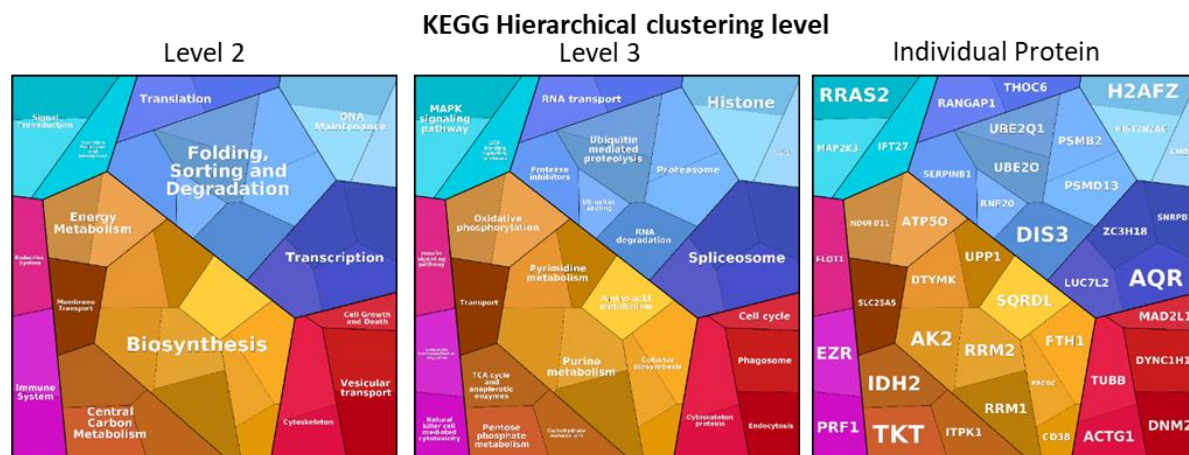


Figure 4.20: NK cells and qPSCs/aPSCs exhibit differentially expressed proteins.

A-B) Heatmaps of differentially expressed proteins in NK cells cultured with qPSC/aPSC (A) and qPSC/aPSCs cultured with NK cells (B). NK cells, qPSC and aPSCs were maintained as separate cell populations following co-culture to ensure the proteome of individual cell types could be assessed. The median Z-Score calculated from $n=3$ biological replicates (each consisting of one technical replicate) was used to plot the heatmaps. Upregulated proteins are shown in red; downregulated proteins are shown in blue. C-D) Volcano plots of proteins differentially expressed in NK cells cultured with aPSCs vs qPSCs (C) and aPSCs cultured with NK cells vs qPSCs cultured with NK cells. T-tests were used to identify statistical significance between 'diseased' (aPSC) and 'healthy' (qPSC) conditions. Upregulated proteins are highlighted in red; downregulated proteins are highlighted in blue. Dr Parthiban Periasamy carried out the initial data alignment and clean up, and provided the R code for the plotting of the heatmaps.

A

Downregulated in NK cells cultured with aPSCs vs qPSCs



B

Upregulated in NK cells cultured with aPSCs vs qPSCs

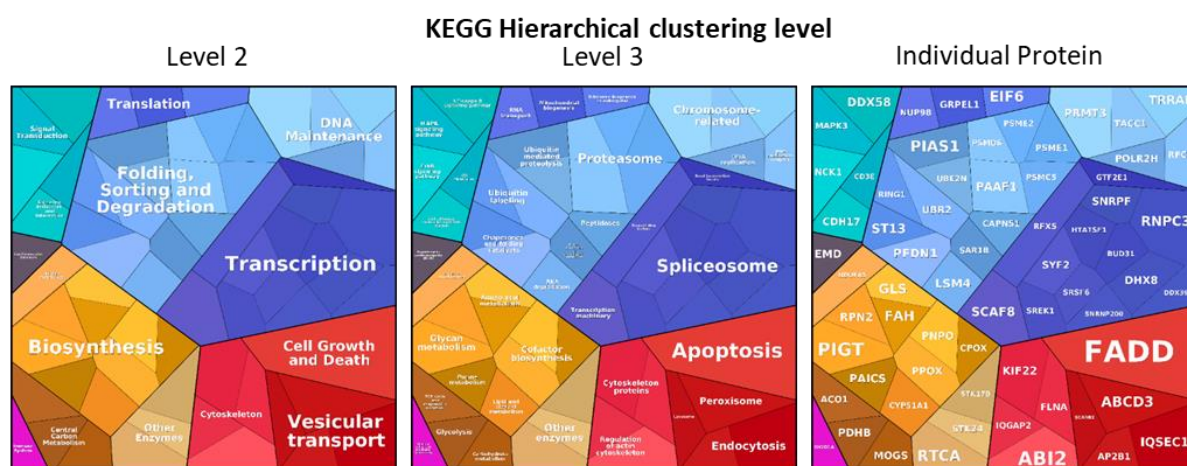
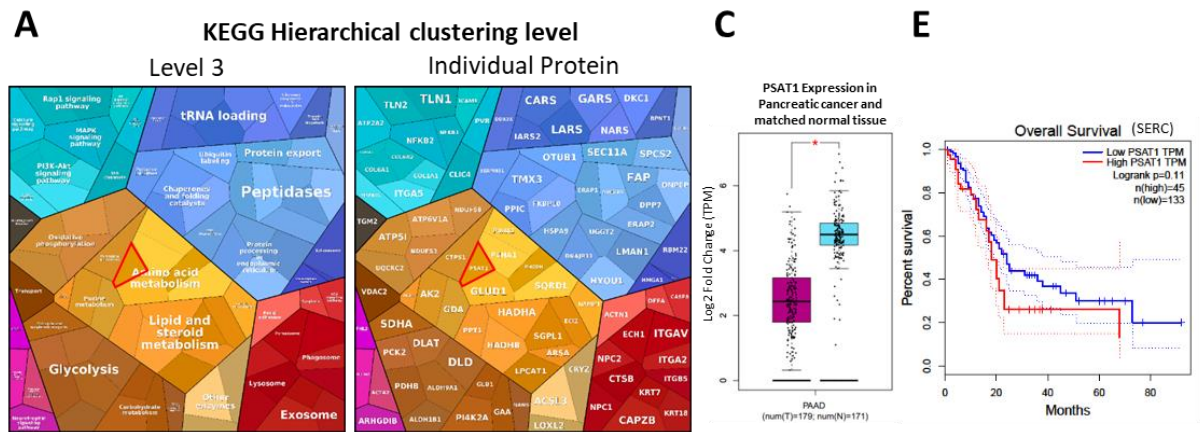


Figure 4.21: Biological Processes down- and up- regulated in NK cells cultured with aPSCs vs those cultured with qPSCs

A-B) Biological Processes down- (A) and up- (B) regulated in NK cells cultured with aPSCs vs those cultured with qPSCs. Down- and up- regulated proteins were identified using T-tests ('diseased' (aPSC) vs 'healthy' (qPSC)) and protein maps created using KEGG pathway gene classifications and Proteomaps software.²⁵⁰ Protein abundance is demonstrated through polygon area, with proteins housed in larger polygons demonstrating greater abundance. Functionally related proteins are clustered into coloured groups.

Downregulated in aPSCs cultured with NK cells vs qPSCs cultured with NK cells



Upregulated in aPSCs cultured with NK cells vs qPSCs cultured with NK cells

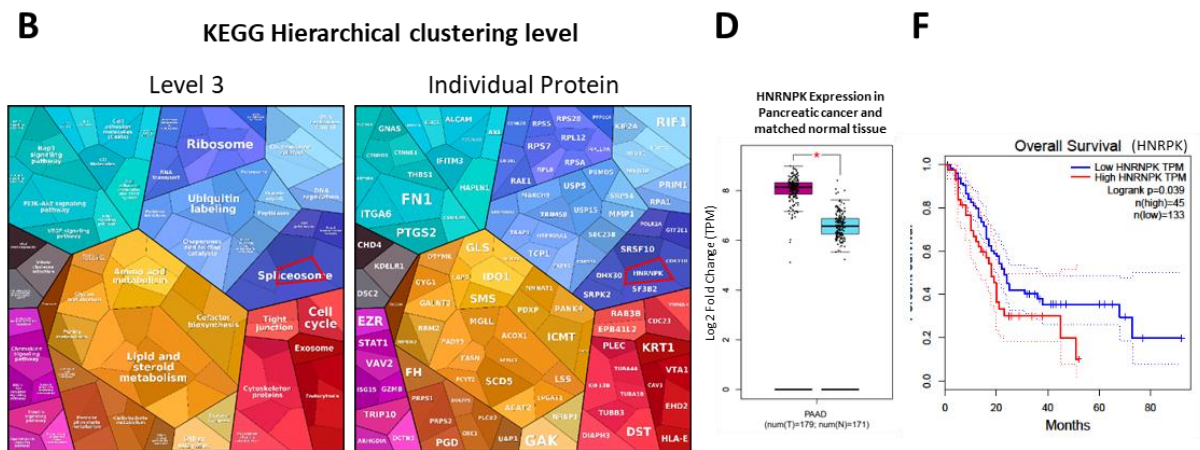


Figure 4.22: Biological Processes down- and up- regulated in qPSCs and aPSCs cultured with NK cells

A-B) Biological Processes down- (A) and up- (B) regulated in aPSCs cultured with NK cells vs qPSCs cultured with NK cells. Significantly down- and up- regulated proteins were identified using T-tests ('diseased' (aPSC) vs 'healthy' (qPSC)) and protein maps created using KEGG pathway gene classifications and Proteomaps software.²⁵⁰ Example proteins explored in publicly available RNA-Seq data sets are highlighted in red. C-D) RNA expression of example proteins assessed in TCGA and GTEx datasets between normal and PDAC tissues (downregulated; PSAT1; C and upregulated; HNRNP; D). E-F) Survival analysis of PDAC patients based on the RNA expression of example proteins identified in the TCGA/GTEx datasets. RNA-sequencing data was analysed using the online web server, GEPIA (Gene Expression Profiling and Interactive Analysis).

Chapter 5 - Results 3 – *Ex Vivo* Optimisations

5.1 Introduction

The advent of multiplex immunohistochemistry (mIHC) has revolutionised classical IHC. Whilst long recognised as the ‘gold standard’ of tissue pathology diagnosis, IHC exhibits several limitations, most notably, the opportunity to label only one marker per tissue section (detailed review in Reference 265).^{276, 277} As such, there has been increasing demand for more advanced techniques to facilitate multi-marker staining and gain important diagnostic and prognostic information from patient samples which is often lost with single marker labelling.²⁷⁷ With the ability to detect multiple markers on a single tissue section, mIHC overcomes this limitation and affords researchers and clinicians the opportunity to assess cellular phenotypes, as well as visualise both cellular location and cell-cell interactions.^{278, 279} In addition, this multi-parameter data can be reproducibly quantified, allowing effective investigation of specific antigens of interest and spatial relationships. Thus, mIHC has been increasingly implemented in both the research and clinical settings²⁷⁷, demonstrating its important role in translational oncology research.^{278, 280}

We developed three mIHC panels for the investigation of NK-CAF interactions in patient samples. In this chapter, we report the *ex vivo* optimisations and troubleshooting undertaken to prepare for the staining of patient TMA slides.

5.2 Immunofluorescent staining

In order to assess the location of and interaction between NK cells and PSC/CAFs in PDAC tissue, we looked to optimise immunofluorescent staining of NK cells in formalin fixed, paraffin embedded tissue samples.

5.2.1 Antibody titration

To facilitate visualisation of NK cells within pancreatic cancer tissues, antibodies for the NK markers CD56, NKG2D and NKG2A were titrated using control tissues. Initial titration results for all markers demonstrated high background fluorescence and poor signal: noise ratio (Figure 5.1).

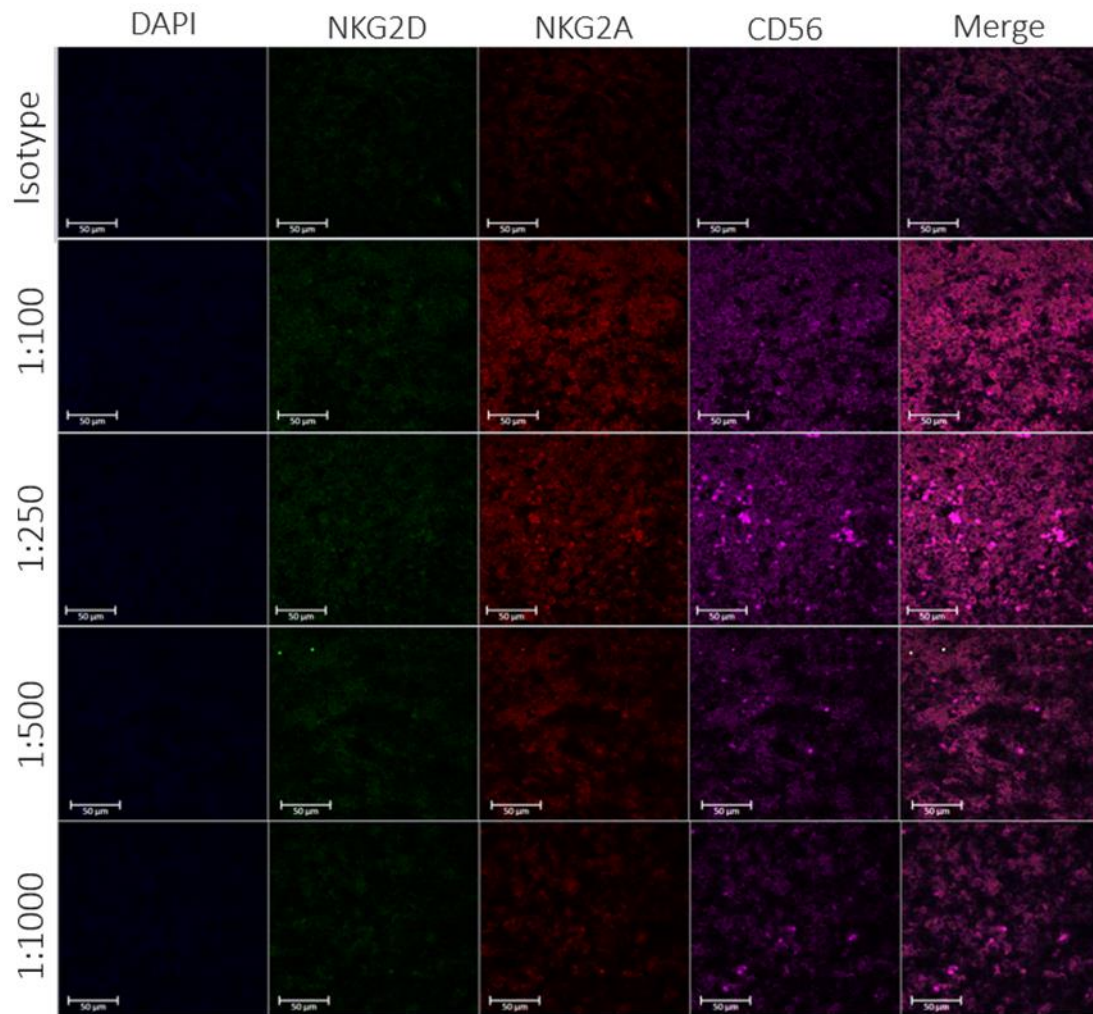


Figure 5.1: Immunofluorescent antibody titration of anti-CD56, anti-NKG2D and anti-NKG2A antibodies in human spleen tissue.

Antibodies were diluted 1:100, 1:250, 1:500 and 1:1000. An isotype control (1:100) is shown in the first panel. Images were acquired on the LSM710 laser scanning confocal microscope. Magnification x40. Scale Bars = 50µm.

5.2.2 Background Troubleshooting

We hypothesised that the high background staining observed may be a result of secondary antibody dilution or ineffective blocking of non-specific staining. As such, we trialled different dilutions of secondary antibodies, as well as a variety of blocking agents.

Secondary antibody dilution demonstrated little impact on background fluorescence levels (Figure 5.2). Moreover, high background fluorescence was observed in all blocking conditions tested (Figure 5.3). No true staining for CD56, NKG2D or NKG2A was evident in any condition tested (Figure 5.2 and Figure 5.3).

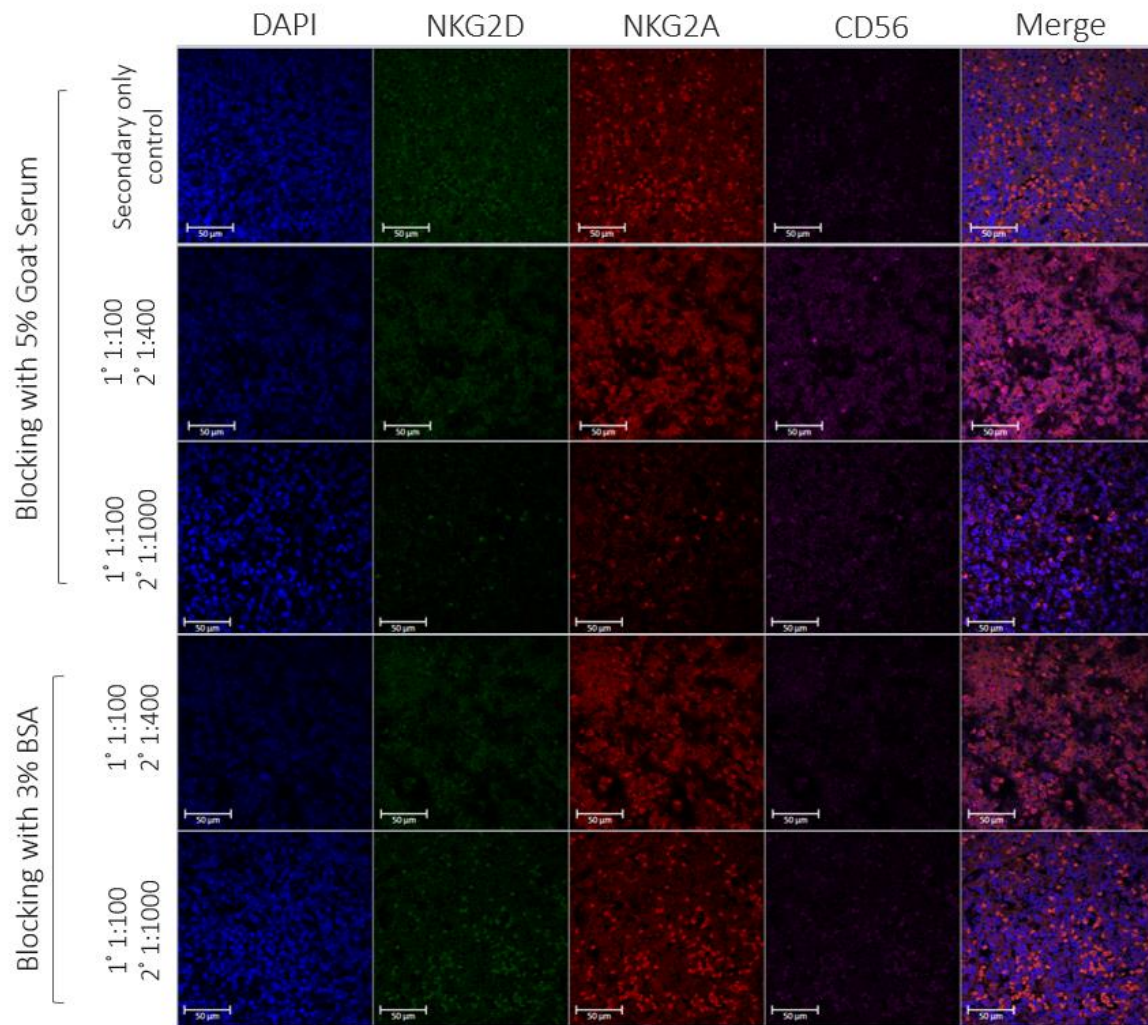


Figure 5.2: Troubleshooting immunofluorescent staining of human spleen tissue.

Anti-CD56, anti-NKG2D and anti-NKG2A were diluted 1:100. Secondary antibodies were titrated 1:400 and 1:1000. These conditions were tested with two blocking agents: 5% goat serum and 3% BSA. A secondary only control is shown in the first panel. Images were acquired on the LSM710 laser scanning confocal microscope. Magnification x40. Scale Bars = 50µm.

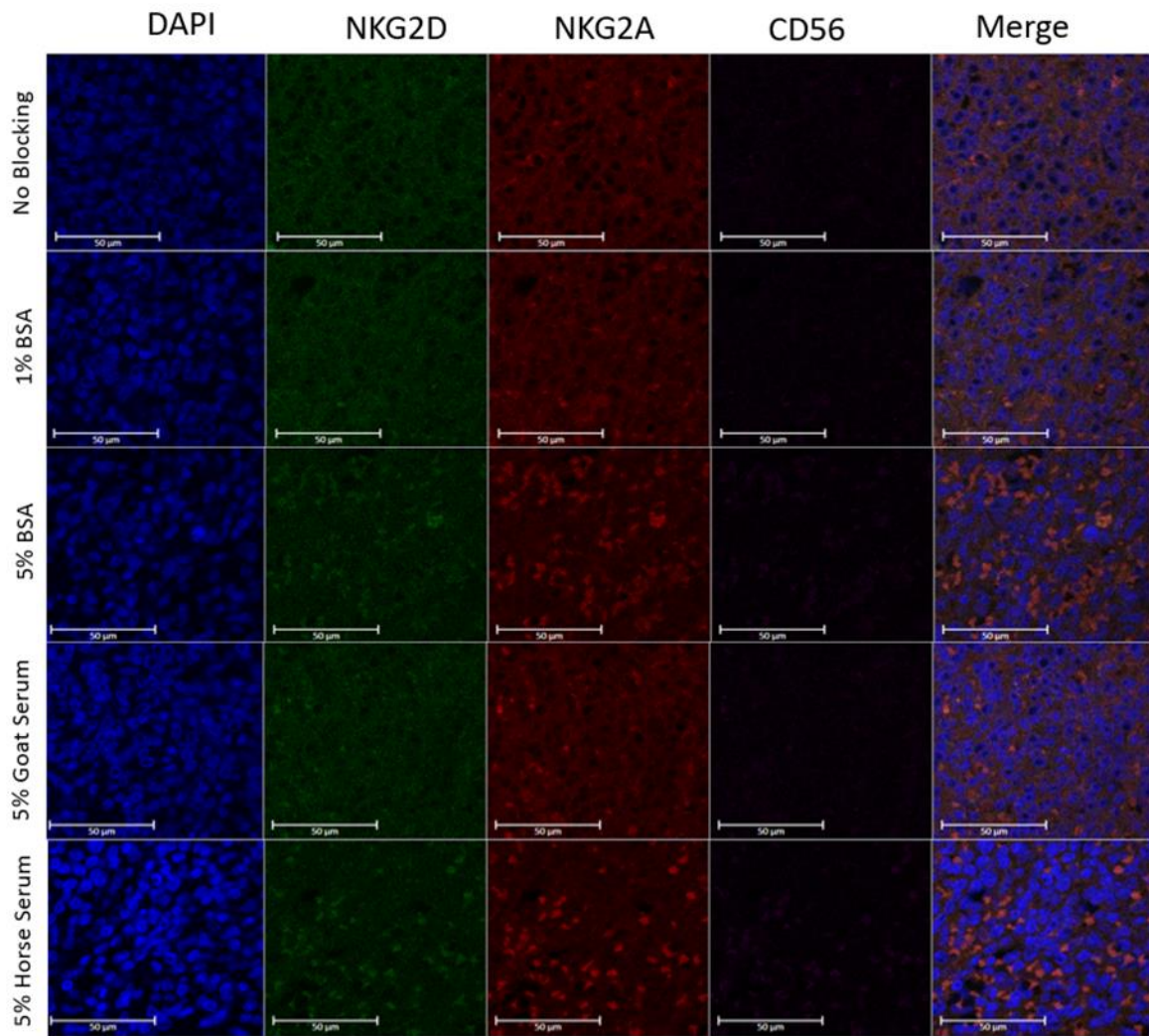


Figure 5.3: Immunofluorescent staining of human spleen tissue with different blocking agents.

Spleen tissues were subjected to five blocking conditions: No blocking, 1% BSA, 5% BSA, 5% goat serum and 5% horse serum. No primary antibodies were used to determine the background staining generated with each blocking condition. Images were acquired on the LSM710 laser scanning confocal microscope. Magnification x40. Scale Bars = 50 μ m.

5.2.3 Antibody titration using a different immunofluorescent protocol

We next trialled a different immunofluorescent staining protocol to determine if positive signal could be achieved in control tissues.

This protocol delivered cleaner staining with a greater signal to noise ratio. Whilst no positive staining was evident for CD56 or NKG2D (Figure 5.4A, B), positive staining for NKG2A was identified at all antibody dilutions tested (Figure 5.4C).

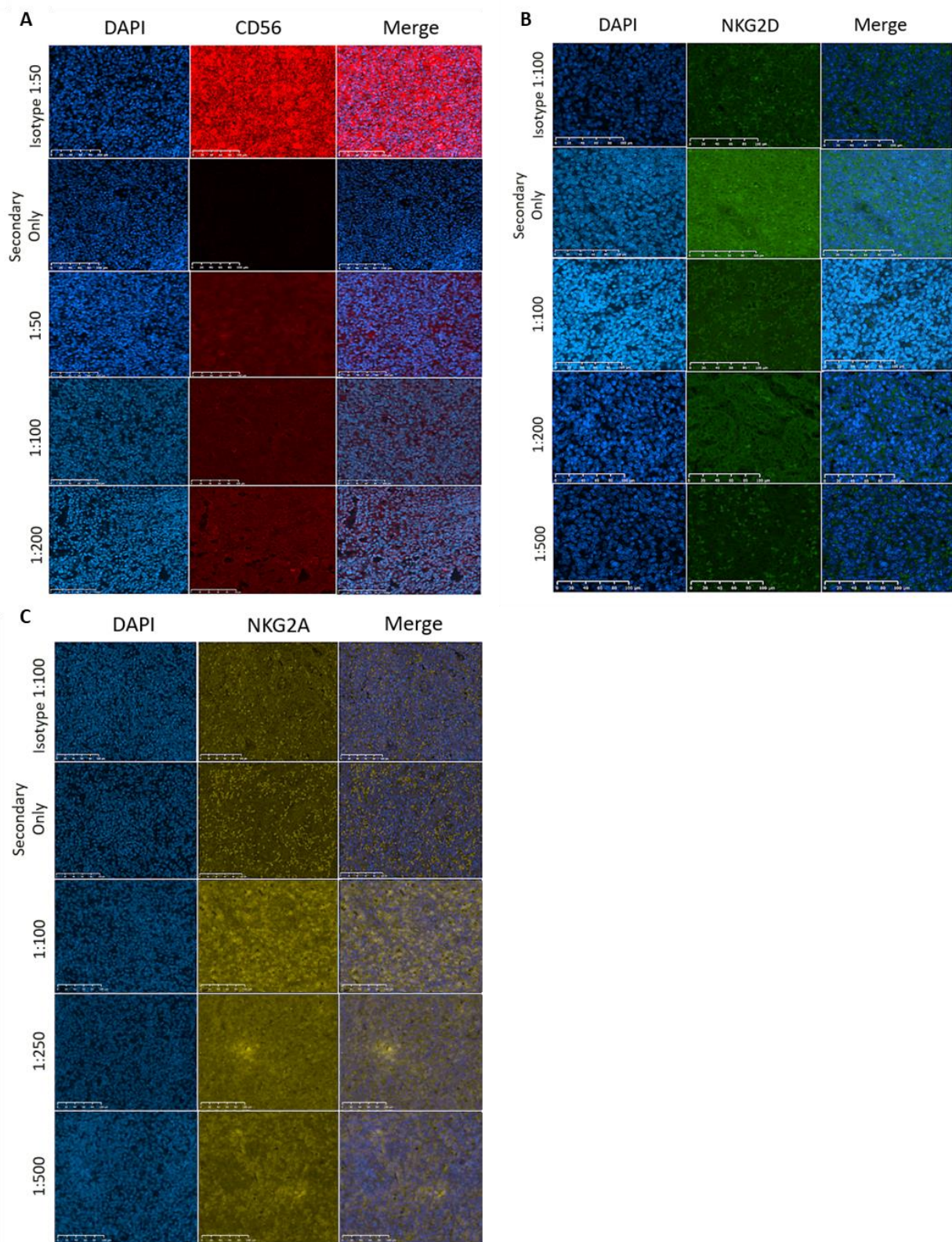


Figure 5.4: Immunofluorescent staining of human spleen tissue using a new protocol.

Antibodies were titrated at the following dilutions: A) Anti-CD56; 1:50, 1:100, 1:200; B) Anti-NKG2D; 1:100, 1:200, 1:500. C) Anti-NKG2A; 1:100, 1:250, 1:500. All antibodies are shown with an isotype and secondary only control. Images were acquired on the NanozoomerS60 slide scanner (Hamamatsu). Slides scanned with 20x magnification lens. Scale bars = 100µm.

5.3 Immunohistochemical Evaluation of Antibody signal

As high background remained a persistent issue with fluorescent staining, we employed immunohistochemistry (IHC) to evaluate antibody signal.

The DAKO CD56 antibody generates positive signal with both microwave and pressure cooker antigen retrieval in human tonsil tissue. Some positive staining was observed for CD56 (abcam) at dilutions of 1:500 and 1:750, however the high background staining observed confounds these results. Dilutions of 1:100 and 1:500 yielded positive staining for NKG2A in both spleen and tonsil tissue (with high background), however no positive signal was observed for NKG2D (Figure 5.5).

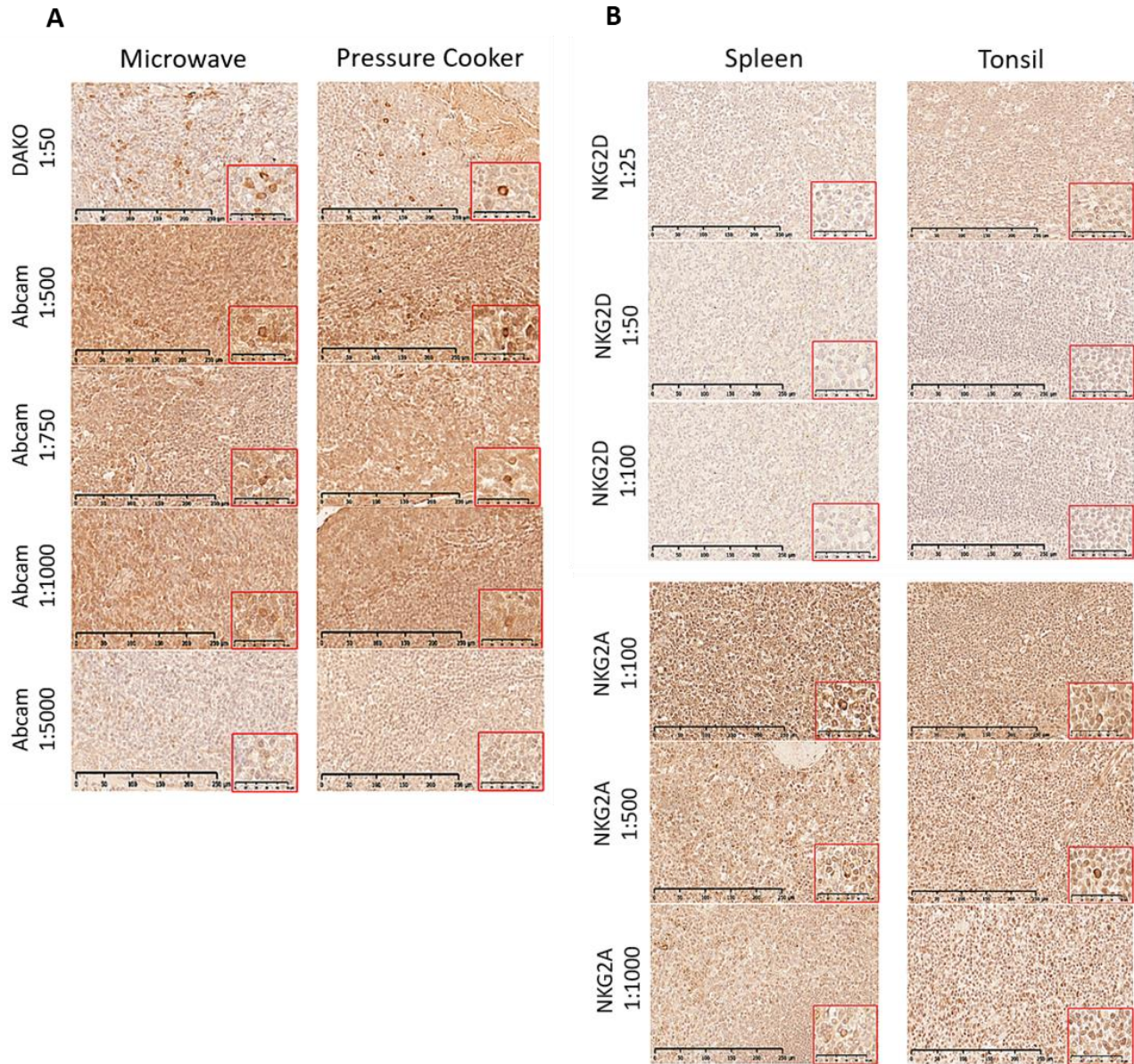


Figure 5.5: Immunohistochemical evaluation of antibody signal strength.

A) Titration of anti-CD56 (Abcam) in human tonsil tissue (1:500, 1:750, 1:1000, 1:500). Antigen retrieval was achieved using citrate buffer (pH 6.0) with either microwave or pressure cooker heating. The anti-CD56 antibody from DAKO serves as a positive control (top). B) Titration of anti NKG2D (1:25, 1:50, 1:100) and NKG2A (1:100, 1:500 and 1:1000) antibodies in human spleen and tonsil tissues. Microwave antigen retrieval was used in this protocol. All slides were imaged on the Nanozoomer210 Brightfield Slide scanner. Slides scanned with 40x magnification lens. Scale Bars = 250µm.

Following identification of positive signal using the CD56 antibody from DAKO, we employed a modified staining protocol to carry out antibody titration.

The DAKO CD56 antibody generated greatest signal at a 1:50 dilution with pressure cooker antigen retrieval (Figure 5.6). Thus, this antibody dilution and antigen retrieval method was chosen to be used for all future manual staining.

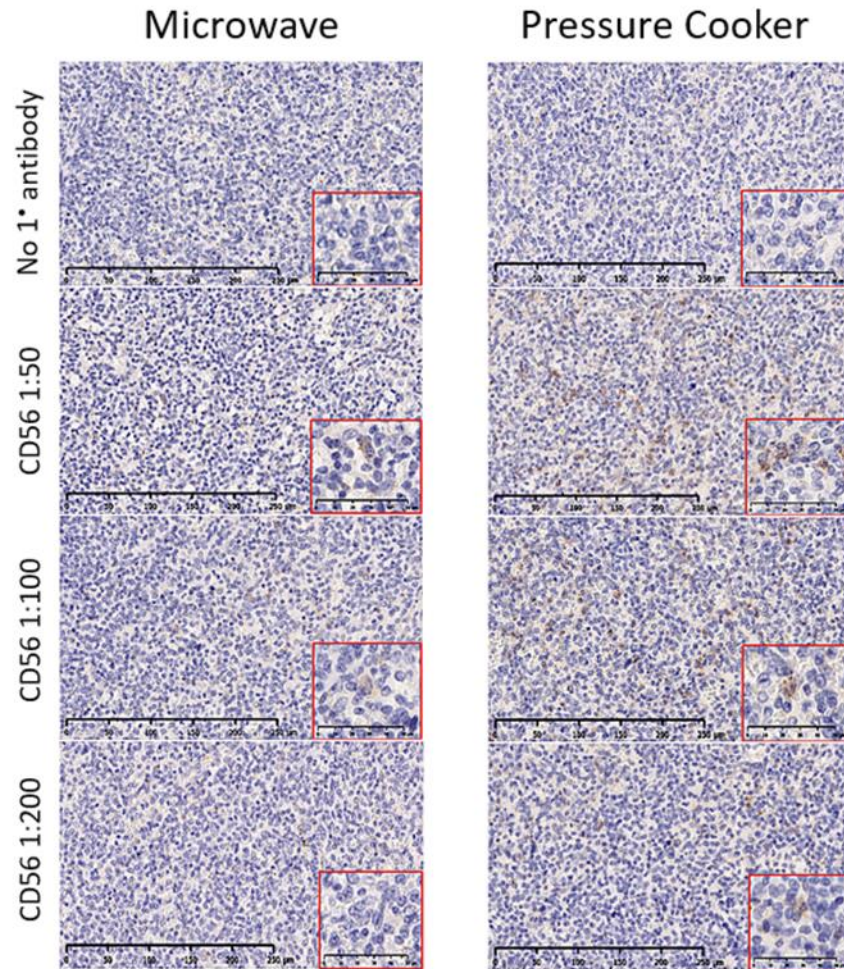


Figure 5.6: Titration of CD56 antibody from DAKO in human spleen tissue.

Antibodies were titrated at 1:50, 1:100 and 1:200. Slides with no primary antibody serve as negative controls (top). Heat induced antigen retrieval was carried out using either microwave or pressure cooker heating with citrate (pH 6.0) antigen retrieval buffer. Slides were scanned on the Nanozoomer210 Brightfield slide scanner using the x40 magnification lens. Scale Bar = 250μm.

5.4 IHC Optimisations for multiplex immunohistochemistry

To facilitate the staining of multiple NK and PSC/CAF markers in patient TMA sections, and thus allow comprehensive assessment of the interaction between NK-PSC/CAF in patient samples, multiplex immunohistochemistry was employed. Ahead of running mIHC on pancreas cancer sections, several antibodies within the designed panels required optimisation. IHC optimisation images for periostin (Figure 5.7; Appendix 9, Appendix 10), myosin -11 (Figure 5.8), CD105 (Figure 5.9) and NKp46 (Figure 5.10) are shown below. Each antibody was optimised for dilution and antigen retrieval method.

It was concluded that the subsequent dilutions/concentrations and epitope retrieval conditions would be used for multiplexed staining: periostin – 1: 1500, ER1; myosin-11 – 1.25µg/mL, ER2; CD105 – 1: 1400, ER2; and NKp46 1: 1000, ER2.

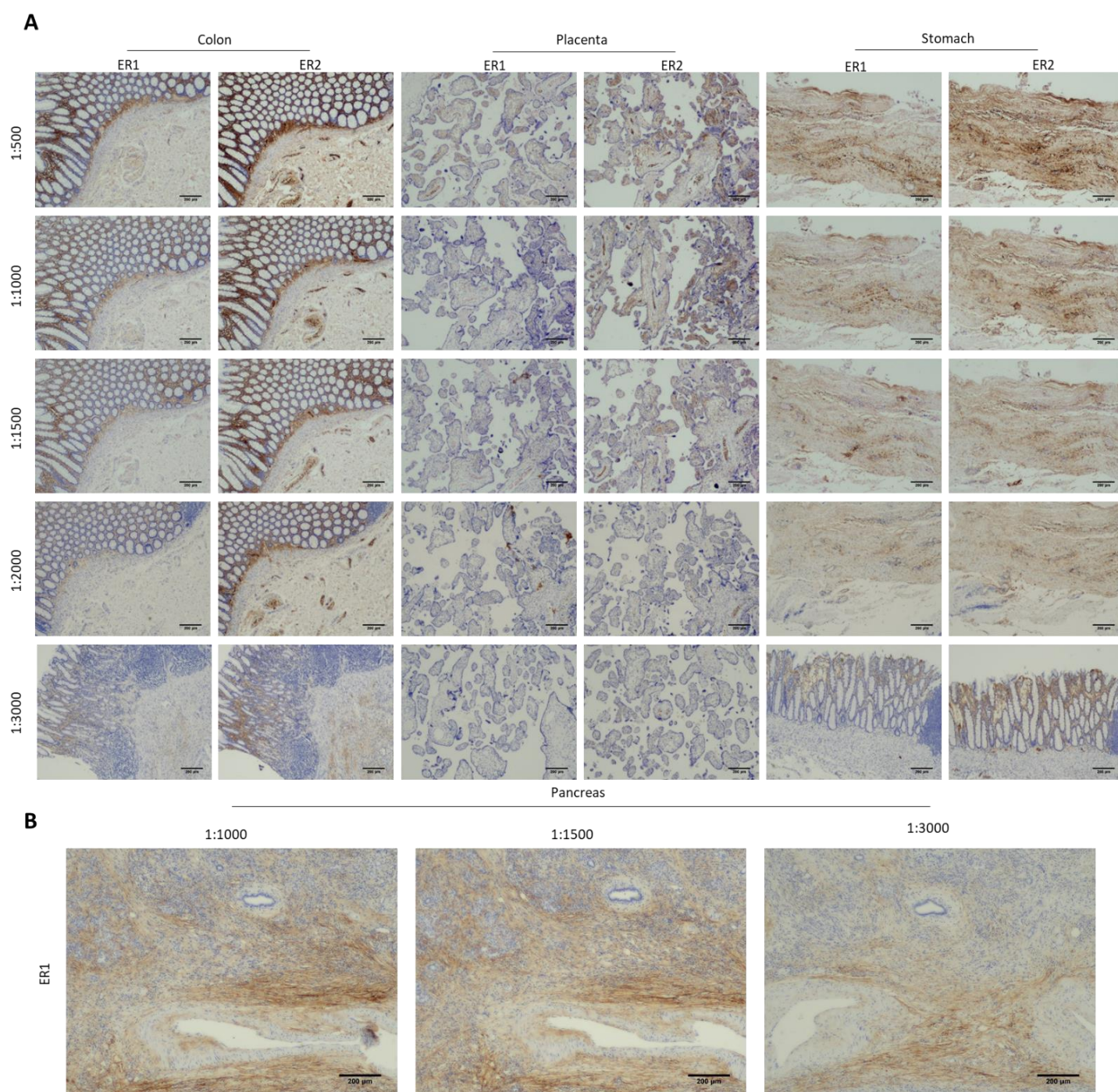


Figure 5.7: Periostin antibody optimisation.

A) Immunohistochemical staining of Periostin (ab215199, Abcam) was carried out on colon, placenta, and stomach positive control tissue. Each dilution was tested using two epitope retrieval conditions ER1 (pH 6.0 citrate-based antigen retrieval) or ER2 (pH 9.0 Tris-based antigen retrieval). Slides were stained using the Leica Bond Max automated staining system. Following staining, slides were dehydrated and mounted with glass coverslips using Dibutylphthalate Polystyrene Xylene (DPX). B) IHC staining of periostin on normal pancreas tissue (1: 1000, 1: 1500, 1: 3000). All slides were imaged using the Olympus CKX53 inverted light microscope and Olympus EP50 camera at magnification x4. Scale bars=200µm were added using ImageJ software. The optimal staining conditions for Periostin were determined to be ER1, dilution 1:1500.

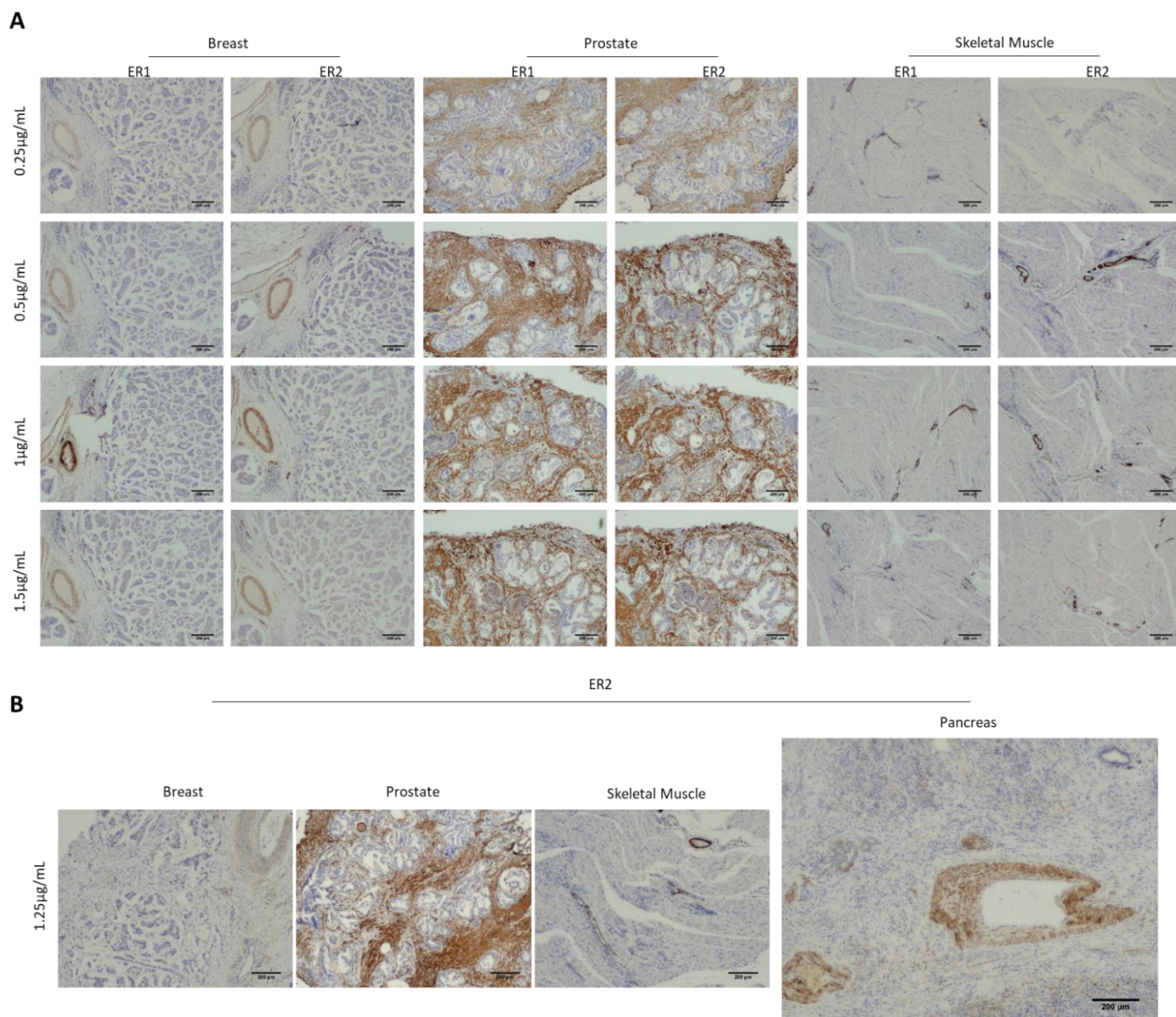


Figure 5.8: Myosin-11 antibody optimisation

A) Immunohistochemical staining of Myosin-11 (NBP2-44533, Novus Biologicals) was carried out on breast, prostate and skeletal muscle positive control tissue. Each dilution was tested using two epitope retrieval conditions ER1 (pH 6.0 citrate-based antigen retrieval) or ER2 (pH 9.0 Tris-based antigen retrieval). Slides were stained using the Leica Bond Max automated staining system. Following staining, slides were dehydrated and mounted as described. Slides were imaged using the Olympus CKX53 inverted light microscope and Olympus EP50 camera at magnification x4. Scale bars=200 μm were added using ImageJ software. B) Trial of the optimised dilution of 1.25 $\mu\text{g/mL}$, ER2 on control sections and normal pancreas tissue. Slides were imaged as described.

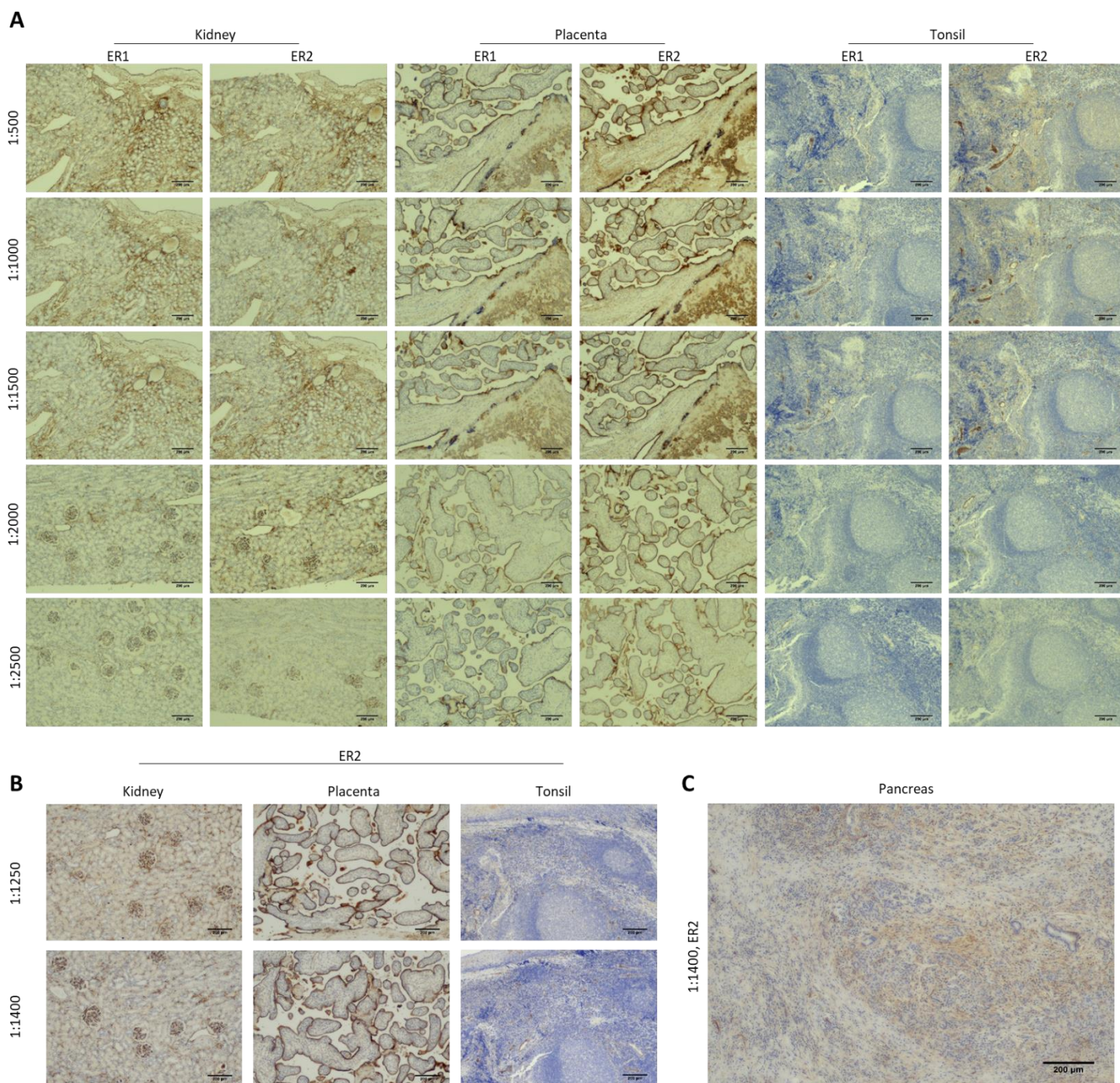


Figure 5.9: CD105 antibody optimisation

A) Immunohistochemical staining of CD105 (14606, Cell Signaling Technology) on Kidney, Placenta and Tonsil positive control tissue. Each dilution was tested using two epitope retrieval conditions ER1 (pH 6.0 citrate-based antigen retrieval) or ER2 (pH 9.0 Tris-based antigen retrieval). Slides were stained using the Leica Bond Max automated staining system. Following staining, slides were dehydrated and mounted with glass coverslips using Dibutylphthalate Polystyrene Xylene (DPX). Slides were imaged using the Olympus CKX53 inverted light microscope and Olympus EP50 camera at magnification x4. Scale bars=200µm were added using ImageJ software. B) Immunohistochemical staining of CD105 on control slides at two final dilutions. C) IHC staining of CD105 on normal pancreas tissue using the optimised dilution and antigen retrieval condition.

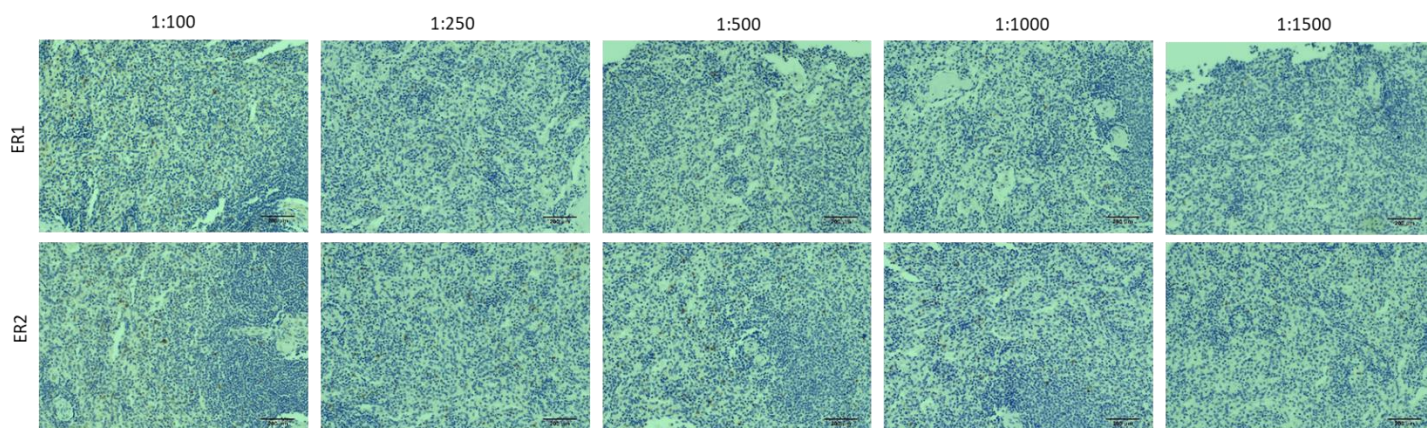


Figure 5.10: NKp46 Antibody optimisation.

Immunohistochemical staining of NKp46 (ab244703, Abcam) on human spleen positive control tissue. Each dilution was tested using two epitope retrieval conditions ER1 (pH 6.0 citrate-based antigen retrieval) or ER2 (pH 9.0 Tris-based antigen retrieval). Slides were stained using the Leica Bond Max automated staining system. Following staining, slides were dehydrated and mounted as described and imaged using the Olympus CKX53 inverted light microscope and Olympus EP50 camera at magnification x4. Scale bars=200µm were added using ImageJ software. The optimal staining conditions for NKp46 were determined to be ER2, dilution 1:1000.

5.5 mIHC full panel trials

We next sought to run trial mIHC staining for each of the panels designed to ensure that each marker could be clearly identified within pancreas tissue. Trial images were unmixed using the triple negative breast cancer library as creation of the pancreas library slides had not been finalised. It is perhaps prudent to note that due to the light staining intensity of NKG2D previously noted by the lab, panel 2 was trialled on tonsil and pancreas cancer tissue to ensure a positive control was present.

We determined that the staining order and antibody intensities for Panels 1 (Figure 5.11) and 3 (Figure 5.13) yielded positive results for all the markers of interest. As such, these panels were taken forward for patient TMA staining. However, for panel 2, very few NKG2D⁺ cells were observable within tonsil tissue, with little to no positive stain being identified with PDAC samples (Figure 5.12).

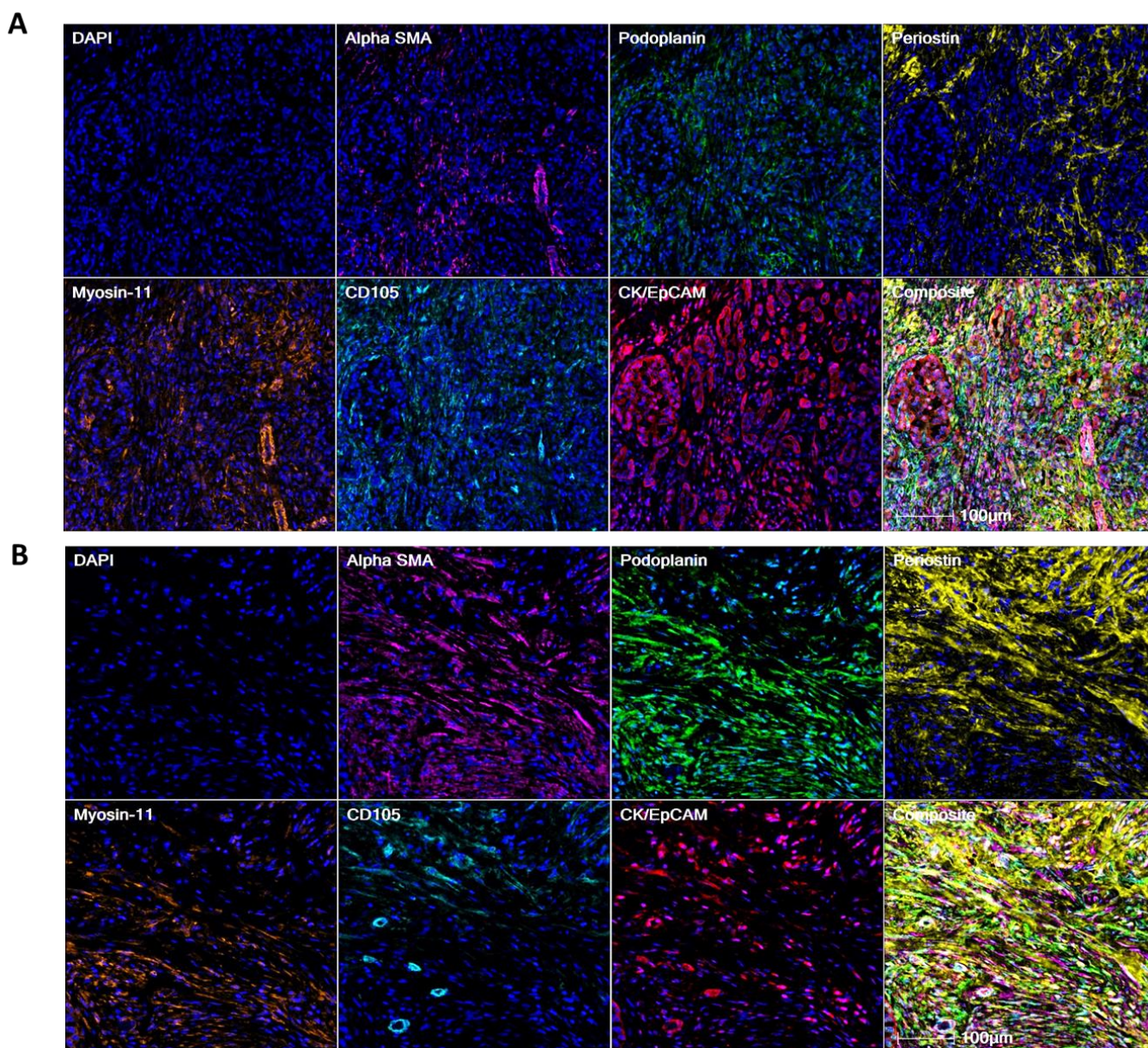


Figure 5.11: mIHC images of Panel 1 trial staining.

A) Representative image of Panel 1 staining on normal pancreas tissue. B) Representative image of Panel 1 staining on pancreatic cancer tissue. DAPI – blue; alpha SMA – magenta; podoplanin – green; periostin – yellow; myosin-11 – orange; CD105 – cyan; cytokeratin/EpCAM – red. Slides were imaged using the Vectra imaging system. Images were spectrally unmixed using a triple negative breast cancer library and inForm software. Images were generated using HALO 3.0 software. Scale bar =100µm.

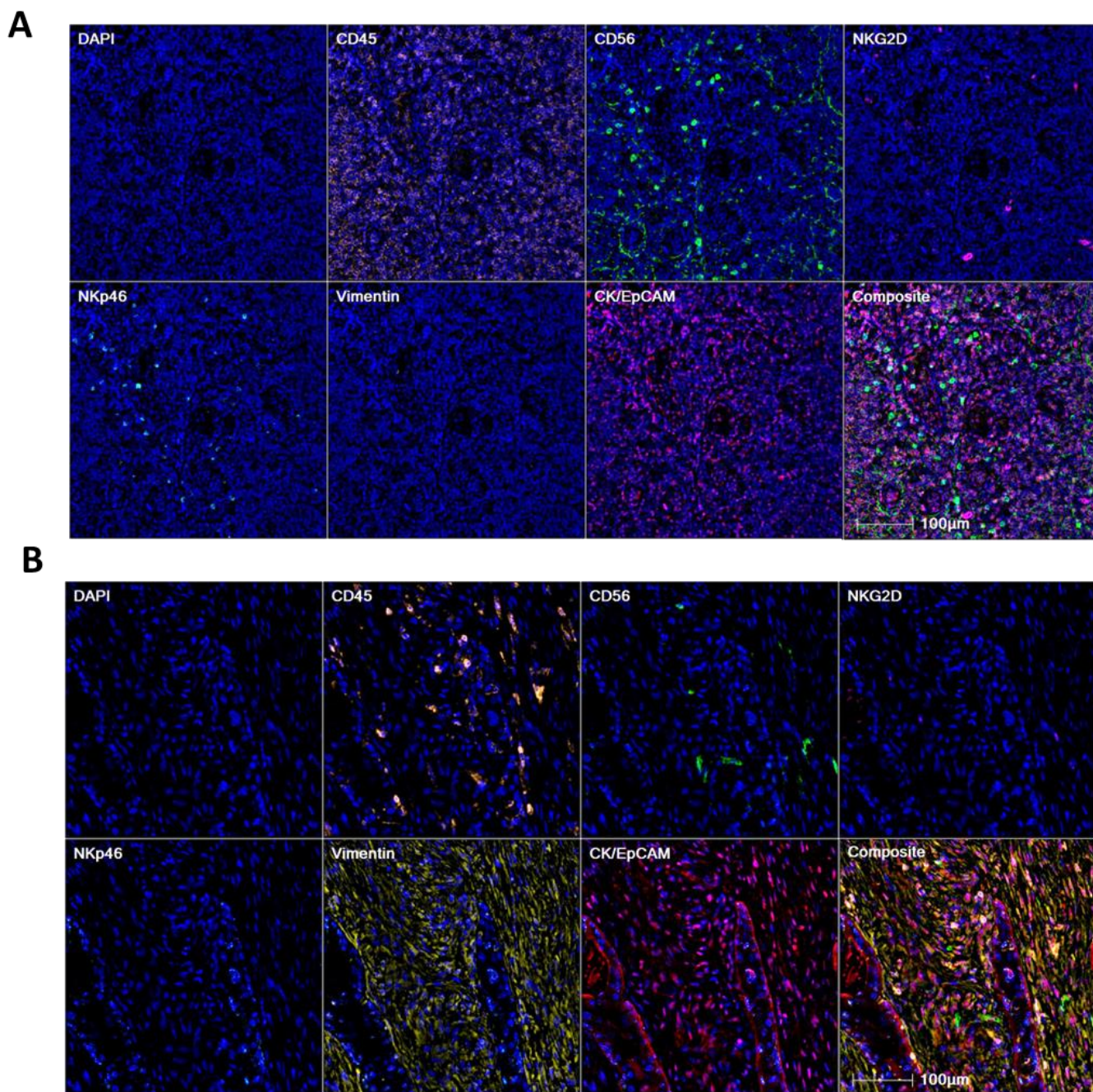


Figure 5.12: mIHC images of Panel 2 trial staining.

A) Representative image of Panel 2 staining on tonsil tissue. B) Representative image of Panel 2 staining on pancreatic cancer tissue. DAPI – blue; CD45 – orange; CD56 – green; NKG2D – Magenta; NKp46 – cyan; Vimentin – yellow; cytokeratin/EpCAM – red. Slides were imaged using the Vectra imaging system. Images were spectrally unmixed using a triple negative breast cancer library and inForm software. Images were generated using HALO 3.0. Scale bar =100µm.

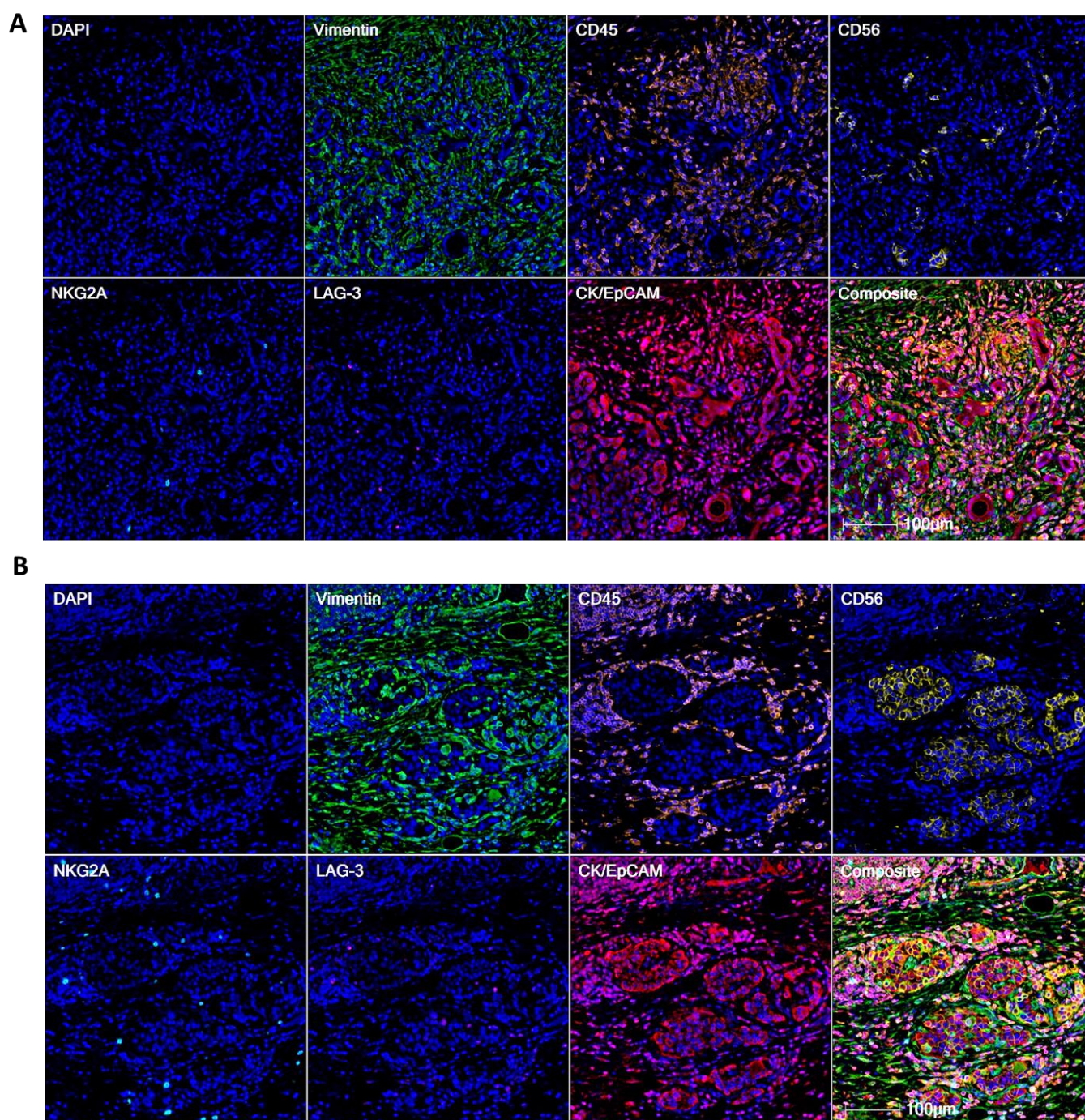


Figure 5.13: mIHC images of Panel 3 trial staining.

A) Representative image of Panel 3 staining on normal pancreas tissue. B) Representative image of Panel 3 staining on pancreatic cancer tissue. DAPI – blue; vimentin – green; CD45 – orange; CD56 – yellow; NKG2A – cyan; LAG-3 – magenta; cytokeratin/EpCAM – red. Slides were imaged using the Vectra Polaris imaging system. Images were spectrally unmixed using a triple negative breast cancer library and inForm software. Images were generated using HALO 3.0. Scale bar =100µm.

5.5.1 NKG2D Troubleshooting

To address the lack of NKG2D staining observed during multiplex immunohistochemical staining, we ran further optimisations for incubation length for the NKG2D antibody (Figure 5.14).

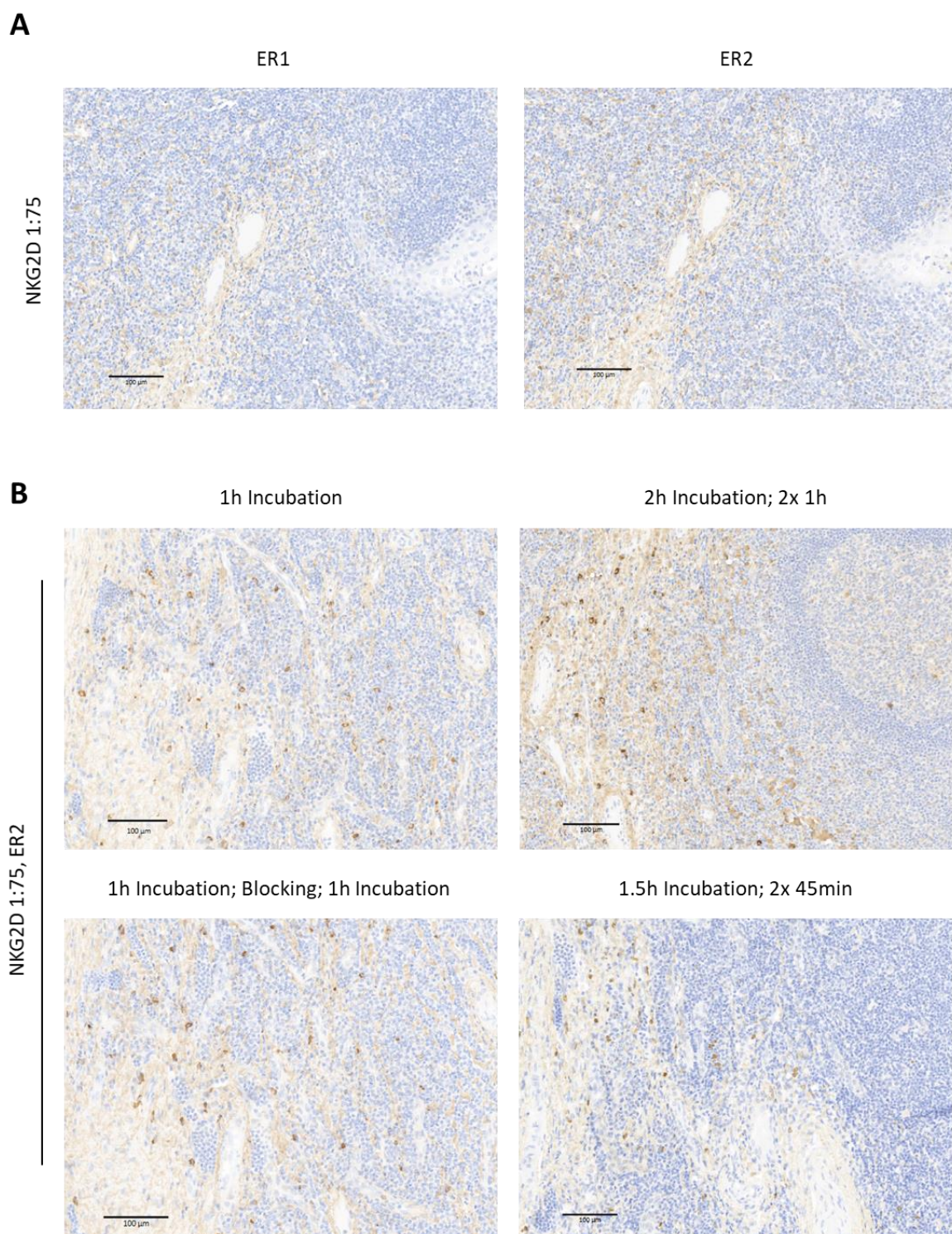


Figure 5.14: NKG2D incubation optimisation.

A) IHC staining of NKG2D (NB100-65956, Novus Biologicals) (1:75) on tonsil positive control tissue using either ER1 (pH6.0 citrate based) or ER2 (pH 9.0 Tris-based) antigen retrieval. The optimal staining condition was determined to be 1:75, ER2. B) IHC staining of NKG2D (1: 75, ER2) on tonsil tissue following different length incubations. Slides were incubated for either 1h, 2h (2x 1h), 1h incubation followed by a blocking step and then a further 1h incubation (2h total), or 1.5h split into 2x 45min incubations. All slides were imaged on the Zeiss AxioScan. Scale bars were added using Zen Lite (Zeiss). Scale bars =100µm.

The optimal NKG2D incubation length was determined to be 1.5h, with staining divided into two incubations of 45 min in order to achieve the desired incubation length without risking the slide drying out.

Following NKG2D optimisation, a trial round of mIHC staining for panel 2 was completed (Figure 5.15). Clear positive populations of all cell markers could be identified and consequently this staining protocol was used to stain PDAC TMA sections.

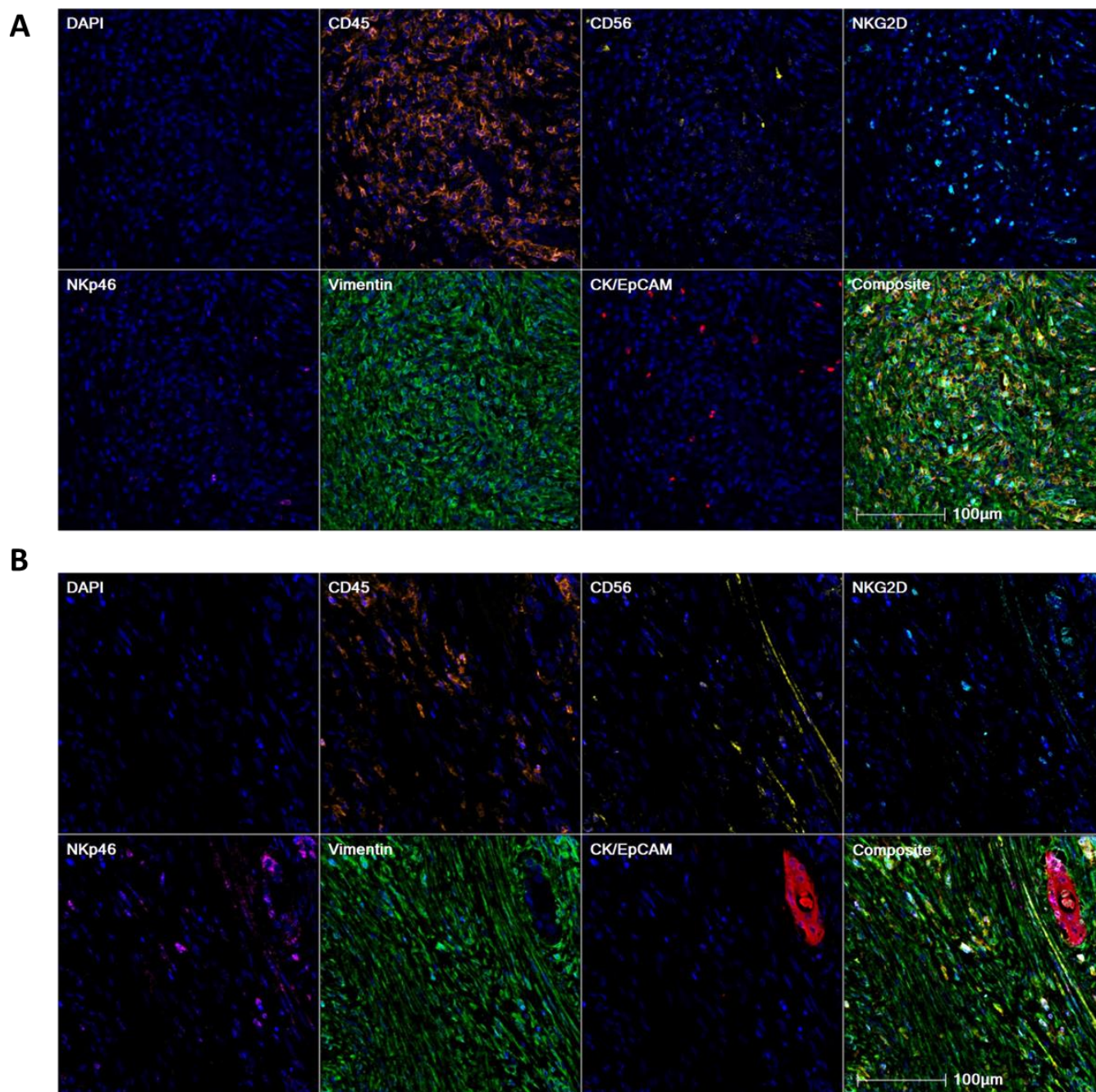


Figure 5.15: mIHC images of Panel 2 trial staining – modified NKG2D incubation.

A) Representative image of Panel 2 staining on normal pancreas tissue. B) Representative image of Panel 2 staining pancreatic cancer tissue. DAPI – blue; CD45 – orange; CD56 – yellow; NKG2D – cyan; NKp46 – magenta; vimentin – green; cytokeratin/EpCAM – red. Slides were imaged using the Vectra Polaris imaging system. Images were spectrally unmixed using a pancreas library and inForm software. Images were generated using HALO 3.0. Scale bar =100µm.

Chapter 6 - Results 4 – *Ex Vivo* Experiments

6.1 Introduction

Cellular localisation within the tumour microenvironment has long been recognised to play a crucial role in patient prognosis.^{61, 281, 282} However, the prognostic value of single cell infiltrate is often variable and inconsistent, with much dependency on the experience of the observer. Moreover, the semi-quantitative cellular assessment achieved with this method provides only rudimentary cell count estimates.²⁸³ Thus, the technical and analytical limitations of classical IHC staining methods are yet to fully address the complex interactions of immune, stromal and tumour cells within the context of cancer.²⁸⁴

Multiplex IHC facilitates quantitative assessment of immune infiltrate within tumoural tissue whilst preserving tissue architecture.²⁸⁵ Moreover, with the ability to stain multiple markers on a single slide, cellular phenotype can be assessed.²⁸⁶ The availability of post-acquisition analysis tools such as HALO (Indica Labs) and QuPath²⁸⁷ facilitate further exploration of the unique cell-cell interactions observed within patient samples, allowing spatial as well as phenotypic analysis.^{241, 277}

Previously we have shown that NK cells and PSCs exhibit a distinct bi-directional interaction *in vitro*. In this chapter, we investigate the spatial interaction of NK and PSC/CAFs in PDAC patient samples through the use of mIHC and post-acquisition tools.

6.2 Multiplex Immunohistochemical analysis of PDAC samples

To assess the location of and interaction between NK and CAFs in PDAC, multiplex immunohistochemical analysis of tissue microarray (TMA) slides containing samples from patients with PDAC and chronic pancreatitis as well as adjacent normal tissue was carried out (Appendix 11). An overview of patient clinical data is outlined in Table 6.1.

Unfortunately, during the creation of the TMA sections the cores for two PDAC patients were lost. Consequently, the number of PDAC patients included within the TMA slides is stated as 98 and not 100 (as included in the clinical data table). All clinical data for these patients were unknown. A summary of the patient samples included in the TMA slides are outlined in Table 6.2 and Table 6.3.

	Normal Adjacent (n=24)		Chronic Pancreatitis (n=3)		PDAC (n=100)	
T (TNM Stage) (%)						
1	-	-	-	-	10	(10)
2	-	-	-	-	34	(34)
3	-	-	-	-	49	(49)
4	-	-	-	-	2	(2)
Unknown	-	-	-	-	5	(5)
N (TNM Stage) (%)						
0	-	-	-	-	35	(35)
1	-	-	-	-	60	(60)
Unknown	-	-	-	-	5	(5)
Resection (%)						
R0	-	-	-	-	62	(62)
R1	-	-	-	-	32	(32)
R2	-	-	-	-	0	(0)
Unknown	-	-	-	-	6	(6)
Differentiation (%)						
Well	-	-	-	-	13	(13)
Moderate	-	-	-	-	50	(50)
Poor	-	-	-	-	29	(29)
Moderate/poor borderline	-	-	-	-	5	(5)
Unknown	-	-	-	-	3	(3)
Sex (%)						
Male	12	(50)	0	(0)	54	(54)
Female	11	(46)	1	(33)	44	(44)
Unknown	1	(4)	2	(67)	2	(2)
Patient Status (%)						
Dead	12	(50)	0	(0)	73	(73)
Alive	4	(17)	0	(0)	15	(15)
Lost to follow-up	5	(21)	1	(33)	9	(9)
Unknown	3	(13)	2	(67)	3	(3)

Table 6.1: Clinical details of patient samples included within TMA blocks.

Final Diagnosis	Number of Patients	Number of Cores
Normal Adjacent	24	101
Chronic Pancreatitis	3	12
PDAC	98	446
Lymphoma	1	4
Mucinous Cystadenocarcinoma	1	6

Table 6.2: Details of tissue types included within TMA slides.

Source of Normal Adjacent tissue	Number of Cases
AMP Adenoma	3
Ampullary Cancer	3
Cholangiocarcinoma	13
Duodenal Adenoma	1
Endocrine	2
IPMN	2

Table 6.3: Sources of normal adjacent tissue included within TMA slides.

Following successful trial runs of each mIHC panel on normal and malignant pancreas (Section 5.5), 7 TMA slides were stained for each multiplex panel (Figure 6.1, Figure 6.2, Appendix 12, Appendix 13, Appendix 14). The resultant scoring data was processed and concordance across panels was established (Appendix 15).

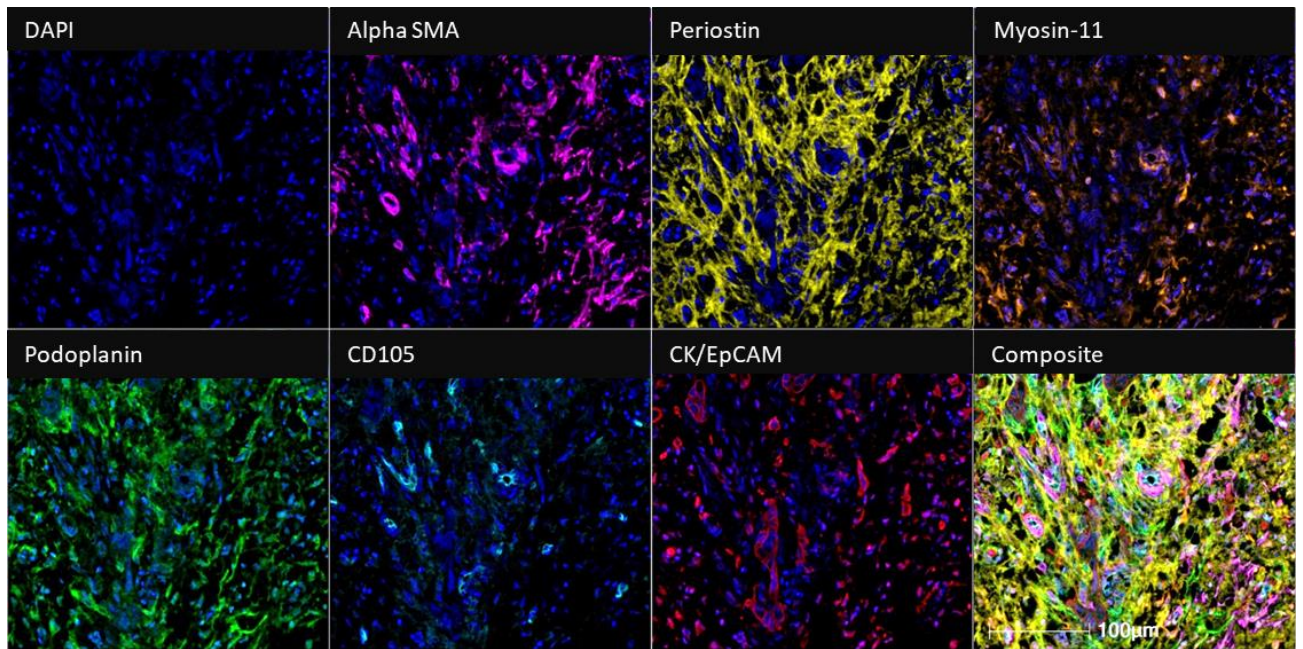


Figure 6.1: Representative image of CAF staining in PDAC.

Samples were stained for alpha SMA –magenta; periostin – yellow; myosin-11 – orange; podoplanin- - green; CD105 – cyan; CK/EpCAM – red using the Opal TSA system (Akoya Biosciences). Nuclei are stained with DAPI– blue. Slides were scanned using the Vectra Polaris (Akoya bioscience). Images were created with HALO software (3.4). Scale bars = 100µm.

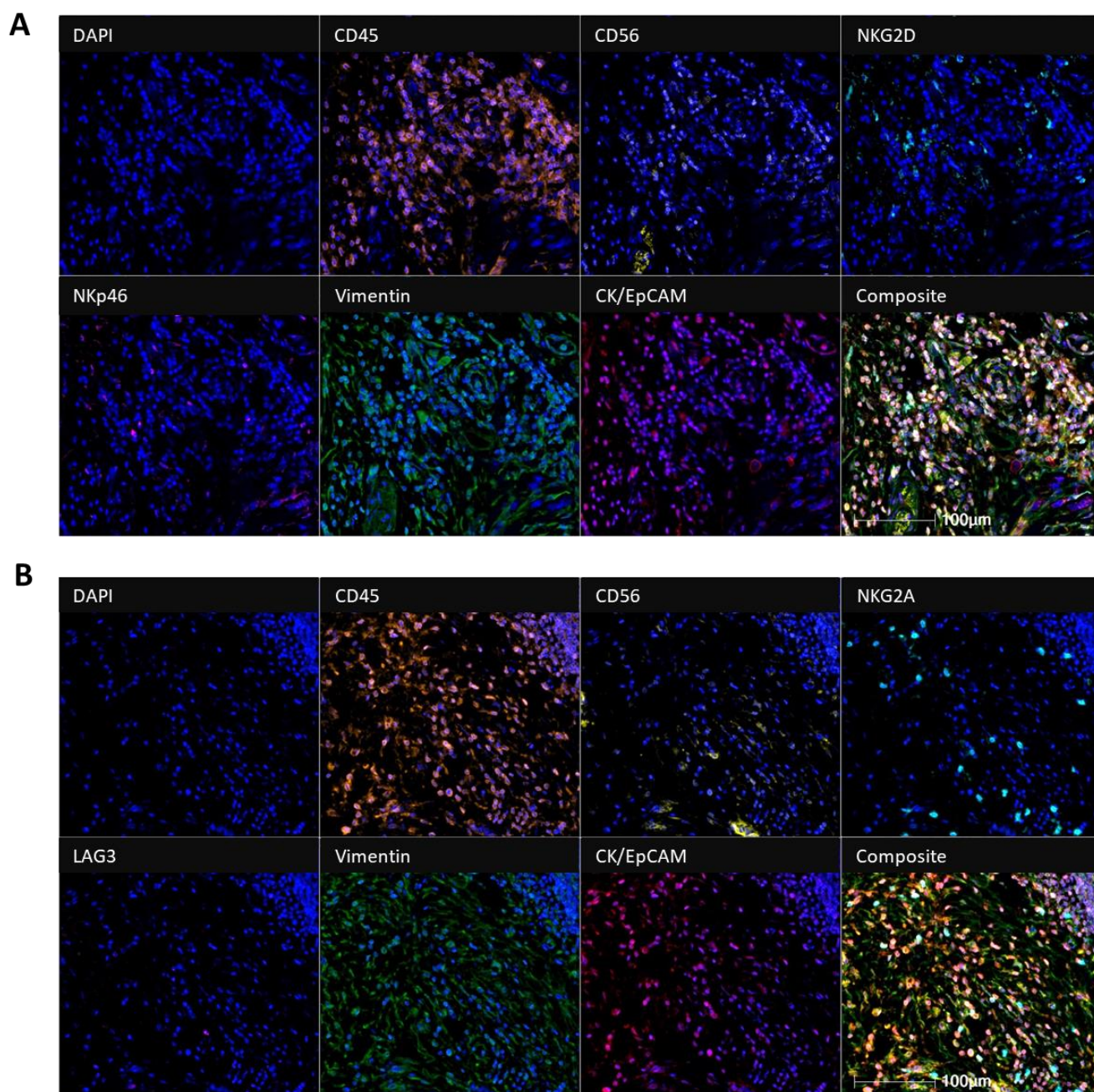


Figure 6.2: Representative images of NK cell staining in PDAC.

A) Representative image of panel 2 staining (NK activating receptors) on PDAC patient tissue. CD45 – orange; CD56 – yellow; NKG2D – cyan; NKp46 – magenta; Vimentin – green; CK/EpCAM – red. Nuclei are stained with DAPI – blue. B) Representative image of panel 3 (NK inhibitory receptors) on PDAC patient tissue. CD45 – orange; CD56 – yellow; NKG2A – cyan; LAG3 – magenta; Vimentin – green; CK/EpCAM – red. Nuclei are stained with DAPI – blue. Patient TMA samples were stained using the Opal TSA system and scanned using the Vectra Polaris (Akoya Biosciences). Images were created with HALO software (3.4). Scale bars = 100µm.

We identified significant inter-tumoural heterogeneity in CAF marker expression as previously described (Figure 6.3).¹⁴⁰ Furthermore, we also report distinct NK phenotypic heterogeneity between patients (Figure 6.4, Appendix 16).

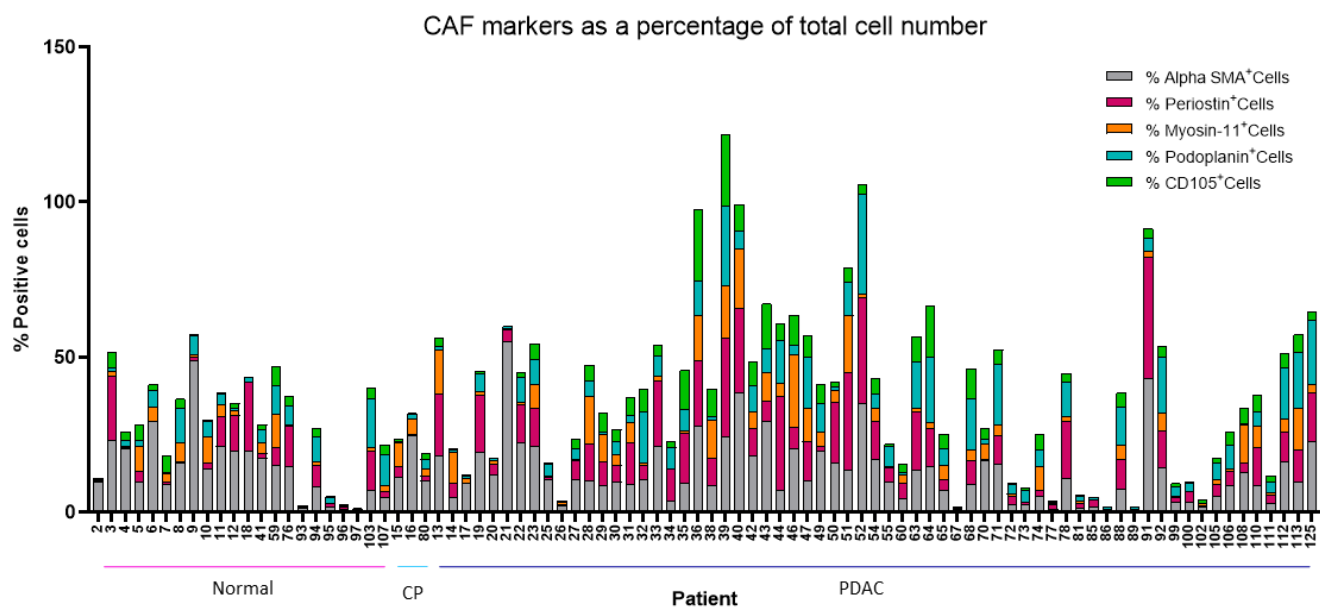


Figure 6.3: Cancer associated fibroblast marker expression across patients.

Expression of CAF markers identified using multiplex immunohistochemical analysis of patient TMA sections. Expression is shown as a percentage of total (DAPI⁺) cell number. Please note some cells may express more than one marker, resulting in >100% cells.

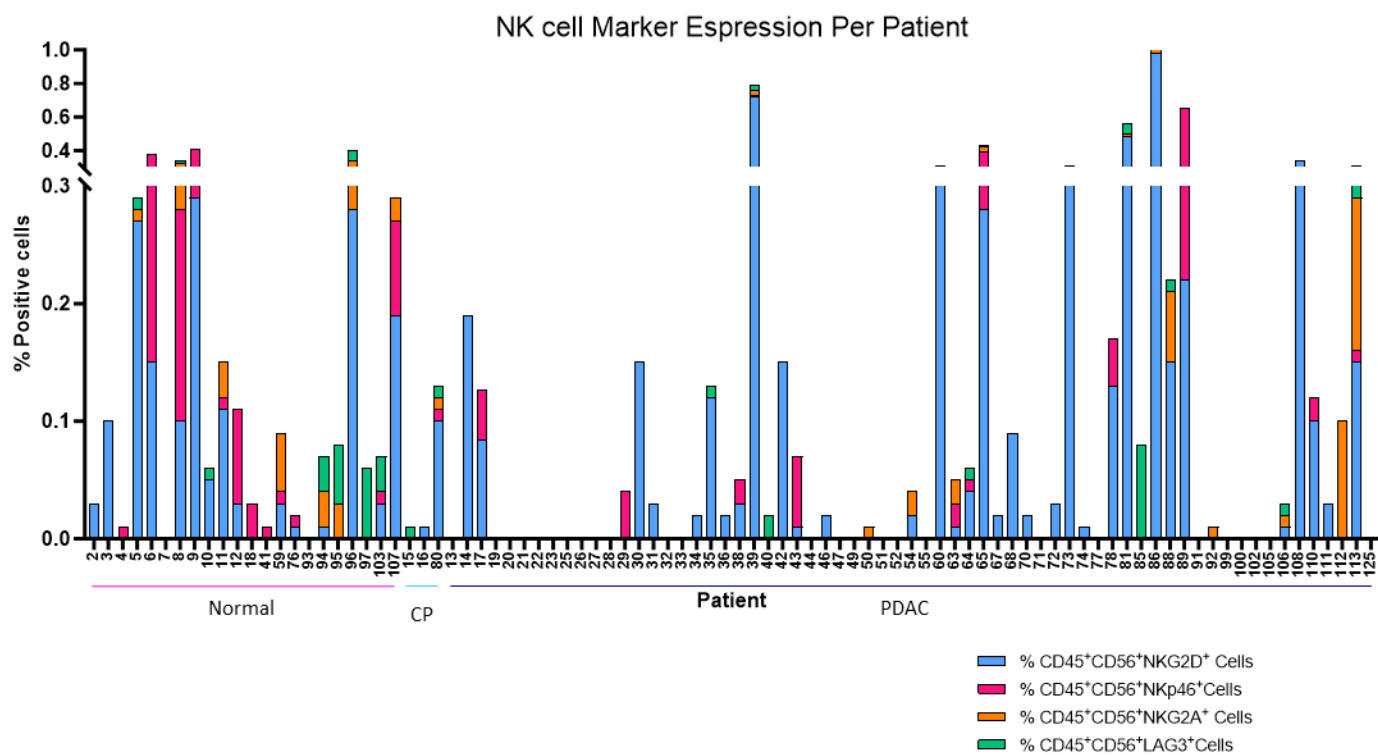


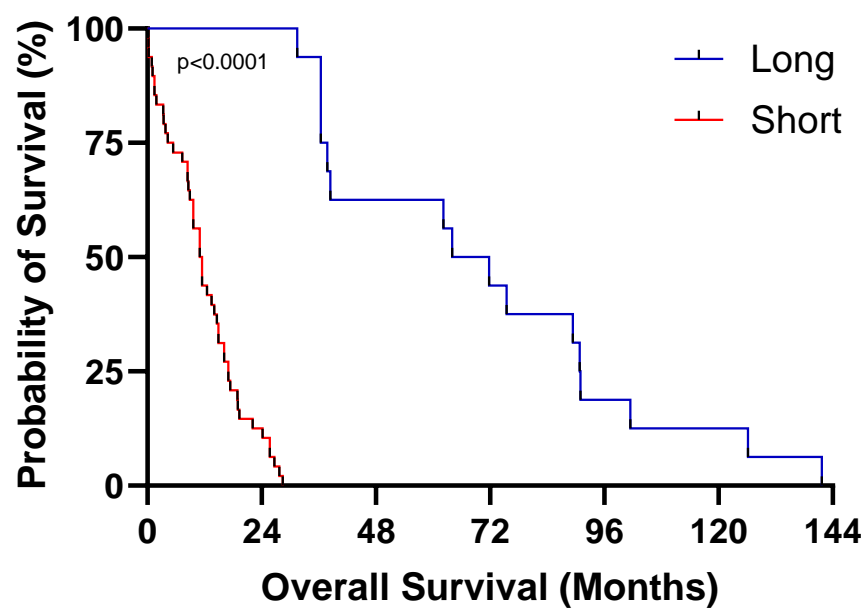
Figure 6.4: NK cell marker expression across patients.

Expression of NK cell markers identified using multiplex immunohistochemical analysis of patient TMA sections. Marker expression is shown as a percentage of total (DAPI⁺) cell number.

6.2.1 Immune cell infiltrate in PDAC

To further investigate NK heterogeneity in PDAC, we sought to determine the impact of NK immune cell infiltrate on short and long survivorship (Figure 6.5 and Figure 6.6).

Patient dichotomisation at 30 months overall survival provided two distinct subgroups ('short' and 'long' survivors) which could be used to assess the impact of immune cell infiltrate on patient prognosis (Figure 6.5).



Number at Risk

Short Survivors	48	6	0	0	0	0	0
Long Survivors	16	16	12	9	4	3	0

Figure 6.5: Survival analysis of short and long survivors.

Kaplan Meier survival analysis of 64 PDAC patients dichotomised into short ($n=48$) and long ($n=16$) survivors (cut-off = 30 months). Statistical significance was identified using the Log-Rank test. Data were analysed using GraphPad Prism (9.0).

We did not identify any significant difference in NK cell infiltrate (CD45⁺CD56⁺) nor any difference in individual NK subsets (CD45⁺CD56⁺NKG2D⁺, CD45⁺CD56⁺NKG2A⁺, CD45⁺CD56⁺NKp46⁺, CD45⁺CD56⁺LAG3⁺) between short and long survivors (Figure 6.6).

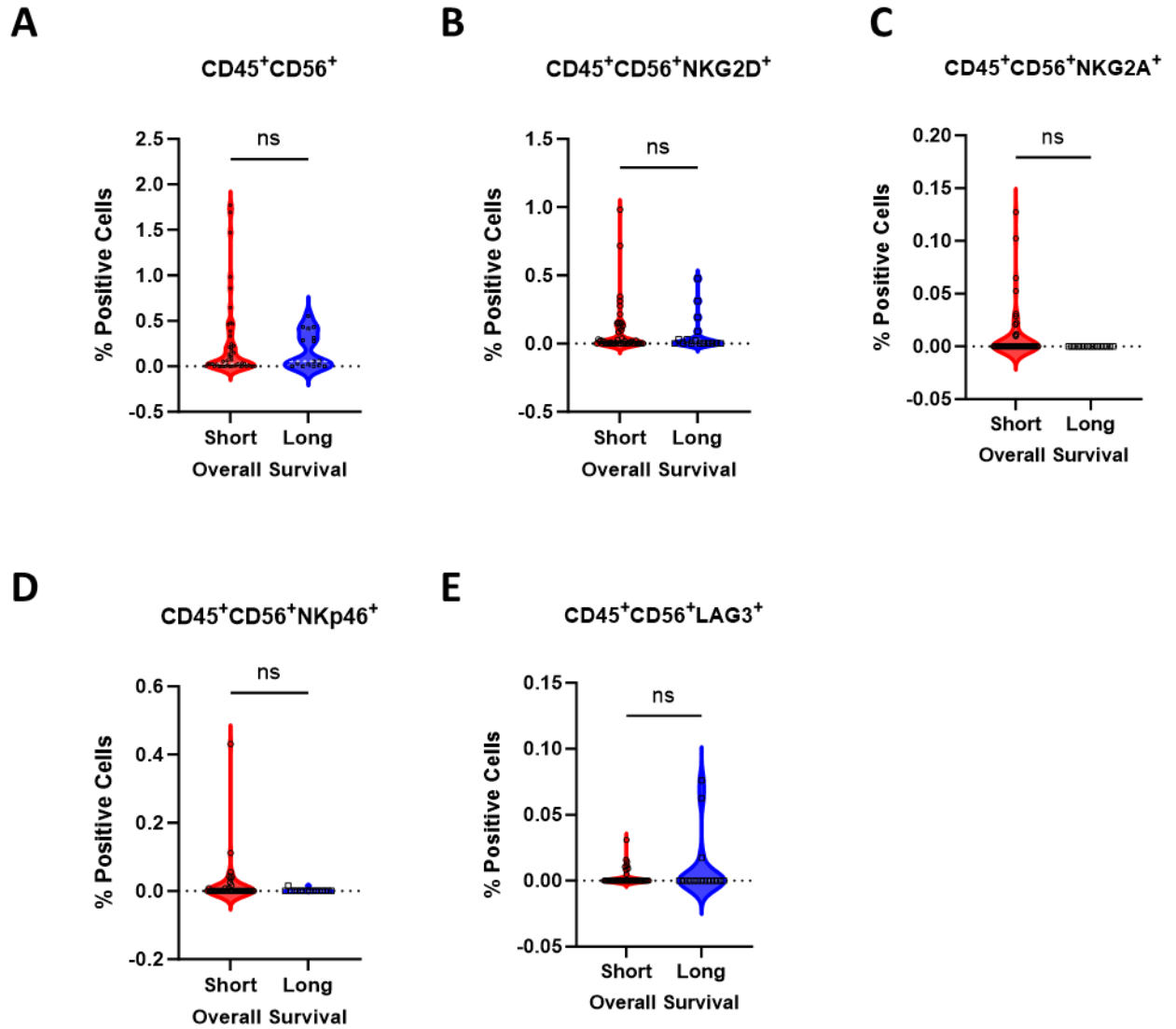


Figure 6.6: NK immune cell infiltrate in short and long survivors.

A-E) Violin plots of percent positive cells for CD45⁺CD56⁺ (A), CD45⁺CD56⁺NKG2D⁺ (B) CD45⁺CD56⁺NKG2A⁺ (C), CD45⁺CD56⁺NKp46⁺ (D) and CD45⁺CD56⁺LAG3⁺ (E) infiltrate in short (n=48) vs long (n=16) survivors. Data are shown as a percentage of total cells. Data were analysed using Mann-Whitney U-tests.

6.2.2 The importance of immune cell proximity to CAFs in PDAC

As we found direct contact to be necessary for the majority of functional and phenotypic changes identified between NK cells and PSCs *in vitro* we next looked to determine the impact of NK cell proximity to CAF cells (within PDAC tissue) on patient survival (Figure 6.7 and Figure 6.8).

Representative images depicting cellular proximity of NK cells and CAFs in PDAC are shown in Figure 6.7.

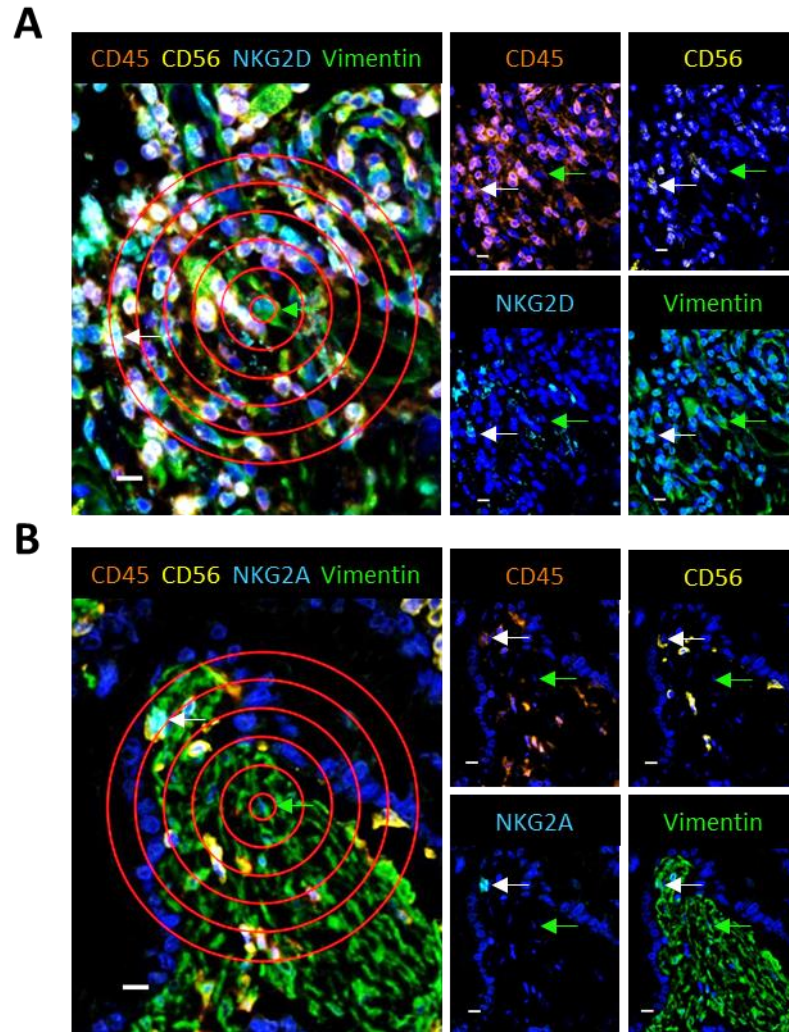


Figure 6.7: Proximity of NK cells and CAFs in PDAC.

A-B) Representative images of CD45⁺CD56⁺NKG2D⁺ (A) and CD45⁺CD56⁺NKG2A⁺ (B) cells in PDAC, and their proximity to Vimentin⁺ cells. Concentric circles were added using ImageJ software and are shown at 10µm intervals. Scale bars = 10µm.

Interestingly, we show that long survivors demonstrate greater spatial separation between NK cells and CAFs than do short survivors (Figure 6.8A). At the NK subset level, NKG2D⁺, but not NKp46⁺/LAG3⁺, cells were found to be at greater distance to CAF cells in long survivors (Figure 6.8B, D, E), whilst NKG2A⁺ NK cells were absent in long survivors (Figure 6.8C). Thus we suggest that it is proximity, and not total NK immune infiltrate, which impacts patient prognosis (Figure 6E). Taken together, these results suggest that NK cells may be less susceptible to CAF education (as previously shown) at greater distances, and thus are more functionally active.

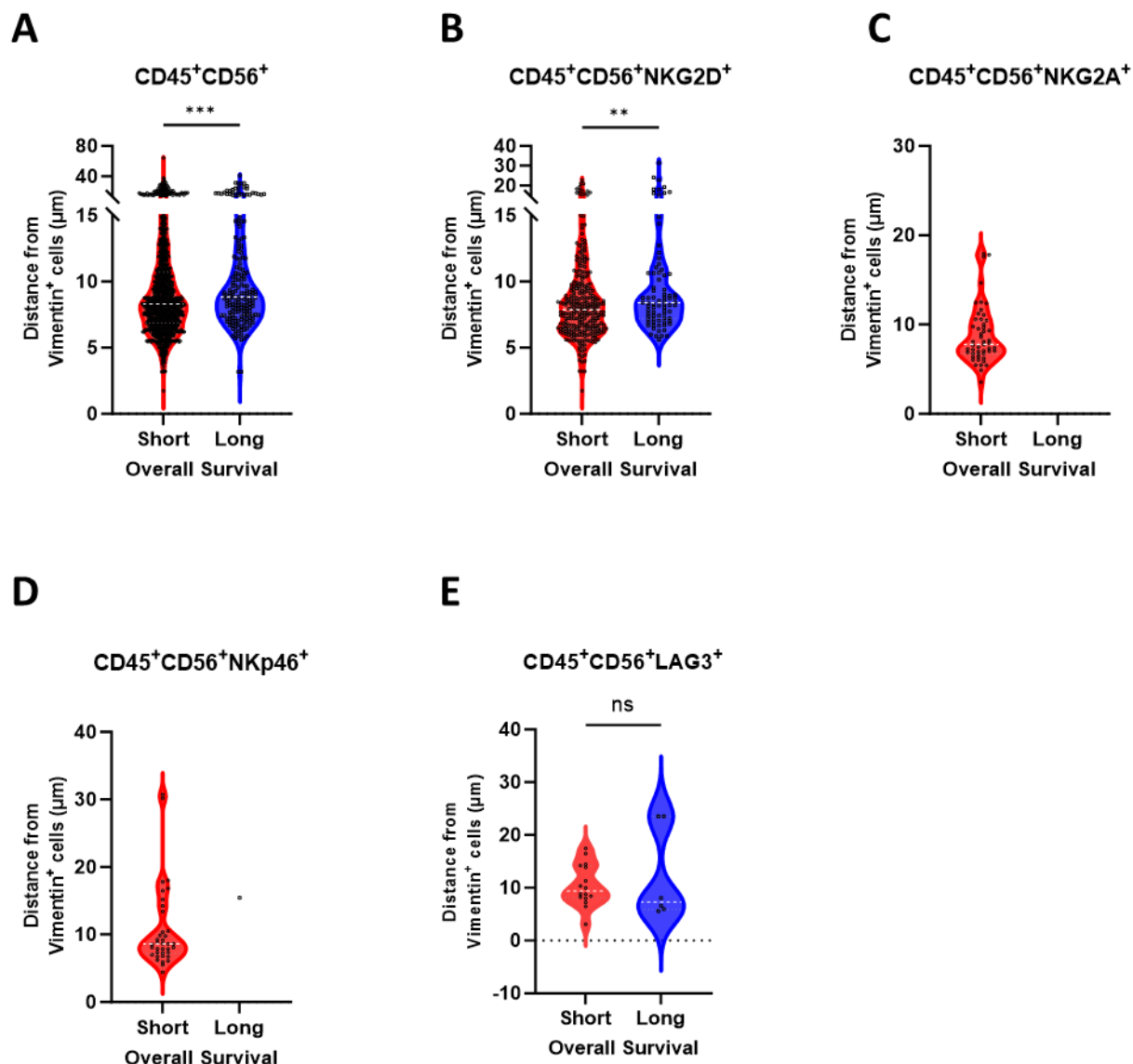


Figure 6.8: Violin plots showing results of proximity analysis between NK and CAF cells in PDAC.

A-E) Violin plots showing results of proximity analysis between $CD45^+CD56^+$ (A), $CD45^+CD56^+NKG2D^+$ (B), $CD45^+CD56^+NKG2A^+$ (C), $CD45^+CD56^+NKp46^+$ (D) and $CD45^+CD56^+LAG3^+$ (E) cells with Vimentin⁺ cells in short (n=48) and long (n=16) survivors. Data were analysed using the proximity analysis tool within the spatial analysis module from HALO (Indica Labs). Statistical analysis was carried out using Mann-Whitney U-tests. ** $p < 0.01$; *** $p < 0.001$; ns-not significant.

To further validate these findings, we investigated the association between NK cell infiltrate/CAF marker expression and short survivorship through odds ratio analysis (conducted by Dr. Jiangfeng Ye, Institute of Molecular and Cell Biology, A*STAR).

We demonstrate that the percentage of cell infiltrate alone does not impact the risk of short survivorship (Figure 6.9A), highlighting the importance of cellular proximity in PDAC.

Interestingly, patients with high alpha SMA expression (myofibroblasts) were found to have greater odds of short survivorship, supporting previous work.^{129, 288} Similarly, patients expressing high levels of periostin expression were also seen to have increased risk of poor overall survival as previously suggested¹⁴⁰, however this does not reach significance (Figure 6.9B).

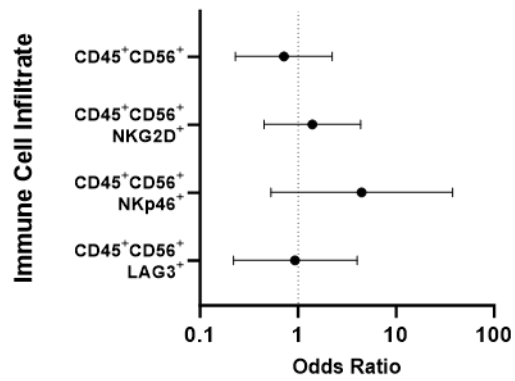
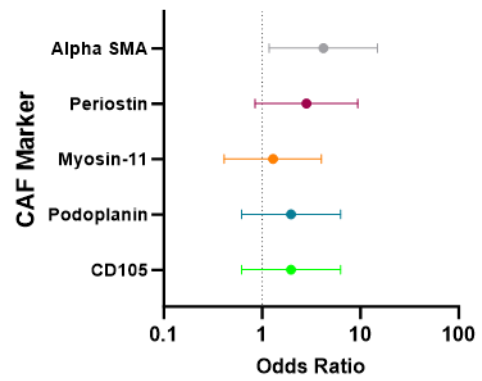
A**B**

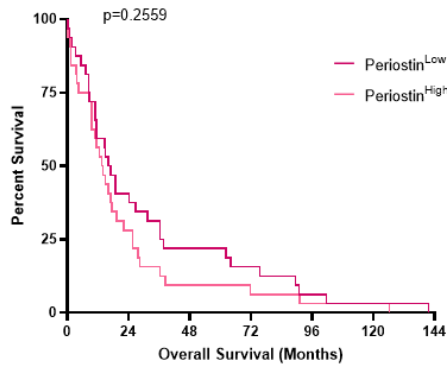
Figure 6.9: Risk of short survival associated with immune cell infiltrate and CAF marker expression.

A-B) Odds ratios and confidence intervals were calculated for the risk of short survival based on immune cell infiltrate (A) or CAF marker expression (B). Significant risk was identified if $p < 0.05$. Analysis carried out by Dr. Jiangfeng Ye.

6.2.3 CAF subtypes in PDAC

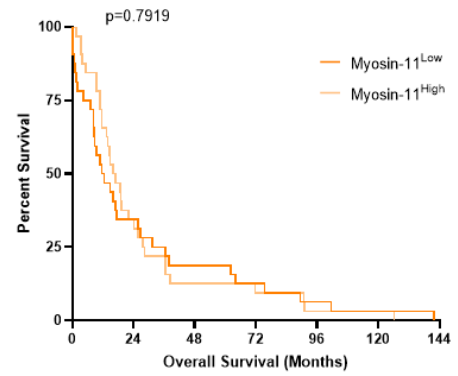
To further characterise the independent role of CAFs in PDAC we carried out Kaplan Meier survival analysis based on high or low expression of previously defined CAF markers^{140, 145} (Figure 6.10).

We note no significant difference in overall survival between high and low expression of any CAF marker, however we do observe a trend in periostin expression which suggests high expression is correlated with worse overall survival (Figure 6.10A). This is further supported by CAF subtype analysis (Figure 6.10E), although this again does not reach significance.

A

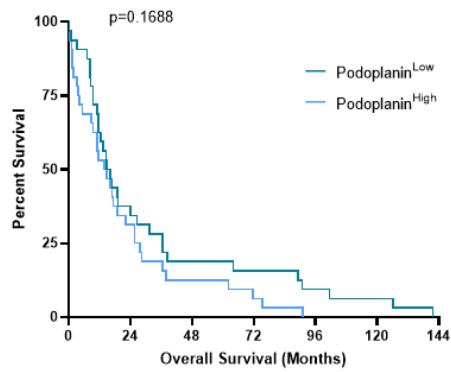
Number at Risk:

Periostin ^{Low}	32	13	7	5	2	1	0
Periostin ^{High}	32	9	3	2	1	1	0

B

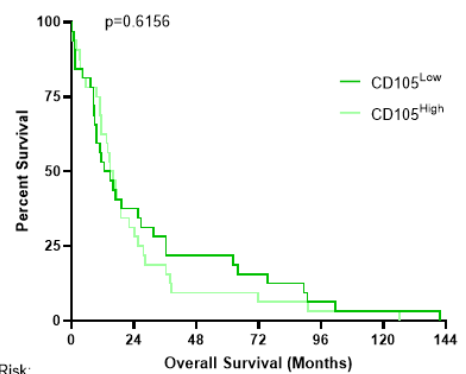
Number at risk:

Myosin ^{Low}	32	11	6	4	2	1	0
Myosin ^{High}	32	11	4	3	1	1	0

C

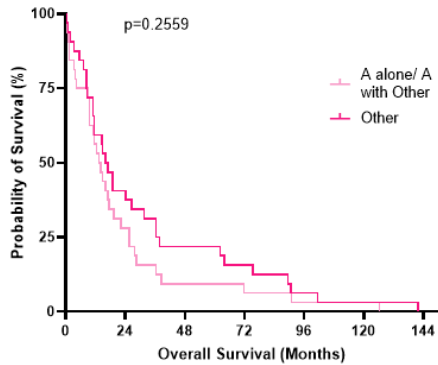
Number at Risk:

Podoplanin ^{Low}	32	12	6	5	3	2	0
Podoplanin ^{High}	32	10	4	3	0	0	0

D

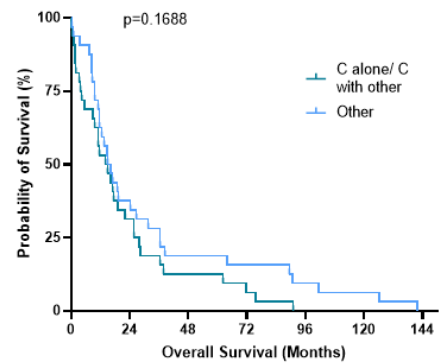
Number at Risk:

CD105 ^{Low}	32	12	8	5	2	1	0
CD105 ^{High}	32	10	3	2	1	1	0

E

Number at Risk:

A Alone/A with Other	32	9	3	2	1	1	0
Other	32	13	7	5	2	1	0

F

Number at Risk:

C Alone / C with other	32	10	4	2	0	0	0
Other	32	12	6	5	3	2	0

Figure 6.10: Survival analysis based on CAF marker expression.

A-F) Kaplan Meier curves depicting patient overall survival dichotomised by high or low expression of Periostin (A), Myosin-11 (B), Podoplanin (C), CD105 (D), or CAF subtype (E, F). Statistical significance was identified using the Log-Rank test.

6.2.4 Correlation between NK cell infiltrate and CAFs in Short/ Long survivors

We next wanted to assess the potential impact of CAF subtype/marker expression on NK cell infiltration in short and long survivors. To assess this interaction we employed correlation analysis.

We demonstrate a significant negative correlation between Alpha SMA⁺ CAFs and CD45⁺CD56⁺/CD45⁺CD56⁺NKG2D⁺ NK cell infiltrate in short survivors (Figure 6.11A). Moreover, short survivors also demonstrate positive correlation between podoplanin/CD105 and LAG3⁺ NK cells (Figure 6.11B). Taken together these findings support the notion that close proximity to CAF cells may result in NK education and decreased functional efficacy.

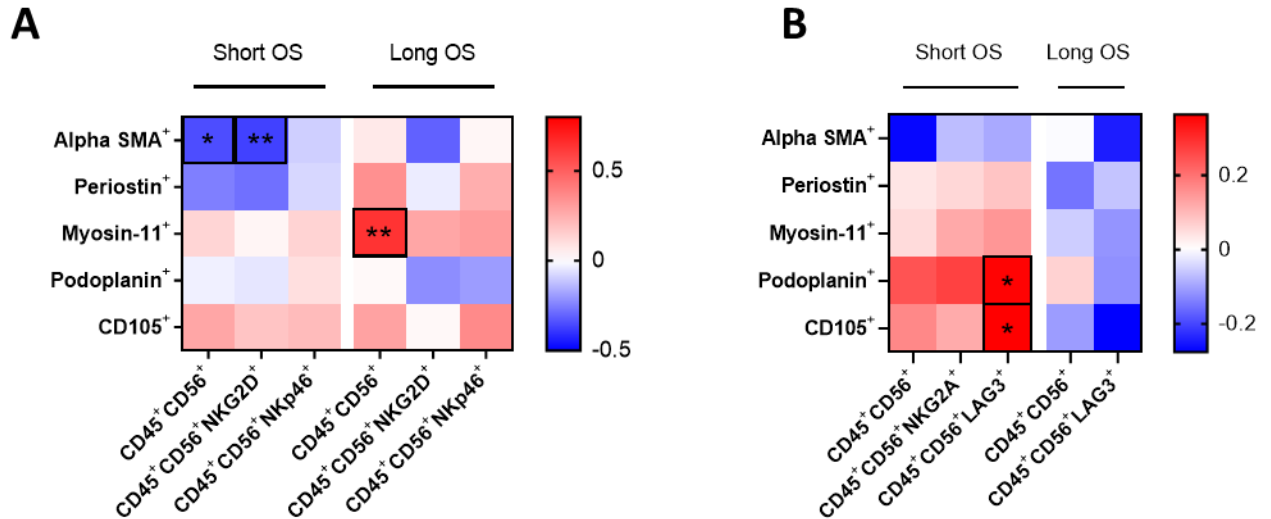


Figure 6.11: Correlation matrices between cancer associated fibroblast (CAF) markers and NK cells in PDAC.

A-B) Correlation between cancer associated fibroblast (CAF) markers and NK cells expressing activating (A) or inhibitory (B) receptors in short (n=48)/long (n=16) survivors. Spearman's Rank correlation analysis was run, and R values used to plot heatmaps. Boxes highlighted in bold denote statistical significance. *p<0.05; **p<0.01.

Chapter 7 – Discussion

My results demonstrate reciprocal changes in NK cells and PSC/CAF upon co-culture which is dependent on PSC activation to CAF. Thus, the co-localisation of specific CAF sub-types with NK cells expressing activating/inhibitory receptors in human pancreatic cancer tissues may have functional significance. I draw on contemporaneous investigations from other fields to compare and contrast my findings, assess limitations of my work and discover future directions of investigations.

7.1 PSC activation confers protection from NK cell lysis whilst qPSC education impairs NK cytotoxicity

Retinoic acid (RA) signalling, directly and indirectly (via stromal cells), modulates NK functional efficacy through both activating and inhibitory roles.²⁸⁹ Using an *in vitro* model of murine hepatic stellate cells (HSC) Radaeva *et al.* demonstrated increased susceptibility of early activated HSC (4- and 7- days culture) to NK induced lysis. This was found to be a result of HSC upregulation of retinoic acid early inducible gene 1 (RAE-1).²⁹⁰ Analogous to UL16 binding proteins (ULBP) identified in humans, RAE-1 is a ligand for the activating receptor NKG2D, which upon activation, stimulates NK induced cellular lysis.²⁹¹ Whilst expressed at low levels in quiescent HSCs, RAE-1 expression changed significantly during HSC activation, with early activated cells expressing high levels of the receptor, and fully activated HSC (21-days culture) demonstrating receptor loss. Importantly, loss of RAE-1 expression in fully activated HSC was shown to confer protection from NK cell lysis.²⁹⁰ Similarly, our results suggest that PSC activation may confer protection against NK cell lysis. Importantly, retinoic acid promotes the expression of RA-inducible genes, a process which has been shown to be regulated by CRABP2.²⁹² Expression of CRABP2 was shown to be lower in activated pancreatic stellate cells (PDAC), when compared with quiescent cells (normal pancreas)²⁹³, correlating with NK-ligand expression. In a study of renal cell carcinoma, *CRABP2* expression was demonstrated to be

prognostic. Specifically, high expression of *CRABP2* was found to correlate with unfavourable survival. Within this risk group, numbers of activated NK cells (as well as Treg, T helper and M0 macrophages) were significantly upregulated. Analysis of immune modulators and exhaustion markers demonstrated significant upregulation of these factors within the unfavourable risk group suggesting an exhausted and immunosuppressive phenotype.²⁹⁴ Thus, *CRABP2* may also play a role in regulating the immune landscape in cancer, although the direct interaction between *CRABP2* and NK cells remains to be elucidated.

Similarly, Fu *et al.* note that liver resident Kuffer cells were able to regulate NK cell activity via NKG2D/RAE-1 signalling in murine models of Primary Biliary Cholangitis.²⁹⁵ NK activation via this pathway was shown to result in increased IFN- γ secretion (which was suggested to target biliary epithelial cells) and target cell killing, resulting in biliary inflammation, a hallmark of this disease.²⁹⁵

In patient derived hepatocellular carcinoma cells, upregulation of the NKG2D ligands MICA and MICB was seen in response to ATRA treatment. This upregulation resulted in increased engagement of NK cells and subsequent IFN- γ release as well as target cell lysis, demonstrating stroma-independent engagement of NK cells against cancer cells.²⁹⁶

Conversely, upon activation, pancreatic stellate cells have been found to secrete a compendium of cytokines and chemokines including, IL-1 β , IL-6 and TNF- α .²⁹⁷ Of particular note is their secretion of IL-6. Huang *et al.* identified impaired NK function in pancreatic cancer as a result of TGF- β induced IL-6 production by cancer associated fibroblasts.²⁹⁸ Similarly, patient derived NK cell function was found to be reduced in response to TGF- β release from activated HSCs.²⁹⁹ Thus, activated PSC secretion of immunosuppressive cytokines may contribute to the protection afforded to activated PSCs observed within our study.

Others have identified a significant direct effect of all-trans retinoic acid on NK cell function. A metabolite of vitamin A, ATRA is an immunomodulatory hormone. Li *et al.* determined a significant dose response between ATRA and NK cell function. Specifically, ATRA was found to inhibit IFN- γ production and the gene expression of granzyme b and the activating receptor NKp46. Additionally, ATRA suppressed NF- κ B activity as well as preventing degradation of I κ B α . This demonstrates a wide range of functional suppression in response to retinoic acid. Interesting, despite its effect on function, ATRA was not found to impair NK proliferation.³⁰⁰ This is consistent with the work of Gunayadin *et al.* In a study of acne vulgaris patients, a condition in which NK cell infiltrate has been correlated with disease severity, treatment with the retinoic acid derived Isotretinoin was not found to reduce the percentage nor absolute number of NK cells within patients.³⁰¹ Additional work demonstrated that ATRA increased the expression of the microRNA miR-23a, a negative regulator of cathepsin C, which has been shown to have a key role in the post-translational modification of granzyme transcripts. Consequently, NK cells with increased miR-23a expression were shown to have reduced functional efficacy. It was suggested that the increased expression of miRNAs may be a result of impaired NF- κ B signalling.³⁰² These findings are consistent with our work which demonstrates a significant reduction in NK cell cytotoxicity in response to culture with quiescent but not activated PSC. Dunham *et al.* demonstrated that HSC were able to metabolise retinol into all-trans retinoic acid upon early activation. It was further suggested that HSC release of the newly converted ATRA induced Treg differentiation in CD4⁺ T cells.³⁰³ Thus, as qPSCs are key stores of retinol⁸⁸, we hypothesise that the NK cellular dysfunction observed in this work may be a result of qPSC paracrine release of retinoic acid.^{292 304} Further work is needed to validate this hypothesis, as the underlying mechanisms of retinol paracrine signalling remain unclear.³⁰⁵ Our findings contrast the work of Huang *et al.* who determined

that education by activated PSC, but not normal PSC reduced expression of the NK cell functional markers, CD107a/b, IFN- γ and granzyme B. We suggest that the difference observed may be a result of methodology. Huang *et al.* measured total expression of functional markers through intracellular flow cytometric analysis, while we employed functional assays. In order to measure degranulation, CD107a/b expression must be detected at the cell surface.²⁵⁵

7.1.1 3D *in vitro* models of NK cell function

The development of 3D culture models has furthered our understanding of the intricate spatial relationship between various cell types. Employing a tumour immune microenvironment (TIME)-on-a-chip model of PDAC, Kim *et al.* report a significant reduction in NK-mediated cancer-cell specific cytotoxicity. The observed NK cell dysfunction was suggested to be in response to secreted cytokines from activated PSCs.³⁰⁶ Importantly, this assay maintained PSCs within a separate chamber from tumoural and NK cells, but allowed media exchange between compartments. Conversely, once seeded, NK cells were free to migrate, infiltrate and interact with tumoural organoids for 48h. Increased cytokine expression in the supernatant of tumour/NK cell cultures further suggested that interaction with tumoural cells may also contribute to NK cell dysfunction. This model allows the exploration of specific mechanisms underlying NK dysfunction and could be applied to further investigate the impact of ATRA-induced PSC quiescence on NK cell function.³⁰⁶

With increasing need to understand the mechanisms of immunosuppression, several 3D *in vitro* models have been developed for the study of NK cells.³⁰⁷ Early models included spinner cultures in which tumour cells were cultured in spinner flasks at constant stirring rates, encouraging cellular aggregation and preventing cell adhesion to culture flasks.³⁰⁷ These

models were then used to assess immune infiltration and *in situ* tumour cytotoxicity.³⁰⁸ Despite the cost-effective and scalable nature of this model, its use has greatly reduced due to several key limitations including the reliance of spheroid formation on cellular collision and the variable size of spheres created within the method.³⁰⁷

Liquid overlay techniques utilise plate coating to prevent the adhesion of cells to culture plastic and to stimulate the formation of spheroid models. Typically, plate coating with agarose or poly-HEMA has been used to generate these spheroid models.³⁰⁷ Ivascu *et al.* demonstrated the production of spheroids within a 24h period following cell seeding and centrifugation. Furthermore, they show that addition of basement membrane extract (Matrigel) aided the development of compact spheroids of homogenous size within 96-well plates.³⁰⁹ Similarly, Giannattasio *et al.* report the development of solid state spheroids 48h after cell seeding when using an agarose base. Interestingly, basement membrane extract was not added to these cultures demonstrating the ability of some tumour and immune cells to form spheroid models without additional matrix proteins.³¹⁰

The hanging drop model has become an increasingly popular method to create spheroid cultures. Initial models based on the development of embryoid bodies³¹¹ seeded multiple cell types within 15-25µL of desired media before plate inversion. These 'drops' were then cultured for several days in which cells aggregated in the base of the droplet, facilitating spheroid formation.³¹² More recently, hanging drop cultures have been supplemented with methylcellulose, which offers a semi-solid matrix to better mimic *in vivo* extracellular conditions.³¹³ Using this method, Lanuza *et al.* demonstrated the ability of allogenic activated NK cells to kill colorectal cancer (CRC) cells within the 3D setting. Furthermore, it was shown that cell death was not observed at low density NK infiltration, whilst high density infiltration

of activated NK cells efficiently killed CRC cells.³¹⁴ Importantly, this method has also been used to study PSC invasion. Murray *et al.* demonstrated that PKN2 knockdown reduced PSC led cancer invasion.³¹⁵ Whilst Coetzee *et al.* identified that FGFR1 was necessary for stellate cell led cancer invasion.¹⁰⁵ Thus, this model may prove beneficial to the 3D study of NK-PSC-cancer cell interactions *in vitro*.

Finally, scaffold-based spheroid cultures attempt to mimic the extracellular-like matrix condition observed in cancer. Typically hydrogel based, including Matrigel and collagen type-I hydrogels, scaffold based spheroid cultures are biologically relevant to study NK transmigration and infiltration.³⁰⁷ Marella *et al.* employed an alginate hydrogel to study the impact of IFN- γ on anti-tumour activity of NK cells in neuroblastoma. Through the use of this model they found an increase in tumoural NK ligands including HLA-1 molecules and PD-L checkpoint ligands which conferred protection from NK cell attack.³¹⁶ Additionally, employing a collagen based spheroid model, Ayuso *et al.* demonstrated NK92 migration towards 3D breast cancer spheroids and identified tumour infiltration within several hours.³¹⁷ Interestingly, Ayuso *et al.* also demonstrate that infiltrated NK cells retain their cytotoxic capabilities suggesting that NK exhaustion is not an immediate process.³¹⁷

Future work investigating the interaction between NK and qPSC/aPSC would benefit from 3D validation of 2D proof of concept assays (performed by me) in the presence of ubiquitous extra-cellular matrix proteins, which are abundantly present in human PDAC tissues. This would facilitate further understanding of the spatial interactions and effect of ECM induced modulation in this bi-/tri- directional relationship.

7.2 NK cells modulate PSC phenotype

A diverse range of molecular mechanisms have been identified in the activation of pancreatic stellate cells including, cytokines and transcription factors, non-coding RNAs, hyperglycaemia and multiple signalling pathways (MAPK, Rho/ROCK, NF- κ B, AKT, JAK/STAT, Hedgehog).³¹⁸ TGF- β is a potent cytokine involved in fibrosis.³¹⁸ Secreted as the large latency complex, containing latency associated peptide (LAP) and latent TGF- β binding protein (LTBP), TGF- β is stored in the extracellular matrix and requires activation via cellular mechanisms. Specifically, LAP interacts with the integrin α v β 5 (amongst others), allowing it to attach to cells whilst being maintained within extracellular stores. Importantly, cells can exert tension on the latency protein via this integrin link causing conformational changes and the release of TGF- β .³¹⁹ Fibronectin has also been shown to release TGF- β through binding with the LTBP. Cellular elasticity, ECM stiffness and mechanical cues were also found to be crucial to the cellular tension applied to the latent TGF- β .³²⁰ Importantly, ATRA treatment was shown to downregulate cellular release of TGF- β through the modulation of myosin contractility and β 1 integrins.³²⁰ This prevented TGF- β acting in an autocrine fashion and potentiating PSC activation.

Active TGF- β binds to TGF- β receptor II which phosphorylates TGF- β receptor I. This activated receptor then phosphorylates Smad2 and Smad3 which in turn bind to Smad4 and translocate to the nucleus. Once inside the nucleus the Smad complex activates the transcription of target genes.³²¹ TGF- β signalling has been shown to stimulate alpha SMA production in a dose dependent manner and increase collagen synthesis, key markers of PSC activation.³²²

NF- κ B signalling has also been found to play a crucial role in fibrosis.³¹⁸ Tumour necrosis factor- α (TNF- α) has been shown to be an activator of the NF- κ B signalling pathway.

Specifically, TNF- α binds to its receptor TNFR1 or TNFR2. TNFR1 then binds to TRADD, initiating the formation of the signalling complex, complex I. The binding of TRADD is followed by the interaction of multiple downstream signalling molecules including TNFR associated factor 2 (or 5), cellular inhibitor of apoptosis protein 1 or 2, receptor interacting serine/threonine protein kinase 1 and the linear ubiquitin chain assembly complex. Activation and association of this pathway stimulates the activation of NF- κ B signalling, as well as MAPK activation. Similarly, TNFR2 binds to TRAF which then activates the downstream complex I signalling pathway, as well as NF- κ B, MAPK and AKT signalling.³²³ PSCs activated by the NF- κ B pathway have been shown to induce the production of the pro-inflammatory and pro-fibrotic factors CCL2, IL-6 and IL-8,^{324, 325} thus highlighting the role of NF- κ B in PSC driven fibrosis.³¹⁸

Hedgehog signalling plays a critical role in multiple biological processes. In pancreatic stellate cells, Hedgehog has been shown to regulate proliferation and invasion. Indian Hedgehog (Ihh) facilitates PSC migration through stimulating chemotaxis and chemical activation, as well as facilitating degradation of the basement membrane via MMP-1 to promote cellular movement.³¹⁸ Sonic Hedgehog (Shh) can activate quiescent PSCs to become activated, stimulate growth and facilitate their invasion.³²⁶ Importantly, several factors have been shown to stimulate Hedgehog activation. In zebrafish models, treatment with retinoic acid was found to stimulate ectopic Shh expression. Moreover, Chang *et al.* also demonstrated that the Shh promoter could be regulated by retinoic acid receptors in response to ATRA.³²⁷ Additionally, using an IFN- γ expressing mouse model to study cerebellar dysplasia, Wang *et al.* determined that mice expressing IFN- γ had significantly increased RNA levels of Shh, Gli-1 and the signalling product Shh precursor protein when compared to non-IFN- γ expressing mice.³²⁸ Non-canonical signalling of the hedgehog pathway via direct interaction with Gli family members has also been shown to be activated downstream of TGF- β , KRAS and Wnt/ β -

catenin signalling.³²⁹ Furthermore, Wang *et al.* also note non-canonical activation of Hedgehog via TNF- α and IL-1 β . TNF- α and IL-1 β were found to transcriptionally upregulate expression of Gli-1 via NF- κ B signalling. This upregulation was found to increase Gli-1 nuclear protein expression and facilitate invasion, migration, and drugs resistance within the context of PDAC.³³⁰

We suggest that NK release of cytokines such as TNF- α and IFN- γ in response to direct contact with PSCs may activate NF- κ B and/or non-canonical Hedgehog signalling resulting in a myofibroblastic shift. Steele *et al.* also suggest a myofibroblastic shift in PSCs following hedgehog activation. Analysis of scRNA-Seq revealed an enrichment of hedgehog target genes including *GLI1* in myofibroblasts when compared to iCAFs.³³¹ Moreover, KPC murine models further revealed significantly high GLI expression in alpha SMA⁺ cells when compared to alpha SMA⁻ cells.³³¹

CD105⁺ cells display a tumour permissive phenotype and express upregulation of the *Acta2* gene suggesting a myofibroblastic phenotype¹⁴⁵, consistent with the findings we present in this work. Additionally, CD105⁺ cells were shown to demonstrate an increase in TGF- β signalling mRNAs when compared to CD105⁻ cells (although only Smad3 was significantly upregulated) suggesting activation via the TGF- β pathway. Interestingly, CD105⁻ cells were shown to express higher levels of ezrin when compared to CD105⁺ cells, although the expression was non-uniform. This was evidenced to demonstrate CAF similarity to mesothelial cells.¹⁴⁵ Previous work has established a significant role for ezrin in the maintenance of cellular shape in rat derived fibroblasts. However, in transformed cells, ezrin was found to be significantly upregulated and hyperphosphorylated. Furthermore, increased ezrin protein concentration at the leading edge of fibroblasts suggested a role in cellular

motility and oncogenic transformation.³³² Our proteomic analysis demonstrated an increase in ezrin expression in aPSCs cultured with NK cells (vs qPSC + NK cells), suggesting that aPSC may express a more oncogenic phenotype when cultured with NK cells than do qPSC.

Podoplanin has been used as a pan-CAF marker, with its gene expression being associated with the general fibroblast phenotype.¹⁴⁵ Despite this classification however, podoplanin⁺ CAFs have been found to display significant prognostic impact in several cancer types. In a meta-analysis of lung cancer patients, podoplanin⁺ CAF infiltration significantly reduced overall survival, progression- and disease-free survival. Moreover, high densities of podoplanin⁺ CAFs correlated with pleural, vascular and lymphatic invasion and lymph node metastasis.³³³ Similarly, node negative, hormone receptor⁺/HER2⁻ breast cancer patients were found to demonstrate a similar correlation between podoplanin expression and worse disease-free and disease-specific survival. Although only expressed in 16% of patient samples, high podoplanin expression was associated with higher Ki67 labelling and greater stromal tumour infiltrating lymphocytes.³³⁴ In PDAC however, the prognostic impact of podoplanin remains unclear. Several studies have reported a correlation between podoplanin and worse prognosis. Hirayama *et al.* demonstrate patients with high podoplanin showed significantly worse disease-free and disease-specific survival.³³⁵ Similarly, Croft *et al.* note high expression of podoplanin at the transcriptional level was associated with poor clinical outcome.³³⁶ Conversely, work by Neuzillet *et al.* demonstrated podoplanin expression to be associated with better clinical outcome. Moreover, of the four CAF subtypes identified, CAFs expressing podoplanin were found to correlate with the best overall prognosis.¹⁴⁰

Interestingly, Hirayama *et al.* note that podoplanin⁺ cells identified within their study expressed alpha SMA suggesting activated PSC origin.³³⁵ We demonstrate a significant

increase in podoplanin expression in aPSCs, but not qPSCs in response to culture with NK cells. Moreover, podoplanin has been demonstrated to further enhance alpha SMA expression and promote activation of PSCs which may account for differences observed between activated and quiescent PSCs.³³⁷ Podoplanin expression has further been demonstrated at the invasive front of cervical squamous cell carcinoma, and murine models of cervical cancer. Gene expression profiling in association with laser capture microscopy revealed an upregulation of interferon response genes in podoplanin positive cells. Furthermore, the expression of podoplanin was found to be stimulated by IFN- γ , TNF- α and TGF- β .³³⁸ Thus, we suggest that NK secretion of IFN- γ /TNF- α in response to cell-cell interaction may account for the upregulation in podoplanin expression observed in PSC/CAF in my experiments.^{339, 340}

7.3 PSCs reciprocally modulate NK phenotype and functional markers

Much work has investigated the role of NK cell receptors in cellular efficacy and response to treatment. NKG2D is an important activating receptor on both NK and T cells and has been shown to be crucial to the formation of the immunological synapse between effector and malignant cells.³⁴¹ Moreover, its expression has been demonstrated to correlate with improved disease free and overall survival in pancreatic cancer.^{342, 343} Conversely, the inhibitory receptors NKG2A and TIM3 have both been shown to play a significant role in tumour escape from immune surveillance.^{344, 345} In addition, NKG2A has been suggested as a marker of NK cell exhaustion.¹⁸³ Thus, NK receptors as well as functional protein expression may play a key role in describing the efficacy or dysfunction of NK cells in malignancy.

Importantly, modulation of NK cell receptor expression has been demonstrated in response to tumoural cells. In colorectal cancer, tumour infiltrating NK cells were shown to have significantly reduced surface expression of NKG2D, NKp30 and NKp46 when compared to

peripheral blood NK cells, suggesting an altered phenotype within this population. It was further determined that CRC tumour cells were responsible for educating the NK cells and for the altered phenotype observed.³⁴⁶ Additionally, in hepatocellular carcinoma, TIM-3 expression on NK cells was found to be significantly greater within tumoural tissue when compared to paratumoural tissues, suggesting that tumoural cells/TME may play a role in NK receptor modulation.³⁴⁷ Consistently, in murine and *in vitro* models of lung cancer, NKG2A expression was found to be significantly increased within tumoural tissue when compared to the control. Furthermore, the expression of NKG2A was greatest in the highly-metastatic model of lung cancer, suggesting that this inhibitory receptor may play a role in metastasis.³⁴⁸ This was further suggested by Liu *et al.* Malignant cells were found to upregulate HLA-E, the ligand for NKG2A, on circulating PDAC tumour cells in order to evade immune detection. Distinct micro-environmental cues may therefore be responsible for the crucial and dynamic relationship involved in NK-target interactions in different disease conditions.³⁴⁴

We demonstrate a significant increase in the inhibitory/exhaustion markers NKG2A and TIM3 in co-culture with qPSC. This finding is consistent with the decreased cell lysis observed against BxPC3 cell lines, and to a lesser extent, MiaPaca2 and Capan2 cells. Similar NK dysfunction in response to increased TIM-3 and NKG2A expression has been demonstrated in oesophageal³⁴⁹ and hepatocellular carcinoma.¹⁸³ Thus we suggest that PSCs may play a regulatory role in NK cell function through the upregulation of inhibitory receptor expression. Importantly, the changes identified in TIM3 were displayed in direct contact, Transwell™ and conditioned media experiments, suggesting that TIM3 modulation by PSCs may be achieved via secreted factors. We also highlight an increase in the percentage of NKG2D⁺ cells at the population, but not individual cell level. Despite its known role in NK cell functionality, recent work has demonstrated an inverse relationship between NKG2D expression on tumour

infiltrating NK cells and degranulation. It was suggested that chronic stimulation of NK cells by tumour cell surface expression of MICA may be responsible for the dysfunction caused.³⁵⁰ Thus, further work is needed to fully elucidate the precise mechanism and role of increased NKG2D expression in response to co-culture with PSCs.

7.4 Co-culture secreted factors

Regarded as a cornerstone of cancer progression, the JAK/STAT pathway has been shown to facilitate tumour development as both an intrinsic driver of cancer growth and metastasis, as well as through modulation of immunosurveillance.³⁵¹ Regulation of the JAK/STAT signalling pathway by IFN- γ has been well documented.³⁵² While earlier mathematical models suggested antifibrotic effects of IFN- γ /STAT1 signalling on PSCs,³⁵³ recent studies have suggested that JAK/STAT engagement leads to PSC proliferation, activation and fibrosis.³¹⁸ Additionally, in regards to NK cell functional efficacy, IFN- γ activation of JAK1, JAK2 and STAT1 was found to upregulate the expression of PD-L1, reducing NK lysis of tumoural cells, mediating escape from immunosurveillance.³⁵⁴ We demonstrated upregulation of IFN- γ and related chemokines in response to direct (but not TranswellTM) co-culture, suggesting that the JAK/STAT signalling pathway may be involved in the phenotypic changes observed.

Fibroblast growth factor (FGF) signalling is a critical pathway involved in tumour-stroma crosstalk.³⁵⁵ In health, FGF signalling plays a crucial role in the development and homeostasis of multiple cell types. However, aberrant expression/control of this pathway has been demonstrated to play a key role in multiple malignancies including glioblastoma, breast, bladder, prostate and pancreatic cancers.³⁵⁶ Thus, targeting of the FGF signalling pathway is becoming an increasingly attractive therapeutic target.³⁵⁵ Acting via autocrine and paracrine routes, FGF2 release from tumour, stromal and endothelial cells has been found to contribute

to cancer progression.³⁵⁷ Coleman *et al.* demonstrated that nuclear translocation of FGF receptor 1 (FGFR1) and FGF2 was necessary for maintaining stellate cell proliferation. Furthermore, blockade of FGFR1, and subsequently FGF2, nuclear translocation prevented PSC invasion in organotypic models.¹⁰³ This suggests a crucial role for PSC induced FGF2 signalling in the progression of pancreatic cancer. Interestingly, FGF2 has demonstrated both pro- and anti-fibrotic effects in HSC. FGFR1 inhibition was shown to suppress HSC growth by regulating cell cycle proteins, suggesting a pro-fibrotic role for FGF2.³⁵⁸ Conversely, murine FGF2 knockout models of hepatic injury demonstrated that upon injury, the level of matrix-collagen derived from HSCs was significantly reduced despite a normal increase in alpha SMA (suggesting HSC migration). These results suggest that FGF2 may have an anti-fibrotic effect in liver injury.³⁵⁹ Interestingly, in hepatocellular carcinoma, FGF2 has been shown to upregulate expression of the NKG2D ligands MICA/B, increasing malignant cell susceptibility to NK- induced lysis.³⁶⁰ Furthermore, Lewis *et al.* demonstrated that FGF2 was a potent stimulator of IFN- γ release by NK cells.³⁶¹ We note dramatic upregulation of FGF2 in response to direct, but not TranswellTM co-culture, suggesting that direct cell-cell interaction may induce activation of this signalling pathway leading to distinct phenotypic changes in both PSC and NK cells.

In summary, our results demonstrate a reciprocal interaction between NK cells and qPSC/aPSCs, resulting in phenotypic changes in both cell types and functional alterations within NK cells. These changes may, in turn, affect NK cell-mediated cancer cell cytotoxicity.

7.5 qPSC/aPSC and NK cells demonstrate a significant bi-directional relationship at the proteomic level

With the advent of multi-omics data, significant progress has been made in understanding cellular changes at the proteomic and transcriptional level. The use of mass-spectrometry

within the proteomic field has allowed the possibility to characterise and quantify the protein signature of desired samples, as well as the ability to investigate complex interactions within a biological sample.^{362, 363} Moreover, through utilising a global proteomic approach, protein detection is not limited by hypothesis, allowing visualisation of the total proteome and direct measurement of cellular protein content.^{362, 363} Whilst several limitations exist within the field of proteomics, including incomplete cellular lysis, sample contamination and membrane protein solubility, the well-established methods for sample preparation and a diverse array of databases to characterise peptide origins post-analysis render proteomics a fast and sensitive technology which holds great potential for both fundamental and clinical research.^{363, 364}

Employing bottom-up global proteomic analysis, we demonstrate significant changes in the key functional pathways including biosynthesis, protein folding, sorting and vesicular transport in NK cells, and lipid and steroid metabolism, glycolysis and spliceosome function in PSCs as a result of co-culture. Similarly, Poznanski *et al.* demonstrated significant proteomic changes between peripheral blood NK cells (low cytotoxicity) and expanded NK cells (highly cytotoxic) following culture within the ascites-TME in ovarian cancer models. Of note, significant changes in biosynthesis pathways were observed within this model. Importantly, it was suggested that the tumour microenvironment may play a crucial role in regulating cellular proteome changes³⁶⁵, validating the changes we observed in NK and PSCs following their interaction.

We further investigated this interaction through the analysis of publicly available RNA-seq datasets. We identified similar downregulation/upregulation in corresponding genes within PSCs, including phosphoserine aminotransferase 1 (*PSAT1*, *SERC*) and heterogeneous nuclear

ribonucleoprotein K (*HNRNPK*, HNRPK) which was shown to have a prognostic impact.³⁶⁶ Specifically, patients with high *HNRNPK* expression were found to have significantly reduced overall survival than did patients with low expression. This finding was consistent with HNRNPK's observed role in the hnRNPK/miR-223/FBXW7 feedback cascade which was found to facilitate pancreatic cancer cell growth and invasion.³⁶⁷ These examples serve to emphasise that post-translational modification may impact functional activity in these interactions, rather than at transcription or translational levels.³⁶⁸ Additionally, activation of the hippo signalling pathway via the hnRNPK-YAP1 axis has been shown to promote pancreatic cancer progression.³⁶⁹ Ren *et al.* demonstrated that HNRNPK translocated to the nucleus of PDAC cells following interaction with SGLT2. Within the nucleus, HNRNPK induced YAP1 expression by acting as a transcription factor. This increased expression of YAP resulted in upregulation of *CTGF* and *CYR61* (via hippo signalling), stimulating cancer cell proliferation and invasion.³⁶⁹ These results suggest that the protumoural roles of HNRNPK are not limited to tumour cells, but may also be induced in stromal cells by NK-PSC interaction.

Chimeric antigen receptor (CAR)-NK cells are receiving increasing interest as therapeutic tools in the treatment of multiple malignancies.³⁷⁰ Li *et al.* report the development of Robo-1-specific CAR-NK cells. An initial case report (PDAC with liver metastasis) noted that the therapy resulted in no significant adverse effects. The patient also demonstrated lesion control within five months, with overall survival of 8 months.³⁷¹ A further Phase I/II study (NCT03941457) is currently underway to observe the occurrence of adverse events, although the status is unknown.³⁷² Importantly, we identified the expression of Robo-1 in both quiescent and activated PSCs, thus CAR-NK therapies may be key to targeting not only tumoural cells, but also PSCs via cellular immunotherapies. Similarly, two early phase I trials (NCT05194709 and NCT05137275) are recruiting for the use of 5T4 CAR-NK cells in advanced

solid cancers and locally advanced and/or metastatic solid tumours (NSCLC, breast, CRC, mesothelioma and other tumours with high expression of 5T4).^{373, 374} 5T4 is a trophoblast glycoprotein which is expressed in a wide variety of cancers. In murine models, overexpression of 5T4 has been associated with downregulation of E-cadherin, a key protein in epithelial to mesenchymal transition. Additionally, Wnt- β catenin signalling was also demonstrated to be modulated by 5T4 through its binding to the co-receptor LRP6, preventing internalisation. This in turn repressed activation of the canonical signalling pathway. Importantly however, 5T4 has also been shown to stimulate non-canonical Wnt pathway activation which has been linked to cellular motility.³⁷⁵ Our proteomic analysis identified the presence of 5T4 within both qPSC and aPSCs following co-culture with NK cells, further highlighting the potential of these novel therapeutics in the targeting of both tumour and stromal cells in solid malignancies.

Previously, we demonstrated NK ability to target and lyse qPSC and aPSC in a contact dependent manner (Figure 4.6A, B; Figure 4.7A). Similarly, Van Audenaerde *et al.* demonstrated enhanced NK cytolytic capacity towards PSCs following IL-15 stimulation.²³² In a first-in human trial, Shan *et al.* utilised IL-15/4-1BBL stimulated donor derived NK cells for the treatment of ultra-high-risk solid tumours (paediatric sarcomas). Activated NK cells were delivered to patients following nonmyeloablative, MHC-matched, T-cell depleted peripheral blood stem cell transplantation. Unfortunately, five out of the nine enrolled patients demonstrated acute graft versus host disease (GVHD) following activated NK cell transplant. Grade 4 GVHD was observed in three patients. It was concluded that NK cell transplant may stimulate subclinical T-cell alloreactivity, resulting in the toxicities observed.³⁷⁶ Thus, whilst allogeneic transfer of stimulated NK cells could be employed to target stellate cells in PDAC,

care must be taken to fully understand the potential reactivity between NK cells and other stromal/immune cells in order to minimise adverse events.

Multiple trials of NK cell-based therapies are currently ongoing both as monotherapy and in combination with additional biological agents and/or drug therapies (Table 7.1).

From the breadth of malignancies targetable, the scope and potential of NK cell therapies is beginning to come to light. This emphasises the increasing importance of understanding the biological interactions within disease in order to fully exploit therapeutic potential.

NCT Number	Study Title	Study Status	Conditions	Biological Interventions	Drug Interventions
NCT00640796	Pilot Study of Expanded, Donor Natural Killer Cell Infusions for Non-B Lineage Hematologic Malignancies and Solid Tumors	Completed	Leukaemia, Myeloid, Acute, Leukaemia, Lymphocytic, Acute, T-Cell, Juvenile Myelomonocytic Leukaemia Lymphoblastic, T-cell Lymphoblastic Lymphoma, Myelodysplastic Syndrome	Haploidentical donor derived natural killer cell infusion using CliniMACS	Chemotherapy
NCT00720785	Natural Killer Cells and Bortezomib to Treat Cancer	Completed	Chronic Myeloid Leukemia (CML), Pancreatic Ca, Colon/Rectal Ca, Multiple Myeloma, Carcinoma, Non-Small -Cell Lung	NK cells	Bortezomib
NCT00823524	Donor Natural Killer Cells After Donor Stem Cell Transplant in Treating Patients With Advanced Cancer	Completed	Brain and Central Nervous System Tumors, Leukaemia, Lymphoma, Lymphoproliferative Disorder, Multiple Myeloma and Plasma Cell Neoplasm, Myelodysplastic/Myeloproliferative Neoplasms, Adult Solid Tumors	Donor natural killer cell infusion	
NCT01212341	Allogeneic Natural Killer (NK) Cell Therapy in Patients With Lymphoma or Solid Tumor	Completed	Malignant Lymphomas, Solid Tumors	Allogeneic NK cells	
NCT01287104	A Phase I Study of NK Cell Infusion Following Allogeneic Peripheral Blood Stem Cell Transplantation From Related or Matched Unrelated Donors in Paediatric Patients With Solid Tumors and Leukemias	Completed	Leukaemia, Lymphoma	Natural Killer (NK) Cell Infusion; Stem Cell Infusion	
NCT01337544	Haploidentical Stem Cell Transplantation and IL-15 NK Cell Infusion for Paediatric Solid Tumours	Terminated	Childhood Solid Tumor	Haploidentical IL-15 Stimulated NK Cells	
NCT01799083	Lower Dose Decitabine Based Therapy in Patients With and/or Chemotherapy Resistant Solid Tumors or B Cell Lymphomas	Unknown	Solid Tumors, B Cell Lymphoma	Decitabine; cytokine-induced killer cell	
NCT01807468	Haploidentical Stem Cell Transplantation and NK Cell Therapy in Patients With High-risk Solid Tumors	Unknown	Neuroblastoma, Ewing Sarcoma, Rhabdomyosarcoma, Osteosarcoma, Soft Tissue Sarcoma	Haploidentical stem cell transplantation and NK cell therapy	
NCT01875601	NK White Blood Cells and Interleukin in Children and Young Adults With Advanced Solid Tumors	Completed	Solid Tumors, Brain Tumors, Sarcoma, Paediatric Cancers, Neuroblastoma	Recombinant human interleukin-15 (rhIL-15); NK Cell Infusion	
NCT01914263	Safety Study of Cord Blood-derived Cytokine-induced Killer Cells in Patients With Solid Tumor After Radical Resection	Unknown	Hepatocellular Carcinoma, Renal Cell Carcinoma, Lung Cancer	Cytokine induced killer cell	
NCT02100891	Phase 2 STR Trial: Haploidentical Transplant and Donor Natural Killer Cells for Solid Tumors	Active not recruiting	Ewing Sarcoma, Neuroblastoma, Rhabdomyosarcoma, Osteosarcoma, CNS Tumors	Allogeneic HCT; Donor NK Cell Infusion	
NCT02130869	A Pilot Study of Immunotherapy Including Haploidentical NK Cell Infusion Following CD133+ Positively-Selected Autologous Hematopoietic Stem Cells in Children With High-Risk Solid Tumors or Lymphomas	Completed	Neuroblastoma, Lymphoma, High-risk Tumor	CD133+ selected autologous stem cell infusion; IL-2; hu14.18K322A; GM-CSF; G-CSF; Haploidentical natural killer cell infusion using CliniMACS	Busulfan; Melphalan; Bendamustine; Etoposide; Cytarabine; Carboplatin; Etoposide phosphate
NCT02839954	CAR-pNK Cell Immunotherapy in MUC1 Positive Relapsed or Refractory Solid Tumor	Unknown	Hepatocellular Carcinoma, Non-small Cell Lung Cancer, Pancreatic Carcinoma, Triple-Negative Invasive Breast Carcinoma, Malignant Glioma of Brain, Colorectal Carcinoma, Gastric Carcinoma	Anti-MUC1 CAR-pNK cells	
NCT03027128	QUILT-3.028: Study of haNK™ for Infusion in Subjects With Metastatic or Locally Advanced Solid Tumors	Completed	Solid Tumor	haNK™ for Infusion	
NCT03047525	Study of DC-CTL Combined With CIK for Advanced Solid Tumor	Unknown	Colorectal Cancer, Renal Cell Carcinoma, Nasopharyngeal Carcinoma, Lung Cancer	Cytokine-induced Killer Cells	
NCT03194959	FATE-NK100 as Monotherapy and in Combination With Monoclonal Antibody in Subjects With Advanced Solid Tumors	Completed	Advanced Solid Tumours (Including Pancreatic Cancer)	FATE-NK100	Cetuximab; Trastuzumab
NCT03415100	Pilot Study of NKG2D-Ligand Targeted CAR-NK Cells in Patients With Metastatic Solid Tumours	Unknown	Solid Tumours	CAR-NK cells targeting NKG2D ligands	
NCT03420963	Donor Natural Killer Cells, Cyclophosphamide, and Etoposide in Treating Children and Young Adults With Relapsed or Solid Tumors	Recruiting	Head and Neck, Melanoma, Solid Tumours, Reproductive Tumours	Cord Blood-derived Expanded Allogeneic Natural Killer Cells	Cyclophosphamide; Etoposide
NCT03634501	Clinical Study on Anti-tumor Effect Induced by Activated Primary Natural Killer (NK) Cells	Unknown	Lung Cancer, Breast Cancer, Colon Cancer, Pancreatic Cancer, Ovarian Cancer	Activated NK	
NCT03815084	A Study of PD1 Combined With DC-NK Cell in the Treatment of Solid Tumors	Unknown	Solid Tumor	PD-1 and DC-NK cells	
NCT03931720	Clinical Research of ROBO1 Specific BICAR-NK/T Cells on Patients With Malignant Tumor	Unknown	Malignant Tumor	BICAR-NK/T cells (ROBO1 CAR-NK/T cells)	
NCT03940820	Clinical Research of ROBO1 Specific CAR-NK Cells on Patients With Solid Tumors	Unknown	Solid Tumor	ROBO1 CAR-NK cells	
NCT03941262	Safety of SNK01 in Subjects With Pathologically Confirmed Metastatic and/or Unresectable Cancer to Conventional Therapy	Active not recruiting	Cancer, Metastatic Cancer, Cancer, Unresectable Carcinoma, Solid Tumor, Adult, Advanced Cancer, Advanced Solid Tumor	SNK01	Avelumab; Pembrolizumab
NCT03941457	Clinical Research of ROBO1 Specific BICAR-NK Cells on Patients With Pancreatic Cancer	Unknown	Pancreatic Cancer	BICAR-NK cells (ROBO1 CAR-NK cells)	
NCT04106167	Long-term, Non-interventional, Observational Study Following Treatment With Fate Therapeutics FT500 Cellular Immunotherapy	Terminated	Advanced Solid Tumor s (Including Pancreatic cancer)	Allogeneic natural killer (NK) cell	
NCT04307142	Haplo / Allogeneic NKG2DL-targeting Chimeric Antigen Receptor-grafted γδ T Cells for Relapsed or Solid Tumour	Unknown	Colorectal Cancer, Triple Negative Breast Cancer, Sarcoma, Nasopharyngeal Carcinoma, Prostate Cancer, Gastric Cancer	Adoptive Cell Transfer of NKG2DL-targeting Chimeric Antigen Receptor-grafted Gamma Delta T cell	
NCT04214717	Study of DC-CIK Combined With Chemotherapy for Advanced Solid Tumor	Recruiting	Solid Tumor	DC-CIK Cells	Chemotherapy
NCT04214730	Study of NK Combined With Chemotherapy for Advanced Solid Tumor	Recruiting	Solid Tumor	NK Cells	Chemotherapy
NCT04464967	Safety and Preliminary Efficacy of SNK01 in Combination With Trastuzumab or Cetuximab in Subjects With Advanced HER2 or EGFR Cancers	Withdrawn	Advanced Solid Tumors (Including Pancreatic Cancer)	SNK01	Trastuzumab; Cetuximab
NCT04476641	A Study of DC-CIK Immunotherapy in the Treatment of Solid Tumors	Unknown	Liver Cancer, Kidney Cancer, Nasopharyngeal Cancer, Lung Cancer, Colorectal Cancer, Breast Cancer	DC-CIK cells	
NCT04557306	Evaluation of Tolerability and Safety of CBT101, an Autologous Natural Killer Cell, in Patients With Solid Cancer	Unknown	Solid Tumor	CBT101 (2-6 x 10 ⁹ cells), every 2 weeks; CBT101 (2-6 x 10 ⁹ cells), every 4 weeks	
NCT04623944	NKX101, Intravenous Allogeneic CAR NK Cells, in Adults With AML or MDS	Recruiting	Relapsed/ AML, AML, Adult, MDS, Myelodysplastic Syndromes	NKX101 - CAR NK cell therapy	
NCT05099549	Safety, Tolerability, and Anti-Tumor Activity of AFM24 in Combination With SNK01 in Subjects With Advanced/Metastatic EGFR-Expressing Cancers	Active not recruiting	Squamous Cell Carcinoma of Head and Neck, Carcinoma, Non-Small Cell Lung, Colorectal Neoplasms, Advanced Solid Tumor, Tumor, Metastatic Tumor	SNK01	AFM24
NCT05137275	Study of Anti-ST4 CAR-raNK Cell Therapy in Locally Advanced or Metastatic Solid Tumors	Recruiting	Locally Advanced or Metastatic Solid Tumors	Anti-ST4 CAR-raNK cells	
NCT05194709	Study of Anti-ST4 CAR-NK Cell Therapy in Advanced Solid Tumors	Recruiting	Advanced Solid Tumors	Anti-CAR-NK Cells	
NCT05213195	NKG2D CAR-NK Cell Therapy in Patients With Metastatic Colorectal Cancer	Recruiting	Metastatic Colorectal Cancer	NKG2D CAR-NK	
NCT05247957	NKG2D CAR-NK Cell Therapy in Patients With Relapsed or Acute Myeloid Leukaemia	Terminated	Safety and Efficacy	CAR-NK cells	
NCT05319249	Natural Killer Cell Immunotherapy in Combination With PARP-inhibition in Acute Myeloid Leukaemia	Not yet recruiting	Acute Myeloid Leukaemia	NK cells	Talazoparib 1 MG [Talzena]
NCT05410717	CLDN6-CAR-NK Cell Therapy for Advanced Solid Tumors	Recruiting	Stage IV Ovarian Cancer, Testis Cancer, Endometrial Cancer, CAR NK	Claudin6 targeting CAR-NK cells	
NCT05528341	NKG2D-CAR-NK92 Cells Immunotherapy for Solid Tumors	Recruiting	Relapsed/ Solid Tumors	NKG2D-CAR-NK92 cells	
NCT05734898	NKG2D CAR-NK & r/AML	Recruiting	AML	NKG2D CAR-NK	
NCT05776355	NKG2D CAR-NK & Ovarian Cancer	Recruiting	Ovarian Cancer	NKG2D CAR-NK	
NCT05880043	A Study of GIC-102 (Allogeneic Natural Killer Cells) in Patients With Advanced Solid Tumors, Non-Hodgkin Lymphoma, and Multiple Myeloma	Recruiting	Advanced Solid Tumors, Relapsed/ Non-Hodgkin Lymphoma, Relapsed/ Multiple Myeloma	GIC-102 (Allogeneic NK cells)	
NCT05955157	Combined S-1 With DC-CIK As Maintenance Therapy For Advanced Pancreatic Ductal Adenocarcinoma	Recruiting	Pancreatic Ductal Adenocarcinoma, Advanced Solid Tumor	Dendritic cell + Cytokine-induced killer cell (DC+CIK) immunotherapy	Tegafur
NCT05990920	Study of Allogeneic Blood-derived Natural Killer Cells to Evaluate Safety and Tolerability in Cancer to Conventional Therapy	Recruiting	Advanced Solid Tumor, Metastatic Cancer	SNK02	

Table 7.1: Clinical Trials involving NK cell therapies (clinicaltrials.gov).

7.6 Prognostic implications of NK cell infiltrate and proximity to CAFs in PDAC

7.6.1 Absolute NK cell infiltrate does not confer prognostic impact

NK cell infiltrate in PDAC has been shown to correlate with patient outcome. Previous work by Hoshikawa *et al*, identified that the percentage of NK cells within both the tumour and peripheral blood of PDAC patients correlated with progression free survival.²¹⁹ Davis *et al*. also note improved overall survival in patients with higher absolute NK cells numbers.²²¹ Similarly, Ogobuiro *et al*. identified significant enrichment in NK cell signatures (as well as CD8⁺ T cells, monocytes and M2 macrophages) in patients with young onset pancreatic cancer (YOPC) when compared to average onset (AOPC) cohorts. As YOPC is associated with significantly greater overall survival (when compared to AOPC), it was suggested that the increased immune signature may play a role in the differential clinicopathological outcomes between the two cohorts.³⁷⁷ Additionally, murine models of pancreatic cancer revealed that NK cells were required for a gemcitabine induced antitumor response following tumour resection.³⁷⁸ Despite this positive correlation between NK cell number and patient outcome, Jun *et al*. suggested that it is the functional state of NK cells, and not total cell number, which is an important prognostic indicator.²²² Furthermore, in a multi-omics study of pancreatic cancer, Yousuf *et al*. identified significantly greater proportions of NK cells within short term survivors (IQR: 7-9 months) when compared with long-term survivors (IQR:45-57). This was also true for B-cells, NKT-cells and alternatively activated macrophages. The lower survival observed within this cohort was determined to be in line with the immunosuppressive nature of these cells as identified by scRNA-seq analysis.³⁷⁹ Consistently, whilst we note the importance of absolute NK cell infiltrate, we did not identify any prognostic relationship between NK cell number and patient overall survival.

7.6.2 NK proximity to CAFs demonstrates prognostic significance and may be used for patient stratification

The dynamic interactions between immune, malignant and stromal cells play a crucial role in determining the effectiveness of immunotherapies.³⁸⁰ Thus, development of clear patient stratification may lead to improved patient care and therapeutic strategies.³⁸¹ In a study of gastric cancer, Li *et al.* note that fibroblasts, NK cells and endothelial cells were the most robust markers of prognosis. As such, these cellular markers were used to stratify patients into four distinct subgroups: $NK^{Low}/Stroma^{Low}$, $NK^{Low}/Stroma^{High}$, $NK^{High}/Stroma^{Low}$, $NK^{High}/Stroma^{High}$. This patient stratification was found to demonstrate significant prognostic impact, with $NK^{High}/Stroma^{Low}$ patients demonstrating the best overall survival. Consequently, it was suggested that improved risk stratification may guide personalised therapies.³⁸² Similarly, a prediction signature based on NK cell marker genes demonstrated clear prognostic implications for low-risk and high-risk scores in lung adenocarcinoma patients. Specifically, patients with low-risk scores were found to exhibit abundant immune cell infiltration. Moreover, immunotherapy response rate was considerably higher in low-risk score patients when compared to the high-risk cohort, demonstrating the therapeutic significance of NK-cell based patient stratification.³⁸³ Similarly, NK-related genes identified in the TCGA-PAAD database generated three stable clusters with distinct characteristics for patient stratification. Survival analysis revealed favourable prognosis in cluster 3, whilst cluster 1 had poorer prognosis. Importantly, immune cell infiltrate was seen to differ between clusters, with cluster 3 demonstrating a significantly higher immune score than did other clusters. Cluster 3 was also found to have a greater response to IFN- γ and increased cytolytic activity. Finally, the greatest expression of the immune checkpoint related genes PD-1 and CTLA-4 was observed in cluster 3, suggesting that this group may respond best to immune checkpoint

blockade. Thus the potential for patient stratification using NK-related genes in PDAC can be clearly observed.³⁸⁴ These results in combination with the prognostic impact of PSC/CAFs previously identified¹⁴⁰ suggest that NK-PSC/CAF interaction may hold important prognostic potential.

To further investigate the role of NK-PSC/CAF interaction in patient outcome, we studied the proximity between these two cell types within PDAC samples. Importantly, NK cell proximity to tumour cells has been shown to have prognostic significance in various cancer types such as metastatic melanoma³⁸⁵, breast cancer³⁸⁶ and PDAC.²²² Mi *et al.* recently report the importance of spatial proximity of adaptive immune cell infiltrate in short and long term survivors in PDAC, providing a precedent for the potential role innate immune cell proximity may play in prognosis.³⁸⁷ Väyrynen *et al.* similarly determined longer cancer specific survival in patients expressing greater proximity between T- and NKT- cells and tumour cells in patients with colorectal cancer.³⁸⁸ In addition, spatial analysis revealed closer proximity of NK cells to tumoural cells in PD-1 treatment responders than in non-responders, revealing a prognostic role for NK cell proximity in malignant melanoma.³⁸⁵ Our findings expand on this foundation and highlight the significance of cellular proximity in the PDAC tumour microenvironment. We demonstrate that patients with greater distance between CD45⁺CD56⁺/CD45⁺CD56⁺NKG2D⁺ NK cells and CAFs (Vimentin⁺ cells) exhibit longer overall survival. These findings highlight the role of NK cell proximity to CAFs in patient overall survival and suggest the potential for patient stratification.

7.7 Limitations

There are several limitations associated with this study which should be considered. Firstly, due to experimental design, baseline proteomic levels were not assessed for NK, qPSC or aPSC

alone, thus the data presented are relative changes between 'healthy' (qPSC) and 'diseased' (aPSC) conditions. As such, this must be taken into consideration when reviewing the results. Secondly, we note that the *in vitro* work displayed herein has been conducted in 2D culture. As this study was a proof of principle, future works including 3D models would be useful to demonstrate the spatial interaction between NK and PSC. Finally, mIHC analysis of PDAC samples was conducted using tissue microarray sections. Whilst it could be argued that whole tissue slides may provide a more comprehensive overview, we have demonstrated tumoural heterogeneity in both CAF and NK cell infiltrate. Furthermore, the use of TMA sections has allowed us to include 64 PDAC patients within the study in a timely manner, providing a synopsis of the interplay of NK and PSCs within PDAC. Additionally, with a median of 3 cores analysed per patient, we present good tissue coverage overall, and suggest that this validates the use of TMA within the current work.

7.8 Future directions

This study provides a firm observational foundation of the bidirectional interplay between NK and PSCs in the context of PDAC, however further work is needed to fully explore the mechanistic underpinning of this dynamic interaction. Specifically, employing 3D organotypic/spheroid models would provide more in-depth analysis of the spatial cross-talk between NK and PSCs *in vitro*, facilitating investigation of specific spatial cell-cell interactions. Recent work employing 3D models of PDAC (established using poly-HEMA coated plates) revealed that targeting periostin expression within PSCs resulted in an increase in NK-cell cytotoxicity against pancreatic cancer cells and PSCs.³⁸⁹ This provides an important foundation on which to further explore NK-PSC/CAF interactions within the 3D *in vitro* setting. Furthermore, within this study, NK activity was measured using the CD107 degranulation assay, validating the use of this assay in spheroid cultures for future work. In addition, further

exploration of our initial proteomic results and their continued validation through phospho-proteomic analysis would facilitate a deeper understanding of the underlying mechanisms involved within this interaction. Through greater mechanistic understanding we may be able to suggest potential biological pathways which may be harnessed for the treatment of PDAC. Several clinical trials are currently ongoing (Section 7.5) targeting markers which were also identified within our proteomic data. This demonstrates the potential to harness NK-PSC interaction in the clinical setting. Thus, further work to validate targets in *in vivo* models is of great importance. Several pre-clinical trials are underway to activate both the innate and adaptive immune response in PDAC. Using KPC mouse models, Piper *et al.* demonstrate a systemic increase in NK cells following treatment with a murine PD-1 targeted-IL2 variant antibody complex.³⁹⁰ Similarly, in orthotopic mouse models of oral squamous cell carcinoma and PDAC, sequential therapy with supercharged NK cells followed by chemotherapy or anti-PD-1 treatment resulted in significantly decreased tumour size and enhanced NK cell function.³⁹¹ In addition to harnessing NK cell function, PKT murine models have demonstrated efficacy of MEK and STAT3 inhibitors in pancreatic cancer. Furthermore, this inhibition was shown to attenuate both myCAFs and iCAFs within the tumour whilst enriching for Ly6a/CD34-expressing CAFs which display a mesenchymal stem-cell like phenotype, demonstrating the ability to induce CAF plasticity within PDAC. Moreover, combination of these treatments with PD-1 immunotherapy significantly improved T-cell cytotoxicity and led to a reduction in tumour volume.³⁹² Thus through employing sequential therapies in the form of CAF targeting and NK cell stimulation or transfer, we may be able to further harness this unique interaction within *in vivo* models of PDAC. Finally, plans to complete 40-plex mIHC using COMET (Lunaphore Technologies, Switzerland) will provide more in-depth analysis of

the spatial interaction between NK and PSC/CAF subtypes within PDAC, as well as their relevance within the larger immune landscape.

7.9 Conclusions

PDAC is a disease with dismal prognosis. Despite increasing interest in targeting PSCs and the potential role for NK cells as therapies, little remains known about the interaction between these two players. We demonstrate for the first time to our knowledge, a significant bidirectional relationship between NK cells and PSCs in the context of PDAC.

We show a propensity for NK cells to target and lyse both qPSC and aPSC in a contact dependent manner. Furthermore, we demonstrate that qPSC education modulates NK functional efficacy against pancreatic cancer cell lines.

We identify significant phenotypic changes in response to co-culture. PSCs demonstrate an increase in alpha SMA, suggesting that NK cells induce a myofibroblastic shift within PSCs in a direct contact dependent manner. Moreover, increase in inhibitory receptor expression in NK cells correlated with reduced functional efficacy. We further demonstrated the bi-directionality of this relationship through global proteomic analysis.

Despite the prognostic significance of total NK cell infiltrate demonstrated previously, we show that NK proximity to CAFs, and not total NK cell infiltrate is correlated with improved overall survival in PDAC patients. Consequently, we suggest that the spatial biology of stromal cells may play a prognostic role in PDAC and may potentially be used as a tool for patient stratification.

Additional work is needed to further explore the complexities of NK-PSC/CAF interactions and to greater understand the mechanistic underpinnings of this key cellular relationship in order to fully harness its therapeutic potential.

References

1. Siegel RL, Miller KD, Fuchs HE, et al. Cancer statistics, 2022. *CA: A Cancer Journal for Clinicians* 2022;72:7-33.
2. Orth M, Metzger P, Gerum S, et al. Pancreatic ductal adenocarcinoma: biological hallmarks, current status, and future perspectives of combined modality treatment approaches. *Radiat Oncol* 2019;14:141.
3. Lee B, Gibbs P. Inflammation, Biomarkers and Immuno-Oncology Pathways in Pancreatic Cancer. *J Pers Med* 2019;9.
4. de Santiago I, Yau C, Heij L, et al. Immunophenotypes of pancreatic ductal adenocarcinoma: Meta-analysis of transcriptional subtypes. *Int J Cancer* 2019;145:1125-1137.
5. Halbrook CJ, Lyssiotis CA, di Magliano MP, et al. Pancreatic cancer: Advances and challenges. *Cell* 2023;186:1729-1754.
6. Yang J, Xu R, Wang C, et al. Early screening and diagnosis strategies of pancreatic cancer: a comprehensive review. *Cancer Communications* 2021;41:1257-1274.
7. Young K, Hughes DJ, Cunningham D, et al. Immunotherapy and pancreatic cancer: unique challenges and potential opportunities. *Ther Adv Med Oncol* 2018;10:1758835918816281.
8. Hu JX, Zhao CF, Chen WB, et al. Pancreatic cancer: A review of epidemiology, trend, and risk factors. *World J Gastroenterol* 2021;27:4298-4321.
9. McGuigan A, Kelly P, Turkington RC, et al. Pancreatic cancer: A review of clinical diagnosis, epidemiology, treatment and outcomes. *World J Gastroenterol* 2018;24:4846-4861.
10. Molina-Montes E, Van Hoogstraten L, Gomez-Rubio P, et al. Pancreatic Cancer Risk in Relation to Lifetime Smoking Patterns, Tobacco Type, and Dose-Response Relationships. *Cancer Epidemiol Biomarkers Prev* 2020;29:1009-1018.
11. Bagnardi V, Rota M, Botteri E, et al. Alcohol consumption and site-specific cancer risk: a comprehensive dose-response meta-analysis. *Br J Cancer* 2015;112:580-93.
12. Naudin S, Li K, Jaouen T, et al. Lifetime and baseline alcohol intakes and risk of pancreatic cancer in the European Prospective Investigation into Cancer and Nutrition study. *Int J Cancer* 2018;143:801-812.
13. Tsai HJ, Chang JS. Environmental Risk Factors of Pancreatic Cancer. *J Clin Med* 2019;8.

14. Wu QJ, Wu L, Zheng LQ, et al. Consumption of fruit and vegetables reduces risk of pancreatic cancer: evidence from epidemiological studies. *Eur J Cancer Prev* 2016;25:196-205.
15. Stolzenberg-Solomon RZ, Cross AJ, Silverman DT, et al. Meat and meat-mutagen intake and pancreatic cancer risk in the NIH-AARP cohort. *Cancer Epidemiol Biomarkers Prev* 2007;16:2664-75.
16. Zhou B, Wu D, Liu H, et al. Obesity and pancreatic cancer: An update of epidemiological evidence and molecular mechanisms. *Pancreatology* 2019;19:941-950.
17. Aune D, Greenwood DC, Chan DSM, et al. Body mass index, abdominal fatness and pancreatic cancer risk: a systematic review and non-linear dose–response meta-analysis of prospective studies. *Annals of Oncology* 2012;23:843-852.
18. Bethea TN, Kitahara CM, Sonderman J, et al. A Pooled Analysis of Body Mass Index and Pancreatic Cancer Mortality in African Americans. *Cancer Epidemiology, Biomarkers & Prevention* 2014;23:2119-2125.
19. Koyanagi YN, Matsuo K, Ito H, et al. Body-Mass Index and Pancreatic Cancer Incidence: A Pooled Analysis of Nine Population-Based Cohort Studies With More Than 340,000 Japanese Subjects. *Journal of Epidemiology* 2018;28:245-252.
20. Bray F, Ferlay J, Soerjomataram I, et al. Global cancer statistics 2018: GLOBOCAN estimates of incidence and mortality worldwide for 36 cancers in 185 countries. *CA: A Cancer Journal for Clinicians* 2018;68:394-424.
21. Cervantes A, Waymouth EK, Petrov MS. African-Americans and Indigenous Peoples Have Increased Burden of Diseases of the Exocrine Pancreas: A Systematic Review and Meta-Analysis. *Dig Dis Sci* 2019;64:249-261.
22. Li X, Xu H, Gao P. ABO Blood Group and Diabetes Mellitus Influence the Risk for Pancreatic Cancer in a Population from China. *Med Sci Monit* 2018;24:9392-9398.
23. Antwi SO, Bamlet WR, Pedersen KS, et al. Pancreatic cancer risk is modulated by inflammatory potential of diet and ABO genotype: a consortia-based evaluation and replication study. *Carcinogenesis* 2018;39:1056-1067.
24. Klein AP, Brune KA, Petersen GM, et al. Prospective risk of pancreatic cancer in familial pancreatic cancer kindreds. *Cancer Res* 2004;64:2634-8.

25. Molina-Montes E, Coscia C, Gómez-Rubio P, et al. Deciphering the complex interplay between pancreatic cancer, diabetes mellitus subtypes and obesity/BMI through causal inference and mediation analyses. *Gut* 2021;70:319-329.
26. Huang BZ, Pandol SJ, Jeon CY, et al. New-Onset Diabetes, Longitudinal Trends in Metabolic Markers, and Risk of Pancreatic Cancer in a Heterogeneous Population. *Clin Gastroenterol Hepatol* 2020;18:1812-1821.e7.
27. Grant TJ, Hua K, Singh A. Molecular Pathogenesis of Pancreatic Cancer. *Prog Mol Biol Transl Sci* 2016;144:241-275.
28. Peltola E, Hannula P, Huhtala H, et al. Long-term morbidity and mortality in patients diagnosed with an insulinoma. *European Journal of Endocrinology* 2021;185:577-586.
29. Sada A, Yamashita TS, Glasgow AE, et al. Comparison of benign and malignant insulinoma. *The American Journal of Surgery* 2021;221:437-447.
30. Johnston ME, 2nd, Carter MM, Wilson GC, et al. Surgical management of primary pancreatic neuroendocrine tumors. *J Gastrointest Oncol* 2020;11:578-589.
31. Anderson CW, Bennett JJ. Clinical Presentation and Diagnosis of Pancreatic Neuroendocrine Tumors. *Surg Oncol Clin N Am* 2016;25:363-374.
32. Vareedayah AA, Alkaade S, Taylor JR. Pancreatic Adenocarcinoma. *Mo Med* 2018;115:230-235.
33. Sarantis P, Koustas E, Papadimitropoulou A, et al. Pancreatic ductal adenocarcinoma: Treatment hurdles, tumor microenvironment and immunotherapy. *World J Gastrointest Oncol* 2020;12:173-181.
34. Kim JY, Hong SM. Precursor Lesions of Pancreatic Cancer. *Oncol Res Treat* 2018;41:603-610.
35. Xing-Mao Z, Hong-Juan Z, Qing L, et al. Pancreatic acinar cell carcinoma-case report and literature review. *BMC Cancer* 2018;18:1083.
36. Gurzu S, Bara T, Sincu M, et al. Solid pseudopapillary neoplasm of pancreas: Two case reports. *Medicine (Baltimore)* 2019;98:e16455.
37. Isobe T, Seki M, Yoshida K, et al. Integrated Molecular Characterization of the Lethal Pediatric Cancer Pancreatoblastoma. *Cancer Res* 2018;78:865-876.
38. Sivapalan L, Kocher HM, Ross-Adams H, et al. The molecular landscape of pancreatic ductal adenocarcinoma. *Pancreatology* 2022;22:925-936.

39. Morris JPt, Wang SC, Hebrok M. KRAS, Hedgehog, Wnt and the twisted developmental biology of pancreatic ductal adenocarcinoma. *Nat Rev Cancer* 2010;10:683-95.
40. Zaccari P, Cardinale V, Severi C, et al. Common features between neoplastic and preneoplastic lesions of the biliary tract and the pancreas. *World J Gastroenterol* 2019;25:4343-4359.
41. Buscail L, Bournet B, Cordelier P. Role of oncogenic KRAS in the diagnosis, prognosis and treatment of pancreatic cancer. *Nature Reviews Gastroenterology & Hepatology* 2020;17:153-168.
42. Löhr M, Klöppel G, Maisonneuve P, et al. Frequency of K-ras mutations in pancreatic intraductal neoplasias associated with pancreatic ductal adenocarcinoma and chronic pancreatitis: a meta-analysis. *Neoplasia* 2005;7:17-23.
43. Hingorani SR, Wang L, Multani AS, et al. Trp53R172H and KrasG12D cooperate to promote chromosomal instability and widely metastatic pancreatic ductal adenocarcinoma in mice. *Cancer Cell* 2005;7:469-83.
44. Wilentz RE, Geradts J, Maynard R, et al. Inactivation of the p16 (INK4A) Tumor-suppressor Gene in Pancreatic Duct Lesions: Loss of Intranuclear Expression¹. *Cancer Research* 1998;58:4740-4744.
45. Yachida S, Iacobuzio-Donahue CA. Evolution and dynamics of pancreatic cancer progression. *Oncogene* 2013;32:5253-5260.
46. Lin JC, Liu TP, Yang PM. CDKN2A-Inactivated Pancreatic Ductal Adenocarcinoma Exhibits Therapeutic Sensitivity to Paclitaxel: A Bioinformatics Study. *J Clin Med* 2020;9.
47. Lüttges J, Gallehdari H, Bröcker V, et al. Allelic Loss Is Often the First Hit in the Biallelic Inactivation of the p53 and DPC4 Genes During Pancreatic Carcinogenesis. *The American Journal of Pathology* 2001;158:1677-1683.
48. Mello SS, Flowers BM, Mazur PK, et al. Multifaceted role for p53 in pancreatic cancer suppression. *Proc Natl Acad Sci U S A* 2023;120:e2211937120.
49. Bailey P, Chang DK, Nones K, et al. Genomic analyses identify molecular subtypes of pancreatic cancer. *Nature* 2016;531:47-52.
50. Stewart MD, Merino Vega D, Arend RC, et al. Homologous Recombination Deficiency: Concepts, Definitions, and Assays. *Oncologist* 2022;27:167-174.

51. Yao W, Maitra A, Ying H. Recent insights into the biology of pancreatic cancer. *EBioMedicine* 2020;53:102655.
52. Chen A. PARP inhibitors: its role in treatment of cancer. *Chin J Cancer* 2011;30:463-71.
53. Golan T, Hammel P, Reni M, et al. Maintenance Olaparib for Germline BRCA-Mutated Metastatic Pancreatic Cancer. *N Engl J Med* 2019;381:317-327.
54. Conroy T, Desseigne F, Ychou M, et al. FOLFIRINOX versus gemcitabine for metastatic pancreatic cancer. *N Engl J Med* 2011;364:1817-25.
55. Von Hoff DD, Ervin T, Arena FP, et al. Increased survival in pancreatic cancer with nab-paclitaxel plus gemcitabine. *N Engl J Med* 2013;369:1691-703.
56. Oettle H, Riess H, Stieler JM, et al. Second-line oxaliplatin, folinic acid, and fluorouracil versus folinic acid and fluorouracil alone for gemcitabine-refractory pancreatic cancer: outcomes from the CONKO-003 trial. *J Clin Oncol* 2014;32:2423-9.
57. Ducreux M, Seufferlein T, Van Laethem J-L, et al. Systemic treatment of pancreatic cancer revisited. *Seminars in Oncology* 2019;46:28-38.
58. Zhu Y-H, Zheng J-H, Jia Q-Y, et al. Immunosuppression, immune escape, and immunotherapy in pancreatic cancer: focused on the tumor microenvironment. *Cellular Oncology* 2023;46:17-48.
59. Zhao L, Singh V, Ricca A, et al. Survival Benefit of Pembrolizumab for Patients With Pancreatic Adenocarcinoma: A Case Series. *J Med Cases* 2022;13:240-243.
60. Marabelle A, Le DT, Ascierto PA, et al. Efficacy of Pembrolizumab in Patients With Noncolorectal High Microsatellite Instability/Mismatch Repair-Deficient Cancer: Results From the Phase II KEYNOTE-158 Study. *J Clin Oncol* 2020;38:1-10.
61. Ene-Obong A, Clear AJ, Watt J, et al. Activated pancreatic stellate cells sequester CD8+ T cells to reduce their infiltration of the juxtatumoral compartment of pancreatic ductal adenocarcinoma. *Gastroenterology* 2013;145:1121-32.
62. Ren B, Cui M, Yang G, et al. Tumor microenvironment participates in metastasis of pancreatic cancer. *Mol Cancer* 2018;17:108.
63. Truong L-H, Pauklin S. Pancreatic Cancer Microenvironment and Cellular Composition: Current Understandings and Therapeutic Approaches. *Cancers* 2021;13:5028.
64. Uzunparmak B, Sahin IH. Pancreatic cancer microenvironment: a current dilemma. *Clin Transl Med* 2019;8:2.

65. Komar G, Kauhanen S, Liukko K, et al. Decreased blood flow with increased metabolic activity: a novel sign of pancreatic tumor aggressiveness. *Clin Cancer Res* 2009;15:5511-7.
66. Zhang Z, Han H, Rong Y, et al. Hypoxia potentiates gemcitabine-induced stemness in pancreatic cancer cells through AKT/Notch1 signaling. *J Exp Clin Cancer Res* 2018;37:291.
67. Wang X, Luo G, Zhang K, et al. Hypoxic Tumor-Derived Exosomal miR-301a Mediates M2 Macrophage Polarization via PTEN/PI3K γ to Promote Pancreatic Cancer Metastasis. *Cancer Res* 2018;78:4586-4598.
68. Hester R, Mazur PK, McAllister F. Immunotherapy in Pancreatic Adenocarcinoma: Beyond “Copy/Paste”. *Clinical Cancer Research* 2021;27:6287-6297.
69. Falcomatà C, Bärthel S, Schneider G, et al. Context-Specific Determinants of the Immunosuppressive Tumor Microenvironment in Pancreatic Cancer. *Cancer Discov* 2023;13:278-297.
70. Thyagarajan A, Alshehri MSA, Miller KLR, et al. Myeloid-Derived Suppressor Cells and Pancreatic Cancer: Implications in Novel Therapeutic Approaches. *Cancers (Basel)* 2019;11.
71. Markowitz J, Brooks TR, Duggan MC, et al. Patients with pancreatic adenocarcinoma exhibit elevated levels of myeloid-derived suppressor cells upon progression of disease. *Cancer Immunol Immunother* 2015;64:149-59.
72. Trovato R, Fiore A, Sartori S, et al. Immunosuppression by monocytic myeloid-derived suppressor cells in patients with pancreatic ductal carcinoma is orchestrated by STAT3. *Journal for immunotherapy of cancer* 2019;7:255-255.
73. Zhang Y, Velez-Delgado A, Mathew E, et al. Myeloid cells are required for PD-1/PD-L1 checkpoint activation and the establishment of an immunosuppressive environment in pancreatic cancer. *Gut* 2017;66:124-136.
74. Huang B, Pan P-Y, Li Q, et al. Gr-1+CD115+ Immature Myeloid Suppressor Cells Mediate the Development of Tumor-Induced T Regulatory Cells and T-Cell Anergy in Tumor-Bearing Host. *Cancer Research* 2006;66:1123-1131.
75. Yang S, Liu Q, Liao Q. Tumor-Associated Macrophages in Pancreatic Ductal Adenocarcinoma: Origin, Polarization, Function, and Reprogramming. *Frontiers in Cell and Developmental Biology* 2021;8.

76. Zhu Y, Herndon JM, Sojka DK, et al. Tissue-Resident Macrophages in Pancreatic Ductal Adenocarcinoma Originate from Embryonic Hematopoiesis and Promote Tumor Progression. *Immunity* 2017;47:323-338.e6.
77. Lankadasari MB, Mukhopadhyay P, Mohammed S, et al. TAMing pancreatic cancer: combat with a double edged sword. *Molecular Cancer* 2019;18:48.
78. Poh AR, Ernst M. Tumor-Associated Macrophages in Pancreatic Ductal Adenocarcinoma: Therapeutic Opportunities and Clinical Challenges. *Cancers (Basel)* 2021;13.
79. Beatty GL, Winograd R, Evans RA, et al. Exclusion of T Cells From Pancreatic Carcinomas in Mice Is Regulated by Ly6C^{low} F4/80⁺ Extratumoral Macrophages. *Gastroenterology* 2015;149:201-210.
80. Krneta T, Gillgrass A, Poznanski S, et al. M2-polarized and tumor-associated macrophages alter NK cell phenotype and function in a contact-dependent manner. *Journal of Leukocyte Biology* 2016;101:285-295.
81. Xia Q, Jia J, Hu C, et al. Tumor-associated macrophages promote PD-L1 expression in tumor cells by regulating PKM2 nuclear translocation in pancreatic ductal adenocarcinoma. *Oncogene* 2022;41:865-877.
82. Li C, Jiang P, Wei S, et al. Regulatory T cells in tumor microenvironment: new mechanisms, potential therapeutic strategies and future prospects. *Molecular Cancer* 2020;19:116.
83. Principe DR, DeCant B, Mascariñas E, et al. TGFβ Signaling in the Pancreatic Tumor Microenvironment Promotes Fibrosis and Immune Evasion to Facilitate Tumorigenesis. *Cancer Res* 2016;76:2525-39.
84. Gao Z, Zhang Q, Zhang X, et al. Advance of T regulatory cells in tumor microenvironment remodeling and immunotherapy in pancreatic cancer. *European Journal of Inflammation* 2022;20:1721727X221092900.
85. Apte MV, Pirola RC, Wilson JS. Pancreatic stellate cells: a starring role in normal and diseased pancreas. *Front Physiol* 2012;3:344.
86. Means AL. Pancreatic stellate cells: small cells with a big role in tissue homeostasis. *Lab Invest* 2013;93:4-7.
87. Sherman MH. Stellate Cells in Tissue Repair, Inflammation, and Cancer. *Annu Rev Cell Dev Biol* 2018;34:333-355.

88. Froeling FE, Feig C, Chelala C, et al. Retinoic acid-induced pancreatic stellate cell quiescence reduces paracrine Wnt- β -catenin signaling to slow tumor progression. *Gastroenterology* 2011;141:1486-97, 1497.e1-14.
89. Ferdek PE, Jakubowska MA. Biology of pancreatic stellate cells-more than just pancreatic cancer. *Pflugers Arch* 2017;469:1039-1050.
90. Xu Z, Vonlaufen A, Phillips PA, et al. Role of pancreatic stellate cells in pancreatic cancer metastasis. *Am J Pathol* 2010;177:2585-96.
91. Fu Y, Liu S, Zeng S, et al. The critical roles of activated stellate cells-mediated paracrine signaling, metabolism and onco-immunology in pancreatic ductal adenocarcinoma. *Molecular Cancer* 2018;17:62.
92. Wu YS, Chung I, Wong WF, et al. Paracrine IL-6 signaling mediates the effects of pancreatic stellate cells on epithelial-mesenchymal transition via Stat3/Nrf2 pathway in pancreatic cancer cells. *Biochim Biophys Acta Gen Subj* 2017;1861:296-306.
93. Huang L, Hu B, Ni J, et al. Transcriptional repression of SOCS3 mediated by IL-6/STAT3 signaling via DNMT1 promotes pancreatic cancer growth and metastasis. *J Exp Clin Cancer Res* 2016;35:27.
94. Qin J-J, Yan L, Zhang J, et al. STAT3 as a potential therapeutic target in triple negative breast cancer: a systematic review. *Journal of Experimental & Clinical Cancer Research* 2019;38:195.
95. Nan L, Qin T, Xiao Y, et al. Pancreatic Stellate Cells Facilitate Perineural Invasion of Pancreatic Cancer via HGF/c-Met Pathway. *Cell Transplant* 2019;28:1289-1298.
96. Sleightholm RL, Neilsen BK, Li J, et al. Emerging roles of the CXCL12/CXCR4 axis in pancreatic cancer progression and therapy. *Pharmacology & Therapeutics* 2017;179:158-170.
97. Malik S, Westcott JM, Brekken RA, et al. CXCL12 in Pancreatic Cancer: Its Function and Potential as a Therapeutic Drug Target. *Cancers (Basel)* 2021;14.
98. Anderson EC, Wong MH. Caught in the Akt: regulation of Wnt signaling in the intestine. *Gastroenterology* 2010;139:718-22.
99. Ahmed YAAR, Mohamed Ali M. Evaluating the evolving evidence: The challenges of molecular-targeted therapy in management of gastric cancer. *Open Journal of Gastroenterology* 2014;4:6-15.

100. Mousavi A. CXCL12/CXCR4 signal transduction in diseases and its molecular approaches in targeted-therapy. *Immunology Letters* 2020;217:91-115.
101. Xu X, Lu Y, Li Y, et al. Sonic Hedgehog Signaling in Thyroid Cancer. *Frontiers in Endocrinology* 2017;8.
102. McCubrey JA, Steelman LS, Chappell WH, et al. Roles of the Raf/MEK/ERK pathway in cell growth, malignant transformation and drug resistance. *Biochimica et Biophysica Acta (BBA) - Molecular Cell Research* 2007;1773:1263-1284.
103. Coleman SJ, Chioni A-M, Ghallab M, et al. Nuclear translocation of FGFR1 and FGF2 in pancreatic stellate cells facilitates pancreatic cancer cell invasion. *EMBO molecular medicine* 2014;6:467-481.
104. Corn PG, Wang F, McKeenan WL, et al. Targeting Fibroblast Growth Factor Pathways in Prostate Cancer. *Clinical Cancer Research* 2013;19:5856.
105. Coetzee AS, Carter EP, Rodríguez-Fernández L, et al. Nuclear FGFR1 promotes pancreatic stellate cell-driven invasion through up-regulation of Neuregulin 1. *Oncogene* 2023;42:491-500.
106. Pothula SP, Pirola RC, Wilson JS, et al. Pancreatic stellate cells: Aiding and abetting pancreatic cancer progression. *Pancreatology* 2020;20:409-418.
107. Di Maggio F, Arumugam P, Delvecchio FR, et al. Pancreatic stellate cells regulate blood vessel density in the stroma of pancreatic ductal adenocarcinoma. *Pancreatology* 2016;16:995-1004.
108. González-González L, Alonso J. Periostin: A Matricellular Protein With Multiple Functions in Cancer Development and Progression. *Frontiers in Oncology* 2018;8.
109. Masamune A, Kikuta K, Watanabe T, et al. Hypoxia stimulates pancreatic stellate cells to induce fibrosis and angiogenesis in pancreatic cancer. *American Journal of Physiology-Gastrointestinal and Liver Physiology* 2008;295:G709-G717.
110. Tang D, Wang D, Yuan Z, et al. Persistent activation of pancreatic stellate cells creates a microenvironment favorable for the malignant behavior of pancreatic ductal adenocarcinoma. *International Journal of Cancer* 2013;132:993-1003.
111. Hrabák P, Kalousová M, Krechler T, et al. Pancreatic stellate cells - rising stars in pancreatic pathologies. *Physiol Res* 2021;70:S597-s616.
112. Daniel SK, Sullivan KM, Labadie KP, et al. Hypoxia as a barrier to immunotherapy in pancreatic adenocarcinoma. *Clinical and translational medicine* 2019;8:10-10.

113. Li C, Cui L, Yang L, et al. Pancreatic Stellate Cells Promote Tumor Progression by Promoting an Immunosuppressive Microenvironment in Murine Models of Pancreatic Cancer. *Pancreas* 2020;49:120-127.
114. Tang D, Yuan Z, Xue X, et al. High expression of Galectin-1 in pancreatic stellate cells plays a role in the development and maintenance of an immunosuppressive microenvironment in pancreatic cancer. *International Journal of Cancer* 2012;130:2337-2348.
115. Lunardi S, Jamieson NB, Lim SY, et al. IP-10/CXCL10 induction in human pancreatic cancer stroma influences lymphocytes recruitment and correlates with poor survival. *Oncotarget* 2014;5:11064-80.
116. Ma Y, Hwang RF, Logsdon CD, et al. Dynamic Mast Cell–Stromal Cell Interactions Promote Growth of Pancreatic Cancer. *Cancer Research* 2013;73:3927-3937.
117. Incio J, Liu H, Suboj P, et al. Obesity-Induced Inflammation and Desmoplasia Promote Pancreatic Cancer Progression and Resistance to Chemotherapy. *Cancer discovery* 2016;6:852-869.
118. Han L, Ma J, Duan W, et al. Pancreatic stellate cells contribute pancreatic cancer pain via activation of SHH signaling pathway. *Oncotarget* 2016;7:18146-18158.
119. Kikuta K, Masamune A, Hamada S, et al. Pancreatic stellate cells reduce insulin expression and induce apoptosis in pancreatic β -cells. *Biochemical and Biophysical Research Communications* 2013;433:292-297.
120. Gonzalez-Rodriguez AP, Villa-Álvarez M, Sordo-Bahamonde C, et al. NK Cells in the Treatment of Hematological Malignancies. *J Clin Med* 2019;8.
121. Morvan MG, Lanier LL. NK cells and cancer: you can teach innate cells new tricks. *Nat Rev Cancer* 2016;16:7-19.
122. Muenst S, Läubli H, Soysal SD, et al. The immune system and cancer evasion strategies: therapeutic concepts. *J Intern Med* 2016;279:541-62.
123. Garcia PE, Scales MK, Allen BL, et al. Pancreatic Fibroblast Heterogeneity: From Development to Cancer. *Cells* 2020;9.
124. Huang H, Brekken RA. Recent advances in understanding cancer-associated fibroblasts in pancreatic cancer. *American Journal of Physiology-Cell Physiology* 2020;319:C233-C243.

125. Huet E, Jaroz C, Nguyen HQ, et al. Stroma in normal and cancer wound healing. *The FEBS Journal* 2019;286:2909-2920.
126. Helms E, Onate MK, Sherman MH. Fibroblast Heterogeneity in the Pancreatic Tumor Microenvironment. *Cancer Discov* 2020;10:648-656.
127. Sousa CM, Biancur DE, Wang X, et al. Pancreatic stellate cells support tumour metabolism through autophagic alanine secretion. *Nature* 2016;536:479-483.
128. Auciello FR, Bulusu V, Oon C, et al. A Stromal Lysolipid-Autotaxin Signaling Axis Promotes Pancreatic Tumor Progression. *Cancer Discov* 2019;9:617-627.
129. Öhlund D, Handly-Santana A, Biffi G, et al. Distinct populations of inflammatory fibroblasts and myofibroblasts in pancreatic cancer. *J Exp Med* 2017;214:579-596.
130. Raskov H, Orhan A, Gaggari S, et al. Cancer-Associated Fibroblasts and Tumor-Associated Macrophages in Cancer and Cancer Immunotherapy. *Frontiers in oncology* 2021;11:668731-668731.
131. Goehrig D, Nigri J, Samain R, et al. Stromal protein β ig-h3 reprogrammes tumour microenvironment in pancreatic cancer. *Gut* 2019;68:693-707.
132. Özdemir BC, Pentcheva-Hoang T, Carstens JL, et al. Depletion of carcinoma-associated fibroblasts and fibrosis induces immunosuppression and accelerates pancreas cancer with reduced survival. *Cancer cell* 2014;25:719-734.
133. Rhim AD, Oberstein PE, Thomas DH, et al. Stromal elements act to restrain, rather than support, pancreatic ductal adenocarcinoma. *Cancer cell* 2014;25:735-747.
134. Lee JJ, Perera RM, Wang H, et al. Stromal response to Hedgehog signaling restrains pancreatic cancer progression. *Proceedings of the National Academy of Sciences of the United States of America* 2014;111:E3091-E3100.
135. van Mackelenbergh MG, Strokes CI, Spijker R, et al. Clinical Trials Targeting the Stroma in Pancreatic Cancer: A Systematic Review and Meta-Analysis. *Cancers* 2019;11:588.
136. Ko AH, LoConte N, Tempero MA, et al. A Phase I Study of FOLFIRINOX Plus IPI-926, a Hedgehog Pathway Inhibitor, for Advanced Pancreatic Adenocarcinoma. *Pancreas* 2016;45:370-5.
137. Manoukian P, Bijlsma M, van Laarhoven H. The Cellular Origins of Cancer-Associated Fibroblasts and Their Opposing Contributions to Pancreatic Cancer Growth. *Frontiers in Cell and Developmental Biology* 2021;9.

138. Zhang T, Ren Y, Yang P, et al. Cancer-associated fibroblasts in pancreatic ductal adenocarcinoma. *Cell Death & Disease* 2022;13:897.
139. Sun Q, Zhang B, Hu Q, et al. The impact of cancer-associated fibroblasts on major hallmarks of pancreatic cancer. *Theranostics* 2018;8:5072-5087.
140. Neuzillet C, Tijeras-Raballand A, Ragulan C, et al. Inter- and intra-tumoural heterogeneity in cancer-associated fibroblasts of human pancreatic ductal adenocarcinoma. *J Pathol* 2019;248:51-65.
141. Sperb N, Tsesmelis M, Wirth T. Crosstalk between Tumor and Stromal Cells in Pancreatic Ductal Adenocarcinoma. *International journal of molecular sciences* 2020;21:5486.
142. Helms EJ, Berry MW, Chaw RC, et al. Mesenchymal Lineage Heterogeneity Underlies Non-Redundant Functions of Pancreatic Cancer-Associated Fibroblasts. *Cancer Discovery* 2021:candisc.0601.2021.
143. Elyada E, Bolisetty M, Laise P, et al. Cross-Species Single-Cell Analysis of Pancreatic Ductal Adenocarcinoma Reveals Antigen-Presenting Cancer-Associated Fibroblasts. *Cancer discovery* 2019;9:1102-1123.
144. Mizutani Y, Kobayashi H, Iida T, et al. Meflin-Positive Cancer-Associated Fibroblasts Inhibit Pancreatic Carcinogenesis. *Cancer Research* 2019;79:5367-5381.
145. Hutton C, Heider F, Blanco-Gomez A, et al. Single-cell analysis defines a pancreatic fibroblast lineage that supports anti-tumor immunity. *Cancer Cell* 2021;39:1227-1244.e20.
146. Menezes S, Okail MH, Jalil SMA, et al. Cancer-associated fibroblasts in pancreatic cancer: new subtypes, new markers, new targets. *J Pathol* 2022;257:526-544.
147. Abel AM, Yang C, Thakar MS, et al. Natural Killer Cells: Development, Maturation, and Clinical Utilization. *Front Immunol* 2018;9:1869.
148. Granzin M, Wagner J, Köhl U, et al. Shaping of Natural Killer Cell Antitumor Activity by Ex Vivo Cultivation. *Front Immunol* 2017;8:458.
149. Poli A, Michel T, Thérésine M, et al. CD56bright natural killer (NK) cells: an important NK cell subset. *Immunology* 2009;126:458-65.
150. Kumar S. Natural killer cell cytotoxicity and its regulation by inhibitory receptors. *Immunology* 2018;154:383-393.

151. Mehta RS, Randolph B, Daher M, et al. NK cell therapy for hematologic malignancies. *International Journal of Hematology* 2018;107:262-270.
152. Urlaub D, Höfer K, Müller ML, et al. LFA-1 Activation in NK Cells and Their Subsets: Influence of Receptors, Maturation, and Cytokine Stimulation. *J Immunol* 2017;198:1944-1951.
153. Seidel U, Schlegel P, Lang P. Natural Killer Cell Mediated Antibody-Dependent Cellular Cytotoxicity in Tumor Immunotherapy with Therapeutic Antibodies. *Frontiers in Immunology* 2013;4.
154. Siemaszko J, Marzec-Przyszlak A, Bogunia-Kubik K. NKG2D Natural Killer Cell Receptor- A Short Description and Potential Clinical Applications. *Cells* 2021;10.
155. Perera Molligoda Arachchige AS. Human NK cells: From development to effector functions. *Innate Immunity* 2021;27:212-229.
156. Wensveen FM, Jelenčić V, Polić B. NKG2D: A Master Regulator of Immune Cell Responsiveness. *Frontiers in Immunology* 2018;9.
157. Zafirova B, Wensveen FM, Gulin M, et al. Regulation of immune cell function and differentiation by the NKG2D receptor. *Cellular and Molecular Life Sciences* 2011;68:3519-3529.
158. Duan S, Guo W, Xu Z, et al. Natural killer group 2D receptor and its ligands in cancer immune escape. *Molecular Cancer* 2019;18:29.
159. Morimoto Y, Yamashita N, Daimon T, et al. MUC1-C is a master regulator of MICA/B NKG2D ligand and exosome secretion in human cancer cells. *J Immunother Cancer* 2023;11.
160. Whalen KA, Rakhra K, Mehta NK, et al. Engaging natural killer cells for cancer therapy via NKG2D, CD16A and other receptors. *mAbs* 2023;15:2208697.
161. Jones AB, Rocco A, Lamb LS, et al. Regulation of NKG2D Stress Ligands and Its Relevance in Cancer Progression. *Cancers* 2022;14:2339.
162. Skořepa O, Pazicky S, Kalousková B, et al. Natural Killer Cell Activation Receptor NKp30 Oligomerization Depends on Its N-Glycosylation. *Cancers (Basel)* 2020;12.
163. Barrow AD, Martin CJ, Colonna M. The Natural Cytotoxicity Receptors in Health and Disease. *Frontiers in Immunology* 2019;10.

164. Memmer S, Weil S, Beyer S, et al. The Stalk Domain of NKp30 Contributes to Ligand Binding and Signaling of a Preassembled NKp30-CD3 ζ Complex. *J Biol Chem* 2016;291:25427-25438.
165. Kellner C, Maurer T, Hallack D, et al. Mimicking an Induced Self Phenotype by Coating Lymphomas with the NKp30 Ligand B7-H6 Promotes NK Cell Cytotoxicity. *The Journal of Immunology* 2012;189:5037-5046.
166. Ponath V, Hoffmann N, Bergmann L, et al. Secreted Ligands of the NK Cell Receptor NKp30: B7-H6 Is in Contrast to BAG6 Only Marginally Released via Extracellular Vesicles. *Int J Mol Sci* 2021;22.
167. Klausz K, Pekar L, Boje AS, et al. Multifunctional NK Cell–Engaging Antibodies Targeting EGFR and NKp30 Elicit Efficient Tumor Cell Killing and Proinflammatory Cytokine Release. *The Journal of Immunology* 2022;209:1724-1735.
168. Luo Q, Luo W, Zhu Q, et al. Tumor-Derived Soluble MICA Obstructs the NKG2D Pathway to Restrain NK Cytotoxicity. *Aging Dis* 2020;11:118-128.
169. Rusakiewicz S, Perier A, Semeraro M, et al. NKp30 isoforms and NKp30 ligands are predictive biomarkers of response to imatinib mesylate in metastatic GIST patients. *Oncoimmunology* 2017;6:e1137418.
170. Delahaye NF, Rusakiewicz S, Martins I, et al. Alternatively spliced NKp30 isoforms affect the prognosis of gastrointestinal stromal tumors. *Nature Medicine* 2011;17:700-707.
171. Gauthier L, Morel A, Anceriz N, et al. Multifunctional Natural Killer Cell Engagers Targeting NKp46 Trigger Protective Tumor Immunity. *Cell* 2019;177:1701-1713.e16.
172. Pessino A, Sivori S, Bottino C, et al. Molecular Cloning of NKp46: A Novel Member of the Immunoglobulin Superfamily Involved in Triggering of Natural Cytotoxicity. *Journal of Experimental Medicine* 1998;188:953-960.
173. Peipp M, Klausz K, Boje AS, et al. Immunotherapeutic targeting of activating natural killer cell receptors and their ligands in cancer. *Clinical and Experimental Immunology* 2022;209:22-32.
174. Hadad U, Thauland TJ, Martinez OM, et al. NKp46 Clusters at the Immune Synapse and Regulates NK Cell Polarization. *Frontiers in immunology* 2015;6:495-495.

175. Lundgren S, Micke P, Elebro J, et al. Topographical Distribution and Spatial Interactions of Innate and Semi-Innate Immune Cells in Pancreatic and Other Periampullary Adenocarcinoma. *Front Immunol* 2020;11:558169.
176. Mikulak J, Oriolo F, Bruni E, et al. Nkp46-expressing human gut-resident intraepithelial V δ 1 T cell subpopulation exhibits high antitumor activity against colorectal cancer. *JCI Insight* 2019;4.
177. Diefenbach A, Colonna M, Koyasu S. Development, Differentiation, and Diversity of Innate Lymphoid Cells. *Immunity* 2014;41:354-365.
178. Wang X, Xiong H, Ning Z. Implications of NKG2A in immunity and immune-mediated diseases. *Frontiers in Immunology* 2022;13.
179. Kaiser BK, Pizarro JC, Kerns J, et al. Structural basis for NKG2A/CD94 recognition of HLA-E. *Proceedings of the National Academy of Sciences* 2008;105:6696-6701.
180. Kaulfuss M, Mietz J, Fabri A, et al. The NK cell checkpoint NKG2A maintains expansion capacity of human NK cells. *Scientific Reports* 2023;13:10555.
181. Marchesi M, Andersson E, Villabona L, et al. HLA-dependent tumour development: a role for tumour associate macrophages? *J Transl Med* 2013;11:247.
182. Kamiya T, Seow SV, Wong D, et al. Blocking expression of inhibitory receptor NKG2A overcomes tumor resistance to NK cells. *J Clin Invest* 2019;129:2094-2106.
183. Sun C, Xu J, Huang Q, et al. High NKG2A expression contributes to NK cell exhaustion and predicts a poor prognosis of patients with liver cancer. *Oncoimmunology* 2017;6:e1264562.
184. Zhang C, Wang X-m, Li S-r, et al. NKG2A is a NK cell exhaustion checkpoint for HCV persistence. *Nature Communications* 2019;10:1507.
185. Wolf Y, Anderson AC, Kuchroo VK. TIM3 comes of age as an inhibitory receptor. *Nature Reviews Immunology* 2020;20:173-185.
186. Ndhlovu LC, Lopez-Vergès S, Barbour JD, et al. Tim-3 marks human natural killer cell maturation and suppresses cell-mediated cytotoxicity. *Blood* 2012;119:3734-3743.
187. So EC, Khaladj-Ghom A, Ji Y, et al. NK cell expression of Tim-3: First impressions matter. *Immunobiology* 2019;224:362-370.
188. Wang F, Hou H, Wu S, et al. Tim-3 pathway affects NK cell impairment in patients with active tuberculosis. *Cytokine* 2015;76:270-279.

189. da Silva IP, Gallois A, Jimenez-Baranda S, et al. Reversal of NK-Cell Exhaustion in Advanced Melanoma by Tim-3 Blockade. *Cancer Immunology Research* 2014;2:410-422.
190. Jiang W, Li F, Jiang Y, et al. Tim-3 Blockade Elicits Potent Anti-Multiple Myeloma Immunity of Natural Killer Cells. *Frontiers in Oncology* 2022;12.
191. Gleason MK, Lenvik TR, McCullar V, et al. Tim-3 is an inducible human natural killer cell receptor that enhances interferon gamma production in response to galectin-9. *Blood* 2012;119:3064-3072.
192. Sun H, Sun C, Xiao W. Expression regulation of co-inhibitory molecules on human natural killer cells in response to cytokine stimulations. *Cytokine* 2014;65:33-41.
193. Workman CJ, Dugger KJ, Vignali DAA. Cutting Edge: Molecular Analysis of the Negative Regulatory Function of Lymphocyte Activation Gene-31. *The Journal of Immunology* 2002;169:5392-5395.
194. Miyazaki T, Dierich A, Benoist C, et al. Independent Modes of Natural Killing Distinguished in Mice Lacking *Lag3*. *Science* 1996;272:405-408.
195. Huard B, Tournier M, Triebel F. LAG-3 does not define a specific mode of natural killing in human. *Immunol Lett* 1998;61:109-12.
196. Ohs I, Ducimetière L, Marinho J, et al. Restoration of Natural Killer Cell Antimetastatic Activity by IL12 and Checkpoint Blockade. *Cancer Research* 2017;77:7059-7071.
197. Narayanan S, Ahl PJ, Bijin VA, et al. LAG3 is a Central Regulator of NK Cell Cytokine Production. *bioRxiv* 2020:2020.01.31.928200.
198. Lefort C, Ley K. Neutrophil arrest by LFA-1 activation. *Frontiers in Immunology* 2012;3.
199. Yuki K, Bu W, Xi J, et al. Isoflurane binds and stabilizes a closed conformation of the leukocyte function-associated antigen-1. *The FASEB Journal* 2012;26:4408-4417.
200. Zhang M, March ME, Lane WS, et al. A signaling network stimulated by β_2 integrin promotes the polarization of lytic granules in cytotoxic cells. *Science Signaling* 2014;7:ra96-ra96.
201. Chaldakov GN. Colchicine, Inflammation and Fibrosis in Cardiovascular Disease: Merging Three Classical Tales. 2018 2018;28.
202. Paul S, Lal G. The Molecular Mechanism of Natural Killer Cells Function and Its Importance in Cancer Immunotherapy. *Frontiers in Immunology* 2017;8.

203. Mentlik AN, Sanborn KB, Holzbaur EL, et al. Rapid lytic granule convergence to the MTOC in natural killer cells is dependent on dynein but not cytolytic commitment. *Molecular biology of the cell* 2010;21:2241-2256.
204. Mukherjee M, Mace EM, Carisey AF, et al. Quantitative Imaging Approaches to Study the CAR Immunological Synapse. *Molecular Therapy* 2017;25:1757-1768.
205. Viswanath DI, Mace EM, Hsu H-T, et al. Quantification of natural killer cell polarization and visualization of synaptic granule externalization by imaging flow cytometry. *Clinical immunology (Orlando, Fla.)* 2017;177:70-75.
206. Brown ACN, Dobbie IM, Alakoskela J-M, et al. Super-resolution imaging of remodeled synaptic actin reveals different synergies between NK cell receptors and integrins. *Blood* 2012;120:3729-3740.
207. Mace EM, Dongre P, Hsu HT, et al. Cell biological steps and checkpoints in accessing NK cell cytotoxicity. *Immunol Cell Biol* 2014;92:245-55.
208. Stinchcombe JC, Salio M, Cerundolo V, et al. Centriole polarisation to the immunological synapse directs secretion from cytolytic cells of both the innate and adaptive immune systems. *BMC biology* 2011;9:45-45.
209. Abarca-Rojano E, Muñiz-Hernández S, Moreno-Altamirano MM, et al. Re-organization of mitochondria at the NK cell immune synapse. *Immunol Lett* 2009;122:18-25.
210. Capuano C, Paolini R, Molfetta R, et al. PIP2-dependent regulation of Munc13-4 endocytic recycling: impact on the cytolytic secretory pathway. *Blood* 2012;119:2252-62.
211. Backes CS, Friedmann KS, Mang S, et al. Natural killer cells induce distinct modes of cancer cell death: Discrimination, quantification, and modulation of apoptosis, necrosis, and mixed forms. *J Biol Chem* 2018;293:16348-16363.
212. Zhu Y, Huang B, Shi J. Fas ligand and lytic granule differentially control cytotoxic dynamics of natural killer cell against cancer target. *Oncotarget* 2016;7:47163-47172.
213. Allen F, Bobanga ID, Rauhe P, et al. CCL3 augments tumor rejection and enhances CD8(+) T cell infiltration through NK and CD103(+) dendritic cell recruitment via IFN γ . *Oncoimmunology* 2018;7:e1393598.
214. Mishra HK, Pore N, Michelotti EF, et al. Anti-ADAM17 monoclonal antibody MEDI3622 increases IFN γ production by human NK cells in the presence of antibody-bound tumor cells. *Cancer Immunol Immunother* 2018;67:1407-1416.

215. Tenuta M, Pandozzi C, Sciarra F, et al. Circulating Natural Killer Cells as Prognostic Value for Non-Small-Cell Lung Cancer Patients Treated with Immune Checkpoint Inhibitors: Correlation with Sarcopenia. *Cancers* 2023;15:3592.
216. Lin Z, Ma J, Ma Y, et al. Prognostic impact of peripheral natural killer cells in primary central nervous system lymphoma. *Front Immunol* 2023;14:1191033.
217. Morinaga T, Iwatsuki M, Yamashita K, et al. Evaluation of HLA-E Expression Combined with Natural Killer Cell Status as a Prognostic Factor for Advanced Gastric Cancer. *Annals of Surgical Oncology* 2022;29:4951-4960.
218. Thacker G, Henry S, Nandi A, et al. Immature natural killer cells promote progression of triple-negative breast cancer. *Science Translational Medicine* 2023;15:eabl4414.
219. Hoshikawa M, Aoki T, Matsushita H, et al. NK cell and IFN signatures are positive prognostic biomarkers for resectable pancreatic cancer. *Biochemical and Biophysical Research Communications* 2018;495:2058-2065.
220. Hu S, Yang J, Shangguan J, et al. Natural killer cell-based adoptive transfer immunotherapy for pancreatic ductal adenocarcinoma in a Kras(LSL-G12D) p53(LSL-R172H) Pdx1-Cre mouse model. *Am J Cancer Res* 2019;9:1757-1765.
221. Davis M, Conlon K, Bohac GC, et al. Effect of Pemetrexed on Innate Immune Killer Cells and Adaptive Immune T Cells in Subjects With Adenocarcinoma of the Pancreas. *Journal of Immunotherapy* 2012;35.
222. Jun E, Song AY, Choi JW, et al. Progressive Impairment of NK Cell Cytotoxic Degranulation Is Associated With TGF- β 1 Deregulation and Disease Progression in Pancreatic Cancer. *Front Immunol* 2019;10:1354.
223. Lin M, Alnaggar M, Liang S, et al. An important discovery on combination of irreversible electroporation and allogeneic natural killer cell immunotherapy for unresectable pancreatic cancer. *Oncotarget* 2017;8:101795-101807.
224. Barrow AD, Colonna M. Tailoring Natural Killer cell immunotherapy to the tumour microenvironment. *Semin Immunol* 2017;31:30-36.
225. Yang C, Cheng H, Zhang Y, et al. Anergic natural killer cells educated by tumor cells are associated with a poor prognosis in patients with advanced pancreatic ductal adenocarcinoma. *Cancer Immunol Immunother* 2018;67:1815-1823.

226. Lim SA, Kim J, Jeon S, et al. Defective Localization With Impaired Tumor Cytotoxicity Contributes to the Immune Escape of NK Cells in Pancreatic Cancer Patients. *Front Immunol* 2019;10:496.
227. Zhao J, Schlößer HA, Wang Z, et al. Tumor-Derived Extracellular Vesicles Inhibit Natural Killer Cell Function in Pancreatic Cancer. *Cancers (Basel)* 2019;11.
228. Konjević GM, Vuletić AM, Mirjačić Martinović KM, et al. The role of cytokines in the regulation of NK cells in the tumor environment. *Cytokine* 2019;117:30-40.
229. Ostrand-Rosenberg S, Sinha P, Beury DW, et al. Cross-talk between myeloid-derived suppressor cells (MDSC), macrophages, and dendritic cells enhances tumor-induced immune suppression. *Semin Cancer Biol* 2012;22:275-81.
230. Peng Y-P, Zhang J-J, Liang W-b, et al. Elevation of MMP-9 and IDO induced by pancreatic cancer cells mediates natural killer cell dysfunction. *BMC cancer* 2014;14:738-738.
231. Bassani B, Baci D, Gallazzi M, et al. Natural Killer Cells as Key Players of Tumor Progression and Angiogenesis: Old and Novel Tools to Divert Their Pro-Tumor Activities into Potent Anti-Tumor Effects. *Cancers* 2019;11:461.
232. Van Audenaerde JRM, De Waele J, Marcq E, et al. Interleukin-15 stimulates natural killer cell-mediated killing of both human pancreatic cancer and stellate cells. *Oncotarget* 2017;8:56968-56979.
233. Huang Q, Huang M, Meng F, et al. Activated pancreatic stellate cells inhibit NK cell function in the human pancreatic cancer microenvironment. *Cell Mol Immunol* 2019;16:87-89.
234. Kyriazis AA, Kyriazis AP, Sternberg CN, et al. Morphological, biological, biochemical, and karyotypic characteristics of human pancreatic ductal adenocarcinoma Capan-2 in tissue culture and the nude mouse. *Cancer Res* 1986;46:5810-5.
235. Barton CM, Staddon SL, Hughes CM, et al. Abnormalities of the p53 tumour suppressor gene in human pancreatic cancer. *Br J Cancer* 1991;64:1076-82.
236. Tan MH, Nowak NJ, Loo R, et al. Characterization of a new primary human pancreatic tumor line. *Cancer Invest* 1986;4:15-23.
237. Froeling FE, Mirza TA, Feakins RM, et al. Organotypic culture model of pancreatic cancer demonstrates that stromal cells modulate E-cadherin, beta-catenin, and Ezrin expression in tumor cells. *Am J Pathol* 2009;175:636-48.

238. Gong JH, Maki G, Klingemann HG. Characterization of a human cell line (NK-92) with phenotypical and functional characteristics of activated natural killer cells. *Leukemia* 1994;8:652-8.
239. Loukopoulos P, Kanetaka K, Takamura M, et al. Orthotopic Transplantation Models of Pancreatic Adenocarcinoma Derived From Cell Lines and Primary Tumors and Displaying Varying Metastatic Activity. *Pancreas* 2004;29.
240. Caldas C, Hahn SA, da Costa LT, et al. Frequent somatic mutations and homozygous deletions of the p16 (MTS1) gene in pancreatic adenocarcinoma. *Nature Genetics* 1994;8:27-32.
241. Apaolaza PS, Petropoulou P-I, Rodriguez-Calvo T. Whole-Slide Image Analysis of Human Pancreas Samples to Elucidate the Immunopathogenesis of Type 1 Diabetes Using the QuPath Software. *Frontiers in Molecular Biosciences* 2021;8.
242. Deer EL, González-Hernández J, Coursen JD, et al. Phenotype and genotype of pancreatic cancer cell lines. *Pancreas* 2010;39:425-35.
243. Berrozpe G, Schaeffer J, Peinado MA, et al. Comparative analysis of mutations in the p53 and K-ras genes in pancreatic cancer. *Int J Cancer* 1994;58:185-91.
244. Moore PS, Sipos B, Orlandini S, et al. Genetic profile of 22 pancreatic carcinoma cell lines. *Virchows Archiv* 2001;439:798-802.
245. Park LM, Lannigan J, Jaimes MC. OMIP-069: Forty-Color Full Spectrum Flow Cytometry Panel for Deep Immunophenotyping of Major Cell Subsets in Human Peripheral Blood. *Cytometry Part A* 2020;97:1044-1051.
246. Bryceson YT, Fauriat C, Nunes JM, et al. Functional analysis of human NK cells by flow cytometry. *Methods Mol Biol* 2010;612:335-52.
247. Somanchi SS, Senyukov VV, Denman CJ, et al. Expansion, purification, and functional assessment of human peripheral blood NK cells. *J Vis Exp* 2011.
248. Neri S, Mariani E, Meneghetti A, et al. Calcein-acetyoxymethyl cytotoxicity assay: standardization of a method allowing additional analyses on recovered effector cells and supernatants. *Clin Diagn Lab Immunol* 2001;8:1131-5.
249. Gu Z, Eils R, Schlesner M. Complex heatmaps reveal patterns and correlations in multidimensional genomic data. *Bioinformatics* 2016;32:2847-2849.
250. Liebermeister W, Noor E, Flamholz A, et al. Visual account of protein investment in cellular functions. *Proc Natl Acad Sci U S A* 2014;111:8488-93.

251. Tang Z, Li C, Kang B, et al. GEPIA: a web server for cancer and normal gene expression profiling and interactive analyses. *Nucleic Acids Research* 2017;45:W98-W102.
252. Wu Y, Zhang C, Jiang K, et al. The Role of Stellate Cells in Pancreatic Ductal Adenocarcinoma: Targeting Perspectives. *Front Oncol* 2020;10:621937.
253. Liu S, Galat V, Galat Y, et al. NK cell-based cancer immunotherapy: from basic biology to clinical development. *Journal of Hematology & Oncology* 2021;14:7.
254. Wang Z, He R, Dong S, et al. Pancreatic stellate cells in pancreatic cancer: as potential targets for future therapy. *Frontiers in oncology*. Volume 13, 2023:1185093.
255. Alter G, Malenfant JM, Altfeld M. CD107a as a functional marker for the identification of natural killer cell activity. *Journal of Immunological Methods* 2004;294:15-22.
256. Lee Y, Shin H, Kim J. In vivo anti-cancer effects of resveratrol mediated by NK cell activation. *Journal of Innate Immunity* 2021;13:94-106.
257. Ahn S, Woo JW, Lee K, et al. HER2 status in breast cancer: changes in guidelines and complicating factors for interpretation. *J Pathol Transl Med* 2020;54:34-44.
258. Estes G, Felgueres MJ, García-Jiménez ÁF, et al. BCG-activation of leukocytes is sufficient for the generation of donor-independent innate anti-tumor NK and $\gamma\delta$ T-cells that can be further expanded in vitro. *OncolImmunology* 2023;12:2160094.
259. Kiesgen S, Messinger JC, Chintala NK, et al. Comparative analysis of assays to measure CAR T-cell-mediated cytotoxicity. *Nature protocols* 2021;16:1331-1342.
260. Park J-E, Kim S-E, Keam B, et al. Anti-tumor effects of NK cells and anti-PD-L1 antibody with antibody-dependent cellular cytotoxicity in PD-L1-positive cancer cell lines. *Journal for ImmunoTherapy of Cancer* 2020;8:e000873.
261. Samson A, Bentham MJ, Scott K, et al. Oncolytic reovirus as a combined antiviral and anti-tumour agent for the treatment of liver cancer. *Gut* 2018;67:562-573.
262. Maecker H, Trotter J. Selecting reagents for multicolor flow cytometry with BD™ LSR II and BD FACSCanto™ systems. *Nature Methods* 2008;5:an6-an7.
263. Factors Regulating the Cytotoxic Activity of the Human Natural Killer Cell Line, NK-92. *Journal of Hematotherapy & Stem Cell Research* 2001;10:369-383.
264. Malchiodi ZX, Weiner LM. Understanding and Targeting Natural Killer Cell-Cancer-Associated Fibroblast Interactions in Pancreatic Ductal Adenocarcinoma. *Cancers (Basel)* 2021;13.

265. Cesmeli S, Goker Bagca B, Caglar HO, et al. Combination of resveratrol and BIBR1532 inhibits proliferation of colon cancer cells by repressing expression of LncRNAs. *Medical Oncology* 2022;39:1-10.
266. Zhang B, Zhang J, Tian Z. Comparison in the effects of IL-2, IL-12, IL-15 and IFN α on gene regulation of granzymes of human NK cell line NK-92. *International Immunopharmacology* 2008;8:989-996.
267. Tomescu C, Chehimi J, Maino VC, et al. Retention of viability, cytotoxicity, and response to IL-2, IL-15, or IFN-alpha by human NK cells after CD107a degranulation. *J Leukoc Biol* 2009;85:871-6.
268. Kasarci G, Ertugrul B, Iplik ES, et al. The apoptotic efficacy of succinic acid on renal cancer cell lines. *Medical Oncology* 2021;38:144.
269. Heshmatian B, Behrouzkia Z, Mohammadian M, et al. Cytotoxic and Radiosensitizing Effects of Folic Acid-Conjugated Gold Nanoparticles and Doxorubicin on Colorectal Cancer Cells. *Adv Pharm Bull* 2022;12:772-779.
270. Prado IB, Laudanna AA, Carneiro CRW. Susceptibility of colorectal-carcinoma cells to natural-killer-mediated lysis: Relationship to CEA expression and degree of differentiation. *International Journal of Cancer* 1995;61:854-860.
271. Bonilla DL, Reinin G, Chua E. Full Spectrum Flow Cytometry as a Powerful Technology for Cancer Immunotherapy Research. *Front Mol Biosci* 2020;7:612801.
272. Miller JS, Lanier LL. Natural Killer Cells in Cancer Immunotherapy. *Annual Review of Cancer Biology* 2019;3:77-103.
273. Montalban-Arques A, Gorkiewicz G, Mulero V, et al. Cytokine intervention: a double edged sword in the NKG2D system regulation. *Immunome Res* 2014;2:1-11.
274. Choi SH, Kim HJ, Park JD, et al. Chemical priming of natural killer cells with branched polyethylenimine for cancer immunotherapy. *Journal for ImmunoTherapy of Cancer* 2022;10:e004964.
275. Supadmanaba IGP, Mantini G, Randazzo O, et al. Interrelationship between miRNA and splicing factors in pancreatic ductal adenocarcinoma. *Epigenetics* 2022;17:381-404.
276. Fincham REA, Bashiri H, Lau MC, et al. Editorial: Multiplex Immunohistochemistry/Immunofluorescence Technique: The Potential and Promise for Clinical Application. *Frontiers in Molecular Biosciences* 2022;9.

277. Tan WCC, Nerurkar SN, Cai HY, et al. Overview of multiplex immunohistochemistry/immunofluorescence techniques in the era of cancer immunotherapy. *Cancer Commun (Lond)* 2020;40:135-153.
278. Parra ER, Jiang M, Solis L, et al. Procedural Requirements and Recommendations for Multiplex Immunofluorescence Tyramide Signal Amplification Assays to Support Translational Oncology Studies. *Cancers (Basel)* 2020;12.
279. Locke D, Hoyt CC. Companion diagnostic requirements for spatial biology using multiplex immunofluorescence and multispectral imaging. *Frontiers in Molecular Biosciences* 2023;10:1051491.
280. Taube JM, Akturk G, Angelo M, et al. The Society for Immunotherapy of Cancer statement on best practices for multiplex immunohistochemistry (IHC) and immunofluorescence (IF) staining and validation. *J Immunother Cancer* 2020;8.
281. Nazemalhosseini-Mojarad E, Mohammadpour S, Torshizi Esafahani A, et al. Intratumoral infiltrating lymphocytes correlate with improved survival in colorectal cancer patients: Independent of oncogenetic features. *Journal of Cellular Physiology* 2019;234:4768-4777.
282. Masugi Y, Abe T, Ueno A, et al. Characterization of spatial distribution of tumor-infiltrating CD8+ T cells refines their prognostic utility for pancreatic cancer survival. *Modern Pathology* 2019;32:1495-1507.
283. Mezheyeuski A, Bergsland CH, Backman M, et al. Multispectral imaging for quantitative and compartment-specific immune infiltrates reveals distinct immune profiles that classify lung cancer patients. *J Pathol* 2018;244:421-431.
284. Backman M, Strell C, Lindberg A, et al. Spatial immunophenotyping of the tumour microenvironment in non-small cell lung cancer. *Eur J Cancer* 2023;185:40-52.
285. Tsujikawa T, Mitsuda J, Ogi H, et al. Prognostic significance of spatial immune profiles in human solid cancers. *Cancer Science* 2020;111:3426-3434.
286. Hernandez S, Rojas F, Laberiano C, et al. Multiplex Immunofluorescence Tyramide Signal Amplification for Immune Cell Profiling of Paraffin-Embedded Tumor Tissues. *Frontiers in Molecular Biosciences* 2021;8.
287. Bankhead P, Loughrey MB, Fernández JA, et al. QuPath: Open source software for digital pathology image analysis. *Scientific Reports* 2017;7:16878.

288. Li B, Pei G, Yao J, et al. Cell-type deconvolution analysis identifies cancer-associated myofibroblast component as a poor prognostic factor in multiple cancer types. *Oncogene* 2021;40:4686-4694.
289. Oliveira LdM, Teixeira FME, Sato MN. Impact of Retinoic Acid on Immune Cells and Inflammatory Diseases. *Mediators of Inflammation* 2018;2018:3067126.
290. Radaeva S, Wang L, Radaev S, et al. Retinoic acid signaling sensitizes hepatic stellate cells to NK cell killing via upregulation of NK cell activating ligand RAE1. *American Journal of Physiology-Gastrointestinal and Liver Physiology* 2007;293:G809-G816.
291. Cerwenka A, Lanier LL. Ligands for natural killer cell receptors: redundancy or specificity. *Immunological Reviews* 2001;181:158-169.
292. Conserva MR, Anelli L, Zagaria A, et al. The Pleiotropic Role of Retinoic Acid/Retinoic Acid Receptors Signaling: From Vitamin A Metabolism to Gene Rearrangements in Acute Promyelocytic Leukemia. *Int J Mol Sci* 2019;20.
293. Hughes CS, ChinAleong J-A, Kocher HM. CRABP2 and FABP5 expression levels in diseased and normal pancreas. *Annals of Diagnostic Pathology* 2020;47:151557.
294. Liao Z, Yao H, Wei J, et al. Development and validation of the prognostic value of the immune-related genes in clear cell renal cell carcinoma. *Transl Androl Urol* 2021;10:1607-1619.
295. Fu HY, Bao WM, Yang CX, et al. Kupffer Cells Regulate Natural Killer Cells Via the NK group 2, Member D (NKG2D)/Retinoic Acid Early Inducible-1 (RAE-1) Interaction and Cytokines in a Primary Biliary Cholangitis Mouse Model. *Med Sci Monit* 2020;26:e923726.
296. Jinushi M, Takehara T, Tatsumi T, et al. Expression and role of MICA and MICB in human hepatocellular carcinomas and their regulation by retinoic acid. *International Journal of Cancer* 2003;104:354-361.
297. Masamune A, Shimosegawa T. Signal transduction in pancreatic stellate cells. *Journal of Gastroenterology* 2009;44:249-260.
298. Huang H, Zhang Y, Gallegos V, et al. Targeting TGF β R2-mutant tumors exposes vulnerabilities to stromal TGF β blockade in pancreatic cancer. *EMBO Molecular Medicine* 2019;11:e10515.

299. Shi J, Zhao J, Zhang X, et al. Activated hepatic stellate cells impair NK cell anti-fibrosis capacity through a TGF- β -dependent emperipolesis in HBV cirrhotic patients. *Sci Rep* 2017;7:44544.
300. Li A, He M, Wang H, et al. All-trans retinoic acid negatively regulates cytotoxic activities of nature killer cell line 92. *Biochemical and biophysical research communications* 2007;352:42-47.
301. Gunaydin SD, Tezcan I. Evaluation of peripheral lymphocyte subsets in acne vulgaris patients before and after systemic isotretinoin treatment. *Indian J Pharmacol* 2022;54:338-344.
302. Sanchez-Martínez D, Krzywinska E, Rathore MG, et al. All-trans retinoic acid (ATRA) induces miR-23a expression, decreases CTSC expression and granzyme B activity leading to impaired NK cell cytotoxicity. *The International Journal of Biochemistry & Cell Biology* 2014;49:42-52.
303. Dunham RM, Thapa M, Velazquez VM, et al. Hepatic stellate cells preferentially induce Foxp3⁺ regulatory T cells by production of retinoic acid. *J Immunol* 2013;190:2009-16.
304. Theodosiou M, Laudet V, Schubert M. From carrot to clinic: an overview of the retinoic acid signaling pathway. *Cellular and Molecular Life Sciences* 2010;67:1423-1445.
305. Ferreira R, Napoli J, Enver T, et al. Advances and challenges in retinoid delivery systems in regenerative and therapeutic medicine. *Nature Communications* 2020;11:4265.
306. Kim H-A, Kim H, Nam M-K, et al. Suppression of the antitumoral activity of natural killer cells under indirect coculture with cancer-associated fibroblasts in a pancreatic TIME-on-chip model. *Cancer Cell International* 2023;23:219.
307. Carannante V, Wiklund M, Önfelt B. In vitro models to study natural killer cell dynamics in the tumor microenvironment. *Front Immunol* 2023;14:1135148.
308. Sutherland RM, MacDonald HR, Howell RL. Multicellular spheroids: a new model target for in vitro studies of immunity to solid tumor allografts. *J Natl Cancer Inst* 1977;58:1849-53.
309. Ivascu A, Kubbies M. Rapid Generation of Single-Tumor Spheroids for High-Throughput Cell Function and Toxicity Analysis. *Journal of Biomolecular Screening* 2006;11:922-932.
310. Giannattasio A, Weil S, Kloess S, et al. Cytotoxicity and infiltration of human NK cells in in vivo-like tumor spheroids. *BMC Cancer* 2015;15:351.

311. Keller GM. In vitro differentiation of embryonic stem cells. *Current Opinion in Cell Biology* 1995;7:862-869.
312. Kelm JM, Timmins NE, Brown CJ, et al. Method for generation of homogeneous multicellular tumor spheroids applicable to a wide variety of cell types. *Biotechnology and Bioengineering* 2003;83:173-180.
313. Ware MJ, Colbert K, Keshishian V, et al. Generation of Homogenous Three-Dimensional Pancreatic Cancer Cell Spheroids Using an Improved Hanging Drop Technique. *Tissue Eng Part C Methods* 2016;22:312-21.
314. Lanuza PM, Viguera A, Olivan S, et al. Activated human primary NK cells efficiently kill colorectal cancer cells in 3D spheroid cultures irrespectively of the level of PD-L1 expression. *Oncoimmunology* 2018;7:e1395123.
315. Murray ER, Menezes S, Henry JC, et al. Disruption of pancreatic stellate cell myofibroblast phenotype promotes pancreatic tumor invasion. *Cell Rep* 2022;38:110227.
316. Marrella A, Dondero A, Aiello M, et al. Cell-Laden Hydrogel as a Clinical-Relevant 3D Model for Analyzing Neuroblastoma Growth, Immunophenotype, and Susceptibility to Therapies. *Front Immunol* 2019;10:1876.
317. Ayuso JM, Truttschel R, Gong MM, et al. Evaluating natural killer cell cytotoxicity against solid tumors using a microfluidic model. *Oncoimmunology* 2019;8:1553477.
318. Jin G, Hong W, Guo Y, et al. Molecular Mechanism of Pancreatic Stellate Cells Activation in Chronic Pancreatitis and Pancreatic Cancer. *J Cancer* 2020;11:1505-1515.
319. Wells RG, Discher DE. Matrix elasticity, cytoskeletal tension, and TGF-beta: the insoluble and soluble meet. *Sci Signal* 2008;1:pe13.
320. Sarper M, Cortes E, Lieberthal TJ, et al. ATRA modulates mechanical activation of TGF- β by pancreatic stellate cells. *Sci Rep* 2016;6:27639.
321. Ohnishi H, Miyata T, Yasuda H, et al. Distinct Roles of Smad2-, Smad3-, and ERK-dependent Pathways in Transforming Growth Factor- β Regulation of Pancreatic Stellate Cellular Functions *. *Journal of Biological Chemistry* 2004;279:8873-8878.
322. Apte MV, Haber PS, Darby SJ, et al. Pancreatic stellate cells are activated by proinflammatory cytokines: implications for pancreatic fibrogenesis. *Gut* 1999;44:534-41.

323. Jang DI, Lee AH, Shin HY, et al. The Role of Tumor Necrosis Factor Alpha (TNF- α) in Autoimmune Disease and Current TNF- α Inhibitors in Therapeutics. *Int J Mol Sci* 2021;22.
324. Papiris SA, Tomos IP, Karakatsani A, et al. High levels of IL-6 and IL-8 characterize early-on idiopathic pulmonary fibrosis acute exacerbations. *Cytokine* 2018;102:168-172.
325. Singh S, Anshita D, Ravichandiran V. MCP-1: Function, regulation, and involvement in disease. *International Immunopharmacology* 2021;101:107598.
326. Li X, Wang Z, Ma Q, et al. Sonic Hedgehog Paracrine Signaling Activates Stromal Cells to Promote Perineural Invasion in Pancreatic Cancer. *Clinical Cancer Research* 2014;20:4326-4338.
327. Chang BE, Blader P, Fischer N, et al. Axial (HNF3 β) and retinoic acid receptors are regulators of the zebrafish sonic hedgehog promoter. *Embo j* 1997;16:3955-64.
328. Wang J, Lin W, Popko B, et al. Inducible production of interferon- γ in the developing brain causes cerebellar dysplasia with activation of the Sonic hedgehog pathway. *Molecular and Cellular Neuroscience* 2004;27:489-496.
329. Sigafos AN, Paradise BD, Fernandez-Zapico ME. Hedgehog/GLI Signaling Pathway: Transduction, Regulation, and Implications for Disease. *Cancers (Basel)* 2021;13.
330. Wang Y, Jin G, Li Q, et al. Hedgehog Signaling Non-Canonical Activated by Pro-Inflammatory Cytokines in Pancreatic Ductal Adenocarcinoma. *J Cancer* 2016;7:2067-2076.
331. Steele NG, Biffi G, Kemp SB, et al. Inhibition of Hedgehog Signaling Alters Fibroblast Composition in Pancreatic Cancer. *Clin Cancer Res* 2021;27:2023-2037.
332. Lamb RF, Ozanne BW, Roy C, et al. Essential functions of ezrin in maintenance of cell shape and lamellipodial extension in normal and transformed fibroblasts. *Curr Biol* 1997;7:682-8.
333. Hu G, Zhong K, Chen W, et al. Podoplanin-positive cancer-associated fibroblasts predict poor prognosis in lung cancer patients. *Onco Targets Ther* 2018;11:5607-5619.
334. Tanaka Y, Ohno T, Kadonaga T, et al. Podoplanin expression in cancer-associated fibroblasts predicts unfavorable prognosis in node-negative breast cancer patients with hormone receptor-positive/HER2 - negative subtype. *Breast cancer (Tokyo, Japan)* 2021;28:822-828.

335. Hirayama K, Kono H, Nakata Y, et al. Expression of podoplanin in stromal fibroblasts plays a pivotal role in the prognosis of patients with pancreatic cancer. *Surg Today* 2018;48:110-118.
336. Croft W, Pearce H, Margielewska-Davies S, et al. Spatial determination and prognostic impact of the fibroblast transcriptome in pancreatic ductal adenocarcinoma. *eLife* 2023;12:e86125.
337. Wang X, Carvalho V, Wang Q, et al. Screening and Identification of Key Genes for Activation of Islet Stellate Cell. *Frontiers in Endocrinology* 2021;12.
338. Kunita A, Baeriswyl V, Meda C, et al. Inflammatory Cytokines Induce Podoplanin Expression at the Tumor Invasive Front. *The American Journal of Pathology* 2018;188:1276-1288.
339. Wang R, Jaw JJ, Stutzman NC, et al. Natural killer cell-produced IFN- γ and TNF- α induce target cell cytotoxicity through up-regulation of ICAM-1. *J Leukoc Biol* 2012;91:299-309.
340. Suzuki H, Kaneko MK, Kato Y. Roles of Podoplanin in Malignant Progression of Tumor. *Cells* 2022;11:575.
341. Giurisato E, Cella M, Takai T, et al. Phosphatidylinositol 3-Kinase Activation Is Required To Form the NKG2D Immunological Synapse. *Molecular and Cellular Biology* 2007;27:8583-8599.
342. Chen J, Xu H, Zhu XX. Abnormal expression levels of sMICA and NKG2D are correlated with poor prognosis in pancreatic cancer. *Ther Clin Risk Manag* 2016;12:11-8.
343. Duan X, Deng L, Chen X, et al. Clinical significance of the immunostimulatory MHC class I chain-related molecule A and NKG2D receptor on NK cells in pancreatic cancer. *Medical Oncology* 2011;28:466-474.
344. Liu X, Song J, Zhang H, et al. Immune checkpoint HLA-E:CD94-NKG2A mediates evasion of circulating tumor cells from NK cell surveillance. *Cancer Cell* 2023;41:272-287.e9.
345. Wang H, Cao K, Liu S, et al. Tim-3 Expression Causes NK Cell Dysfunction in Type 2 Diabetes Patients. *Frontiers in Immunology* 2022;13.
346. Rocca YS, Roberti MP, Arriaga JM, et al. Altered phenotype in peripheral blood and tumor-associated NK cells from colorectal cancer patients. *Innate Immunity* 2013;19:76-85.

347. Tan S, Xu Y, Wang Z, et al. Tim-3 Hampers Tumor Surveillance of Liver-Resident and Conventional NK Cells by Disrupting PI3K Signaling. *Cancer Research* 2020;80:1130-1142.
348. Jin S, Deng Y, Hao JW, et al. NK cell phenotypic modulation in lung cancer environment. *PLoS One* 2014;9:e109976.
349. Zheng Y, Li Y, Lian J, et al. TNF- α -induced Tim-3 expression marks the dysfunction of infiltrating natural killer cells in human esophageal cancer. *Journal of Translational Medicine* 2019;17:165.
350. Secchiari F, Nuñez SY, Sierra JM, et al. The MICA-NKG2D axis in clear cell renal cell carcinoma bolsters MICA as target in immuno-oncology. *Oncolmunology* 2022;11:2104991.
351. Brooks AJ, Putoczki T. JAK-STAT Signalling Pathway in Cancer. *Cancers (Basel)* 2020;12.
352. Majoros A, Platanitis E, Kernbauer-Hölzl E, et al. Canonical and Non-Canonical Aspects of JAK-STAT Signaling: Lessons from Interferons for Cytokine Responses. *Front Immunol* 2017;8:29.
353. Rateitschak K, Karger A, Fitzner B, et al. Mathematical modelling of interferon- γ signalling in pancreatic stellate cells reflects and predicts the dynamics of STAT1 pathway activity. *Cellular Signalling* 2010;22:97-105.
354. Bellucci R, Martin A, Bommarito D, et al. Interferon- γ -induced activation of JAK1 and JAK2 suppresses tumor cell susceptibility to NK cells through upregulation of PD-L1 expression. *Oncoimmunology* 2015;4:e1008824.
355. Carter EP, Coetzee AS, Tomas Bort E, et al. Dissecting FGF Signalling to Target Cellular Crosstalk in Pancreatic Cancer. *Cells* 2021;10.
356. Clayton NS, Wilson AS, Laurent EP, et al. Fibroblast growth factor–mediated crosstalk in cancer etiology and treatment. *Developmental Dynamics* 2017;246:493-501.
357. Akl MR, Nagpal P, Ayoub NM, et al. Molecular and clinical significance of fibroblast growth factor 2 (FGF2 /bFGF) in malignancies of solid and hematological cancers for personalized therapies. *Oncotarget* 2016;7:44735-44762.
358. Lin N, Chen S, Pan W, et al. NP603, a novel and potent inhibitor of FGFR1 tyrosine kinase, inhibits hepatic stellate cell proliferation and ameliorates hepatic fibrosis in rats. *American Journal of Physiology-Cell Physiology* 2011;301:C469-C477.

359. Yu C, Wang F, Jin C, et al. Role of Fibroblast Growth Factor Type 1 and 2 in Carbon Tetrachloride-Induced Hepatic Injury and Fibrogenesis. *The American Journal of Pathology* 2003;163:1653-1662.
360. Tsunematsu H, Tatsumi T, Kohga K, et al. Fibroblast growth factor-2 enhances NK sensitivity of hepatocellular carcinoma cells. *International Journal of Cancer* 2012;130:356-364.
361. Lewis CE, Ramshaw AL, Lorenzen J, et al. Basic fibroblast growth factor and interleukins 4 and 6 stimulate the release of IFN-gamma by individual NK cells. *Cell Immunol* 1991;132:158-67.
362. Deracinois B, Flahaut C, Duban-Deweer S, et al. Comparative and Quantitative Global Proteomics Approaches: An Overview. *Proteomes* 2013;1:180-218.
363. Dupree EJ, Jayathirtha M, Yorkey H, et al. A Critical Review of Bottom-Up Proteomics: The Good, the Bad, and the Future of This Field. *Proteomes* 2020;8:14.
364. Al-Amrani S, Al-Jabri Z, Al-Zaabi A, et al. Proteomics: Concepts and applications in human medicine. *World J Biol Chem* 2021;12:57-69.
365. Poznanski SM, Singh K, Ritchie TM, et al. Metabolic flexibility determines human NK cell functional fate in the tumor microenvironment. *Cell Metabolism* 2021;33:1205-1220.e5.
366. Zhou R, Shanas R, Nelson MA, et al. Increased expression of the heterogeneous nuclear ribonucleoprotein K in pancreatic cancer and its association with the mutant p53. *Int J Cancer* 2010;126:395-404.
367. He D, Huang C, Zhou Q, et al. HnRNPK/miR-223/FBXW7 feedback cascade promotes pancreatic cancer cell growth and invasion. *Oncotarget* 2017;8:20165-20178.
368. Xu Y, Wu W, Han Q, et al. Post-translational modification control of RNA-binding protein hnRNPK function. *Open Biol* 2019;9:180239.
369. Ren D, Sun Y, Zhang D, et al. SGLT2 promotes pancreatic cancer progression by activating the Hippo signaling pathway via the hnRNPK-YAP1 axis. *Cancer Lett* 2021;519:277-288.
370. Lamers-Kok N, Panella D, Georgoudaki A-M, et al. Natural killer cells in clinical development as non-engineered, engineered, and combination therapies. *Journal of Hematology & Oncology* 2022;15:164.

371. Li C, Yang N, Li H, et al. Robo1-specific chimeric antigen receptor natural killer cell therapy for pancreatic ductal adenocarcinoma with liver metastasis. *J Cancer Res Ther* 2020;16:393-396.
372. Wang Z. Clinical Research of ROBO1 Specific BiCAR-NK Cells on Patients With Pancreatic Cancer. In: ClinicalTrials.gov [Internet]. Bethesda (MD): U.S. National Library of Medicine. Available from: <http://clinicaltrials.gov/show/NCT03941457> ClinicalTrials.gov Identifier: NCT03941457. Accessed 1st Oct 2023.
373. Lu PP. Study of Anti-5T4 CAR-NK Cell Therapy in Advanced Solid Tumors. In: ClinicalTrials.gov [Internet]. Bethesda (MD): U.S. National Library of Medicine. Available from: <https://www.clinicaltrials.gov/study/NCT05194709> ClinicalTrials.gov Identifier: NCT05194709. Accessed 1st Oct 2023.
374. Li J. Study of Anti-5T4 CAR-raNK Cell Therapy in Locally Advanced or Metastatic Solid Tumors. In: ClinicalTrials.gov [Internet]. Bethesda (MD): U.S. National Library of Medicine. Available from: <https://www.clinicaltrials.gov/study/NCT05137275> ClinicalTrials.gov Identifier: NCT05137275. Accessed 1st Oct 2023.
375. Stern PL, Harrop R. 5T4 oncofoetal antigen: an attractive target for immune intervention in cancer. *Cancer Immunology, Immunotherapy* 2017;66:415-426.
376. Shah NN, Baird K, Delbrook CP, et al. Acute GVHD in patients receiving IL-15/4-1BBL activated NK cells following T-cell-depleted stem cell transplantation. *Blood* 2015;125:784-92.
377. Ogobuiro I, Baca Y, Ribeiro JR, et al. Multi-omic characterization reveals a distinct molecular landscape in young-onset pancreatic cancer. *medRxiv* 2023.
378. Gürlevik E, Fleischmann-Mundt B, Brooks J, et al. Administration of Gemcitabine After Pancreatic Tumor Resection in Mice Induces an Antitumor Immune Response Mediated by Natural Killer Cells. *Gastroenterology* 2016;151:338-350.e7.
379. Yousuf S, Qiu M, Voith von Voithenberg L, et al. Spatially Resolved Multi-Omics Single-Cell Analyses Inform Mechanisms of Immune Dysfunction in Pancreatic Cancer. *Gastroenterology* 2023;165:891-908.e14.
380. Ying L, Yan F, Xu D. Cancer patient stratification based on the tumor microenvironment. *J Thorac Dis* 2020;12:4522-4526.

381. Halama N. The next age of immunotherapy: optimisation, stratification and therapeutic synergies. *British Journal of Cancer* 2019;120:1-2.
382. Li B, Jiang Y, Li G, et al. Natural killer cell and stroma abundance are independently prognostic and predict gastric cancer chemotherapy benefit. *JCI Insight* 2020;5.
383. Song P, Li W, Guo L, et al. Identification and Validation of a Novel Signature Based on NK Cell Marker Genes to Predict Prognosis and Immunotherapy Response in Lung Adenocarcinoma by Integrated Analysis of Single-Cell and Bulk RNA-Sequencing. *Frontiers in Immunology* 2022;13.
384. Lan Y, Jia Q, Feng M, et al. A novel natural killer cell-related signatures to predict prognosis and chemotherapy response of pancreatic cancer patients. *Frontiers in Genetics* 2023;14.
385. Lee H, Quek C, Silva I, et al. Integrated molecular and immunophenotypic analysis of NK cells in anti-PD-1 treated metastatic melanoma patients. *OncolImmunology* 2019;8:e1537581.
386. Muntasell A, Rojo F, Servitja S, et al. NK Cell Infiltrates and HLA Class I Expression in Primary HER2+ Breast Cancer Predict and Uncouple Pathological Response and Disease-free Survival. *Clinical Cancer Research* 2019;25:1535-1545.
387. Mi H, Sivagnanam S, Betts CB, et al. Quantitative Spatial Profiling of Immune Populations in Pancreatic Ductal Adenocarcinoma Reveals Tumor Microenvironment Heterogeneity and Prognostic Biomarkers. *Cancer Res* 2022;82:4359-4372.
388. Väyrynen JP, Haruki K, Lau MC, et al. Spatial Organization and Prognostic Significance of NK and NKT-like Cells via Multimarker Analysis of the Colorectal Cancer Microenvironment. *Cancer Immunol Res* 2022;10:215-227.
389. Karakas D, Erkisa M, Akar RO, et al. Targeting Periostin Expression Makes Pancreatic Cancer Spheroids More Vulnerable to Natural Killer Cells. *Biomedicines* 2023;11:270.
390. Piper M, Hoen M, Darragh LB, et al. Simultaneous targeting of PD-1 and IL-2R $\beta\gamma$ with radiation therapy inhibits pancreatic cancer growth and metastasis. *Cancer Cell* 2023;41:950-969.e6.
391. Kaur K, Chen PC, Ko MW, et al. Sequential therapy with supercharged NK cells with either chemotherapy drug cisplatin or anti-PD-1 antibody decreases the tumor size and significantly enhances the NK function in Hu-BLT mice. *Front Immunol* 2023;14:1132807.

392. Datta J, Dai X, Bianchi A, et al. Combined MEK and STAT3 Inhibition Uncovers Stromal Plasticity by Enriching for Cancer-Associated Fibroblasts With Mesenchymal Stem Cell-Like Features to Overcome Immunotherapy Resistance in Pancreatic Cancer. *Gastroenterology* 2022;163:1593-1612.

Appendix

CD107 Degranulation Assay

- 1) Label FACS tubes
- 2) Harvest, count & resuspend PBMCs @ 5×10^6 /ml in RPMI+10%FCS
- 3) Harvest, count & resuspend target cell lines @ 5×10^6 /ml in cell line-specific media
- 4) Add 300µl of RPMI+10%FCS to each tube
- 5) Add 100µl of PBMCs (i.e. 5×10^5 cells) to appropriate tubes
- 6) Add 100µl of target cells (i.e. at a 1:1 ratio with effectors) to appropriate tubes
- 7) Cover tubes loosely with Parafilm & incubate for 1hr at 37°C
- 8) Make up master-mix (in RPMI+10%FCS) of brefeldin A and antibodies, allowing for 100µl to be added to all tubes:

5µl of CD107a-FITC / tube

5µl of CD107b-FITC / tube

Brefeldin A at 1:1000 dilution / tube (0.5 µl)

3µl of CD3-PerCP / tube

2µl of CD56-PE / tube

- 1) Add 100µl of master-mix to tubes
- 2) Cover tubes loosely with Parafilm and return to incubator for 3-4hr

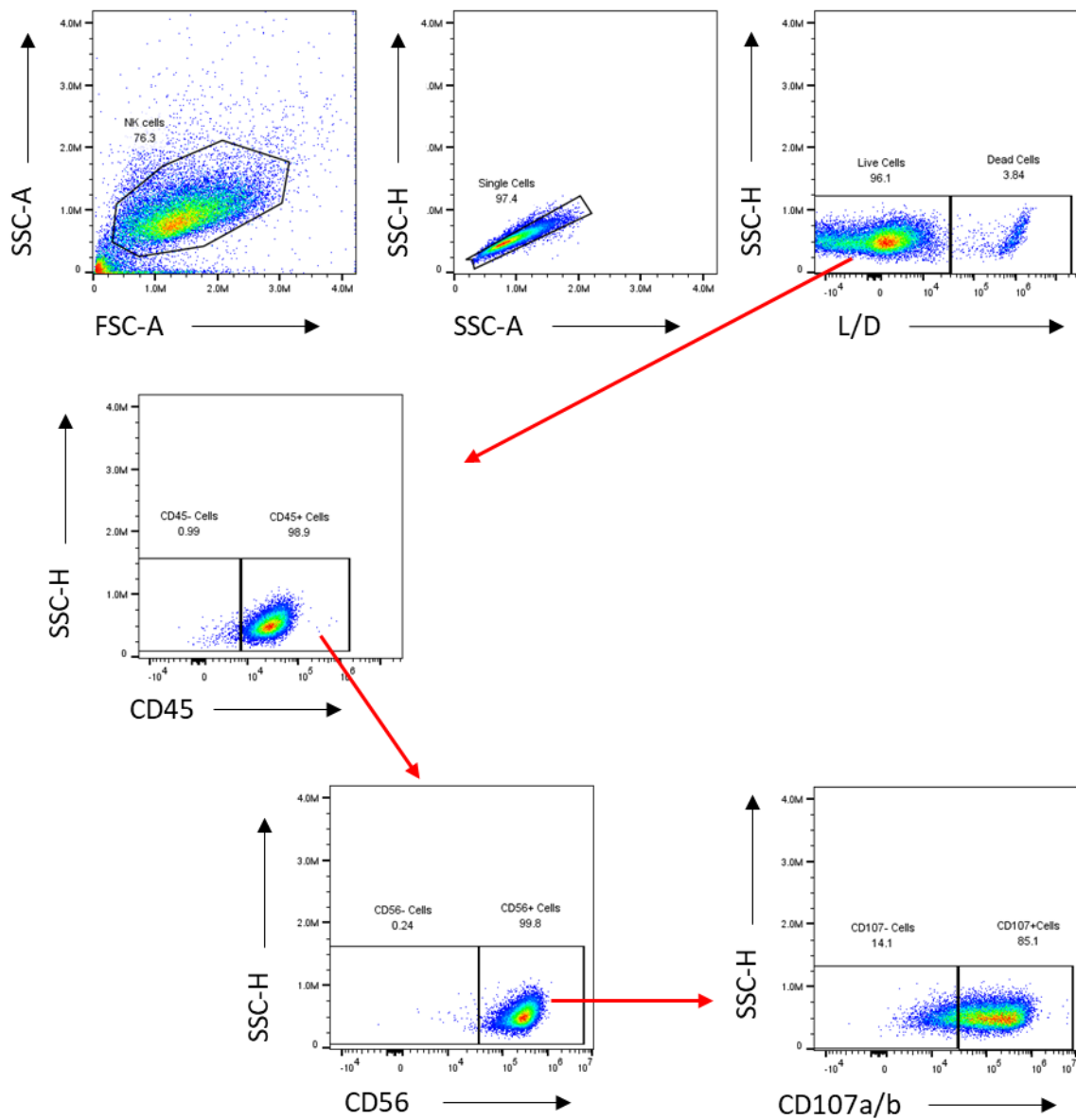
After incubation:

Add 2 ml FACS buffer to each tube & spin (400 g, 5min, acc 9, brake 9)

- 1) Discard supernatant

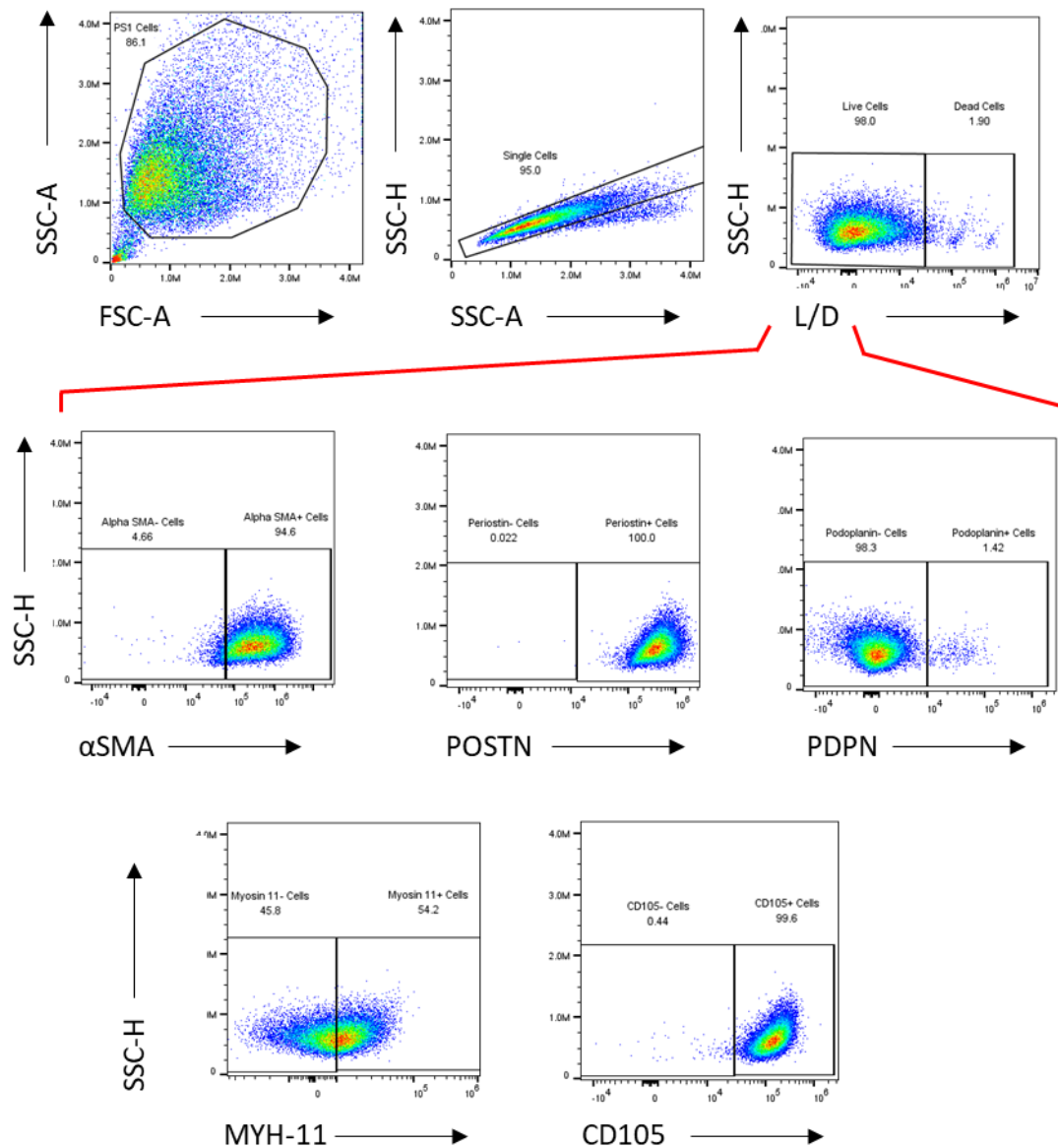
Fix cells in 150µl 1% PFA, cover with foil & keep at 4°C until data acquisition

Appendix 1: CD107 degranulation assay protocol provided by the Samson Lab.



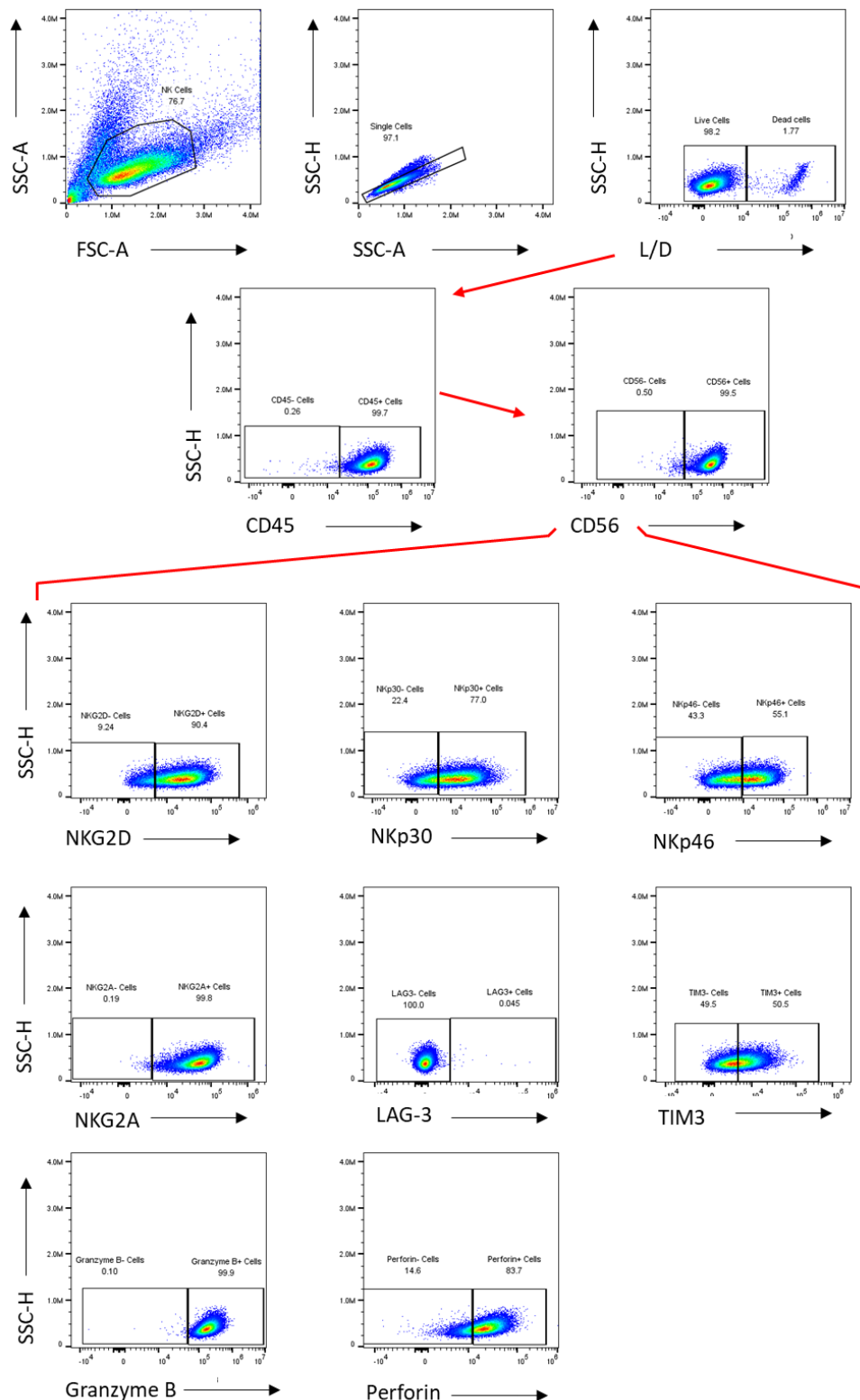
Appendix 2: Gating strategy for CD107 degranulation assays.

Cells were gated on single cells and live cells before identifying cells positive for CD45. CD56⁺ cells were identified from the CD45⁺ population before gating CD107a/b⁺ cells from the CD56⁺ pool.



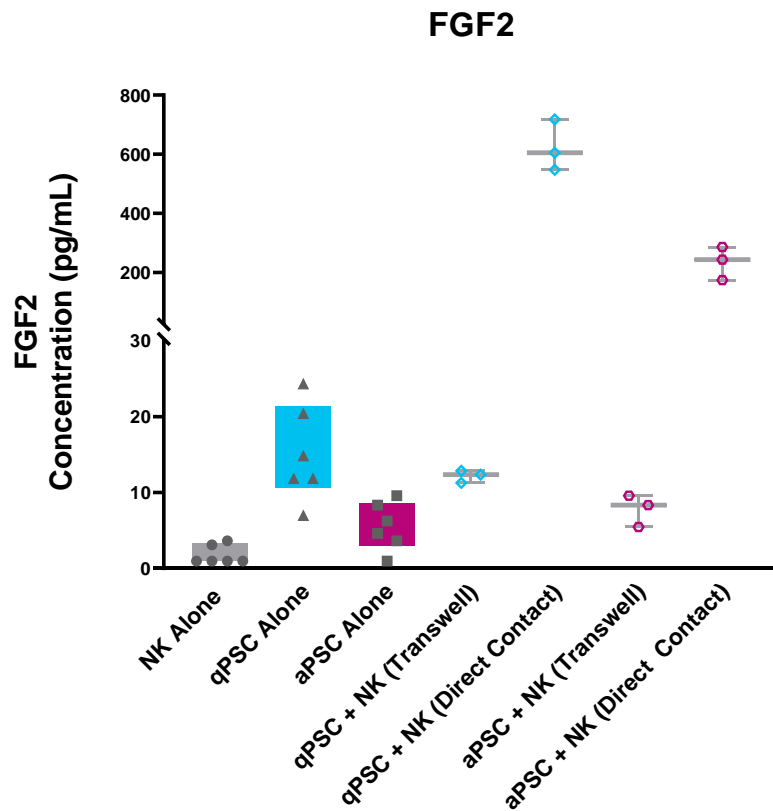
Appendix 3: Gating strategy for flow cytometric analysis of PSC markers in response to co-culture with NK cells.

PSCs were identified from their forward/side scatter profile. Doublets were then excluded, and live cells identified from the single cell gate. Individual PSC markers (alpha SMA, periostin, myosin-11, podoplanin and CD105) were then gated from the live cell population.



Appendix 4: Gating strategy for flow cytometric analysis of NK cell markers in response to co-culture with quiescent or activated PSCs.

NK cells were gated based on the forward/side scatter profile. Doublets were excluded and live cells identified from the single cell population. CD45 was then used to identify lymphocytes and from this population CD56⁺ cells were identified. All subsequent markers were gated from the CD45⁺CD56⁺ population.



Appendix 5: FGF2 expression in response to Direct and Transwell™ culture.

Abundance of FGF2 secreted in mono- and co-culture of NK and PSCs in direct contact and Transwell™ conditions. Analyte concentrations are displayed as picograms per mL. Data were analysed using Kruskal-Wallis analysis with Dunn's Post Hoc tests.

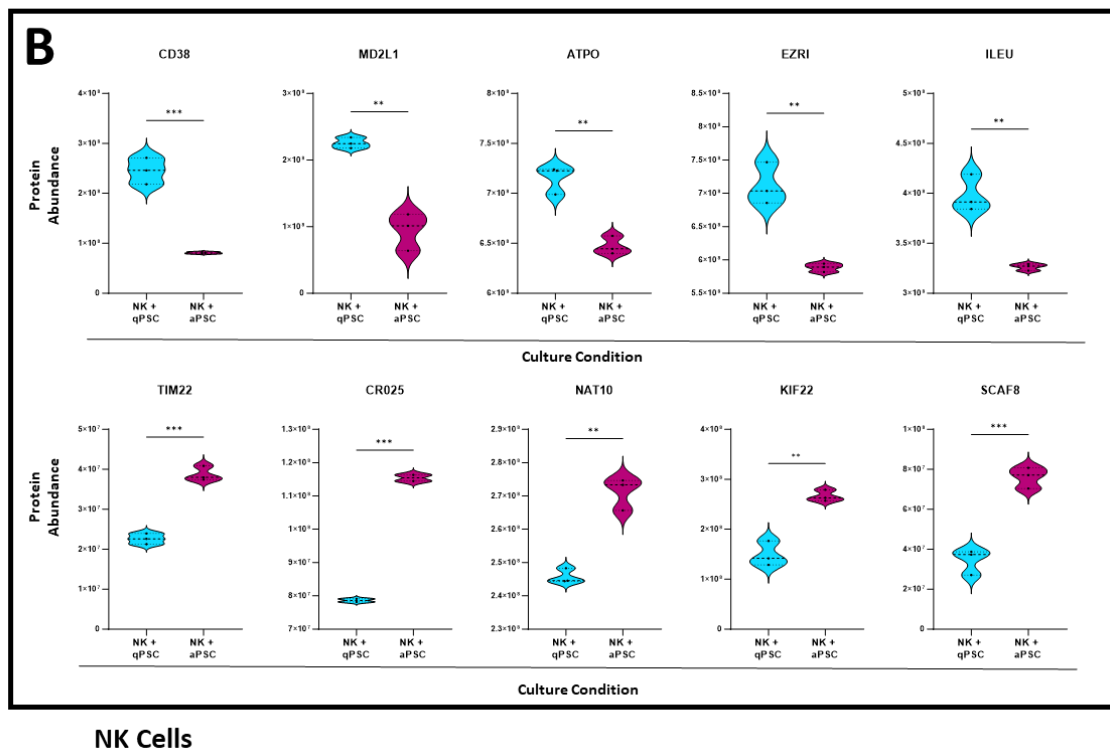
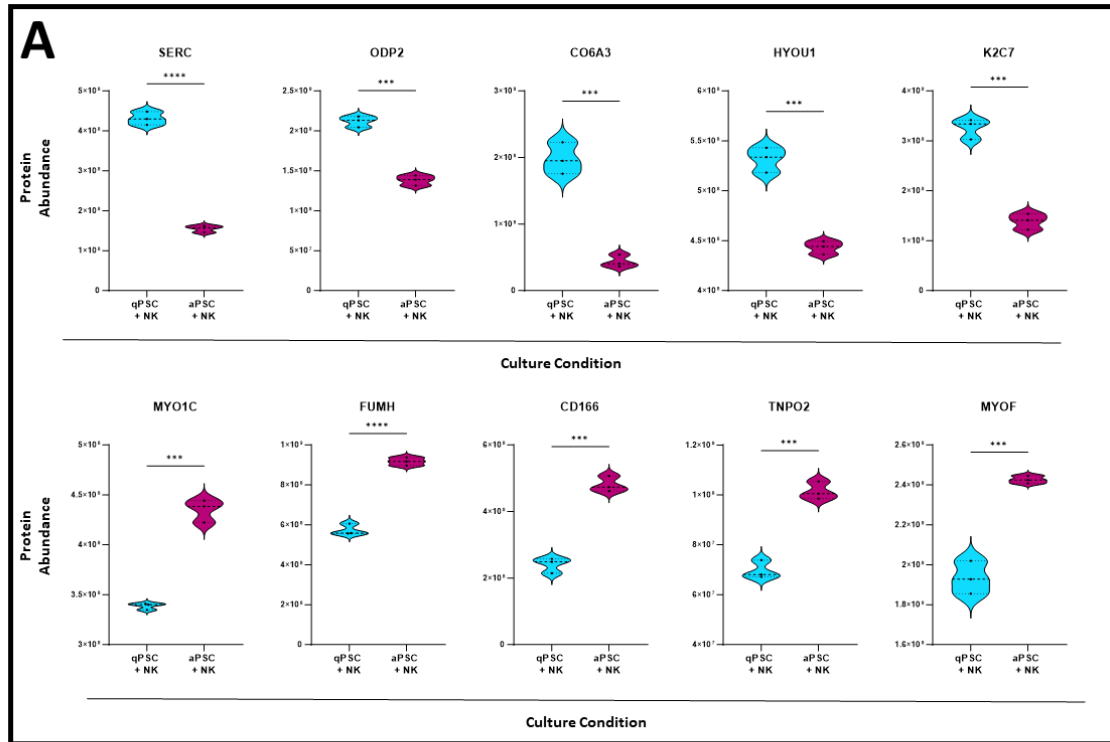
Analyte	Direct Contact					Transwell				
	NK Cells Alone	qPSC Alone	qPSC + NK Cells	aPSC Alone	aPSC + NK cells	NK Cells Alone	qPSC Alone	qPSC + NK Cells	aPSC Alone	aPSC + NK cells
APRIL	49.72	149.01	391.31	65.01	278.65	70.88	126.12	139.83	32.49	89.00
BAFF	39.28	121.92	342.91	86.47	381.77	27.82	77.63	106.13	70.33	90.74
CCL11	0.59	1.50	2.80	1.13	3.18	0.50	1.12	1.37	0.85	1.36
CCL2	1.17	4124.66	2087.49	3794.07	1896.73	1.46	5779.51	2204.26	2548.21	3507.58
CCL20	39.46	160.17	570.26	185.82	298.21	47.72	107.49	136.38	166.91	177.62
CCL24	22.57	47.06	91.97	25.87	98.20	18.88	44.80	50.91	22.83	42.46
CCL26	0.45	2.68	6.05	0.19	5.31	0.50	1.00	2.64	0.65	1.80
CCL3	6990.29	13.83	1105.05	6.12	828.84	1856.90	11.49	824.47	3.55	992.36
CCL4	2100.35	6.09	33430.87	2.31	20787.80	1288.49	2.90	2018.53	2.31	1794.86
CCL7	6.59	13.32	191.50	17.64	175.32	7.46	12.44	11.96	15.72	18.00
CCL8	0.21	0.41	706.59	0.17	681.48	0.15	0.28	0.47	0.10	0.83
CD30	48.81	207.91	406.36	51.56	397.89	39.85	135.15	210.55	36.61	112.69
CD40L	6.94	23.05	42.98	11.80	40.91	7.84	17.26	24.46	6.90	16.43
CTLA-8	35.58	87.74	163.44	36.80	166.81	34.86	65.42	88.71	29.81	63.17
CX3CL1	4.20	10.51	15.34	6.77	14.82	5.10	9.52	9.60	3.28	7.51
CXCL1	3.40	14.15	22.85	14.07	22.89	4.42	12.02	12.92	13.98	12.84
CXCL10	3.98	36.19	2565.38	20.09	2565.38	4.02	31.01	276.83	15.95	1052.44
CXCL11	16.08	11.88	5226.78	6.03	2787.32	16.15	8.98	40.88	6.08	89.21
CXCL12	85.00	996.72	704.80	1737.81	1344.53	94.85	779.51	736.74	1409.25	1410.89
CXCL13	11.60	40.05	69.81	33.40	72.67	17.01	34.89	39.55	25.74	36.58
CXCL5	3.01	12.42	23.26	3.73	22.24	1.42	8.98	13.07	1.65	6.24
CXCL9	3.12	35.22	2128.06	11.75	1383.91	2.15	32.50	37.41	4.18	24.84
FGF-2	1.68	17.22	623.47	6.48	234.73	1.85	12.82	12.16	4.63	7.78
G-CSF	9.26	42.12	78.88	37.10	69.91	21.85	35.78	44.12	31.50	46.39
GM-CSF	5.47	30.20	62.92	18.48	55.88	10.51	24.20	21.51	11.51	18.77
HGF	3.82	25.94	74.03	8.20	60.53	3.88	16.78	22.83	5.63	12.97
IFNa	0.71	5.46	14.56	1.00	14.46	0.88	4.39	5.79	1.12	3.85
IFNg	38.59	85.15	304.65	23.73	413.08	27.93	67.34	97.21	13.90	62.70
IL-1a	5.56	13.22	30.79	5.56	23.44	5.56	9.67	12.01	5.56	5.56
IL-1b	7.63	14.89	43.90	7.38	39.51	4.70	12.03	14.22	8.20	13.25
IL-2R	401.06	1002.07	3166.10	360.56	2507.55	345.93	694.87	1022.67	259.19	548.13
IL-3	14.50	47.30	103.41	21.33	83.89	14.86	38.00	55.23	14.58	22.34
IL-4	5.77	35.14	83.12	6.31	78.81	7.31	17.80	34.37	2.96	17.31
IL-5	27.85	36.73	181.64	15.79	133.29	28.68	32.95	52.78	15.32	24.87
IL-6	99.73	3269.56	4940.31	1137.16	5058.13	77.36	1526.66	2139.67	758.21	1310.49
IL-7	0.75	0.28	1.63	0.29	1.64	0.70	0.21	1.01	0.19	1.28
IL-8	2.06	1069.08	1505.54	478.95	1695.61	0.86	766.10	681.09	306.80	299.13
IL-9	2.37	72.44	88.50	24.93	83.50	3.13	57.16	58.54	17.95	30.93
IL-10	22.34	4.43	68.87	1.89	116.11	17.98	3.40	10.12	2.54	17.47
IL-12p70	2.27	3.18	4.51	2.07	4.93	2.07	2.15	3.56	1.92	2.33
IL-13	1.48	3.49	6.39	1.93	5.96	1.84	1.72	3.40	1.61	3.01
IL-15	0.29	4.90	10.30	0.88	10.42	0.20	3.37	5.34	0.42	3.43
IL-16	15.92	8.51	19.86	8.51	19.04	12.20	8.51	9.46	8.51	10.39
IL-18	5.84	30.80	102.84	31.30	134.63	5.84	17.35	40.58	14.30	40.08
IL-20	1.47	5.95	11.45	2.91	11.70	0.99	4.76	7.12	1.56	4.37
IL-21	7.10	35.16	49.79	15.15	41.22	6.00	25.29	31.16	11.85	19.41
IL-22	2.69	84.27	109.36	10.72	92.88	2.69	69.06	60.16	16.41	43.66
IL-23	15.23	80.33	69.10	17.67	90.55	24.98	32.19	27.13	0.12	31.17
IL-27	55.41	129.67	269.92	48.04	291.30	75.29	125.14	139.41	49.09	104.70
IL-31	3.02	18.96	51.98	5.66	46.56	7.97	30.61	3.02	10.13	3.02
LIF	3.82	363.47	556.61	291.61	445.66	4.24	264.29	317.67	226.11	265.61
M-CSF	138.70	1273.19	1875.18	428.27	1792.03	16.58	1124.93	1289.15	326.07	605.67
MDC	26.50	57.98	93.08	37.73	92.28	36.37	46.06	67.88	34.25	46.01
MIF	31.59	6.91	146.68	1.85	85.19	27.11	2.71	23.28	1.27	23.83
MMP-1	3.23	11156.06	8536.49	28570.34	36893.39	4.01	4847.68	5095.25	20833.25	20434.96
NGFb	4.62	28.97	65.67	9.86	67.24	6.73	24.05	34.17	8.20	19.91
SCF	1.13	2.35	4.21	1.82	4.43	1.25	1.88	2.18	1.48	1.68
TNFA	2.46	9.69	22.91	4.63	19.19	1.86	6.60	11.27	2.96	8.16
TNFB	28.14	40.95	202.81	9.79	170.68	15.90	40.01	54.43	7.70	39.79
TNF-RII	25.20	1.85	46.55	1.23	41.60	19.62	1.23	17.33	1.23	20.80
TRAIL	16.83	67.87	113.58	35.22	112.32	15.27	58.22	62.13	26.90	49.57
TSLP	2.80	12.17	25.00	4.78	22.12	3.77	10.35	9.57	5.54	8.16
TWEAK	358.17	358.17	358.17	358.17	358.17	358.17	358.17	358.17	358.17	358.17
VEGF-A	13.43	8021.40	5865.13	255.60	228.06	11.90	3864.46	3596.83	184.60	202.02

Appendix 6: Concentrations of secreted cytokines and chemokines identified in direct and Transwell™ co-culture.

Mean observed concentration for each analyte is depicted as pg/mL. Analytes identified as out of range are represented as the highest/lowest observed value for the analyte. Data for direct contact co-culture are shaded in white, whilst those for Transwell™ separated assays are shaded in grey.

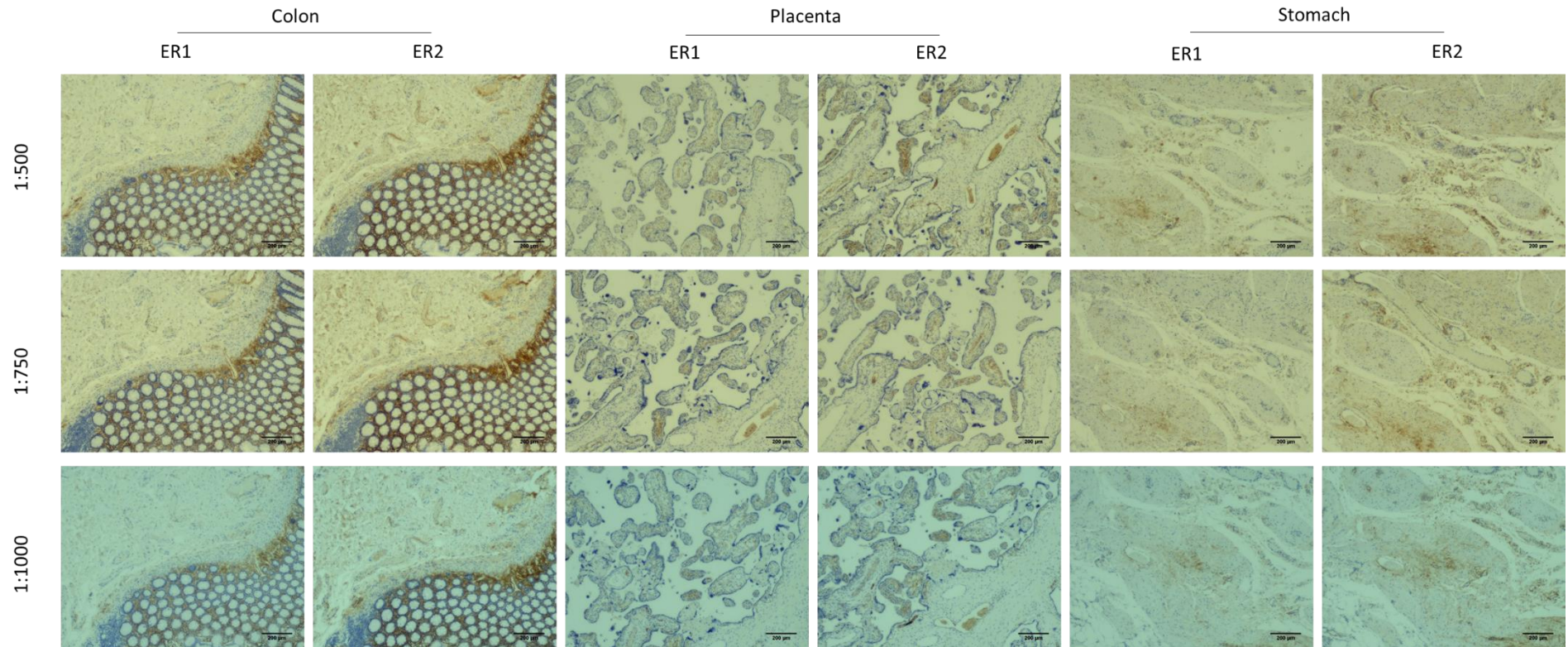
Analyte	Fold Change				
	NK Cells Alone	qPSC Alone	qPSC + NK Cells	aPSC Alone	aPSC + NK cells
APRIL	1.425420661	0.8463827	0.35732661	0.4997693	0.319397093
BAFF	0.708223712	0.636729	0.309498119	0.8133071	0.237684449
CCL11	0.852272727	0.7450111	0.487514863	0.7551622	0.428721174
CCL2	1.251428571	1.4012069	1.055936306	0.6716282	1.849272433
CCL20	1.2093259	0.6711063	0.239158517	0.8982187	0.595631714
CCL24	0.836656328	0.9519088	0.553570134	0.8823757	0.432348948
CCL26	1.126865672	0.3718905	0.436123348	3.4210526	0.33919598
CCL3	0.265640513	0.831244	0.746098204	0.5792052	1.197292591
CCL4	0.613465036	0.4769989	0.060379324	1	0.086341975
CCL7	1.132524026	0.9337003	0.062472802	0.8909675	0.10264844
CCL8	0.714285714	0.6829268	0.00066517	0.5882353	0.001217931
CD30	0.81630702	0.6500249	0.518144831	0.7100925	0.28322973
CD40L	1.129140663	0.7485541	0.569101908	0.584911	0.401499104
CTLA-8	0.979765808	0.7455457	0.542777313	0.8100371	0.378706738
CX3CL1	1.214115781	0.9055168	0.625814863	0.483998	0.506633686
CXCL1	1.302257115	0.8494345	0.565490082	0.9936034	0.561089268
CXCL10	1.010041841	0.8568534	0.107911239	0.7938931	0.410248514
CXCL11	1.004561476	0.7553997	0.007821259	1.0077391	0.032005654
CXCL12	1.115843137	0.7820719	1.045327494	0.8109329	1.049350456
CXCL13	1.466245332	0.8713168	0.566585494	0.7707356	0.503417274
CXCL5	0.472283814	0.7232958	0.561989394	0.4436494	0.28057554
CXCL9	0.688367129	0.9227638	0.017580985	0.3560284	0.017946692
FGF-2	1.105367793	0.7444832	0.019509092	0.7141388	0.033158665
G-CSF	2.35925126	0.8496241	0.559372887	0.849043	0.663599084
GM-CSF	1.92195122	0.8013464	0.341880795	0.6229479	0.335918392
HGF	1.015693112	0.6469228	0.308402378	0.6861789	0.214285714
IFNa	1.244131455	0.8029286	0.397893773	1.1129568	0.266021208
IFNg	0.72373877	0.7908315	0.319098419	0.5858146	0.151785354
IL-1a	1	0.7317196	0.389953448	1	0.237201365
IL-1b	0.615283843	0.8081486	0.323866657	1.1115628	0.335470807
IL-2R	0.862538128	0.6934313	0.323007615	0.7188632	0.218593473
IL-3	1.024827586	0.8034393	0.534070397	0.6838074	0.266340843
IL-4	1.266166282	0.5065933	0.413515139	0.4688161	0.21960917
IL-5	1.029559598	0.897259	0.290561744	0.9698185	0.186615315
IL-6	0.775660951	0.4669298	0.433104783	0.6667546	0.259086356
IL-7	0.924778761	0.746988	0.619631902	0.6363636	0.782520325
IL-8	0.419773096	0.7166006	0.452388174	0.6405565	0.1764167
IL-9	1.322535211	0.7891128	0.661431262	0.7202461	0.370459082
IL-10	0.804685169	0.7669173	0.146950629	1.3433099	0.150427743
IL-12p70	0.911764706	0.6771488	0.789940828	0.9290323	0.4719405
IL-13	1.240449438	0.4937918	0.532359081	0.8310345	0.504751258
IL-15	0.689655172	0.688904	0.518278874	0.4810606	0.328854766
IL-16	0.766701571	1	0.476246433	1	0.545772799
IL-18	1	0.5633589	0.394561131	0.4567139	0.297736952
IL-20	0.672727273	0.7989922	0.622125182	0.534937	0.373325734
IL-21	0.845539906	0.7194463	0.625786585	0.7822261	0.470926001
IL-22	1	0.8195159	0.550126497	1.5315708	0.470016149
IL-23	1.639964981	0.4007469	0.392590091	0.0067925	0.34424238
IL-27	1.358840161	0.9650404	0.516480395	1.0217859	0.359427388
IL-31	2.639072848	1.6143435	0.058095543	1.7881107	0.064867187
LIF	1.110820244	0.727146	0.570732175	0.7753938	0.595989439
M-CSF	0.119538572	0.88355	0.687477669	0.7613636	0.337978602
MDC	1.372499685	0.794515	0.729291265	0.9079343	0.498609255
MIF	0.857986917	0.3928571	0.158709238	0.6895307	0.279738613
MMP-1	1.243801653	0.4345332	0.596879201	0.7291916	0.553892084
NGFb	1.457761733	0.8299586	0.520328917	0.8319242	0.29603926
SCF	1.10619469	0.8	0.518196203	0.8131868	0.379518072
TNFa	0.753721245	0.6808803	0.491924924	0.6393089	0.425469076
TNFB	0.565031983	0.9771266	0.26837486	0.7871253	0.233111341
TNF-RII	0.778674428	0.6648649	0.372189603	1	0.500040067
TRAIL	0.907290016	0.8577673	0.546999266	0.7638429	0.44129867
TSLP	1.346428571	0.8507258	0.382717696	1.1591068	0.369047619
TWEAK	1	1	1	1	1
VEGF-A	0.885856079	0.4817684	0.613256306	0.7222353	0.885791958

Appendix 7: Fold change in analyte concentration (identified by Luminex multiplex ELISA) observed between Transwell™ separated and direct co-culture conditions.



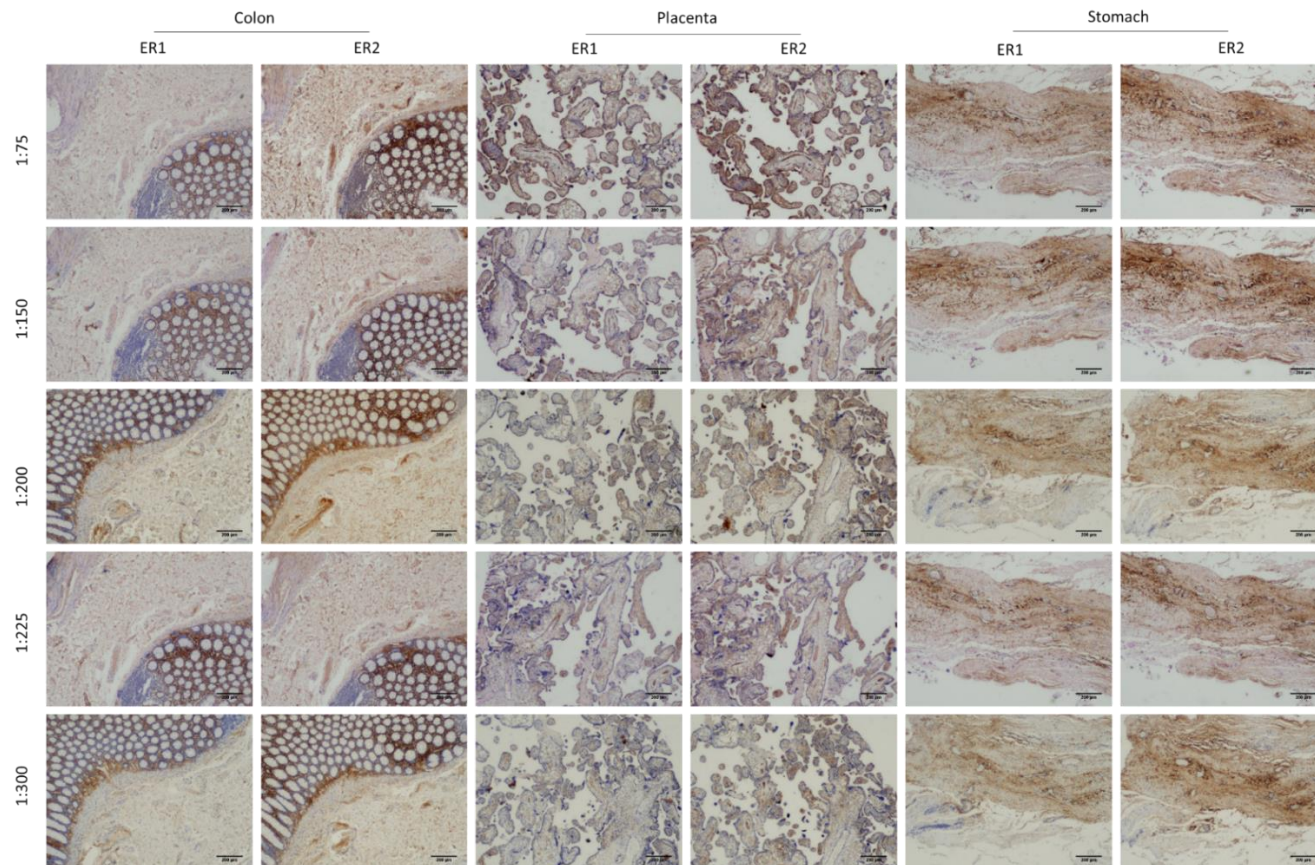
Appendix 8: Top upregulated and downregulated proteins in PSCs and NK cells in response to co-culture.

A). Top five upregulated and downregulated proteins in qPSC/aPSCs following 24h culture with NK cells. B). Top five upregulated and downregulated proteins in NK cells following 24h culture with qPSC/aPSCs. Data were analysed using unpaired T-tests. * $p < 0.05$; ** $p < 0.01$; *** $p < 0.001$; **** $p < 0.0001$.



Appendix 9: Initial antibody titrations for periostin using a second antibody clone.

Immunohistochemical staining of Periostin (MA5-26675, ThermoFisher) was carried out on colon, placenta, and stomach positive control tissue. Each dilution was tested using two epitope retrieval conditions ER1 (pH 6.0 citrate-based antigen retrieval) or ER2 (pH 9.0 Tris-based antigen retrieval). Slides were stained using the Leica Bond Max automated staining system. Following staining, slides were dehydrated and mounted with glass coverslips using Dibutylphthalate Polystyrene Xylene (DPX). All slides were imaged using the Olympus CKX53 inverted light microscope and Olympus EP50 camera at magnification x4. Scale bars=200µm were added using ImageJ software.



Appendix 10: Additional antibody titration for periostin (second clone).

Immunohistochemical staining of Periostin (MA5-26675, ThermoFisher) was carried out on colon, placenta, and stomach positive control tissue. Each dilution was tested using two epitope retrieval conditions ER1 (pH 6.0 citrate-based antigen retrieval) or ER2 (pH 9.0 Tris-based antigen retrieval). Slides were stained using the Leica Bond Max automated staining system. Following staining, slides were dehydrated and mounted as described. All slides were imaged using the Olympus CKX53 inverted light microscope and Olympus EP50 camera at magnification x4. Scale bars=200µm were added using ImageJ software. It was concluded that this antibody would not be used for further staining as greater signal to noise ratio was achieved using the alternative periostin clone (ab215199, Abcam).

A

Normal Adjacent	
Patient	Number of cores
2	3
3	1
4	2
5	2
6	3
7	3
8	3
9	1
10	2
11	3
12	3
18	3
41	3
59	5
76	4
93	1
94	4
95	4
96	1
97	2
103	6
107	9
Total Number	68

B

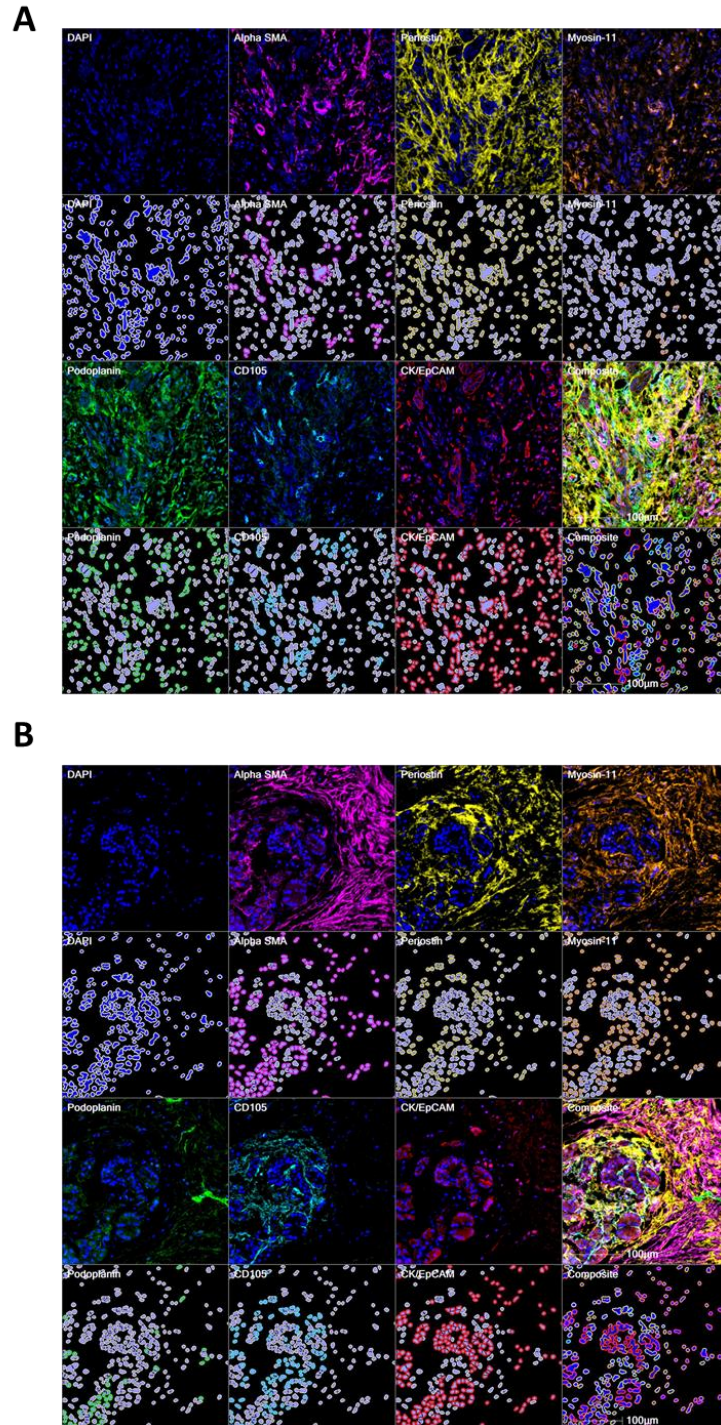
Chronic Pancreatitis	
Patient	Number of cores
15	3
16	3
80	4
Total Number	10

C

PDAC		PDAC (Continued)	
Patient	Number of cores	Patient	Number of cores
13	3	55	4
14	3	60	3
17	2	63	6
19	2	64	6
20	2	65	6
21	3	67	4
22	3	68	3
23	3	70	5
25	1	71	2
26	1	72	3
27	3	73	1
28	1	74	2
29	2	77	3
30	2	78	4
31	3	81	4
32	3	85	3
33	3	86	1
34	3	88	6
35	3	89	1
36	3	91	6
38	3	92	6
39	3	99	4
40	3	100	1
42	3	102	2
43	1	105	3
44	3	106	6
46	3	108	1
47	3	110	3
49	2	111	3
50	3	112	3
51	3	113	4
52	1	125	1
54	4	Total Number	194

Appendix 11: Number of cores analysable for each patient.

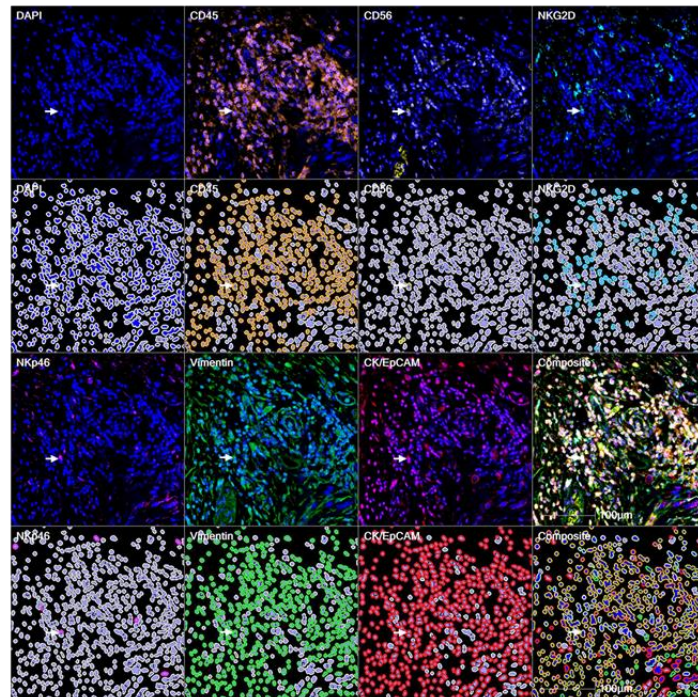
A-C) The number of cores analysable for patients with a final diagnosis of normal (A), chronic pancreatitis (B) or PDAC (C) following mIHC staining. These numbers take into account cores removed due to lack of concordance across panels.



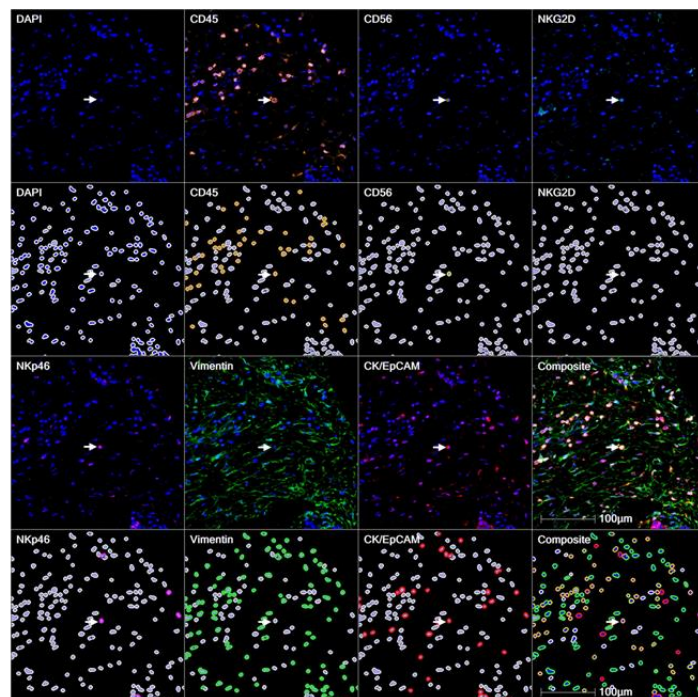
Appendix 12: Representative images of Panel 1 staining with HALO scoring masks.

A-B) Representative images of CAF staining in patient PDAC sections. Samples were stained for alpha SMA –magenta; periostin – yellow; myosin-11 – orange; podoplanin- - green; CD105 – cyan; CK/EpCAM – red using the Opal TSA system (Akoya Biosciences). Nuclei are stained with DAPI – blue. Slides were imaged using the Vectra Polaris (Akoya bioscience). Images were created with HALO software (3.4). Scoring masks for each marker are displayed below the tissue section. Scale bars = 100µm.

A



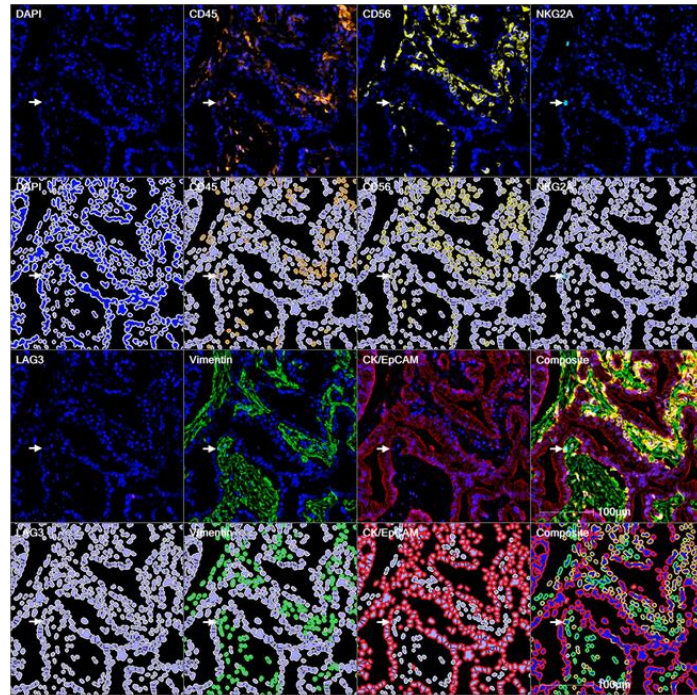
B



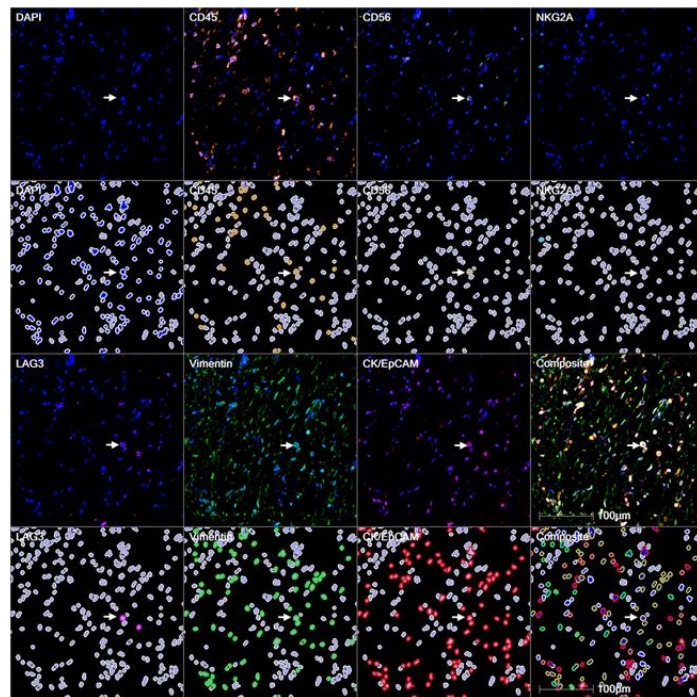
Appendix 13: Representative images of Panel 2 staining with scoring masks.

A-B) Representative image of panel 2 (NK activating receptors) on TMA samples. CD45 – orange; CD56 – yellow; NKG2D – cyan; Nkp46 – magenta; Vimentin – green; CK/EpCAM – red. Nuclei are stained with DAPI – blue. Patient TMA samples were stained using the Opal TSA system and scanned using the Vectra Polaris (Akoya Biosciences). Images were created with HALO software (3.4). Scoring masks for each marker are displayed below the tissue section. Arrows indicate examples of CD45⁺CD56⁺NKG2D⁺ (A) and CD45⁺CD56⁺Nkp46⁺ (B) cells. Scale bars = 100µm.

A

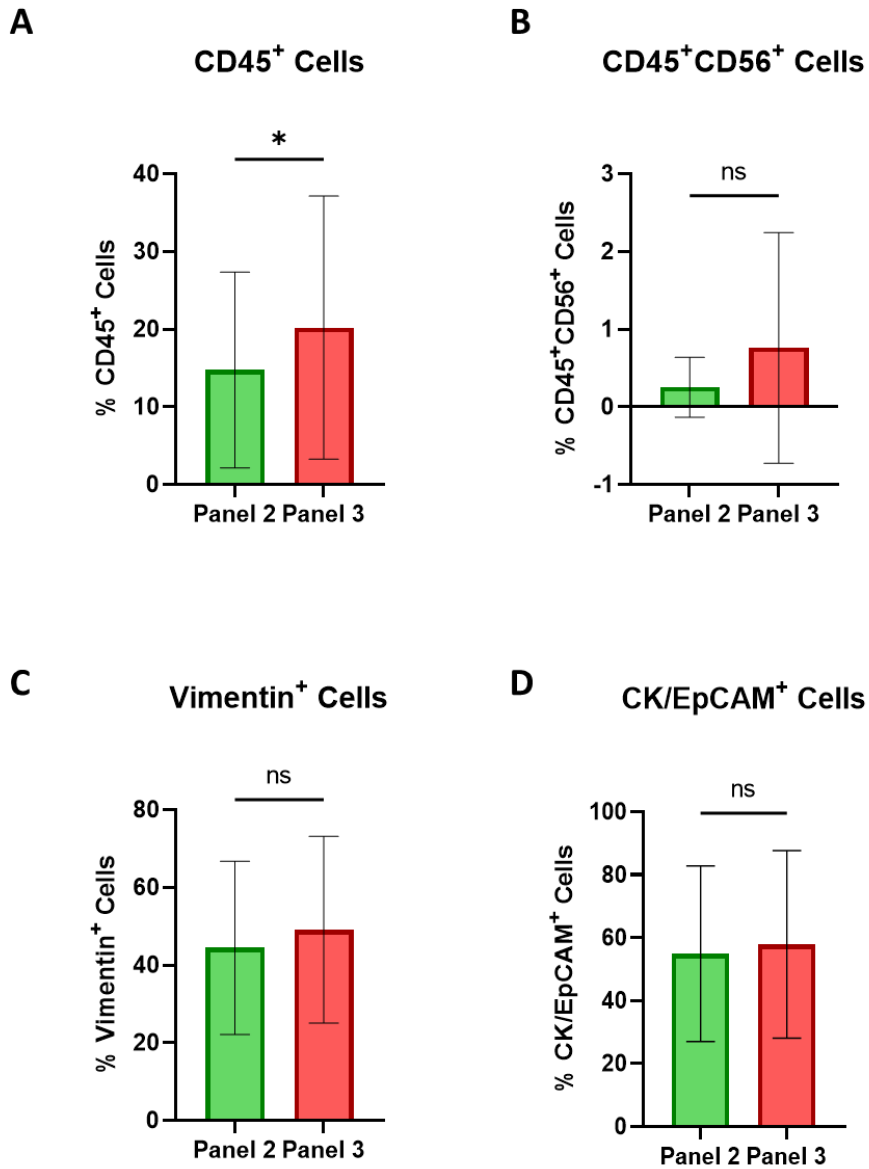


B



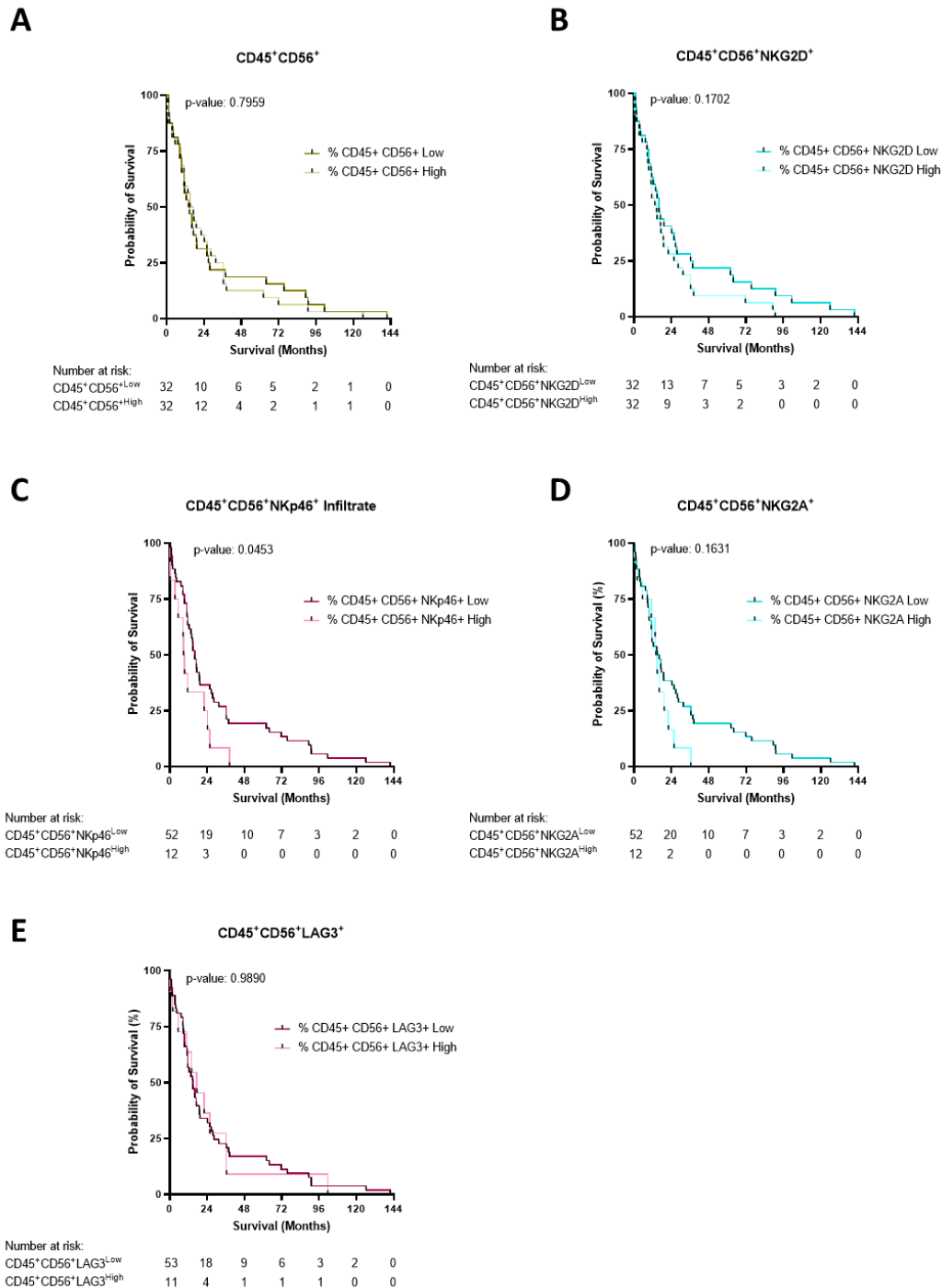
Appendix 14: Representative images of Panel 3 staining on TMA sections with scoring masks.

A-B) Representative image of panel 3 (NK inhibitory receptors) on TMA Sections. CD45 – orange; CD56 – yellow; NKG2A – cyan; LAG3 – magenta; Vimentin – green; CK/EpCAM – red. Nuclei are stained with DAPI – blue. Patient TMA samples were stained using the Opal TSA system and scanned using the Vectra Polaris (Akoya Biosciences). Images were created with HALO software (3.4). Scoring masks for each marker are displayed below the tissue section. Arrows indicate examples of CD45⁺CD56⁺NKG2A⁺ (A) and CD45⁺CD56⁺LAG3⁺ (B) cells. Scale bars = 100µm.



Appendix 15: Comparison of lineage markers between panels 2 and 3.

A-D) The expression of CD45⁺ (A), CD45⁺CD56⁺ (B), Vimentin⁺ (C) and CK/EpCAM⁺ (D) cells observed per patient in mIHC staining panels 2 and 3. Data were analysed using Mann Whitney U Tests. * $p < 0.05$. Whilst there was some variation in CD45⁺ cells observed between panels 2 and 3 it was concluded that the concordance across panels was acceptable to proceed with downstream proximity and survival analysis.



Appendix 16: Kaplan Meier survival analysis dichotomised by high and low expression of NK cell markers.

A-E) Kaplan Meier Survival curves based on high or low expression of CD45⁺CD56⁺ (A), CD45⁺CD56⁺NKG2D⁺ (B), CD45⁺CD56⁺NKp46⁺ (C), CD45⁺CD56⁺NKG2A⁺ (D), CD45⁺CD56⁺LAG3⁺ (E). Significance was identified using the Log-Rank test. Due to the low percentage of immune infiltrate for CD45⁺CD56⁺NKp46⁺, CD45⁺CD56⁺NKG2A⁺ and CD45⁺CD56⁺LAG3⁺ subsets, the number of patients at risk differs greatly between 'high' and 'low' expression groups. This must be considered when reviewing the significance in overall survival identified in the CD45⁺CD56⁺NKp46⁺ subset.